

2015-09-29

# Experimental and Theoretical Investigation on Compressive Behaviour of CFRP- and SFRP Confined Concrete Cylinders

Salameh, Nisreen

---

Salameh, N. (2015). Experimental and Theoretical Investigation on Compressive Behaviour of CFRP- and SFRP Confined Concrete Cylinders (Master's thesis, University of Calgary, Calgary, Canada). Retrieved from <https://prism.ucalgary.ca>. doi:10.11575/PRISM/26056

<http://hdl.handle.net/11023/2554>

*Downloaded from PRISM Repository, University of Calgary*

UNIVERSITY OF CALGARY

Experimental and Theoretical Investigation on Compressive Behaviour of  
CFRP- and SFRP-Confined Concrete Cylinders

by

Nisreen Salameh

A THESIS

SUBMITTED TO THE FACULTY OF GRADUATE STUDIES  
IN PARTIAL FULFILMENT OF THE REQUIREMENTS FOR THE  
DEGREE OF MASTER OF SCIENCE

GRADUATE PROGRAM IN CIVIL ENGINEERING

CALGARY, ALBERTA

SEPTEMBER, 2015

© Nisreen Salameh 2015

## **Abstract**

A combined experimental and theoretical investigation into the compressive behaviour of CFRP- and SFRP-confined concrete is presented in this thesis. The experimental investigation included testing of small-scale unreinforced CFRP- and SFRP-confined concrete cylinders under axial compression. Fundamental aspects of compression behaviours such as failure mode, ultimate strength, ultimate strain, stress-strain response, ductility enhancement were closely examined. The theoretical investigation included performance assessment of some existing empirical, analytical and design code confinement. Modification to one of the existing models is proposed. The new model provided more accurate predictions of the ultimate strength, ultimate axial strain and stress-strain response of FRP-confined concrete. Furthermore, the Drucker-Prager (DP) plasticity model parameters were derived and implemented in numerical Finite Element analyses to simulate the behaviour of FRP-confined concrete. It has been found that the DP model can give close predictions of confined concrete compressive behaviour should accurate material parameters be defined.

## **Acknowledgements**

First and Foremost, I would like to express my deepest gratitude to my supervisor Dr. Raafat El-Hacha for his patience, unlimited support and insightful feedback throughout the research and writing this thesis. I could not have asked a better mentor and instructor for my research than Dr. El-Hacha.

I am most grateful to my examination committee members: Dr. Nigel Shrive, Dr. Markus Dann and Dr. Maen Hussein. Their contribution to this work is greatly appreciated.

I would like to thank my colleagues Khaled Abdelrahman and Hamid Omran for their friendship and support. I am also thankful to all the technical staff in the structural lab at the Civil Engineering Department, Mr. Terry Quinn, Mr. Dan Tilleman, Mr. Don Anson, Mr. Mirsad Berbic and Mr. Dan Larson, for their assistance during the experimental works.

I would like also to acknowledge SIKA Canada for donating the CFRP sheets and the epoxy adhesive; Hardwire LLC for donating the SFRP sheets and the University of Calgary for partially funding this research.

Finally, I would like to thank my long suffering husband, Ayed and my kids; Nathaly, Jad and Fadi of which their incredible encouragement, enthusiasm and optimism have gave me the strength to keep going and dragged me to the finish line. I unquestionably could not have accomplished this without them.

## **Dedication**

This work is dedicated to the memory of my mother,

I hope this would have made her proud.

## Table of Contents

Abstract.....	ii
Acknowledgements.....	iii
Dedication.....	iv
Table of Contents.....	v
List of Tables.....	xi
List of Figures and Illustrations.....	xiv
List of Symbols, Abbreviations and Nomenclature.....	xxii
CHAPTER ONE: INTRODUCTION.....	1
1.1 Background.....	1
1.2 Objectives.....	2
1.3 Research Significance.....	4
1.4 Scope of Work.....	6
1.5 Organization of the Thesis.....	8
1.6 Summary.....	10
CHAPTER TWO: LITERATURE REVIEW.....	11
2.1 Introduction.....	11
2.2 FRP Composite Materials.....	11
2.2.1 Reinforcing Fibres.....	13
2.2.1.1 Glass Fibres.....	13
2.2.1.2 Carbon Fibres.....	15
2.2.1.3 Aramid Fibres.....	16
2.2.1.4 Basalt Fibres.....	16
2.2.1.5 Steel Fibres.....	17
2.2.2 Matrix Materials.....	18
2.2.2.1 Polymer Matrix Materials.....	19
2.3 Mechanical Behaviour of FRP Composites.....	21
2.4 Mechanics of FRP-Confined Concrete.....	23
2.5 Preceding Research and State-of-the-Art of FRP-Confined Concrete.....	25
2.5.1 Experimental Programs.....	26
2.5.1.1 Xiao and Wu (2000).....	27
2.5.1.2 Karabinis and Rousakis (2002).....	28
2.5.1.3 Lam and Teng (2004).....	28
2.5.1.4 Li (2006).....	28
2.5.1.5 Youssef et al. (2007).....	29
2.5.2 Theoretical Developments.....	29
2.5.2.1 Empirical Models.....	31
2.5.2.2 Analytical Models.....	43
2.5.2.3 Numerical Models.....	48
2.5.2.4 FRP-Confinement Models in the Canadian Design Codes.....	53
2.6 Preceding Research and State-of-the-Art of SFRP-Confined Concrete.....	55
2.6.1 Experimental Programs.....	55
2.6.1.1 Mashrik (2011) and El-Hacha and Mashrik (2011).....	55
2.6.1.2 Abdelrahman (2011) and Abdelrahman and El-Hacha (2012).....	56

2.6.1.3 Napoli and Realfonzo (2013).....	57
2.6.2 Theoretical Works .....	59
2.6.2.1 Empirical Models.....	59
2.6.2.2 Analytical Models.....	59
2.6.2.3 Numerical Models.....	59
2.7 Summary .....	62
<b>CHAPTER THREE: EXPERIMENTAL PROGRAM.....</b>	<b>63</b>
3.1 Introduction.....	63
3.2 Experimental Program Overview .....	63
3.2.1 FRP Wrap Configuration Designation .....	65
3.3 Material Properties.....	66
3.3.1 Concrete.....	66
3.3.2 SFRP Sheets .....	66
3.3.3 CFRP Sheets.....	67
3.3.4 Epoxy Adhesive.....	69
3.4 Cylinders Fabrication.....	70
3.4.1 Concrete Casting Procedure .....	70
3.4.2 Cylinder's Ends Preparation.....	70
3.4.3 FRP System Installation Procedure .....	71
3.4.3.1 Cylinder's Surface Preparation.....	71
3.4.3.2 Fabric and Epoxy Preparation.....	72
3.4.3.3 FRP Fabric Installation .....	72
3.4.4 Strain Gauge Installation Procedure.....	75
3.4.4.1 Surface Preparation.....	75
3.4.4.2 Gauge Mounting .....	76
3.4.4.3 Curing .....	77
3.4.4.4 Soldering.....	77
3.4.4.5 Verification .....	78
3.4.5 Cylinder's Surface Finishing Procedure.....	79
3.5 Instrumentation .....	79
3.5.1 Strain Gauges.....	79
3.5.2 Linear Strain Converter LSC.....	81
3.5.3 Digital Image Correlation (DIC) Technique .....	82
3.6 Test Setup .....	83
3.7 Loading .....	83
3.8 Summary.....	84
<b>CHAPTER FOUR: COMPRESSIVE BEHAVIOUR OF CFRP-AND SFRP-CONFINED CONCRETE CYLINDERS .....</b>	<b>86</b>
4.1 Introduction.....	86
4.2 Ancillary Test Results.....	86
4.2.1 Concrete.....	86
4.3 Test Results Statistical Analysis .....	88
4.4 Compressive Behaviour of CFRP-and SFRP- Confined Cylinders.....	93
4.4.1 Failure Mechanism .....	93
4.4.1.1 CFRP-Confined Concrete Cylinders .....	93

4.4.1.2 SFRP-Confined Concrete Cylinders .....	93
4.4.2 Ultimate Axial Strength.....	96
4.4.2.1 CFRP-Confined Concrete Cylinders .....	96
4.4.2.2 SFRP-Confined Concrete Cylinders .....	100
4.4.3 Ultimate Axial Strain.....	104
4.4.3.1 CFRP-Confined Concrete Cylinders .....	104
4.4.3.2 SFRP-Confined Concrete Cylinders .....	108
4.4.4 Ultimate Lateral Strain .....	113
4.4.4.1 CFRP-Confined Concrete Cylinders .....	113
4.4.4.2 SFRP-Confined Concrete Cylinders .....	115
4.4.5 Load-Deformation Behaviour .....	117
4.4.5.1 Stress-Strain Behaviour .....	118
4.4.5.2 Dilation Behaviour.....	122
4.4.6 Axial and Lateral Strain Variation over FRP-Confined Cylinder's Surface .	126
4.4.6.1 Validation of the DIC Technique.....	127
4.4.6.2 Axial and Lateral Strain Variation in CFRP-Confined Concrete Cylinders .....	132
4.4.6.3 Axial and Lateral Strain Variation in SFRP-Confined Concrete Cylinders .....	139
4.4.7 FRP Strain Efficiency.....	144
4.4.7.1 CFRP Sheet Strain Efficiency.....	144
4.4.7.2 SFRP Sheet Strain Efficiency .....	145
4.4.7.3 Failure Theories of FRP Wraps .....	146
4.5 Performance Comparison between CFRP- and SFRP-Confined Cylinders .....	148
4.5.1 Performance Parameters .....	148
4.5.1.1 Confinement Effectiveness Coefficients ( $kl$ ) .....	148
4.5.1.2 Strain Ductility Index, ( $\mu_{cu}$ ) .....	148
4.5.1.3 Energy Ductility Index, ( $\omega_{cu}$ ).....	149
4.5.2 Effect of Different Parameters.....	152
4.5.2.1 Effect of FRP Jacket Thickness .....	152
4.5.2.2 Effect of FRP Type.....	158
4.5.2.3 Effect of Unconfined Concrete Compressive Strength.....	164
4.6 Summary.....	168

## CHAPTER FIVE: ANALYTICAL MODELING OF FRP-CONFINED CONCRETE CYLINDERS .....

5.1 Introduction.....	169
5.2 FRP Confinement Models Overview.....	169
5.2.1 Empirical/ Analytical Confinement models .....	169
5.2.2 Confinement Models Adopted by the Canadian Design Codes .....	172
5.3 Performance Analysis of Confinement Models.....	173
5.3.1 Models' Performance in Prediction of $f'_{cu}$ .....	174
5.3.2 Models' Performance in Prediction of $\epsilon_{cu}$ .....	184
5.3.3 Axial Stress-Strain Behaviour Prediction.....	192
5.4 Proposed Analytical Confinement Model.....	202
5.4.1 Performance of the Proposed Stress-Strain Model.....	204
5.5 Summary.....	208

CHAPTER SIX: FINITE ELEMENT MODELING OF FRP-CONFINED CONCRETE	
CYLINDERS .....	210
6.1 Introduction.....	210
6.2 Concrete Plasticity .....	210
6.3 Concrete Constitutive Model.....	212
6.3.1 Extended Linear Drucker-Prager Plasticity Model .....	212
6.3.1.1 Yield criterion and Hardening-Softening Rule.....	212
6.3.1.2 Flow Rule.....	219
6.3.1.3 Implementation in ABAQUS.....	222
6.4 Modeling of FRP-Confined Concrete Cylinders .....	223
6.4.1 Model Geometry.....	223
6.4.2 Material Properties .....	223
6.4.2.1 FRP .....	223
6.4.2.2 Concrete .....	224
6.4.3 Element Types .....	224
6.4.4 Boundary Conditions and Loading Control .....	224
6.5 Sensitivity Analysis .....	225
6.5.1 Effect of FE Mesh Size.....	226
6.5.2 Effect of FE Element Type.....	228
6.5.3 Effect of Concrete Poisson's Ratio.....	229
6.6 FE Results and Discussion.....	230
6.6.1 Model Validation.....	230
6.6.1.1 Ultimate Axial Strength and Ultimate Axial Strain.....	231
6.6.1.2 Stress – Strain Response.....	233
6.6.2 Parametric Study .....	236
6.6.3 Effect of FRP Jacket Thickness.....	236
6.6.4 Effect of FRP Mechanical Properties .....	239
6.7 Summary.....	241
CHAPTER SEVEN: SUMMARY, CONCLUSIONS AND RECOMMENDATIONS	242
7.1 Introduction.....	242
7.2 Research Summary .....	242
7.3 Conclusions.....	243
7.3.1 Compressive Behaviour of FRP-Confined Concrete .....	243
7.3.2 Analytical Modeling of FRP-Confined Concrete.....	248
7.3.3 FE Numerical Modeling of FRP-Confined concrete.....	248
7.4 Recommendations for Future Work .....	249
REFERENCES .....	251
APPENDIX A: FAILURE MODES.....	274
A.1. Group I.....	274
A.1.1. C37.3-CFRP1 .....	274
A.1.2. C37.3-CFRP2 .....	275
A.1.3. C37.3-CFRP3 .....	276
A.1.4. C37.3-SFRP1 .....	277
A.1.5. C37.3-SFRP2.....	278

A.1.6. C37.3-SFRP3 .....	279
A.2. Group II.....	280
A.2.1. C42.4-CFRP1 .....	280
A.2.2. C42.4-CFRP2 .....	281
A.2.3. C42.4-CFRP3 .....	282
A.2.4. C42.4-SFRP1 .....	283
A.2.5. C42.4-SFRP2.....	284
A.2.6. C42.4-SFRP3.....	285
APPENDIX B: STRESS-STRAIN CURVES .....	286
B.1. Group I .....	286
B.1.1. C37.3-CFRP1.....	286
B.1.2. C37.3-CFRP2.....	287
B.1.3. C37.3-CFRP3.....	288
B.1.4. C37.3-SFRP1 .....	289
B.1.5. C37.3-SFRP2 .....	290
B.1.6. C37.3-SFRP3 .....	291
B.2. Group II.....	292
B.2.1. C42.4-CFRP1 .....	292
B.2.2. C42.4-CFRP2.....	293
B.2.3. C42.4-CFRP3.....	294
B.2.4. C42.4-SFRP1 .....	295
B.2.5. C42.4-SFRP2 .....	296
B.2.6. C42.4-SFRP3 .....	297
APPENDIX C: LATERAL STRAIN PROFILE EVOLUTION .....	298
C.1. Group I .....	298
C.1.1. C37.3-CFRP1.....	298
C.1.2. C37.3-CFRP2.....	299
C.1.3. C37.3-CFRP3.....	300
C.1.4. C37.3-SFRP1 .....	301
C.1.5. C37.3-SFRP2 .....	302
C.1.6. C37.3-SFRP3 .....	303
C.2. Group II.....	304
C.2.1. C42.4-CFRP1 .....	304
C.2.2. C42.4-CFRP2.....	305
C.2.3. C42.4-CFRP3.....	306
C.2.4. C42.4-SFRP1 .....	307
C.2.5. C42.4-SFRP2 .....	308
C.2.6. C42.4-SFRP3 .....	309
APPENDIX D: AXIAL AND LATERAL STRAIN DISTRIBUTION AT FAILURE..	310
D.1. Group I.....	310
D.1.1. C37.3-CFRP1 .....	310
D.1.2. C37.3-CFRP2 .....	311
D.1.3. C37.3-CFRP3 .....	312
D.1.4. C37.3-SFRP1 .....	313

D.1.5. C37.3-SFRP2 .....	314
D.1.6. C37.3-SFRP3 .....	315
D.2. Group II.....	316
D.2.1. C42.4-CFRP1 .....	316
D.2.2. C42.4-CFRP2 .....	317
D.2.3. C42.4-CFRP3 .....	318
D.2.4. C42.4-SFRP1 .....	319
D.2.5. C42.4-SFRP2 .....	320
D.2.6. C42.4-SFRP3 .....	321

## List of Tables

Table 2-1: Typical mechanical properties of common grades of glass fibres, Bank (2006) .....	14
Table 2-2: Typical elastic properties of common grades of carbon fibres, Bank (2006) .....	15
Table 2-3: Typical elastic properties of basalt fibres, Parnas et al. (2007).....	17
Table 2-4: Hardening/softening models parameters, Jiang and Wu (2012) .....	53
Table 2-5: Concrete Damage Plasticity (CDP) model parameter, Abdelrahman and El-Hacha (2014).....	61
Table 3-1: Summary of test specimens .....	64
Table 3-2: Summary of concrete mix design .....	66
Table 3-3: Typical properties of single 3×2 roving (cord), HARDWIRE (2014) .....	67
Table 3-4: Typical properties of SFRP sheet, HARDWIRE (2014).....	67
Table 3-5: Typical properties of SFRP composite system, HARDWIRE (2014) .....	67
Table 3-6: Typical properties of carbon fibre, SikaWrap® Hex 230C (2014).....	68
Table 3-7: Typical properties of carbon cured laminate, SikaWrap® Hex 230C (2014).....	68
Table 3-8: Typical mechanical/physical properties of Sikadure®-330, Sikadure®-330 (2014) ....	69
Table 3-9: Strain gauge properties, Micro-Measurement (2014) .....	81
Table 4-1: Concrete ancillary test results.....	87
Table 4-2: Summary of ANOVA analysis results for unconfined concrete cylinders .....	87
Table 4-3: Summary of ANOVA analysis results of FRP jacket thickness parameter significance .....	91
Table 4-4: Summary of ANOVA analysis results of FRP jacket type significance .....	91
Table 4-5: Summary of ANOVA analysis results of concrete compressive strength significance .....	92
Table 4-6: Key test results for CFRP-wrapped cylinders .....	97
Table 4-7: Summary of ultimate axial strength for CFRP-wrapped cylinders .....	97
Table 4-8: Key test results for SFRP-wrapped cylinders.....	101

Table 4-9: Summary of ultimate axial strength for SFRP-wrapped cylinders.....	101
Table 4-10: Summary of ultimate axial strain for CFRP-wrapped cylinders .....	112
Table 4-11: Summary of ultimate axial strain for SFRP-wrapped cylinders.....	112
Table 4-12: Summary of lateral strain for CFRP-wrapped cylinders .....	117
Table 4-13: Summary of lateral strain for SFRP-wrapped cylinders .....	117
Table 4-14: Ultimate axial and lateral strain readings from foil and virtual gauges for CFRP-confined cylinders .....	131
Table 4-15: Ultimate axial and lateral strain readings from foil and virtual gauges for SFRP-confined cylinders .....	132
Table 4-16: Axial and lateral strain variation at failure for CFRP-confined cylinders .....	138
Table 4-17: Axial and lateral strain variation at failure for SFRP-confined cylinders .....	144
Table 4-18: CFRP strain efficiency .....	145
Table 4-19: SFRP sheet strain efficiency.....	146
Table 4-20: Summary of performance parameters for CFRP-confined cylinders .....	150
Table 4-21: Summary of performance parameters for SFRP-confined cylinders .....	151
Table 4-22: Effect of FRP lateral stiffness and FRP ultimate confinement pressure .....	163
Table 5-1: Summary of empirical/ analytical confinement models.....	170
Table 5-2: Strength enhancement coefficient, $k_l$ , for FRP-confined concrete .....	172
Table 5-3: Summary of the Canadian codes confinement models .....	173
Table 5-4: Empirical models prediction of $f'_{cu}$ .....	175
Table 5-5: Analytical models prediction of $f'_{cu}$ .....	175
Table 5-6: Design codes confinement models prediction of $f'_{cu}$ .....	176
Table 5-7: Confinement models accuracy in the prediction of $f'_{cu}$ .....	180
Table 5-8: Empirical models prediction of $\epsilon_{cu}$ .....	185
Table 5-9: Analytical models prediction of $\epsilon_{cu}$ .....	185
Table 5-10: Confinement models accuracy in the prediction of $\epsilon_{cu}$ .....	188

Table 5-11: Proposed model prediction of $f'_{cu}$ and $\epsilon_{cu}$ .....	204
Table 5-12: The proposed model accuracy in the prediction of $f'_{cu}$ .....	204
Table 5-13: The proposed model accuracy in the prediction of $\epsilon_{cu}$ .....	205
Table 6-1: Summary of mesh size sensitivity analysis .....	227
Table 6-2: Summary of element type sensitivity analysis .....	229
Table 6-3: Summary of Poisson's ratio sensitivity analysis .....	230
Table 6-4: Details of the reference experimental programs.....	231
Table 6-5: Numerical and experimental results comparison .....	231
Table 6-6: Summary of FEA results for SFRP jacket thickness variation .....	237
Table 6-7: Summary of FEA results for FRP type variation .....	239

## List of Figures and Illustrations

Figure 2-1: Classification of two-phase composite materials, Daniel and Ishai (1994).....	12
Figure 2-2: FRP composites: (a) Unidirectional lamina (b) Multidirectional laminate, Daniel and Ishai (1994) .....	13
Figure 2-3: Bidirectional glass fabric, World-Trades.com (2014) .....	14
Figure 2-4: Bidirectional carbon fabric, World-Trades.com (2014).....	15
Figure 2-5: Aramid Fibre, World-Trades.com (2014).....	16
Figure 2-6: Multi-directional basalt fabric, GBF.com (2015) .....	17
Figure 2-7: Steel wire cords: (a) 3x2 cords (b) 12X wire cord (c) 3SX wire cord, HARDWIRE (2014) .....	18
Figure 2-8: Classification of matrix materials, Gunaslan et al. (2014).....	19
Figure 2-9: Schematic representation of molecule arrangement: (a) Thermoplastic (b) Thermoset, GangaRao et al. (2007) .....	19
Figure 2-10: Stress-strain curves for FRP unidirectional composites: (a) Tensile strength dominated by fibres (b) Tensile strength dominated by matrix, Daniel and Ishai (1994) ....	23
Figure 2-11: FRP confinement mechanism: (a) FRP jacket (b) Concrete core, Ozbakkaloglu et al. (2013).....	24
Figure 2-12: Typical stress-strain curve of FRP-confined concrete, Ozbakkaloglu et al. (2013).....	25
Figure 2-13: Stress – strain model by Fardis and Khalili (1982).....	33
Figure 2-14: Stress – strain model by Toutanji (1999).....	36
Figure 2-15: Stress – strain model by Lam and Teng (2003) .....	38
Figure 2-16: Stress – strain model by Berthet et al. (2005).....	41
Figure 2-17: Stress – strain model by Fahmy and Wu (2010).....	42
Figure 2-18: Iterative procedure - Spoelstra and Monti analytical model .....	45
Figure 2-19: Stress – strain model by Spoelstra and Monti (1999) .....	47
Figure 2-20: Stress – strain model by Teng et al. (2007).....	48
Figure 2-21: SFRP sheets: (a) low (b) medium (c) high density, Napoli and Realfonzo (2013) .	58

Figure 2-22: Modified Hognestad compression stress-strain curve, Hognestad (1951).....	60
Figure 2-23: Tensile stress-displacement model of confined concrete, ABAQUS (2009).....	61
Figure 3-1: SFRP sheet .....	67
Figure 3-2: CFRP sheet.....	68
Figure 3-3: Sikadure <sup>®</sup> -330.....	69
Figure 3-4: Concrete cylinders end surfaces treatment: (a) Before grinding, (b) After grinding.	71
Figure 3-5: Grinding machine: (a) Isometric view, (b) Front view .....	71
Figure 3-6: Procedures for wrapping cylinders with CFRP sheets.....	73
Figure 3-7: Procedures for wrapping cylinders with SFRP sheet.....	75
Figure 3-8: Soldering machine.....	77
Figure 3-9: Strain gauge installation: (a) After gauge mounting, (b) After Soldering .....	78
Figure 3-10: Surface finish: (a) White paint, (b) Final finish .....	79
Figure 3-11: Instrumentation of strain gauge: (a) Unconfined, (b) Confined cylinder .....	80
Figure 3-12: Conventional foil strain gauge .....	81
Figure 3-13: Linear Strain Converter (LSC): (a) Isometric view (b) Top view .....	82
Figure 3-14: Test set-up - east side (west side similar) .....	83
Figure 3-15: Testing machine: (a) Loading frame (b) Hydraulic pump (c) Pressure transducer .	84
Figure 4-1: Experiment results (a) Axial stress (b) Axial strain (c) Lateral strain for all confinement configurations .....	89
Figure 4-2: Typical failure mode of CFRP-wrapped cylinders .....	93
Figure 4-3: Typical failure mechanism: (a) SFRP rupture- (b) Full debonding- (c) Mixed failure modes.....	94
Figure 4-4: Catastrophic failure of an SFRP-wrapped cylinder .....	95
Figure 4-5: SFRP sheet – concrete interface.....	95
Figure 4-6: Average ultimate axial strength for CFRP-wrapped cylinders with respect to: (a) Unconfined concrete strength (b) Number of CFRP layers .....	98

Figure 4-7: Percentage increase in axial strength for CFRP-wrapped cylinders with respect to: (a) Unconfined concrete strength (b) Number of CFRP layers .....	99
Figure 4-8: Average ultimate axial strength for SFRP-wrapped cylinders with respect to: (a) Unconfined compressive strength (b) Number of SFRP layers .....	102
Figure 4-9: Percentage increase in axial strength of SFRP-wrapped cylinders with respect to: (a) Unconfined compressive strength (b) Number of SFRP layers .....	103
Figure 4-10: Ultimate axial strain for CFRP-wrapped cylinders with respect to: (a) Unconfined compressive strength (b) Number of CFRP layers .....	106
Figure 4-11: Percentage increase in axial strain of CFRP-wrapped cylinders with respect to (a) Unconfined compressive strength (b) Number of CFRP layers .....	107
Figure 4-12: Ultimate axial strain for SFRP-wrapped cylinders with respect to: (a) Unconfined compressive strength (b) Number of SFRP layers .....	110
Figure 4-13: Percentage increase in axial strain of SFRP-wrapped cylinders with respect to: (a) Unconfined compressive strength (b) Number of SFRP layers .....	111
Figure 4-14: Lateral strain for CFRP-wrapped cylinders with respect to: (a) Unconfined compressive strength (b) Number of CFRP layers .....	114
Figure 4-15: Ultimate lateral strain for SFRP-confined cylinders with respect to: (a) Unconfined compressive strength (b) Number of SFRP layers .....	116
Figure 4-16: Stress-strain curve of CFRP-confined cylinders for: (a) C37.3 (b) C42.4.....	119
Figure 4-17: Stress-strain curves of SFRP-confined cylinders for: (a) C37.3 (b) C42.4.....	121
Figure 4-18: Dilation behaviour of CFRP-confined cylinders for: (a) C37.3 (b) C42.4 .....	123
Figure 4-19: Axial strain-lateral strain plots for CFRP-confined cylinders .....	124
Figure 4-20: Dilation behaviour of SFRP-wrapped cylinders (a) C37.3 (b) C42.4.....	125
Figure 4-21: lateral strain-axial strain curve of SFRP-wrapped cylinders .....	126
Figure 4-22: Typical instrumentation: (a) DICT setup (b) Conventional strain gauges (c) vertical strain patches (d) Horizontal strain patches .....	127
Figure 4-23: Comparison between foil and virtual strain gauges at mid height of confined cylinders for: (a) C37.3-CFRP (b) C37.3-SFRP (c) C42.4-CFRP (d) C42.4-SFRP.....	130
Figure 4-24: Lateral strain profile evolution for: (a) C37.3-CFRP1 (b) C37.3-CFRP2 (c) C37.3-CFRP3.....	134

Figure 4-25: Lateral strain profile evolution for: (a) C42.4-CFRP1 (b) C42.4-CFRP2 (c) C42.4-CFRP3 .....	135
Figure 4-26: Axial and lateral strain distribution at failure for: (a) C37.3-CFRP1 (b) C37.3-CFRP2 (c) C37.3-CFRP3.....	136
Figure 4-27: Lateral strain profile evolution for: (a) C42.4-CFRP1 (b) C42.4-CFRP2 (c) C42.4-CFRP3 .....	137
Figure 4-28: Lateral strain profile evolution for: (a) C37.3-SFRP1 (b) C37.3-SFRP2 (c) C37.3-SFRP3 .....	140
Figure 4-29: Lateral strain profile evolution for: (a) C42.4-SFRP1 (b) C42.4-SFRP2 (c) C42.4-SFRP3 .....	141
Figure 4-30: Lateral strain profile evolution for: (a) C37.3-SFRP1 (b) C37.3-SFRP2 (c) C37.3-SFRP3 .....	142
Figure 4-31: Lateral strain profile evolution for: (a) C42.4-SFRP1 (b) C42.4-SFRP2 (c) C42.4-SFRP3 .....	143
Figure 4-32: FRP failure mechanism theory (a) Uniform (b) Localized strain failure, Pessiki et al. (2001) .....	147
Figure 4-33: Definition of ductility indices: (a) Stain ductility index (b) Energy ductility index.....	149
Figure 4-34: Effect of FRP jacket thickness on confinement effectiveness coefficient for: (a) CFRP- (b) SFRP-confined cylinders .....	155
Figure 4-35: Effect of FRP jacket thickness on strain ductility index for: (a) CFRP- (b) SFRP-confined cylinders .....	156
Figure 4-36: Effect of FRP jacket thickness on energy ductility index for: (a) CFRP- (b) SFRP-confined cylinders .....	157
Figure 4-37: Effect of FRP type on confinement effectiveness for: (a) C37.3 (b) C42.4 .....	159
Figure 4-38: Effect of FRP type on strain ductility index for: (a) C37.3 (b) C42.4 .....	160
Figure 4-39: Effect of FRP type on energy ductility index for: (a) C37.3 (b) C42.4 .....	161
Figure 4-40: Effect of concrete strength on confinement effectiveness for: (a) CFRP- (b) SFRP-confined cylinders .....	165
Figure 4-41: Effect of concrete strength on strain ductility index for: (a) CFRP- (b) SFRP-confined cylinders .....	166

Figure 4-42: Effect of concrete strength on energy ductility index for: (a) CFRP- (b) SFRP- confined cylinders .....	167
Figure 5-1: Empirical models' performance in the prediction of $f'_{cu}/f'_{co}$ .....	177
Figure 5-2: Analytical models' performance in the prediction of $f'_{cu}/f'_{co}$ .....	178
Figure 5-3: Canadian codes confinement models' performance in the prediction of $f'_{cu}/f'_{co}$ .....	179
Figure 5-4: Confinement models accuracy in the prediction of $f'_{cu}$ for: (a) the whole experimental set (b) CFRP and SFRP experimental sets.....	181
Figure 5-5: Confinement models SSE in the prediction of $f'_{cu}$ for: (a) the whole experimental set (b) CFRP and SFRP experimental sets.....	183
Figure 5-6: Empirical models' performance in the prediction $\epsilon_{cu}/\epsilon_{co}$ .....	187
Figure 5-7: Analytical models' performance in the prediction of $\epsilon_{cu}/\epsilon_{co}$ .....	188
Figure 5-8: Confinement models accuracy in $\epsilon_{cu}$ predictions for: (a) the whole experimental set (b) CFRP and SFRP experimental sets.....	189
Figure 5-9: Confinement models SSE in $\epsilon_{cu}$ predictions for: (a) the whole experimental set (b) CFRP and SFRP experimental sets .....	191
Figure 5-10: Comparison of Toutanji, 1999 Empirical model with experimental results of: (a) C37.3-CFRP (b) C42.4-CFRP (c) C37.3-SFRP (d) C42.4-SFRP.....	194
Figure 5-11: Comparison of Berthet et al., 2005 Empirical models with experimental results of: (a) C37.3-CFRP (b) C42.4-CFRP (c) C37.3-SFRP (d) C42.4-SFRP .....	196
Figure 5-12: Comparison of Spoelstra and Monti, 1999 analytical model with experimental stress-strain curve of: (a) C37.3-CFRP (b) C42.4-CFRP (c) C437.3-SFRP (d) C42.4-SFRP .....	198
Figure 5-13: Comparison of Teng et al., 2007 Analytical models with experimental results of: (a) C37.3-CFRP (b) C42.4-CFRP (c) C37.3-SFRP (d) C42.4-SFRP .....	200
Figure 5-14: Proposed models' performance in the prediction of $f'_{cu}/f'_{co}$ .....	205
Figure 5-15: Proposed models' performance in the prediction of $\epsilon_{cu}/\epsilon_{co}$ .....	206
Figure 5-16: Comparison of the proposed analytical model with experimental results for: (a) C37.3-CFRP (b) C42.4-CFRP (c) C37.3-SFRP (d) C42.4-SFRP.....	208
Figure 6-1: Failure surface of extended DP model in ABAQUS: (a) in the deviatoric plane (b) in the meridian p-t plane (ABAQUS 6.9) .....	214
Figure 6-2: Mohr-Coulomb and DP failure surfaces in the deviatoric plane, Chen (1982) .....	215

Figure 6-3: Experimental friction angle at different equivalent plastic strain: (a) $\epsilon_p=0.010$ (b) $\epsilon_p=0.020$ (c) $\epsilon_p=0.025$ (d) $\epsilon_p=0.030$ .....	217
Figure 6-4: Proposed friction angle model .....	217
Figure 6-5: Linear DP yield surface and flow direction in the meridian plane .....	221
Figure 6-6: FE modeling of FRP-confined concrete cylinders - model geometry .....	223
Figure 6-7: FE modeling of FRP-confined concrete cylinders - boundary condition and loading.....	225
Figure 6-8: Sensitivity analysis – mesh size .....	227
Figure 6-9: Mesh size sensitivity analysis results.....	228
Figure 6-10: Element type sensitivity analysis results.....	229
Figure 6-11: Poisson’s ratio sensitivity analysis results .....	230
Figure 6-12: Numerical and experimental results comparison of ultimate strength.....	232
Figure 6-13: Numerical and experimental results comparison of ultimate strain.....	232
Figure 6-14: Numerical and experimental results comparison for SFRP-confined cylinders: (a) C37.3-CFRP (b) C42.4-CFRP (c) C37.3-SFRP (d) C42.4-SFRP .....	234
Figure 6-15: Numerical and experimental results comparison for Xiao and Wu (2000) .....	235
Figure 6-16: Numerical and experimental results comparison for Lam and Teng (2004) .....	235
Figure 6-17: Numerical and experimental results comparison for Abdelrahman (2011).....	236
Figure 6-18: Effect of SFRP jacket thickness on: (a) Confinement effectiveness (b) Strain enhancement .....	238
Figure 6-19: Effect of SFRP jacket thickness on stress – strain response .....	238
Figure 6-20: Effect of FRP jacket type on: (a) Confinement effectiveness (b) Strain enhancement .....	240
Figure 6-21: Effect of FRP jacket type on the stress – strain response .....	240
Figure A-1: Failure modes of group I – C37.3-CFRP1 .....	274
Figure A-2: Failure modes of group I – C37.3-CFRP2 .....	275
Figure A-3: Failure modes of group I – C37.3-CFRP3 .....	276

Figure A-4: Failure modes of group I – C37.3-SFRP1.....	277
Figure A-5: Failure modes of group I – C37.3-SFRP2.....	278
Figure A-6: Failure modes of group I – C37.3-SFRP3.....	279
Figure A-7: Failure modes of group II – C42.4-CFRP1.....	280
Figure A-8: Failure modes of group II – C42.4-CFRP2.....	281
Figure A-9: Failure modes of group II – C42.4-CFRP3.....	282
Figure A-10: Failure modes of group II – C42.4-SFRP1.....	283
Figure A-11: Failure modes of group II – C42.4-SFRP2.....	284
Figure A-12: Failure modes of group II – C42.4-SFRP3.....	285
Figure B-1: Stress-strain curves for group I – C37.3-CFRP1.....	286
Figure B-2: Stress-strain curves for group I – C37.3-CFRP2.....	287
Figure B-3: Stress-strain curves for group I – C37.3-CFRP3.....	288
Figure B-4: Stress-strain curves for group I – C37.3-SFRP1.....	289
Figure B-5: Stress-strain curves for group I – C37.3-SFRP2.....	290
Figure B-6: Stress-strain curves for group I – C37.3-SFRP3.....	291
Figure B-7: Stress-strain curves for group II – C42.4-CFRP1.....	292
Figure B-8: Stress-strain curves for group II – C42.4-CFRP2.....	293
Figure B-9: Stress-strain curves for group II – C42.4-CFRP3.....	294
Figure B-10: Stress-strain curves for group II – C42.4-SFRP1.....	295
Figure B-11: Stress-strain curves for group II – C42.4-SFRP2.....	296
Figure B-12: Stress-strain curves for group II – C42.4-SFRP3.....	297
Figure C-1: Lateral strain profiles for group I – C37.3-CFRP1.....	298
Figure C-2: Lateral strain profiles for group I – C37.3-CFRP2.....	299
Figure C-3: Lateral strain profiles for group I – C37.3-CFRP3.....	300
Figure C-4: Lateral strain profiles for group I – C37.3-SFRP1.....	301

Figure C-5: Lateral strain profiles for group I – C37.3-SFRP2 .....	302
Figure C-6: Lateral strain profiles for group I – C37.3-SFRP3 .....	303
Figure C-7: Lateral strain profiles for group II – C42.4-CFRP1 .....	304
Figure C-8: Lateral strain profiles for group II – C42.4-CFRP2 .....	305
Figure C-9: Lateral strain profiles for group II – C42.4-CFRP3 .....	306
Figure C-10: Lateral strain profiles for group II – C42.4-SFRP1.....	307
Figure C-11: Lateral strain profiles for group II – C42.4-SFRP2.....	308
Figure C-12: Lateral strain profiles for group II – C42.4-SFRP3.....	309
Figure D-1: Axial and lateral strain at failure distribution for Group I – C37.3-CFRP1 .....	310
Figure D-2: Axial and lateral strain at failure distribution for Group I – C37.3-CFRP2 .....	311
Figure D-3: Axial and lateral strain at failure distribution for Group I – C37.3-CFRP3 .....	312
Figure D-4: Axial and lateral strain at failure distribution for Group I – C37.3-SFRP1 .....	313
Figure D-5: Axial and lateral strain at failure distribution for Group I – C37.3-SFRP2.....	314
Figure D-6: Axial and lateral strain at failure distribution for Group I – C37.3-SFRP3.....	315
Figure D-7: Axial and lateral strain at failure distribution for Group II – C42.4-CFRP1 .....	316
Figure D-8: Axial and lateral strain at failure distribution for Group II – C42.4-CFRP2 .....	317
Figure D-9: Axial and lateral strain at failure distribution for Group II – C42.4-CFRP3 .....	318
Figure D-10: Axial and lateral strain at failure distribution for Group II – C42.4-SFRP1.....	319
Figure D-11: Axial and lateral strain at failure distribution for Group II – C42.4-SFRP2.....	320
Figure D-12: Axial and lateral strain at failure distribution for Group II – C42.4-SFRP3.....	321

## List of Symbols, Abbreviations and Nomenclature

<b>Symbol</b>	<b>Definition</b>
$c$	Cohesion
$D$	Diameter of circular section
$E_2$	Slope of the linear second branch of the axial stress – axial strain curve
$E_{co}$	Elastic modulus of unconfined concrete
$E_{frp}$	Elastic modulus of FRP material
$E_{ic}$	Initial elastic modulus of the first branch of the axial stress-axial strain
$E_{il}$	Initial elastic modulus of the first branch of the axial stress-lateral strain
$E_l$	FRP jacket lateral stiffness
$E_{fc}$	Ultimate elastic modulus of the first branch of the axial stress-axial strain
$E_{fl}$	Ultimate elastic modulus of the first branch of the axial stress-lateral
$E_c^*$	Equivalent concrete axial elastic modulus of concrete
$E_l^*$	Equivalent concrete lateral elastic modulus of concrete
$E_{sec}$	Secant elastic modulus
$E_{secu}$	Secant elastic modulus at ultimate
$f_c(\varepsilon_c)$	Concrete axial stress - axial strain relation
$f_c(\varepsilon_l)$	Concrete axial stress - lateral strain relation
$f_{frp}$	Ultimate tensile strength of FRP
$f_l$	Lateral confining pressure
$f_l(\varepsilon_l)$	Lateral confining pressure - lateral strain relation
$f_{lu}$	Ultimate lateral confining pressure
$f_{lu,a}$	Actual ultimate lateral confining pressure
$f_o$	Intercept of the axial stress axis by the second linear branch of the axial stress - axial strain curve
$f'_c$	Current axial stress
$f'_{cc}$	Peak strength of confined concrete
$f'_{co}$	Peak strength of unconfined concrete
$f'_{cu}$	Ultimate strength of confined concrete
$f'_{ct}$	Axial stress at the transition point in the axial stress-axial strain curve
$i$	Variable refers to axial or lateral
$k$	Strain hardening-softening function
$k_l$	Lateral confinement effectiveness coefficient
$k_c$	Cross section shape factor

$n$	Number of FRP layers
$t_{frp}$	Thickness of FRP jacket
$\nu_c$	Poisson's ratio for unconfined concrete
$\varepsilon_c$	Current axial strain
$\varepsilon_c^p$	Axial plastic strain
$\varepsilon_l^p$	Lateral plastic strain
$\tilde{\varepsilon}_p$	Equivalent plastic strain
$\varepsilon_c(\varepsilon_l)$	Axial strain - lateral strain relation
$\varepsilon_{cc}$	Axial strain of confined concrete at peak stress, $f'_{cc}$
$\varepsilon_{co}$	Axial strain of unconfined concrete at peak stress, $f'_{co}$
$\varepsilon_{ct}$	Axial strain at the transition point in the axial stress-axial strain curve
$\varepsilon_{cu}$	Ultimate axial strain of confined concrete
$\varepsilon_{frp}$	FRP material rupture strain as provided by manufacturer or determined from flat coupon test.
$\varepsilon_{frp,a}$	Actual rupture strain of FRP jacket as measured from compression test
$\varepsilon_l$	Current lateral strain
$\varepsilon_{lu}$	Ultimate lateral strain
$\varepsilon_{lt}$	Lateral strain at the transition point in the axial stress- lateral strain curve
$\varepsilon_v$	Volumetric strain
$\theta_l$	Slope of the second branch of the axial stress – lateral strain curve
$\gamma$	Strain ratio in Berthet et al model
$\varphi$	Friction angle
$\phi_{frp}$	FRP resistance reduction factor
$\phi$	Angle of internal friction
$\rho$	Lateral stiffness ratio
$\beta$	Dilation angle
$\sigma_c$	Axial stress
$\sigma_l$	Lateral stress

### Abbreviations

<i>AFRP</i>	Aramid fibre reinforced polymer
ANOVA	Analysis of variance
BFRP	Basalt fibre reinforced polymer
<i>CDP</i>	Concrete damage plasticity

<i>CFRP</i>	Carbon fibre reinforced polymer
<i>COV</i>	Coefficient of variation
<i>df</i>	Number of degree of freedom in ANOVA Analysis
<i>DIC</i>	Digital image correlation
<i>DP</i>	Drucker-Prager
<i>FE</i>	Finite element
<i>FRP</i>	Fibre reinforced polymer
<i>GFRP</i>	Glass fibre reinforced polymer
<i>LSC</i>	Linear strain converter
<i>MC</i>	Mohr-Coulomb
<i>MS</i>	Mean of the sum of the squared deviation of the mean, ANOVA analysis
<i>SD</i>	Standard deviation
<i>SDFV</i>	Solution dependent field variable
<i>SFRP</i>	Steel fibre reinforced polymer
<i>SG</i>	Strain gauge
<i>SS</i>	Sum of the squared deviation from the mean in ANOVA analysis
<i>SSE</i>	Sum of squared errors

## Chapter One: **Introduction**

### **1.1 Background**

The use of Fibre Reinforced Polymer (FRP) composites for strengthening and/or retrofitting concrete structural members dates back to the late 1980s in Europe and Japan, followed rapidly by research and applications in the United States and Canada (Bank (2006)). Initial research, particularly in Europe, focused on flexural strengthening of structural members. However, the urgent need to retrofit deficient civil infrastructure, in particular for earthquake-induced seismic loading, directed much of the research efforts in Japan and United States toward strengthening concrete columns using FRP composite fabrics and sheets to enhance their axial load-carrying capacity and axial and flexural deformability.

The FRP confinement technique offers numerous advantages over conventional concrete and steel jacketing which were the accepted technologies to strengthen and repair structural concrete columns. Concrete jacketing requires formwork and results in a significant increase in the weight and cross-section of the column. Steel jacketing is labour intensive, costly and susceptible to corrosion. Fibre wrapping, on the other hand, depending on the type of fibre, offers high strength to weight and high stiffness to weight ratio, high durability performance and outstanding corrosion resistance, fatigue damage resistance and flexible and efficient installation techniques (ISIS Education Module 2 (2006)).

As a result, the FRP confinement technique has received considerable attention in the last few decades. Experimental investigations and theoretical developments have been carried out in parallel. The majority of existing research literature mostly focuses on FRP composite materials commonly encountered in strengthening and retrofitting applications, namely, unidirectional carbon FRP (CFRP), glass FRP (GFRP) or aramid FRP (AFRP). Also, basalt FRP (BFRP), first

developed in the former Soviet Union during the cold war, has been recently utilised in concrete columns retrofitting applications (Fahmy and Wu (2010)). Most recently, steel FRP (SFRP) composite material has been introduced as an alternative material to the more conventional CFRP, GFRP and AFRP for concrete column strengthening and retrofitting applications (Mashrik (2011); Abdelrahman (2011); Napoli and Realfonzo (2013)). This new material possesses many advantages such as cost effectiveness, relatively inherent ductility of the steel cords that make up the SFRP reinforcing fibres (Minnaugh (2006)) and superior performance, when compared to CFRP, even under severe environmental exposure (Mashrik (2011); Abdelrahman (2011), Abdelrahman and El-Hacha (2011)). In view of these many advantages, the use of this new material in concrete column strengthening and retrofitting applications is worth investigating further.

## **1.2 Objectives**

Considering the very limited research knowledge pertaining the SFRP composite material; the objectives of this research are threefold; to study the compressive behaviour of SFRP-confined concrete under monotonic concentric uniaxial compressive loading; to develop an analytical model that accurately predicts the ultimate strength, ultimate strain and stress-strain behaviour of the FRP composite system; and to identify the concrete material parameters for the Drucker-Prager (DP) plasticity type model for immediate use in Finite Element (FE) modeling of the FRP-confined concrete system. In particular, the research work presented in this thesis has the following eight specific objectives:

- Conduct an extensive experimental program on small-scale normal strength concrete cylinders confined with CFRP and SFRP sheets and subjected to monotonic concentric uniaxial loading. The main experimental parameters are the unconfined concrete

compressive strength, thickness and type of FRP wraps. Once experimental results are obtained, the single factor analysis of variance (ANOVA) test is performed to evaluate the significance of the effect of parameters under investigation on the ultimate strength of confined cylinders and ensure that different cylinders' groups within the same category are statistically different before results are further analysed;

- Obtain a solid understanding of the compressive behaviour of SFRP-confined concrete with a particular focus on the failure mode, stress-strain behaviour, ultimate axial strength, ultimate axial and lateral strain, ductility and dilation behaviour. Furthermore, the compressive behaviour of SFRP-confined concrete is compared to that of CFRP-confined concrete;
- Determine the strain efficiency of the SFRP and CFRP wraps from careful investigation of the axial and lateral strain variation over the surface of the SFRP-and CFRP-confined concrete cylinders using the Digital Image Correlation (DIC) technique. Parameters that might affect the FRP strain efficiency such as the type and thickness of FRP jacket and the unconfined concrete compressive strength are also investigated;
- Carry out performance assessment for nine of the foremost existing empirical/analytical confinement models in addition to two confinement models adopted by Canadian design codes by comparing the ultimate axial strength, ultimate axial strain and the stress-strain behaviour obtained from the herein experimental program against the theoretical values predicted by these selected empirical/analytical models;
- Develop a new analytical predictive model that is capable of accurately predicting the ultimate conditions and the entire stress-strain response of concrete confined by FRP sheets;

- Develop a FE model for predicting the axial compressive behaviour of FRP-confined concrete. Mathematical models for confined concrete material's parameters in the framework of a DP plasticity type model, namely the friction angle, the hardening/softening rule and the dilation angle, are proposed; and
- Validate the proposed concrete constitutive model and the FE model by performing a comparison between the numerical predictions from the FE model against the experimental results from the tests described herein and three sets of independent experimental results published by different researchers.
- Once the FE model is validated with experimental results, a parametric study is performed by studying the effect of varying the thickness and type of FRP wrap on the strength and deformability of FRP-confined concrete.

### **1.3 Research Significance**

The majority of the research knowledge currently available in the literature is pertinent to the behaviour of concrete confined with CFRP, GFRP and ARFP sheets. Limited knowledge pertinent to the relatively newly-introduced SFRP sheets exists. Therefore, this research will extend the literature database of SFRP-confined concrete by performing an experimental investigation on unreinforced small-scale SFRP-confined concrete subjected to concentric monotonic uniaxial compression. Furthermore, in this research, the same test matrix fabricated using SFRP sheets was duplicated using CFRP sheets. This experimental program on unreinforced small-scale CFRP-confined concrete provides an important addition to the existing experimental database related to CFRP and allows for performance comparison between SFRP- and CFRP-confined concrete cylinders.

Preceding research on FRP-confined concrete mostly focused on the axial strength and deformability enhancement due to FRP confinement. However, little attention has been paid to the axial and lateral strain variation over the surface of FRP-confined concrete. The current lack of knowledge of the magnitude of the axial strain variation, and more importantly, the lateral strain variation over the full surface of FRP-confined concrete shed some doubt on the capability of localized discrete strain gauges, used in the majority of experimental programs, to capture the true FRP strain at failure accurately. The result has caused researchers to build a high margin of conservatism in the FRP strain efficiencies proposed for design purposes. The current research implements the DIC technique to quantify the axial and lateral strain variation over the full surface of the FRP-confined concrete. Numerous parameters influencing the strain variation such as FRP type, FRP wrap thickness and unconfined concrete strength are also investigated. This resulting knowledge of strain variation over the surface of the FRP confined concrete cylinder will assist in specifying a more reliable and accurate lateral strain efficiencies for different FRP composite systems for design purposes and will eventually allow for more efficient use of FRP wraps in strengthening and retrofitting applications.

Various empirical and analytical models have been developed in the last two decades to predict the ultimate conditions and the stress-strain behaviour of FRP-confined concrete. However, the accuracy of these models depends significantly on the size and reliability of the test database and the range of parameters used in the model calibration for the former and on the active-confinement base model and the dilation relationship used in the model development for the latter. The concern is that the ultimate axial strain and the stress-strain behaviour are still poorly predicted by the majority of existing confinement models, Lorenzis and Tepfers (2003); Teng and Lam (2004), Bisby, Dent and Green (2005). This research critically reviews some of the

foremost existing empirical and analytical confinement models and develops a new analytical model that fits quite well with the experimental results obtained from the experimental investigation described herein and can accurately predict the characteristic compressive behaviour of FRP-confined concrete.

Numerical modeling using the FE technique satisfies equilibrium and displacement compatibility requirements (at the nodal level) and accounts for the constitutive relationships between all the materials involved. Hence, composite systems such as the FRP-confined concrete and the interaction between the different system components are modeled in a more rational way using the FE technique compared to the empirical and analytical modeling approaches. However, due to the complex and highly nonlinear behaviour of confined concrete, an accurate constitutive model for concrete for direct use in the FE modeling has yet to be developed. This research proposes a new constitutive law for concrete in the framework of plasticity theory. The proposed constitutive law is implemented in the FE model. The proposed FE model, in the author's opinion, captures accurately all the characteristic stress-strain and dilation behaviours of both CFRP-and SFRP-confined concrete cylinders.

#### **1.4 Scope of Work**

The research methodology adopted combined experimental investigation with theoretical development. The experimental program of the present research was aimed at studying the behaviour of FRP-confined concrete cylinders under concentric monotonic uniaxial compressive loading. The main parameters in this investigation are the unconfined specified (targeted) concrete compressive strength (35 and 45 MPa), the type of FRP (SFRP and CFRP) and the number of FRP layers (1, 2 and 3). The DIC technique was implemented along with conventional foil strain gauges and Linear Strain Conversion (LSC) measuring devices to

quantify the axial and lateral strain variation over the surface of the FRP-confined concrete cylinders.

The experimental program was divided into two groups depending on the targeted concrete unconfined compressive strength, each group consisting of twenty one (21) circular unreinforced small-scale (150 mm diameter  $\times$  300 mm high) concrete cylinders that included three (3) unwrapped control cylinders, nine (9) concrete cylinders wrapped with one, two and three layers of CFRP sheets and nine (9) concrete cylinders wrapped with one, two and three layers of SFRP sheets. For each confinement configuration, three (3) nominally identical cylinders were fabricated and tested for comparison purposes. This experimental database serves as a benchmark for verification purposes of the proposed analytical model and forms the database for the numerical model development.

The theoretical development presented in this research includes both analytical and numerical modelling of FRP-confined concrete. For the development of the new analytical model, several existing empirical and analytical models theoretical predictions of ultimate stress, ultimate strain and stress-strain response are compared against the herein experimental results. One model is then selected for refinement purposes. The refinement includes the use of a different model to calculate the peak stress at any selected active confining pressure. The modified model, through comparison with the present experimental database, exhibits superior performance over all the reviewed confinement models in predicting the ultimate strength, ultimate strain and the entire stress-strain behaviour of SFRP- and CFRP-confined concrete cylinder.

The numerical modeling includes the development of three-dimensional (3D) FE model using the general purposes FE software ABAQUS. Since the accuracy of any FE model mainly depends on the accuracy of the constitutive law of its constituents, particular attention has been

paid to the development of a constitutive law of confined concrete within the framework of the Drucker-Prager (DP) plasticity model. The DP plasticity model's three main parameters namely, friction angle, hardening/softening rule and dilation angles, are basically extracted from the current experimental results and plotted as functions of the most influencing factors. The closest mathematical models that best represent each of these parameters are utilised and the coefficients are then determined by regression analysis using the least square method. The proposed constitutive law is then implemented in a 3D FE model and verified against the current experimental database and three sets of independent experimental results available in the literature.

### **1.5 Organization of the Thesis**

The experimental and theoretical investigations are presented in this thesis in seven chapters, details of which are summarized below.

Chapter two reviews some of the preceding research on FRP-confined concrete with a particular focus on experimental and theoretical investigations conducted on SFRP-confined concrete. The chapter starts with a brief introduction to the FRP composite system and its constituents. The mechanical behaviour of the constituents of FRP composites as well as the mechanism of FRP confinement is discussed next. The most related preceding experimental research conducted on FRP-confined concrete are briefly reviewed, followed by the state-of-the-art empirical and analytical models for predicting the behaviour of FRP-confined concrete. Selected FE models proposed for FRP-confined concrete are briefly reviewed toward the end of the chapter.

Chapter three presents the experimental program conducted on unreinforced small-scale concrete cylinders confined with CFRP and SFRP and subjected to concentric monotonic uniaxial compression. A brief overview of the test program is first given. Details of the test specimens,

material properties and the main experimental parameters examined which include the concrete strength, type of FRP and numbers of FRP layers are then presented. The procedures for the preparation of the specimen are then described, including the formation of the mould for casting concrete and the wet-layup process for wrapping the specimens. The test set-up and test instrumentation are also introduced.

Chapter four presents the experimental results and observations, in addition to general discussion with the focus on the failure mode, ultimate axial stress, ultimate axial and lateral strain, stress-strain behaviour, ductility and dilation behaviour of SFRP confined concrete. The compressive behaviour of SFRP-confined concrete and CFRP-confined concrete are then compared so that the significant parameters that affect the behaviour of FRP-confined concrete are well-identified.

The ANOVA test is also performed to study the significance of different parameters (concrete strength, type of FRP, number of layers) on the ultimate strength of concrete cylinders.

Chapter five presents a detailed performance assessment of eleven selected confinement models available in the literature. Seven empirical models, two analytical models and two confinement models from Canadian design codes are thoroughly reviewed and compared to each other's and against the current experimental test results to assess each model's accuracy in predicting the ultimate axial strength, ultimate axial strain and the entire stress-strain response. Based on the conclusions drawn from this assessment, a new analytical model is proposed and then verified against the current experimental results.

In Chapter six, a constitutive model for confined concrete based on DP plasticity theory is presented. The chapter starts with an overview of concrete plasticity. The DP type plasticity model with a particular focus on the linear extended DP type plasticity model built in the general purpose FE software ABAQUS is reviewed. The proposed constitutive concrete model is then

presented in which the three main components of concrete DP type plasticity model, namely, the friction angle, the hardening/softening rule and the dilation angle are derived based on a regression analysis of the experimental results obtained herein. Verification of the proposed FE model against the current test database and three sets of independent experimental results by different researchers that are available in the literature is also presented.

The thesis closes with Chapter seven where major conclusions drawn from previous chapters are reviewed and major findings from the current research are highlighted. Areas that need further investigation are also summarized.

## **1.6 Summary**

This chapter presented the background of the use of the FRP composite in strengthening and/or retrofitting of deficient and/or deteriorated concrete columns. The main advantages of this strengthening system over the more conventional strengthening techniques such as steel and concrete jacketing were briefly reviewed. The research significance, objectives and the scope of the current research work were introduced. The layout of the thesis content was described towards the end of this chapter.

The next chapter presents an extensive literature review of FRP-confined concrete including experimental investigations in addition to theoretical developments including empirical, analytical and numerical modeling of FRP-confined concrete. The state-of-the-art knowledge pertinent to the SFRP-confined concrete is focused on throughout the course of the literature review presented in the next chapter.

## Chapter Two: **Literature Review**

### **2.1 Introduction**

FRP-confined concrete under axial loading has received a lot of research attention over the last few decades. This chapter aims to provide a brief review of the state-of-the-art knowledge on the behaviour of normal strength concrete cylinders confined with FRP sheets and subjected to concentric axial loading. The FRP composite materials and various types of fibre reinforcements and resin matrices are first introduced followed by a general review of the mechanical behaviours of the FRP composites. The mechanics of FRP confinement is discussed next. Preceding research on FRP-confined concrete including experimental investigations and theoretical developments are reviewed toward the end of the chapter.

### **2.2 FRP Composite Materials**

FRP composite material is a manufactured material consisting, on the microscopic scale, of two or more distinct phases of constituent materials. The resulting composite material possesses unique mechanical properties and exhibits superior performance characteristics that cannot be achieved by any of the constituent materials alone, Huang and Zhou (2011). The majority of the composite material consists of two-phase constituents: the first is the reinforcement phase, and the second is the continuous phase, in which the reinforcement phase is embedded. The continuous phase is commonly referred to as the matrix. The reinforcement phase can be in the form of particles of various sizes, short fibres or whiskers, or continuous fibres. Two-phase composite materials are classified, depending on the type, geometry and orientation of the reinforcement phase, into three categories, particulate composites, discontinuous or short fibre composites and continuous fibre composites, as illustrated in Figure 2-1.

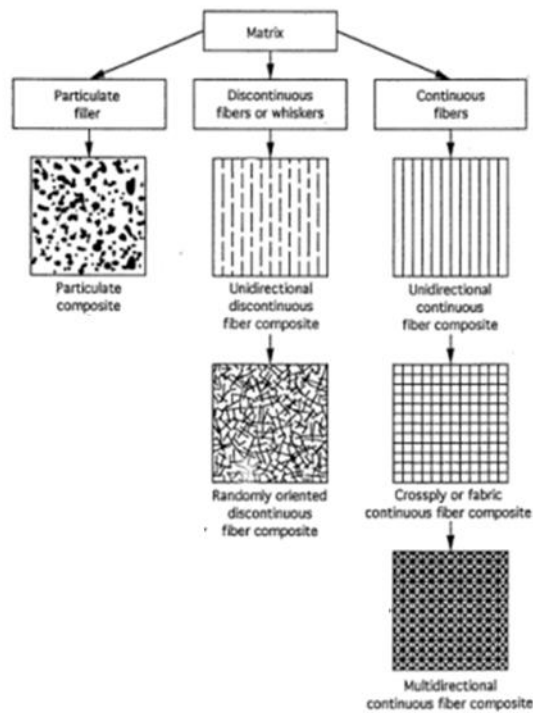


**Figure 2-1: Classification of two-phase composite materials, Daniel and Ishai (1994)**

Continuous fibre composites are in common use in structural engineering applications. The continuous fibres can be all parallel (unidirectional continuous fibre composite), can be oriented at right angles to each other (woven fabric continuous fibre composite) or can be oriented along several directions (multidirectional continuous fibre composite), Daniel and Ishai (1994). A single layer of unidirectional continuous fibre composite is commonly referred to as a unidirectional lamina or a ply while a stack of two or more of unidirectional lamina at various orientations is commonly referred to as laminate. Figure 2-2 shows a unidirectional lamina and multidirectional laminate.

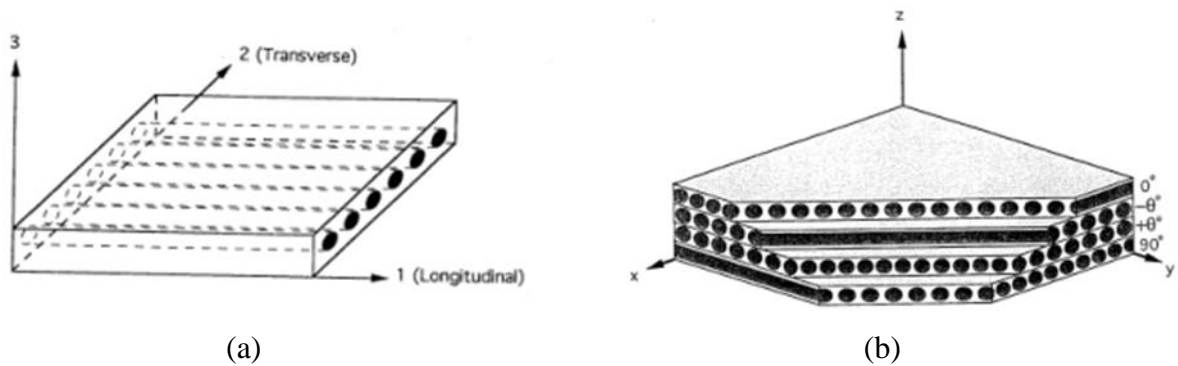


**Figure 2-2: FRP composites: (a) Unidirectional lamina (b) Multidirectional laminate, Daniel and Ishai (1994)**

### **2.2.1 Reinforcing Fibres**

A single continuous fibre or a filament is characterized by its high tensile strength and its extremely small diameter, typically ranging from 5 - 20  $\mu\text{m}$ , Mazumdar (2002). Reinforcing fibres consist of thousands of these indefinitely long individual filaments. Primary desirable characteristics of reinforcing fibres are high strength, high stiffness and relatively low density. Reinforcing fibres provide the strength and the stiffness to the FRP composite material. The fibres in most common use in structural engineering applications are glass, carbon, and aramid. Fibres made from basalt rock have been also recently manufactured, Fahmy and Wu (2010). Glass, carbon, aramid, and basalt reinforcing fibres along with the newly introduced steel fibres are discussed next.

#### **2.2.1.1 Glass Fibres**

Glass fibres are used in a wide variety of structural engineering products like reinforcing bars for concrete, strengthening fabrics and structural profile shapes. Glass filament has a diameter ranging from 3 - 24  $\mu\text{m}$  and has a distinctive bright white colour and is considered as an isotropic material. Bidirectional glass fabrics are shown in Figure 2-3.

There are various grades of glass fibres, manufactured for different applications; C-glass grade is commonly used for corrosion resistant application, E-glass is used often for structural engineering products due to its high electrical resistivity; and S-glass is used to produce high strength products used widely in the aerospace industry. Typical elastic properties of common grades of glass fibres are given in Table 2-1.



**Figure 2-3: Bidirectional glass fabric, World-Trades.com (2014)**

**Table 2-1: Typical mechanical properties of common grades of glass fibres, Bank (2006)**

Grade of Glass Fibre	Tensile Modulus (GPa)	Tensile Strength (MPa)	Max. Elongation (%)
E	72.5	3400	2.5
A	73	2760	2.5
C	74	2350	2.5
S	88	4600	3.0

Glass fibres have a relatively low tensile modulus and are sensitive to moisture, hence, requiring protection by the resin system. They are also sensitive to abrasion during handling; have low fatigue resistance and are susceptible to creep rupture. On the other hand, the glass fibres have high tensile strength; high chemical resistance; excellent thermal and electrical insulating properties and are the least expensive among the reinforcing fibres.

### 2.2.1.2 Carbon Fibres

Carbon fibres have diameters ranging from 5 - 10  $\mu\text{m}$ , have a charcoal-black colour and are considered to be transversely isotropic. These are manufactured for structural engineering applications in a variety of forms; sheets and fabrics; strips and pre-stressing tendons.

Bidirectional carbon fabric is shown in Figure 2-4.

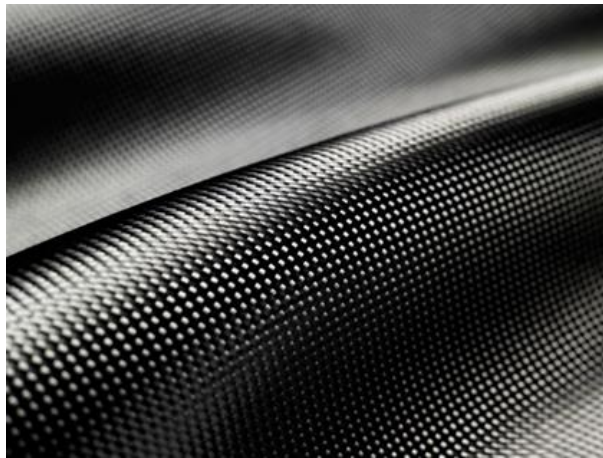


**Figure 2-4: Bidirectional carbon fabric, World-Trades.com (2014)**

Common grades of carbon fibres include standard modulus, intermediate modulus, high strength and ultrahigh modulus. Typical elastic properties for common grades of carbon fibres are given in Table 2-2.

**Table 2-2: Typical elastic properties of common grades of carbon fibres, Bank (2006)**

Grade of Carbon Fibre	Tensile Modulus (GPa)	Tensile Strength (MPa)	Max. Elongation (%)
Standard	250	3700	1.2
High strength	250	4800	1.4
High modulus	500	3000	0.5
Ultra-high modulus	800	2400	0.2

Carbon fibres offer high tensile strength to weight ratio, high elastic modulus; excellent dimensional stability due to their low thermal expansion coefficient and are very durable. They are, however, expensive, thermally and electrically conductive and measures must be taken to

prevent their contact with metallic materials as research has suggested that this can lead to degradation of the polymer resin and to corrosion of the metallic material.

### 2.2.1.3 Aramid Fibres

Aramid fibres offer the highest tensile strength to weight ratio among reinforcing fibres, they provide good impact strength and are dimensionally stable. However, their relatively high cost, difficulty during cutting and machining, high moisture absorption, loss of strength and modulus at high temperatures and low compressive strength have limited their use in structural engineering applications. They have yellow colour and are similar in cost to carbon fibres.

Aramid fibre is shown in Figure 2-5.

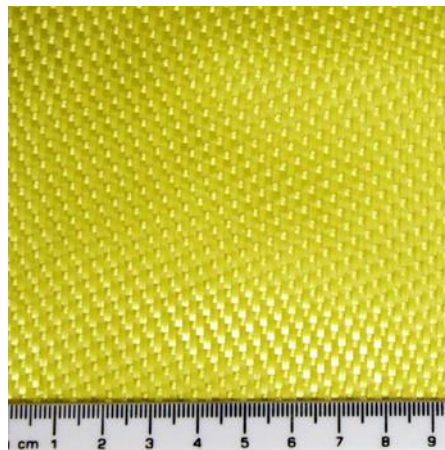


**Figure 2-5: Aramid Fibre, World-Trades.com (2014)**

### 2.2.1.4 Basalt Fibres

Basalt fibres are produced from basalt, an igneous rock formed by the rapid cooling of basaltic lava. The fibres are manufactured by melting the rock at 1300 °C-1700 °C and then extruding it through small nozzles to produce continuous basalt fibres. Basalt fibres have a similar chemical composition to glass fibres but have higher stiffness and strength, have 10 times better electrical

insulating properties than glass and unlike most glass fibres are highly resistant to alkaline, acidic and salt attack, Parnas et al. (2007).

Compared to carbon and aramid, basalt fibres are used in a wider temperature range  $-269^{\circ}\text{C}$ - $700^{\circ}\text{C}$ , have higher corrosion resistance, higher compression and shear strength and better environmental adaptability, Fahmy and Wu (2010). The price of basalt is higher than those of E-glass but less than S-glass, aramid or carbon fibres. Typical elastic properties for basalt fibres are given in Table 2-3

**Table 2-3: Typical elastic properties of basalt fibres, Parnas et al. (2007)**

Tensile Modulus (GPa)	Tensile Strength (MPa)	Max. Elongation (%)	Compression Strength (MPa)
89	4840	3.15	3792

Basalt fibre colour varies from brown to dull green depending on the ferrous content. Typical commercially available basalt fibres are shown in Figure 2-6.



**Figure 2-6: Multi-directional basalt fabric, GBF.com (2015)**

#### 2.2.1.5 Steel Fibres

Steel fibres have introduced recently for use in FRP strengthening fabrics as a cost-effective alternative to carbon and glass fibres, Abdelrahman (2011). Composites made from steel fibres

are 70% thinner and 25% lighter than composites made from glass fibres. Steel fibres are priced like glass fibres yet perform superior to carbon fibres, HARDWIRE (2014).

Steel fibres are ultra-high strength carbon steel filaments, coated with a micro-line brass or galvanized coating. Individual steel filaments range from 2 to 50 wires twisted together into cords. The twist angle is controlled based on the type of application; highly twisted cords are manufactured for optimum tensile strain and better ductility, slightly twisted cords allow for better resin penetration, hence better bonding, while straight cords with a twisted over wrap provide balanced tensile and compressive behaviour, HARDWIRE (2014). Typical commercially available steel wire cords are shown in Figure 2-7.

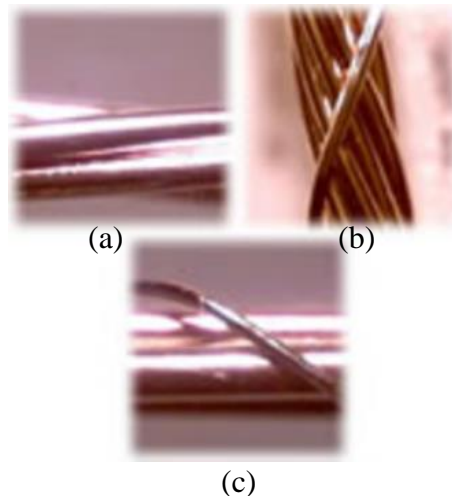


**Figure 2-7: Steel wire cords: (a) 3×2 cords (b) 12X wire cord (c) 3SX wire cord, HARDWIRE (2014)**

### ***2.2.2 Matrix Materials***

The matrix material in the composite binds the fibres together and transfers the load to the reinforcing fibres by adhesion and/or friction. The matrix material, which has comparatively lower mechanical properties than reinforcing fibres, provides rigidity and protection against mechanical damage and chemical and environmental exposure.

The matrix phase of FRP composite materials can be made of polymer, metal, or ceramic, as shown in Figure 2-8.

Polymer composite materials are commonly used in structural engineering applications rather than metal or ceramic matrix, therefore, only polymer matrix is reviewed here.

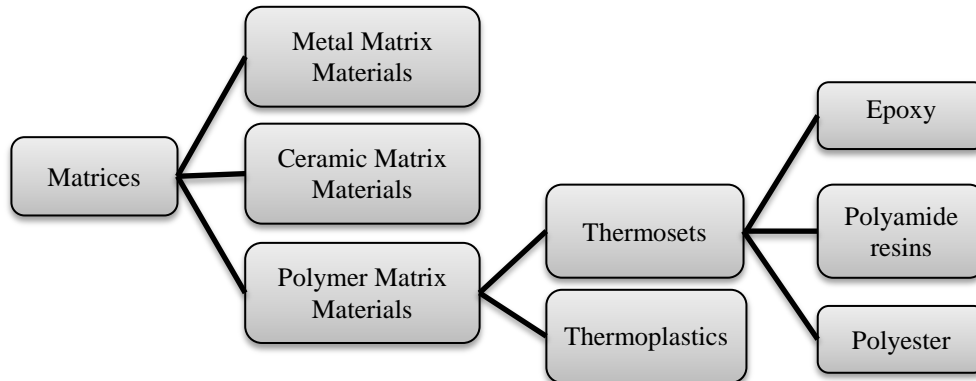


**Figure 2-8: Classification of matrix materials, Gunaslan et al. (2014)**

### 2.2.2.1 Polymer Matrix Materials

Polymer matrix material is composed of long-chain molecules made from many smaller and repeating units called monomers. Polymers can be classified, according to the molecular arrangement, into thermoplastics and thermoset polymers. A schematic representation of the molecular arrangement in thermoplastic and thermoset polymers is illustrated in Figure 2-9.

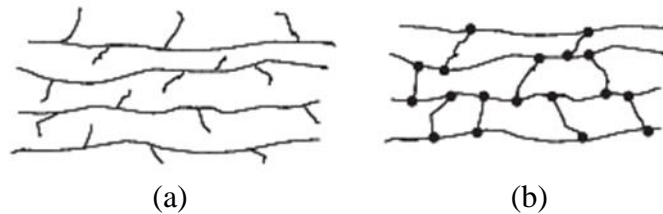


**Figure 2-9: Schematic representation of molecule arrangement: (a) Thermoplastic (b) Thermoset, GangaRao et al. (2007)**

#### 2.2.2.1.1 Thermoplastic Polymers

Thermoplastic molecules consist of linear molecules without any chemical cross-linking between them; hence, they are flexible and re-formable by heating and cooling. Thermoplastic polymers are more ductile, tougher and have lower stiffness and strength than thermoset polymers.

#### 2.2.2.1.2 Thermoset Polymers

Thermoset polymers harden through a series of chemical reactions called curing. At the end of curing process, they formed a tightly cross-linking three-dimensional network of polymer chains. Hence, as opposed to thermoplastic polymers, they are brittle and cannot be re-melted or reshaped. They also offer higher thermal and dimensional stability, better rigidity and higher electrical, chemical and solvent resistance than thermoplastic polymers.

Thermoset polymers are used more frequently than thermoplastic polymers in producing composites. This is mainly attributed to their ability to cure at room temperature, better bonding with reinforcing fibres and good creep resistance, GangaRao et al. (2007). The most commonly used thermoset polymers in concrete columns retrofitting applications are epoxy resins, which are reviewed next.

##### 2.2.2.1.2.1 Epoxy

Epoxy resins are frequently used in wet-lay-up application due to their numerous advantages over other types of resins; they cure well at room temperature, exhibit low shrinkage during curing, have excellent resistance to chemicals and solvents, and they adhere perfectly to a wide range of fibres and surfaces. However, their major drawbacks include relatively high cost, difficulty during handling due to their high viscosity, and long cure time, GangaRao et al. (2007).

### **2.3 Mechanical Behaviour of FRP Composites**

The mechanical behaviour of FRP composite materials can be viewed from a micro-mechanical or macro-mechanical perspective. In micro-mechanics, the composite material is analysed at a microscopic level, i.e., the composite material constituent phases are considered separately and the mechanical behaviour is predicted based on the volume fractions and properties of the constituents and their interaction. Micro-mechanics can also predict the stress and strain state in the constituent phases as well as the local failure mechanism such as fibre failure (tensile, compressive, shear), matrix failure (tensile, buckling, splitting) or interface failure (deboning), Daniel and Ishai (1994). In macro-mechanics, on the other hand, the composite material is considered as one homogenous material with its own average stiffness and strength properties. Failure criteria are expressed in terms of an average ultimate stress or ultimate strain without reference to any particular local failure mechanism. At the laminate level, the overall behaviour of the laminate can be determined as a function of the individual lamina properties and their stacking sequence using lamination theory.

The mechanical behaviour of FRP composites generally depends on a number of factors such as the mechanical properties and the volume fractions of the constituents; the orientation of the fibres in the matrix, the properties of the fibre-matrix interfacial bond and the manufacturing method (ISIS Education Module 2, 2006).

As previously mentioned in Section 2.2, the FRP composites mostly encountered in structural engineering application are unidirectional. Hence, only the mechanical behaviours of unidirectional composites are discussed further.

The stress-strain behaviour of unidirectional composites, especially in the direction of the fibres, is predominantly linearly elastic. The mechanical properties of unidirectional composites, in the

fibres direction, are usually dominated by fibre properties, while the mechanical properties, perpendicular to fibre direction, are usually dominated by matrix properties, volume fraction of the composite constituents and the adhesion between the fibre-matrix interfaces.

The ultimate tensile strength of unidirectional composites, in the fibre direction, depends significantly on the failure tensile strain and the volume fraction of the composite constituents, and two failure behaviours may be encountered: fibre dominated failure or matrix dominated failure as shown in Figure 2-10.

If the failure tensile strain of the fibre is lower than that of the matrix and the fibre volume fraction is large (more than 10%) then the composite fails when ultimate tensile strain of the fibres is reached. On the other hand, if the fibre volume fraction is small (less than 10%) then the fibre initial fracture is not critical and load is transferred from fibre to matrix which continues to carry the load until their failure strain is reached.

On the other hand, if the failure tensile strain of the matrix is lower than that of the fibre, and the fibre volume fraction is small, then the composite fails when ultimate tensile strain of the matrix is reached. However, if the fibre volume fraction is large, then matrix failure is not critical as the majority of the load is transferred to the fibres which continue to carry the load until their failure strain is reached.

The ultimate compressive strength of unidirectional composites, in the fibre direction, is typically 50-80% of respective tensile strength, ISIS Education Module 2 (2006).

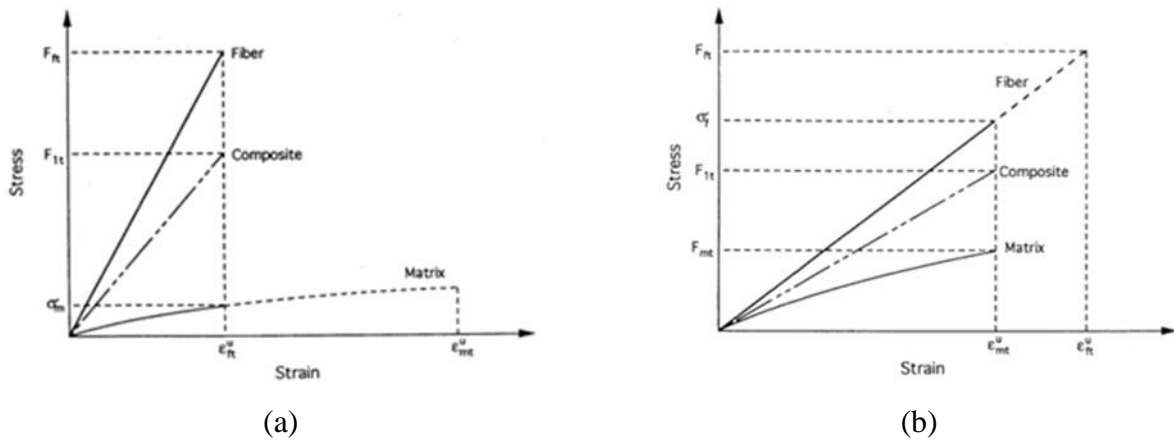


**Figure 2-10: Stress-strain curves for FRP unidirectional composites: (a) Tensile strength dominated by fibres (b) Tensile strength dominated by matrix, Daniel and Ishai (1994)**

## 2.4 Mechanics of FRP-Confined Concrete

The unique performance characteristics of FRP-confined circular concrete sections can be identified as follows:

- FRP jacket exerts a lateral confinement on concrete core that is passive in nature, i.e., the FRP jacket is only activated after the concrete strength is reached and the concrete core starts to dilate in the lateral direction;
- Due to the linear elastic behaviour of the FRP, as axial load on the concrete increases, the FRP jacket exerts a continuously increasing confining pressure on the concrete core that is proportional to the concrete core lateral dilation, as opposed to the active confinement which exerts a constant confining pressure or the steel confinement which exerts a constant confining pressure after yielding;
- In FRP-confined circular concrete sections, the FRP lateral confining pressure,  $f_l$ , is assumed uniformly distributed around the circumferences of the circular section, as illustrated in Figure 2-11. Lateral confining pressure at ultimate,  $f_{lu}$ , can then be

calculated, by satisfying equilibrium and displacement compatibility between FRP jacket and the concrete core, using Equation 2-1.

$$f_{lu} = \frac{2t_{frp}E_{frp}\varepsilon_{frp}}{D} \quad \text{Equation 2-1}$$

where  $t_{frp}$  is the thickness,  $E_{frp}$  is the elastic modulus and  $\varepsilon_{frp}$  is the rupture strain of FRP jacket,  $D$  is the diameter of the cylinder.

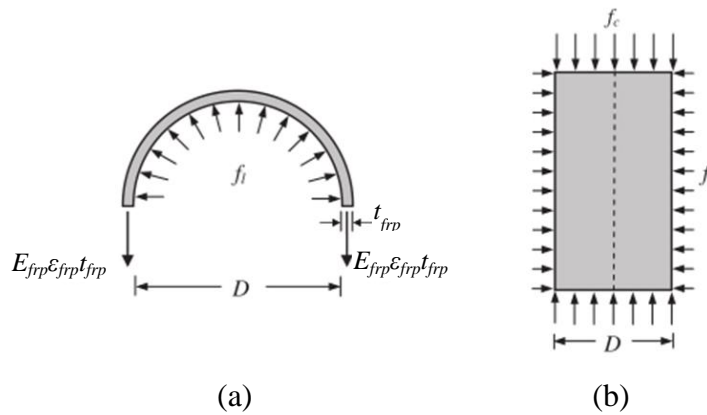


**Figure 2-11: FRP confinement mechanism: (a) FRP jacket (b) Concrete core, Ozbakkaloglu et al. (2013)**

- The volumetric strain depends mainly on the lateral stiffness of the FRP jacket; while concrete confined by flexible FRP jacket exhibits continuously increasing volume dilation after volume compaction, concrete confined with stiffer FRP jacket exhibits continuous volume compaction.

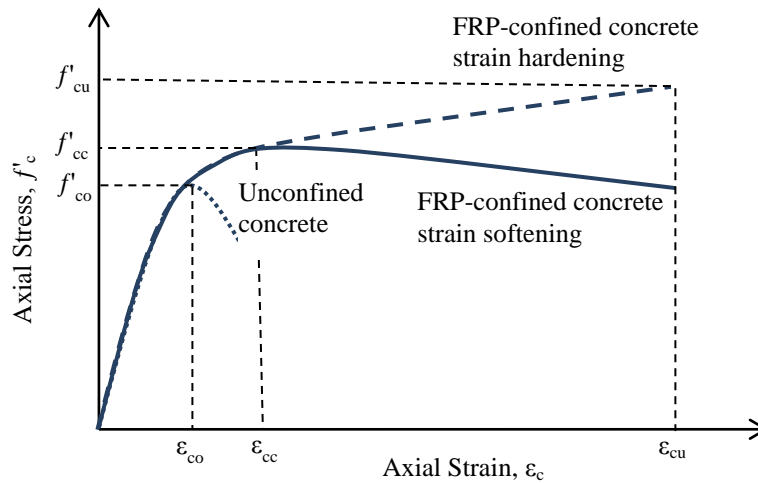


**Figure 2-12: Typical stress-strain curve of FRP-confined concrete, Ozbakkaloglu et al. (2013)**

## 2.5 Preceding Research and State-of-the-Art of FRP-Confined Concrete

The concept of concrete confinement for performance enhancement was originally established in 1927 by the pioneering work of Richart et al. (1928) on concrete subjected to triaxial stress state. Since then, the concept has been widely investigated both experimentally and theoretically, and has been utilized in the form of spiral and circular reinforcement, concrete and steel jacketing, and, relatively recently, FRP jacketing. Steel-confined concrete behaves differently from FRP-confined concrete, Mirmiran and Shahawy (1996), Samaan et al. 1998, Saafi et al. 1999 and Spoelstra and Monti (1999) and hence, will not be discussed further. On the other hand, the unique characteristics of FRP-confined concrete and the confinement mechanism for all types of FRP jackets are still the same. It is imperative then to review the milestones of previous experimental research and modeling development performed on FRP-confined concrete to establish solid ground for the current investigation on the SFRP-confined concrete and to provide more insight on the subsequent experimental and theoretical findings of the current research.

### ***2.5.1 Experimental Programs***

Significant experimental research efforts have been directed towards investigating the compressive behaviour of small-scale unreinforced concrete cylinders confined with FRP spirals: Ahmad et al. (1991), Saadatmanesh et al. (1994) and Nanni and Bradford (1995), with FRP tubes: Mirmiran et al. (1998), Saafi et al. (1999), Tegola and Manni (1999), and Fam and Rizkalla (2001), or with FRP wraps: Demers and Neale (1994), Howie and Karbhari (1994), Picher et al. (1996), Soudki and Green (1996), Miyauchi et al. (1997), Karbhari and Gao (1997), Watanaba et al. (1997), Toutanji (1999), Xiao and Wu (2000), Zhang et al. (2000), Rochette and labossiere (2000), Aire et al. (2001), Karabinis and Rousakis (2002), Lam and Teng (2004), Li (2006), Teng et al. (2007b) and Jiang and Teng (2007) and Youssef et al. (2007). Small-scale unreinforced concrete prisms of square and rectangular sections have been also experimentally investigated: Mirmiran et al. (1998), Pessiki et al. (2001), Parvin and wang (2001), Shehata et al. (2002), Masia et al. (2004), Wang et al. (2008) and Benzaid et al. (2008). Limited numbers of experimental tests were carried out on small-scale reinforced concrete specimens: Hosotani et al. (1997), Harries et al. (1998), Demers and Neale (1999), and Matthys et al. (1999). FRP-confined high strength concrete has been also investigated: Harmon and Slattery (1992), Miyauchi et al. (1999).

Experimental investigations have been also conducted on large scale unreinforced concrete columns of circular sections: Demers and Neale (1999), Purba and Mufti (1999), Pessiki et al. (2001), Lin and Liao (2004), Esfahani and Kianoush (2005) and Ilki et al (2006), of square and rectangular sections: Restrepol and De Vino (1996), Rochette and labossiere (2000), Wang and Restrepo (2001), Pessiki et al. (2001), Chun and Park (2002), Pulido et al. (2002), Tan (2002), Campione and Miragia (2003), Chaallal et al. (2003), Lam and Teng (2003d), Maalej et al.

(2003), Ilki et al. (2004), Esfahani and Kianoush (2005), Rocca et al. (2006), Campione (2006), Rousakis et al. (2007) and Kumutha et al. (2007), and of elliptical sections: Pan et al. (2002), and Teng and Lam (2002). Only limited experimental investigations have been carried out on large scale reinforced concrete columns: Demers (1994), Feng et al. (2002), Pessiki et al. (2001), Tsai and Lin (2002) and Rajasekaran et al. (2008), on large-scale reinforced and prestressed concrete columns: Shrive et al. (2003), and on the compressive behavior under cyclic compression loading: Mirmiran and Shahawy (1997a), Rodriques and da Silva (2001a, 2001b), Ilki and kumbasar (2002), Lam et al. (2004) and Lam et al. (2006).

In the next section, only few selected papers on the experimental investigation of small-scale unreinforced concrete cylinders confined with FRP wraps and uniaxially loaded are reviewed. The review is presented in chronological order and focuses on the aim of the investigation, test matrix information, the material used, loading method, and the key findings.

#### 2.5.1.1 Xiao and Wu (2000)

Xiao and Wu (2000) performed an experimental program on 36 small scale concrete cylinders (152 mm × 305mm) confined by CFRP and subjected to uniaxial compression. The main experimental parameters investigated were the compressive strength of unconfined concrete (33.7, 43.8 and 55.2 MPa) and the thickness of the CFRP jacket (0.381, 0.762, 1.143 mm). Xiao and Wu reported strength and ductility enhancement due to CFRP confinement. They also reported the FRP rupture strain that is less than the ultimate tensile strain from flat coupon tests. Xia and Wu concluded that concrete strength and confinement modulus are the most influential parameters on the stress-strain behaviour of FRP-confined concrete.

#### 2.5.1.2 Karabinis and Rousakis (2002)

Karabinis and Rousakis (2002) investigated the compressive behaviour of 22 CFRP-confined concrete cylinders (200 mm × 320 mm) under axial monotonic compression loading. The parameters investigated were the unconfined concrete compressive strength (47.5 and 43.5 MPa), and CFRP jacket thickness (0.117, 0.234 and 0.351 mm). They reported an increase in strength and ductility due to CFRP confinement and a bilinear stress-strain response with the slope of the second branch sharpening as the stiffness of the confining jacket increased resulting in higher strength and higher ductility.

#### 2.5.1.3 Lam and Teng (2004)

Lam and Teng (2004) conducted an experimental investigation on 27 small scale (152 mm × 305 mm) confined concrete cylinders that were tested in three phases. Each phase included 6 confined cylinders and three unconfined cylinders and encompassed a wide range of experimental parameters such as the type of FRP (CFRP and GFRP), different number of layers (1, 2 and 3), and different overlap lengths (100, 150, 250 and 400 mm).

Lam and Teng reported a failure mode of FRP rupture outside the overlapping zone and bilinear stress-strain behaviour for all tested FRP-confined cylinders.

#### 2.5.1.4 Li (2006)

Li (2006) investigated the behaviour of 39 small scale (150 mm × 300 mm) FRP-confined concrete tested in two phases, the first phase encompassed 24 concrete cylinders jacketed with E-glass unidirectional Fabric, the parameters investigated were the fibre orientation (90°/90°, 60°/30°, 45°/45°, -45°/45°, 90°/0°, 0°/0°) and the FRP jacket thickness (0.738 and 1.476 mm). The second phase encompassed 15 FRP tube-encased concrete cylinders. The parameters

investigated were the concrete strength (31.1, 35.2, 49.5 and 82.0 MPa) and both bonded and unbonded concrete-tube arrangement.

Li reported that the FRP jacket is only activated after the unconfined compressive strength of concrete core is reached. For the encased cylinders, bonded encased FRP concrete exhibited superior behaviour in terms of strength and ductility compared to unbonded tube-encased concrete and that the increase in concrete compressive strength resulted in a reduction in confinement effectiveness.

#### 2.5.1.5 Youssef et al. (2007)

Youssef et al. (2007) conducted an experimental program that included testing of 87 large unreinforced concrete specimens and 30 small-scale (152mm × 300 mm) concrete cylinders. The main parameters investigated were cross-section geometry, confinement modulus and unconfined concrete compressive strength. They reported that the stress-strain behaviour of FRP-confined concrete typically exhibits 3 distinct stages; initial linear elastic behaviour, transition zones followed by a linear behaviour until failure characterized by an ascending or descending tendency depending on the cross-section geometry and the amount of confinement provided.

#### ***2.5.2 Theoretical Developments***

Theoretical models have been developed to predict the behaviour of FRP-confined concrete either empirically in closed form expressions based on test results, analytically by an incremental iterative process, or numerically using finite element modeling.

Empirical models, also referred to as design-oriented models, Teng and Lam (2004), employ best fitting or regression analysis of available experimental data. Hence, the accuracy of these models depends on the size and reliability of the test database and the range of parameters used in the model calibration.

Analytical models, also referred to as analysis-oriented models, Teng and Lam (2004), are mathematical models in which the response of confined concrete core, FRP confining device and their interaction are explicitly considered by satisfying equilibrium and displacement compatibility through an iterative process. They are accurate and versatile, easily extendable to other confining materials.

The axial stress-strain curve of FRP-confined concrete is obtained in the analysis-oriented model through an incremental iterative process in which for a given axial stress, the lateral strain and hence the lateral confining pressure is obtained via the lateral-axial strain relationship, then the corresponding axial stress is obtained from the active-confinement based model, leading to identification of one point on the FRP-confined concrete stress-strain curve; repeating the procedure resulting in a curve crossing a family of stress-strain curves for the same concrete under different levels of active confinement pressure. Hence, the accuracy of an analysis-oriented model depends significantly on the active-confinement base model and the lateral-axial strain (dilation) relationship used in the model development.

In addition to the empirical and analytical models, numerical models using the finite element method were also developed. FE models satisfy the principles of equilibrium, compatibility (at nodal level) and accounts for the material constitutive laws; hence, the accuracy of these models significantly depends on the accuracy of the constitutive models adopted to simulate the materials behaviour.

In the following sections, a brief review of selected papers is presented to describe milestones and state-of-the-art of FRP- confined concrete modeling development. Equations are presented using unified notations rather than notations of the original paper to allow for cross-reference and quick comparison of concepts and main parameters between authors. For the definition of all

notations used in the following review, reader can refer to the list of symbols section at the beginning of this thesis.

#### 2.5.2.1 Empirical Models

The majority of the empirical models in literature have been developed for confined concrete in circular sections and propose expressions to predict the ultimate strength: Mirmiran (1996), Lin and Chen (2001), Lam and Teng (2002), Al-Salloum and Siddiqui (2009), Girgin et al. (2009) Wu and Wang (2009), Masmoudi (2010), Park et al. (2011), Realfonso and Napoli (2011), and Wang and Wu (2011), the ultimate strength and corresponding axial strain: Kono et al. (1998), Ilki et al. (2002), Shehata et al. (2002), Bisby et al. (2005), Mandal et al. (2005), and Wu et al. (2006), the ultimate strength, strain in addition to the axial stress – axial strain response: Fardis and Khalili (1982), Saadatmanesh et al. (1994), Karbhari and Gao (1997), Jolly and Lillistone (1998), Samaan et al. (1998), Miyauchi et al. (1999), Xiao and Wu (2000), Lam and Teng (2003c), Xiao and Wu (2003), Ilki et al. (2004), Saiidi et al. (2005), Youssef et al. (2007), Wu et al. (2009), Fahmy and Wu (2010), Wu and Wang (2010), and Yu and Teng (2011), or propose expressions to predict the ultimate conditions in addition to the entire axial stress – axial strain and axial stress-lateral strain response: Saafi et al. (1999), Toutanji (1999), and Berthet et al. (2006). Only a few propose expressions to predict the axial stress – axial strain response: Ahmad et al. (1991), and Demers and Neale (1994), and a few account for the strain hardening and/or strain softening behaviour of FRP-confined concrete explicitly: Miyauchi et al. (1999), Li et al. (2003), and Yan and Pantelides (2007). Only a few models account for the specimen size effect on the stress-strain response: Matthys et al. (2006), Theriault et al. (2004), and Carey and Harries (2005), non-circular sections: Wu and Wei (2010), Zhang et al. (2010) and Youssef et al. (2007), cyclic type of loading: Abbasnia and Ziaadiny (2010), Lam and Teng (2009) and Rousakis et al.

(2007), and sections with internal steel-reinforcement: Campione and Minafo (2010), Chastre, Silva (2010) and Eid and Dancygier (2006).

In the following review, the model of Fardis and Khalili (1982) was selected to represent one of the early models developed based on active or steel confined concrete models; Lam and Teng (2003) was selected as a simple, accurate and broadly recognized empirical model; the models of Toutanji (1999) and Berthet et al. (2005) were selected as both models provide the entire stress – strain response of confined concrete, Fahmy and Wu (2010) was selected to represent one of the most recent empirical models developed in the last decade.

#### 2.5.2.1.1 Fardis and Khalil (1982)

Early attempts for developing FRP-confined concrete models merely extended the already existing models developed for steel-confined concrete. Fardis and Khalili (1982) extended the well-known steel-confined concrete models to quantify the increase in strength and ductility of FRP-tube encased concrete. Based on models by Richart et al. (1928) and Newman and Newman (1969), Fardis and Khalili (1982) developed Equation 2-2 and Equation 2-3, respectively to predict the ultimate axial strength,  $f'_{cu}$ . They also proposed Equation 2-4 to predict the corresponding ultimate axial strain,  $\epsilon_{cu}$ , and finally Equation 2-5 to generate the axial stress-axial strain curve for FRP-tube encased concrete as shown in Figure 2-13.

$$f'_{cu} = f'_{co} \left[ 1 + 4.1 \frac{f_{lu}}{f'_{co}} \right] \quad \text{Equation 2-2}$$

$$f'_{cu} = f'_{co} \left[ 1 + 3.7 \left[ \frac{f_{lu}}{f'_{co}} \right]^{0.86} \right] \quad \text{Equation 2-3}$$

$$\epsilon_{cu} = 0.002 + 0.001 \frac{E_{frp} t_{frp}}{D f'_{co}} \quad \text{Equation 2-4}$$

**Equation 2-5**

$$f_c(\epsilon_c) = \frac{E_{co}\epsilon_c}{1 + \epsilon_c \left[ \frac{E_{co}}{f'_{cu}} - \frac{1}{\epsilon_{cu}} \right]}$$

where  $f'_{co}$  is the unconfined concrete strength at peak,  $E_{co}$  is the elastic modulus of unconfined concrete,  $f_c(\epsilon_c)$  is the axial stress – axial strain relation and  $\epsilon_c$  is the axial strain.

Although the model was originally developed for rigid FRP tube-confined concrete, Nanni and Bradford (1995) showed later that the model accurately predicts the strength of FRP-wrapped concrete but grossly underestimates the ductility.

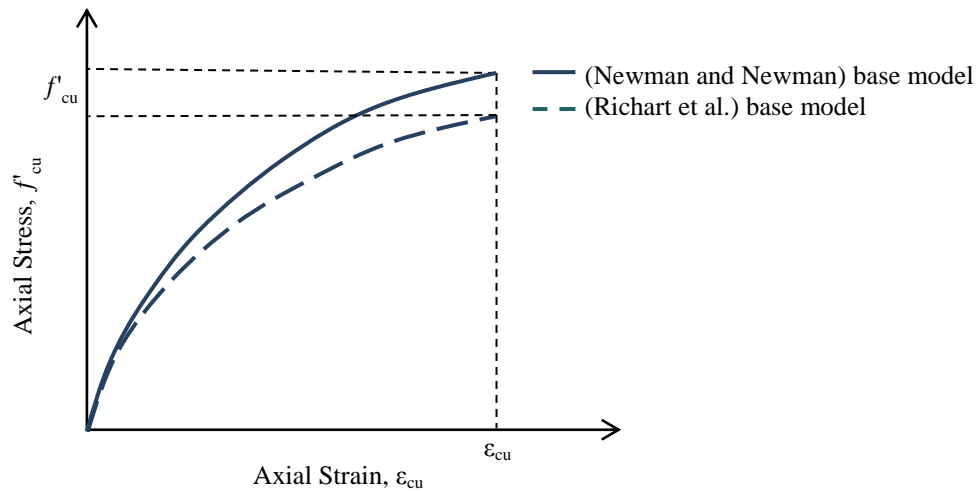


**Figure 2-13: Stress – strain model by Fardis and Khalili (1982)**

2.5.2.1.2 Toutanji (1999)

Toutanji (1999) extended a model first developed by Sargin (1971) to predict the entire axial and lateral stress-strain curve of FRP-confined concrete. The proposed model features two curves and a defined transition point as illustrated in Figure 2-14.

For region where  $\epsilon_{lt} = 0.002 \leq \epsilon_l \leq \epsilon_{lu}$ ; the second branch of the axial stress-axial strain can be generated using Equation 2-6 - Equation 2-9.

$$f_l(\varepsilon_l) = E_l \varepsilon_l \quad \text{Equation 2-6}$$

$$E_l = \frac{2t_{frp}E_{frp}}{D} \quad \text{Equation 2-7}$$

$$f_c(\varepsilon_l) = f'_{co} \left[ 1 + 3.5 \left[ \frac{f_l(\varepsilon_l)}{f'_{co}} \right]^{0.85} \right] \quad \text{Equation 2-8}$$

$$\varepsilon_c(\varepsilon_l) = \varepsilon_{co} \left[ 1 + [310.57\varepsilon_l + 1.9] \left[ \frac{f_c(\varepsilon_l)}{f'_{co}} - 1 \right] \right] \quad \text{Equation 2-9}$$

where  $f_l(\varepsilon_l)$  is the lateral confining pressure as a function of lateral strain,  $\varepsilon_{co}$  is the axial strain at peak unconfined concrete strength,  $\varepsilon_l$  is the lateral strain,  $E_l$  is the FRP lateral stiffness,  $f_c(\varepsilon_l)$  is the axial stress – lateral strain relation, and  $\varepsilon_c(\varepsilon_l)$  is the axial strain – lateral strain relation.

The transition point in the axial stress-axial strain curve, ( $f'_{ct}$ ,  $\varepsilon_{ct}$ ), corresponding to a lateral strain of 0.002, is calculated from Equation 2-10 - Equation 2-11.

$$\varepsilon_{ct} = \varepsilon_{co} \left[ 1 + 0.0448 \left[ \frac{E_l}{f'_{co}} \right]^{0.85} \right] \quad \text{Equation 2-10}$$

$$f'_{ct} = f'_{co} \left[ 1 + 0.0178 \left[ \frac{E_l}{f'_{co}} \right]^{0.85} \right] \quad \text{Equation 2-11}$$

where  $f'_{ct}$  is the axial stress at transition point, and  $\varepsilon_{ct}$  is the axial strain at the transition point.

For the regions where  $0 \leq \varepsilon_c \leq \varepsilon_{ct}$  and  $0 \leq \varepsilon_l \leq \varepsilon_{lt} = 0.002$ , the first branch of the axial stress-axial strain and axial stress lateral strain is generated using Equation 2-12. The variable  $i$  in Equation 2-12 can be used to refer to the axial or lateral corresponding parameters.

$$f_c(\varepsilon_i) = \frac{E_{ii}\varepsilon_i}{1 + \left[ \frac{E_{ij}}{f'_{ct}} - \frac{2}{\varepsilon_{it}} + \frac{E_{fi}E_{ij}\varepsilon_{it}}{f'_{ct}{}^2} \right] \varepsilon_i + \left[ \frac{1}{\varepsilon_{it}{}^2} - \frac{E_{fi}E_{ij}}{f'_{ct}{}^2} \right] \varepsilon_i^2} \quad \text{Equation 2-12}$$

$$E_{ic} = 10200 \sqrt[3]{f'_{co}} \quad \text{Equation 2-13}$$

$$E_{fc} = 0.3075 \frac{f'_{co}}{\varepsilon_{co}} \quad \text{Equation 2-14}$$

$$E_{il} = 51000 \sqrt[3]{f'_{co}} \quad \text{Equation 2-15}$$

$$E_{fl} = 7.557 E_l \left( \frac{f'_{co}}{E_l} \right)^{0.15} \quad \text{Equation 2-16}$$

$$\varepsilon_{lt} = 0.002 \quad \text{Equation 2-17}$$

where  $E_{ic}$  and  $E_{fc}$  are the initial and final elastic modulus of the first branch of the axial stress-axial strain curve,  $E_{il}$  and  $E_{fl}$  are the initial and final elastic modulus of the first branch of the axial stress-lateral strain curve,  $\varepsilon_{lt}$  is the lateral strain at the transition point,  $f'_{ct}$  is the axial stress at the transition point, and  $i$  is a variable that refers to axial or lateral.

The model terminates as soon as the ultimate compressive strength, Equation 2-18, and the ultimate strain, Equation 2-19 are reached.

$$f'_{cu} = f'_{co} \left[ 1 + 3.5 \left( \frac{f'_{lu}}{f'_{co}} \right)^{0.85} \right] \quad \text{Equation 2-18}$$

$$\varepsilon_{cu} = \varepsilon_{co} \left[ 1 + (310.57 \varepsilon_{frp} + 1.9) \left( \frac{f'_{cu}}{f'_{co}} - 1 \right) \right] \quad \text{Equation 2-19}$$

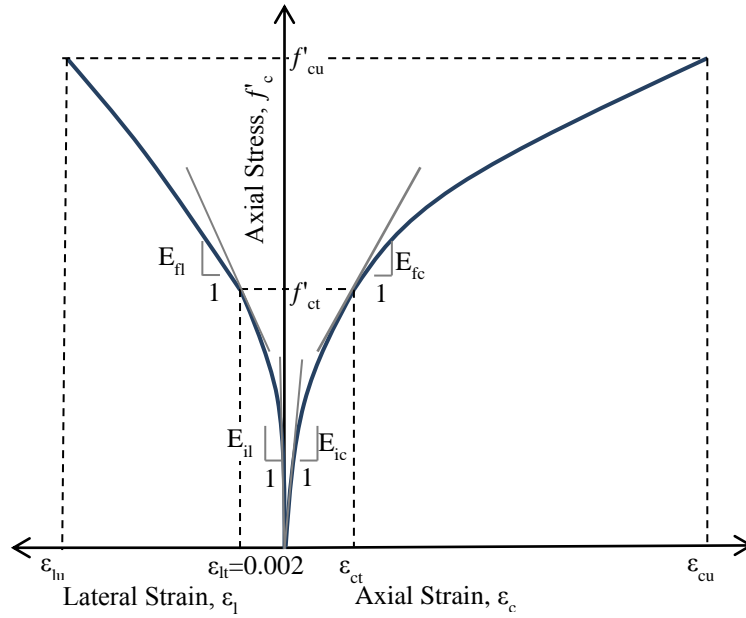


**Figure 2-14: Stress – strain model by Toutanji (1999)**

### 2.5.2.1.3 Lam and Teng (2003)

Based on a database of 76 FRP-wrapped plain concrete circular specimens from existing literature, Lam and Teng (2003) proposed a stress-strain curve that consists of a parabolic first portion and a straight-line second portion, as illustrated in Figure 2-15. The proposed model is strictly applicable for sufficiently confined concrete, that is,

$$\frac{f_{lu,a}}{f'_{co}} \geq 0.07 \quad \text{Equation 2-20}$$

where  $f_{lu,a}$  is the actual lateral confining pressure.

The entire stress-strain curve can be generated by the following expressions:

For region where  $0 \leq \epsilon_c \leq \epsilon_{ct}$  :

$$f_c(\epsilon_c) = E_{co}\epsilon_c - \frac{(E_{co} - E_2)^2}{4f_o} \epsilon_c^2 \quad \text{Equation 2-21}$$

Where  $E_2$  is the slope of the second branch of the axial stress – axial strain curve and  $f_o$  is the intercept of the axial stress axis by the second branch of the axial stress – axial strain curve.

For region where  $\varepsilon_{ct} \leq \varepsilon_c \leq \varepsilon_{cu}$  :

$$f_c(\varepsilon_c) = f_o + E_2 \varepsilon_c \quad \text{Equation 2-22}$$

The transition axial strain is given by Equation 2-23.

$$\varepsilon_{ct} = \frac{2f_o}{(E_{co} - E_2)} \quad \text{Equation 2-23}$$

$$f_o = f'_{co} \quad \text{Equation 2-24}$$

$$E_2 = \frac{f'_{cu} - f_o}{\varepsilon_{cu}} \quad \text{Equation 2-25}$$

The ultimate compressive strength and the ultimate strain are given by Equation 2-27 and Equation 2-28, respectively.

$$f_{lu,a} = \frac{2E_{frp}t_{frp}\varepsilon_{frp,a}}{D} \text{ with } \varepsilon_{frp,a} = 0.586\varepsilon_{frp} \quad \text{Equation 2-26}$$

$$\frac{f'_{cu}}{f'_{co}} = 1 + 3.3 \frac{f_{lu,a}}{f'_{co}} \quad \text{Equation 2-27}$$

$$\frac{\varepsilon_{cu}}{\varepsilon_{co}} = 1.75 + 12 \left[ \frac{f_{lu,a}}{f'_{co}} \right] \left[ \frac{\varepsilon_{frp,a}}{\varepsilon_{co}} \right]^{0.45} \quad \text{Equation 2-28}$$

where  $\varepsilon_{frp,a}$  is the actual rupture strain of the FRP jacket as measured from the compression test

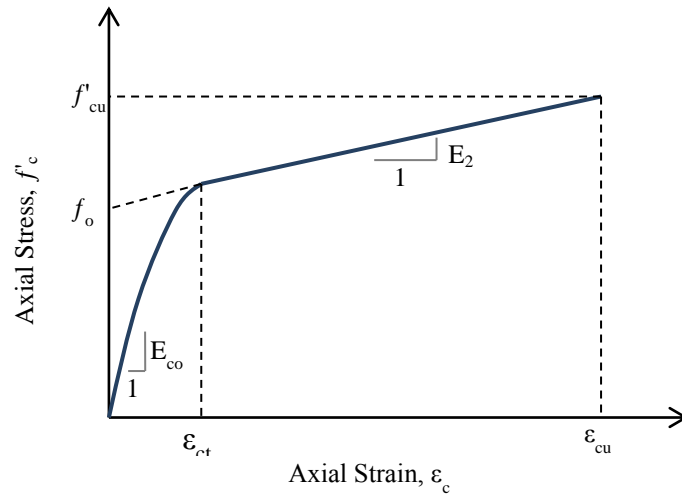


**Figure 2-15: Stress – strain model by Lam and Teng (2003)**

2.5.2.1.4 Berthet et al. (2006)

Berthet et al. (2006) developed a model to predict the ultimate behaviour and the stress-strain response of FRP-confined concrete. The model is adaptable to different unconfined concrete strength including high performance concrete.

Berthet et al. adopted the model of Richart et al. (1928) but suggested a modified value for confinement efficiency,  $k_l$  based on a rigorous regression analysis to account for concrete strength effect on the ultimate behaviour. Berthet et al model takes the following form

$$f'_{cu} = f'_{co} + k_l f_{lu} \quad \text{Equation 2-29}$$

$$k_l = 3.45, \quad 20 \leq f'_{co} \leq 50 \text{ MPa} \quad \text{Equation 2-30}$$

$$k_l = \frac{9.5}{(f'_{co})^{1/4}}, \quad 50 \leq f'_{co} \leq 200 \text{ MPa} \quad \text{Equation 2-31}$$

where  $k_l$  is the lateral confinement effectiveness coefficient.

The relation between the axial strain and transverse strain:

$$\varepsilon_l = \nu_c \varepsilon_c, \quad \varepsilon_c \leq \varepsilon_{co} = 0.002 \quad \text{Equation 2-32}$$

$$\varepsilon_l = \nu_c \varepsilon_{co} + \gamma(\varepsilon_c - \varepsilon_{co}), \quad \varepsilon_c \geq \varepsilon_{co} = 0.002 \quad \text{Equation 2-33}$$

$$\gamma = \frac{1}{\sqrt{2}} \left( \frac{E_l}{f'_{co}} \right)^{-2/3} \quad \text{Equation 2-34}$$

$$E_l = \frac{2E_{frp}t_{frp}}{D} \quad \text{Equation 2-35}$$

where  $\nu_c$  is the Poisson's ratio for concrete, and  $\gamma$  is the strain ratio

Hence, the ultimate axial strain of confined concrete is:

$$\varepsilon_{cu} = \varepsilon_{co} + \frac{(\varepsilon_{frp} - \nu_c \varepsilon_{co})}{\gamma} \quad \text{Equation 2-36}$$

Berthet et al. proposed a stress-strain model comprises of two distinct parts, the first part is parabolic representing the elastic behaviour and is derived based on elasticity and strain compatibility between FRP jacket and concrete core; the second part is linear representing the plastic behaviour and is based on experimental data.

For the region where  $\varepsilon_{lt} = 0.002 \leq \varepsilon_l \leq \varepsilon_{frp}$ , the second branch of the proposed stress- strain model and the transition points are found from Equation 2-37-Equation 2-42.

$$f'_{ct} = f'_{cu} - \theta_l(\varepsilon_{frp} - \varepsilon_{lt}) \quad \text{Equation 2-37}$$

$$\varepsilon_{lt} = 0.002 \quad \text{Equation 2-38}$$

$$\theta_l = (2.73E_l - 163) \quad \text{Equation 2-39}$$

$$\varepsilon_{ct} = \varepsilon_{co} + \frac{(\varepsilon_{lt} - \nu_c \varepsilon_{co})}{\gamma} \quad \text{Equation 2-40}$$

$$f_c(\varepsilon_l) = f'_{ct} + \theta_l(\varepsilon_l - \varepsilon_{lt}) \quad \text{Equation 2-41}$$

where  $\theta_l$  is the slope of the second slope of the axial stress – lateral strain curve.

Also, Equation 2-41 can be restated as function of the axial strain as follows:

$$f_c(\varepsilon_c) = f'_{ct} + \theta_l[(v_c - \gamma)\varepsilon_{co} - \varepsilon_{lt}] + \theta_l\gamma\varepsilon_c \quad \text{Equation 2-42}$$

The first branch of the proposed model followed a model developed by Ahmad and Shah (1982) and takes the following general form:

$$f_c(\varepsilon) = \frac{A\varepsilon}{1 + B\varepsilon + C\varepsilon^2} \quad \text{Equation 2-43}$$

From Equation 2-43, the first branch of the axial stress-lateral strain relation is generated by replacing  $\varepsilon$  by  $\varepsilon_l$  in Equation 2-43, and where the constants  $A$ ,  $B$  and  $C$  are calculated from the following equations:

$$A = E_l^* \quad \text{Equation 2-44}$$

$$B = \frac{E_l^*}{f'_{ct}} - \frac{2}{\varepsilon_{lt}} + \theta_l \frac{E_l^* \varepsilon_{lt}}{f'_{ct}{}^2} \quad \text{Equation 2-45}$$

$$C = \frac{1}{\varepsilon_{lt}^2} - \theta_l \frac{E_l^*}{f'_{ct}{}^2} \quad \text{Equation 2-46}$$

where  $E_l^*$  is the equivalent transverse modulus of concrete .

$$E_l^* = \frac{E_{co}}{v_c} \left[ 1 + \frac{E_l}{E_{co}} (1 - v_c) \right] \quad \text{Equation 2-47}$$

Similarly, the first branch of the axial stress-axial strain model is found by  $\varepsilon$  replacing  $\varepsilon_c$  in Equation 2-43, and the constants  $A$ ,  $B$  and  $C$  are re-evaluated using Equation 2-44-Equation 2-47 with  $E_l^*$  and  $\varepsilon_{lt}$  are replaced with  $E_c^*$  and  $\varepsilon_{ct}$ , respectively, where  $E_c^*$  is the equivalent axial modulus of concrete.

$$E_c^* = E_{co} \left[ \frac{E_{co} + (1 - v_c)E_l}{E_{co} + (1 - v_c - 2v_c^2)E_l} \right] \quad \text{Equation 2-48}$$

Berthet et al. reported a good agreement of the predicted stress-strain behaviours when compared to their own experimental results and others from the literature.

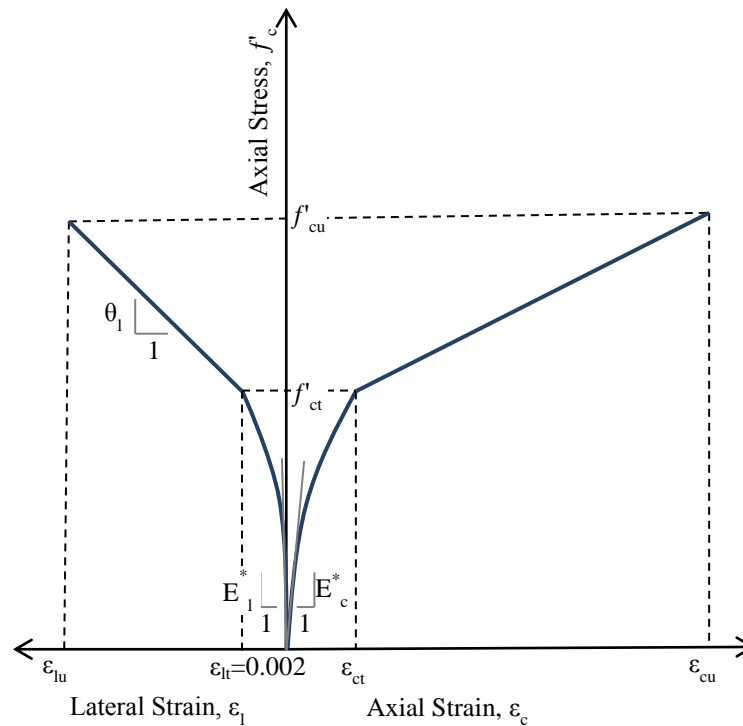


**Figure 2-16: Stress – strain model by Berthet et al. (2005)**

#### 2.5.2.1.5 Fahmy and Wu (2010)

Fahmy and Wu (2010) proposed a stress-strain model of FRP-confined concrete similar to the model developed by Lam and Teng (2003b) and consists of two parts: the first is parabolic, which meets with a second ascending part that has a linear slope  $E_2$  that intersects the axial stress axis at  $f_o = f'_{co}$ , as shown in Figure 2-16. The first parabolic part is generated using the formula developed by Lam and Teng, Equation 2-21. The slope of the second linear part is calculated using Equation 2-49, which was modified from a model originally adopted by Samaan et al.(1998)

$$E_2 = m_2(245.61f'_{co}{}^{m_1} + 0.6728E_l) \quad \text{Equation 2-49}$$

$$m_1 = 0.2, m_2 = 1.73 \text{ if } f'_{co} > 40 \text{ MPa} \quad \text{Equation 2-50}$$

$$m_1 = 0.5, m_2 = 0.83 \text{ if } f'_{co} \leq 40 \text{ MPa} \quad \text{Equation 2-51}$$

Fahmy and Wu reported that among the models they investigated, the Samaan et al. model exhibited the least dispersion: however, the model overestimated the ultimate strength. Hence, they calibrated  $k_l$  based on the available database with explicit consideration of the effect of unconfined compressive strength. The proposed ultimate strength and corresponding axial strain are calculated using Equation 2-52 and Equation 2-53, respectively.

$$f'_{cu} = f'_{co} + k_l f_{lu} \quad \text{Equation 2-52}$$

$$\epsilon_{cu} = \frac{f'_{co} - f_o}{E_2} \quad \text{Equation 2-53}$$

$$k_l = 4.5 f_{lu}^{-0.3}, f'_{co} \leq 40 \text{ MPa} \quad \text{Equation 2-54}$$

$$k_l = 3.75 f_{lu}^{-0.3}, f'_{co} > 40 \text{ MPa} \quad \text{Equation 2-55}$$

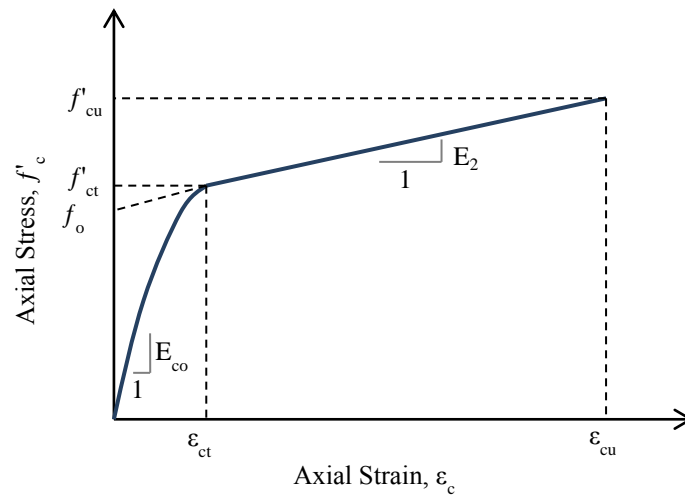


Figure 2-17: Stress – strain model by Fahmy and Wu (2010)

### 2.5.2.2 Analytical Models

Numerous analysis-oriented models have been developed to predict the behaviour of FRP-confined concrete: Mirmiran and Shahawy (1997), Spoelstra and Monti (1999), Fam and Rizkalla (2001), Chun and Park (2002), Harries and Kharel (2002), Moran and Pantelides (2002), Marques et al. (2004), Binici (2005), Teng et al. (2007), Jiang and Teng (2007), Xiao et al. (2010). Only the models by Spoelstra and Monti (1999) and Teng et al. (2007) are reviewed next..

#### 2.5.2.2.1 Spoelstra and Monti (1999)

Utilizing Popovics (1973) and Mander et al. (1988) works, Spoelstra and Monti (1999) developed an analytical, incremental-iterative model that predicts the behaviour of concrete confined by FRP, steel jackets or conventional transverse spiral or circular reinforcement. The model accounts for continuous interaction of concrete core with the confining device by satisfying equilibrium and displacement compatibility.

The proposed curve can be looked upon as a curve crossing a series of Mander's curve, each one applicable to the level of confining pressure corresponding to the current lateral strain. The stress-strain curve is generated by following the procedures outlined next

- For any value of  $\varepsilon_c$ , calculate the peak axial stress of concrete  $f'_{cc}$  and corresponding strain,  $\varepsilon_{cc}$ , under a specific constant confinement pressure,  $f_l$ , using the Mander et al.(1988) expression which was based on the “five parameter” multiaxial failure surface by Willam and Warnke (1975) employed as follows:

$$\frac{f'_{cc}(f_l)}{f'_{co}} = 2.254 \sqrt{1 + 7.94 \frac{f_l}{f'_{co}}} - 2 \frac{f_l}{f'_{co}} - 1.254 \quad \text{Equation 2-56}$$

$$\varepsilon_{cc}(f'_{cc}) = \varepsilon_{co} \left[ 1 + 5 \left[ \frac{f'_{cc}}{f'_{co}} - 1 \right] \right] \quad \text{Equation 2-57}$$

where  $f'_{cc}$  is the strength at peak for unconfined concrete, and  $\varepsilon_{cc}$  is axial strain corresponding to stress at peak.

- The current stress is calculated next using the Popovic (1975) model:

$$f_c(f'_{cc}) = \frac{f'_{cc}(f_l) \cdot x \cdot r}{r - 1 + x^r} \quad \text{Equation 2-58}$$

$$x = \frac{\varepsilon_c}{\varepsilon_{cc}} \quad \text{Equation 2-59}$$

$$r = \frac{E_{co}}{E_{co} - E_{sec}} \quad \text{Equation 2-60}$$

$$E_{sec} = f'_{cc} / \varepsilon_{cc} \quad \text{Equation 2-61}$$

where  $r$  is a constant to account for the brittleness of concrete, and  $E_{sec}$  is the secant elastic modulus.

- The lateral strain  $\varepsilon_l$  is now updated:

$$\varepsilon_l(\varepsilon_c, f_l) = \frac{E_{co}\varepsilon_c - f'_c}{2\beta f'_c} \quad \text{Equation 2-62}$$

$$\beta = \frac{E_{co}}{f'_{co}} - \frac{1}{\varepsilon_{co}} \quad \text{Equation 2-63}$$

where  $f'_c$  is the current axial stress, and  $\beta$  is a constant representing a property of concrete.

- The lateral confinement pressure,  $f_l$ , is also updated:

$$f_l(\varepsilon_l) = \frac{2t_{frp}E_{frp}\varepsilon_l}{D} \quad \text{Equation 2-64}$$

This iterative process is repeated until  $f_l$  converges. The whole procedure is repeated for each  $\varepsilon_l$ , over the complete stress-strain curve. The iterative procedure required to construct the stress-strain curve is illustrated in Figure 2-18.

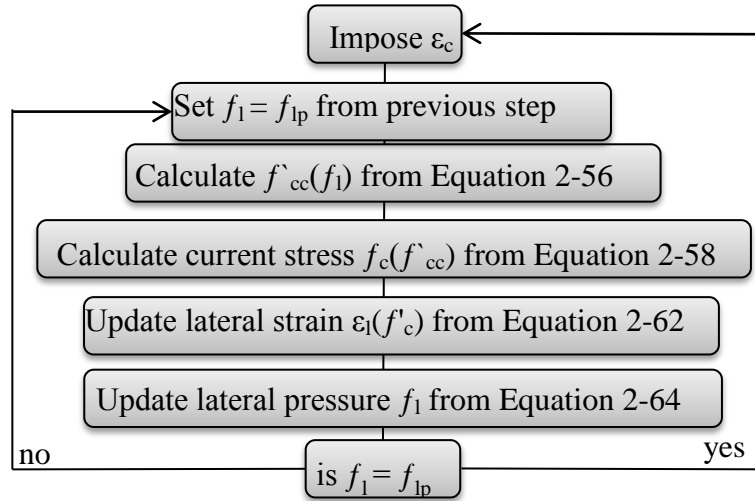


**Figure 2-18: Iterative procedure - Spoelstra and Monti analytical model**

Spoelstra and Monti proposed exact expressions for the ultimate compressive strength of confined concrete that can be evaluated by following the procedures outlined next;

- The peak stress and the correspondent strain corresponding to the ultimate confinement,  $f_{lu}$ , is first evaluated using Mander's stress-strain curve:

$$f'_{cc} = f'_{co} \left[ 2.254 \sqrt{1 + 7.94 \frac{f_{lu}}{f'_{co}}} - 2 \frac{f_{lu}}{f'_{co}} - 1.254 \right] \quad \text{Equation 2-65}$$

$$\varepsilon_{cc} = \varepsilon_{co} \left[ 1 + 5 \left[ \frac{f'_{cc}}{f'_{co}} - 1 \right] \right] \quad \text{Equation 2-66}$$

- The secant modulus of elasticity at ultimate,  $E_{secu}$  is calculated next:

$$E_{secu} = \frac{E_{co}}{1 + 2\beta\varepsilon_{frp}} = \frac{E_{co}}{1 + 2\beta f_{frp}/E_{frp}} \quad \text{Equation 2-67}$$

where  $f_{frp}$  is the ultimate tensile strength of the FRP jacket.

- Finally, the ultimate compressive stress,  $f'_{cu}$  and strain,  $\varepsilon_{cu}$  are calculated by:

$$\varepsilon_{cu} = \varepsilon_{cc} \left[ \frac{E_{sec}[E_{co} - E_{secu}]}{E_{secu}[E_{co} - E_{sec}]} \right]^{1 - \frac{E_{sec}}{E_{co}}} \quad \text{Equation 2-68}$$

$$f'_{cu} = E_{secu} \varepsilon_{cu} \quad \text{Equation 2-69}$$

Spoelstra and Monti also developed two approximate formulas for the ultimate compressive stress and strain of confined concrete for design practice as follows:

$$f'_{cu} = f'_{co} \left[ 0.2 + 3 \sqrt{\bar{f}_{lu}} \right] \quad \text{Equation 2-70}$$

$$\varepsilon_{cu} = \varepsilon_{co} \left[ 0.2 + 1.25 \bar{E}_c \varepsilon_{frp} \sqrt{\bar{f}_{lu}} \right] \quad \text{Equation 2-71}$$

$$\bar{f}_{lu} = \frac{f_{lu}}{f'_{co}}, \bar{E}_c = \frac{E_{co}}{f'_{co}} \quad \text{Equation 2-72}$$

where  $\bar{f}_{lu}$  is the effective ultimate lateral confining pressure, and  $\varepsilon_{cu}$  is the effective elastic modulus.

The proposed model was compared with experimental tests of Picher et al. (1996), Kawashima et al. (1997) and Mirmiran and Shahawy (1997), it showed a good agreement in both the stress-axial strain and stress-lateral strain response.

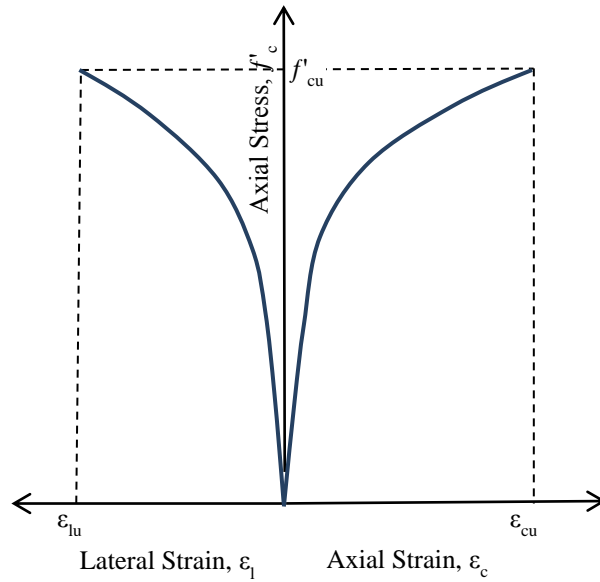


**Figure 2-19: Stress – strain model by Spoelstra and Monti (1999)**

#### 2.5.2.2.2 Teng et al. (2007)

Teng et al. (2007) developed a stress-strain model in which the response of the concrete core and the FRP jacket and their interaction has been explicitly considered. The model is applicable not only to FRP-confined concrete and confined concrete with different materials but also to concrete confined with steel tubes.

The lateral strain-axial strain relation is proposed as follows:

$$\frac{\varepsilon_c}{\varepsilon_{co}} = 0.85 \left( 1 + 8 \frac{f_l}{f'_{co}} \right) \left\{ \left[ 1 + 0.75 \frac{-\varepsilon_l}{\varepsilon_{co}} \right]^{0.7} - \exp \left[ -7 \left( \frac{-\varepsilon_l}{\varepsilon_{co}} \right) \right] \right\} \quad \text{Equation 2-73}$$

Once the lateral strain-axial strain relationship is available, the axial stress-strain response can be generated based on the active confinement model originally proposed by Popovics (1973), Equation 2-58-Equation 2-61, and use Equation 2-74 and Equation 2-75 to calculate the peak stress and strain at any level of confinement Equation 2-56.

$$\frac{f'_{cc}}{f'_{co}} = 1 + 3.5 \frac{f_l}{f'_{co}} \quad \text{Equation 2-74}$$

$$\frac{\varepsilon_{cc}}{\varepsilon_{co}} = 1 + 17.5 \frac{f_l}{f'_{co}} \quad \text{Equation 2-75}$$

For the application of their model, they suggested the use of  $E_{co} = 4730\sqrt{f'_{co}}$ , and  $\varepsilon_{co} = 0.0022$  unless the values are available from tests.

Through comparison with independent test data available from the literature, Teng et al. reported adequate accuracy of the proposed model.

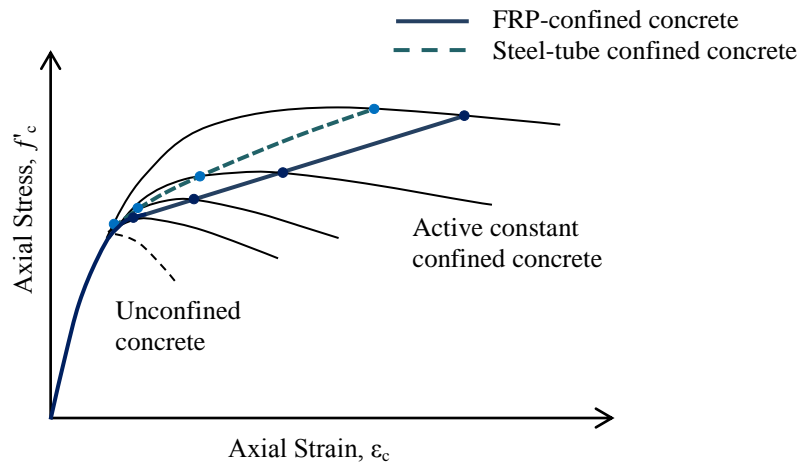


**Figure 2-20: Stress – strain model by Teng et al. (2007)**

### 2.5.2.3 Numerical Models

Many constitutive models that have been proposed for FE modeling of FRP-confined concrete adopted the plasticity type model: Karabinis and Kiousis (1994), Karabinis and Kiousis (1996), Lan (1998), Karabinis and Rousakis (2002), Fang (1999), Mirmiran et al. (2000), Shahawy et al. (2000), Mahfouz et al. (2001), Oh (2002), Malvar et al. (2004), Parvin and Jamwal (2006), Tsionis and Pinto (2007), Rousakis et al. (2007), Eid and Paultre (2007), Rousakis et al. (2008), Karabinis et al. (2008), Papanikalaou and Kappos (2007), Yu et al. (2010) and Jiang and Teng

(2012), plastic-damage type model: Cervenka and Papanikolaou (2008), Luccioni and Rougier (2005), Yan and Pantelides (2006).

In the following sections, only selected papers on concrete constitutive model development in the framework of the DP plasticity model will be discussed.

#### 2.5.2.3.1 Mirmiran et al. (2000)

Mirmiran et al. (2000) utilized a non-associative DP plasticity model. They related DP model parameters, friction angle,  $\varphi$ , and the hardening-softening function,  $k$ , to the Mohr-Coulomb (MC) angle of internal friction,  $\phi$ , and cohesion,  $c$  as follows:

$$\tan \varphi = \frac{2 \sin \phi}{\sqrt{3}(3 - \sin \phi)} \quad \text{Equation 2-76}$$

$$k = \frac{6c \cos \phi}{\sqrt{3}(3 - \sin \phi)} \quad \text{Equation 2-77}$$

The angle of internal friction,  $\phi$ , and the cohesion,  $c$ , are related to the unconfined concrete strength,  $f'_{co}$  and confinement effectiveness coefficient,  $k_l$  by the following expressions:

$$f'_{co} = \frac{2c \cos \phi}{(1 - \sin \phi)} \quad \text{Equation 2-78}$$

$$k_l = \frac{(1 + \sin \phi)}{(1 - \sin \phi)} \quad \text{Equation 2-79}$$

The theoretical confinement effectiveness coefficient,  $k_l$  is either taken directly from any linear confinement model in the form shown in Equation 2-80 or calculated indirectly using Equation 2-81 by first calculating the ultimate confined concrete strength,  $f'_{cu}$  using any nonlinear confinement model, such as the model proposed by Mander et al.(1988), Equation 2-82, or the model proposed by Samaan et al. (1998), Equation 2-83.

$$f'_{cu} = f'_{co} + k_l f_{lu} \quad \text{Equation 2-80}$$

$$k_l = \frac{(f'_{cu} - f'_{co})}{f_{lu}} \quad \text{Equation 2-81}$$

$$f'_{cu} = f'_{co} \left[ -1.254 + 2.254 \sqrt{1 + \frac{7.94 f_{lu}}{f'_{co}}} - 2 \frac{f_{lu}}{f'_{co}} \right] \quad \text{Equation 2-82}$$

$$f'_{cu} = f'_{co} + 3.38 f_{lu}^{0.7} \quad \text{Equation 2-83}$$

However, Rochette and Labossiere (1996) suggested a direct approach to evaluate  $\phi$  and  $c$ .

$$\phi = \sin^{-1} \left[ \frac{3}{1 + \frac{2f'_{co}(MPa)}{\sqrt{3}}} \right] \quad \text{Equation 2-84}$$

$$c(Mpa) = (f'_{co}(Mpa) - 5\sqrt{3}) \frac{3 - \sin \phi}{6 \cos \phi} \quad \text{Equation 2-85}$$

Mirmiran et al. (2000) performed a calibration study to establish the values of the DP parameters to best fit the experimental data. They reported that, for concrete strength between 29.6 MPa-32 MPa, the best fit to experimental result is obtained by setting the cohesion, internal friction angle and dilation angle to 8.275MPa, 28° and zero, respectively. However, they pointed out that their developed FE model fails to capture the dilation behaviour of confined concrete and that further improvement need to be done.

#### 2.5.2.3.2 Yu et al. (2010)

Yu, et al. (2010) critically reviewed the existing DP concrete plasticity models and evaluated their accuracy in predicting the behaviour of actively-confined and passively-confined concrete

using experimental observations and FE numerical analysis. They reported that none of the existing DP plasticity models is capable of modeling the behaviour of confined concrete as they lack one or more of the following features: (a) a yield criterion that includes the third deviatoric stress invariant; (b) a hardening/softening rule that is dependent on the confining pressure; (c) a flow rule that is dependent on both the confining pressure and the rate of confinement increment. Yu et al. proposed modifications to the DP concrete plasticity model that includes all three features mentioned above. These modifications were implemented in the general purpose FE software ABAQUS by modifying its built-in extended DP model.

The yield surface criterion proposed by Yu et al. features a constant friction angle,  $\tan \varphi$ , of 0.2624 and a non-circular failure surface in deviatoric plane based on a shear strength ratio,  $K$ , of 0.78 instead of the 0.725, found from experimental results, due to software limitation.

Yu et al. also used the Solution Dependent Field Variable (SDFV) available in ABAQUS to define the dependency of the hardening/softening rule on the confining pressure and the dependency of the flow rule on the confining pressure, plastic deformation and the rate of confinement increment.

#### 2.5.2.3.3 Jiang and Wu (2012)

Jiang and Wu (2012) proposed a modified DP type plasticity model for FE analysis of FRP-confined concrete and used the extended DP model built in ABAQUS. They developed explicit expressions to evaluate the model parameters; yield criterion, hardening/softening rule and flow rule through analytical studies of experimental results of 29 small-scale (152 mm × 305 mm) FRP-confined concrete cylinders tested by Teng et al. (2007) and Jiang and Teng (2007).

Jiang and Wu defined the DP model parameters as a function of the lateral stiffness ratio,  $\rho$ , provided by the confining jacket, Equation 2-86. They argued that specimens with different FRP stiffness and unconfined concrete strengths but with a similar value of  $\rho$  had the same dilation behaviour. Hence, they concluded that  $\rho$  is the dominant factor that affects the dilation curve,  $\beta(\varepsilon_c^p)$ . The proposed plastic dilation model,  $\beta(\varepsilon_c^p)$ , is given by Equation 2-87 through Equation 2-92

$$\rho = \frac{2E_{frp}t_{frp}}{Df'_{co}} \quad \text{Equation 2-86}$$

$$\beta(\varepsilon_c^p) = \frac{\beta_o + (M_o + \lambda_1\beta_o)\varepsilon_c^p + \lambda_2\beta_u(\varepsilon_c^p)^2}{1 + \lambda_1\varepsilon_c^p + \lambda_2(\varepsilon_c^p)^2} \quad \text{Equation 2-87}$$

$$\beta_o = -37 \quad \text{Equation 2-88}$$

$$M_o = 157000 \quad \text{Equation 2-89}$$

$$\lambda_1 = 11.61\rho + 980 \quad \text{Equation 2-90}$$

$$\lambda_2 = 5700\rho + 225000 \quad \text{Equation 2-91}$$

$$\beta_u = 101.66 \exp(-0.06\rho) - 37.5 \quad \text{Equation 2-92}$$

where  $\beta_o$  and  $M_o$  are the initial and the corresponding slope of  $\beta$  curve at  $\varepsilon_c^p = 0$ ,  $\lambda_1$ ,  $\lambda_2$  and  $\beta_u$  are functions of  $\rho$ .

The friction angle parameter is defined as:

$$\varphi = 56.44^\circ - 226\tilde{\varepsilon}_p \quad \text{Equation 2-93}$$

where  $\tilde{\varepsilon}_p$  is the equivalent principal plastic strain.

The hardening/softening parameter,  $k$ , is defined as a function of equivalent principal plastic strain,  $\tilde{\varepsilon}_p$ , and lateral stiffness ratio,  $\rho$ , as follows:

$$k_{(\tilde{\varepsilon}_p, \rho)} = k_o + E_p \frac{\tilde{\varepsilon}_p}{1 + \eta \tilde{\varepsilon}_p} + p_{1(\rho)} \tilde{\varepsilon}_p^2 + p_{2(\rho)} \tilde{\varepsilon}_p \quad \text{Equation 2-94}$$

$$p_1 = \frac{\rho}{a_1 + a_2 \rho + a_3 \sqrt{\rho}} \quad \text{Equation 2-95}$$

$$p_2 = \frac{b_1 \rho + b_2}{\rho + b_3} \quad \text{Equation 2-96}$$

The hardening/softening model parameters are shown in Table 2-4.

**Table 2-4: Hardening/softening models parameters, Jiang and Wu (2012)**

$k_o$	$E_p$	$\eta$	$a_1$	$a_2$	$a_3$	$b_1$	$b_2$	$b_3$
0.25	2700	6587	0.12	0.0044	-0.023	-0.75	-41.06	2.52

The proposed friction angle, hardening/softening function and plastic dilation models were imported into ABAQUS in a tabular format. The user-defined field subroutine option available in ABAQUS was used to define the additional independent material parameter. The model was verified against 97 FRP-confined column specimens covering a range of concrete strengths from 31.4 MPa to 52.05 MPa and lateral stiffness ratios from 3.9 to 113.35. Good agreement between test results and model predictions was reported.

#### 2.5.2.4 FRP-Confinement Models in the Canadian Design Codes

##### 2.5.2.4.1 The FRP Building Code CAN/CSA S806-12

The confinement model adopted by CAN/CSA S806-12 design code is based on a model by Saatcioglu and Razvi (1992). However, the model was modified by introducing the shape factor,  $k_c$  (1 for circular cross sections) and a reduction factor of 0.85 to the unconfined concrete strength. The model takes the form

$$f'_{cu} = 0.85 f'_{co} + k_l k_c f_{lu} \quad \text{Equation 2-97}$$

$$k_l = 6.7(k_c f_{lu})^{-0.17} \quad \text{Equation 2-98}$$

where  $k_c$  is the cross-section shape factor.

In the calculation of the ultimate confinement pressure by the FRP sheets, the CAN/CSA S806-12 design code limits the FRP ultimate tensile strength to the minimum of  $0.006E_{frp}$  and

$\phi_{frp}f_{frp}$ , i.e.

$$f_{lu} = \frac{2t_{frp}\phi_{frp}f_{frp}}{D} \leq \frac{2t_{frp}0.006E_{frp}}{D} \quad \text{Equation 2-99}$$

where  $\phi_{frp}$  is the FRP material resistance reduction factor.

The code specifies  $\phi_{frp} = 0.65$  for any type of FRP sheets.

#### 2.5.2.4.2 The Canadian Highway Bridge Design Code CAN/CSA-S6-14

The confinement model adopted by the CAN/CSA S6-14 design code takes the form

$$f'_{cu} = f'_{co} + 2f_{lu} \quad \text{Equation 2-100}$$

$$f_{lu} = \frac{2\phi_{frp}t_{frp}f_{frp}}{D} \quad \text{Equation 2-101}$$

The material resistance reduction factor for FRP sheets,  $\phi_{frp}$ , in the bridge code varied depending on the type of FRP sheets used and the type of application. For externally bonded applications, the code recommends 0.8, 0.7, and 0.65 for CFRP, GFRP and AFRP, respectively.

No materials resistance factor for SFRP sheets was provided.

## **2.6 Preceding Research and State-of-the-Art of SFRP-Confined Concrete**

### ***2.6.1 Experimental Programs***

#### **2.6.1.1 Mashrik (2011) and El-Hacha and Mashrik (2011)**

Mashrik (2011) and El-Hacha and Mashrik (2011) performed an extensive experimental program to study the performance of CFRP- and SFRP-confined small-scale unreinforced concrete cylinders (150 mm × 300 mm) and square prisms (150 mm × 150 mm × 300 mm). The experimental program included 156 specimens which were tested under concentric monotonic axial compression until failure. The experimental program examined the effect of a wide range of parameters on the compressive behaviour of CFRP- and SFRP-confined concrete such as specimen cross section (circular and square); type of FRP sheet (CFRP and SFRP); concrete compressive strength (25, 30 and 35 MPa); number of FRP layers (1, 2 and 3), corner radius for square sections (3, 6, 10 and 25 mm); FRP overlap length (25, 50, 75 and 100 mm) and the effect of different environmental exposures such as prolonged temperature (45 °C for 135 days), high temperature along with relative humidity (60 °C along with 96% relative humidity for 42 days) and freeze-thaw cycles (90 and 456 cycles between -34 °C to +34 °C and relative humidity of 75% for temperature above +20 °C).

Mashrik and El-Hacha (2012) concluded that:

- Confinement of concrete sections with CFRP and SFRP sheets improved the axial capacity and ductility for both circular and square specimens with respect to unconfined specimens and increasing the number of FRP layers for the same concrete compressive strength increased the axial compressive strength and ultimate strain for both circular and square specimens.

- Increasing the length of the overlap increases the strength and ductility of confined concrete and for the same overlap length, performance enhancement in SFRP-confined specimens were more prominent than in CFRP-confined specimens. A minimum overlap of 50 mm for CFRP-confined concrete and a minimum of 100 mm for SFRP-confined concrete were recommended for effective FRP confinement.
- FRP confinement is more effective in circular specimens rather than corresponding square specimens; however, the overall performance of square specimens is enhanced as corner radius increases, a minimum 25 mm corner radius was recommended.
- Under severe environmental exposure, CFRP-confined specimens exhibit a reduction in strength and ductility while SFRP-confined specimen's strength and ductility was unaltered. SFRP sheets, on the other hand, show signs of degradation in the form of rust, while CFRP sheets were unaffected.
- SFRP is more cost effective than CFRP in terms of material cost and performance enhancement.

#### 2.6.1.2 Abdelrahman (2011) and Abdelrahman and El-Hacha (2012)

Abdelrahman (2011) and Abdelrahman and El-Hacha (2012) performed an experimental program on 18 large scale reinforced and unreinforced circular concrete columns (300 mm × 1200 mm) under monotonic axial concentric compression loading and investigated the effectiveness of SFRP jacket as compared to CFRP jacket in enhancing the performance of concrete columns. The experimental parameters include the type of FRP (CFRP and SFRP), steel internal reinforcement, wrap orientation (0° and 90°/0°) and environmental exposures ( normal room temperature, freeze-thaw cycles ranging of -34 °C to +34 °C for 252 and 446 cycles for unreinforced and reinforced columns respectively).

Furthermore, Abdelrahman and El-Hacha (2012) performed an experimental program on 18 circular concrete specimens of 150 mm diameter and varying heights of 300, 600 and 900 mm wrapped with one layer of SFRP sheets to study the effect of the slenderness ratio ( $H/D$ , where  $H$  is the height and  $D$  is the diameter of the cylinder, respectively) on the compressive behaviour of confined concrete

Abdelrahman and El-Hacha (2012) major observations were:

- Wrapping circular specimens with SFRP sheets was very effective in enhancing the performance of concrete in terms of strength and ductility, and the performance of the SFRP-confined columns, regardless of the column type (reinforced or unreinforced), wrapping orientation, and type of environmental exposure, was found to be superior to that of columns confined with CFRP.
- Provision of an FRP sheet in the longitudinal direction had negligible effect on the ultimate strength but significantly enhanced the ultimate axial strain and ultimate lateral strain when compared to corresponding columns confined in the lateral direction only.
- Increasing the slenderness ratio of concrete columns significantly reduces the overall performance of SFRP-confined concrete columns in terms of ultimate axial strength, ultimate axial and lateral strain and ductility.

#### 2.6.1.3 Napoli and Realfonzo (2013)

Napoli and Realfonzo (2013) performed an extensive experimental program to investigate the compressive behaviour of unreinforced concrete cylinders (150 mm × 300 mm) confined with SFRP. The test matrix included 252 cylinders; the main parameters investigated were the concrete compressive strength (8, 15, 30 and 35 MPa), the number of SFRP layers (1, 2 and 3) and SFRP densities (4 wires/25.4 mm, 12 wires/25.4 mm and 20 wires/25.4 mm corresponding

to low, medium and high density, respectively). SFRP sheets of low, medium and high density are shown in Figure 2-21.

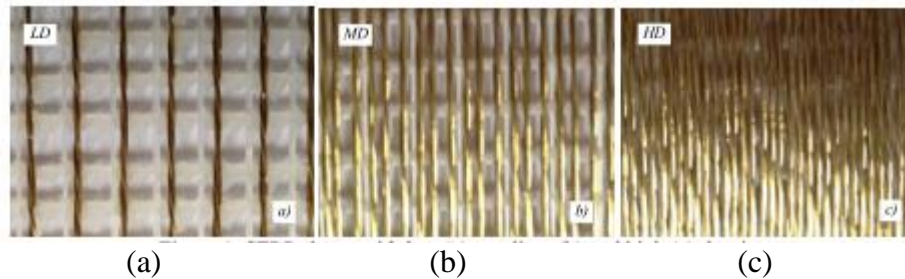


**Figure 2-21: SFRP sheets: (a) low (b) medium (c) high density, Napoli and Realfonzo (2013)**

Preliminary results from 49 concrete cylinders, all of which had unconfined compressive strength of 15 MPa and were variably confined by 1, 2, or 3 SFRP sheets with equal or different SFRP fibre densities, revealed that:

- The compressive behaviour of confined concrete was significantly enhanced as the number of SFRP layers were increased; one layer of low density SFRP sheets doubled the strength and increased the corresponding strain to more than six times higher than those exhibited by unconfined concrete, whereas the use of 3 layers of different combination of medium and high density SFRP sheets enhanced the performance of confined concrete in terms of strength and strain by approximately 8 and 2 times higher than corresponding strength and strain of unconfined concrete.
- The majority of specimens failed by rupture of the SFRP sheet initiated at the overlap while some specimens exhibited a failure mode that is a combination of rupture and debonding.

- SFRP-confined concrete cylinders exhibit a bilinear stress-strain response, where the initial slope is very similar to that of unconfined concrete while the second branch is continuously ascending up to cylinder failure.

## 2.6.2 Theoretical Works

### 2.6.2.1 Empirical Models

#### 2.6.2.1.1 Abdelrahman and El-Hacha (2014)

Based on their own experimental database of 18 concrete specimens; 9 wrapped with one layer of SFRP sheets and 9 unwrapped, all of which had a diameter of 150 mm and varying heights of 300 mm, 600 mm and 900 mm and subjected to monotonic, concentric uniaxial compression, Abdelrahman and El-Hacha (2014) developed a model that is capable of predicting the ultimate axial strain of SFRP-wrapped concrete. The model was developed based on a parabolic relationship between the strain ratio and the confinement ratio and takes the following form:

$$\frac{\varepsilon_{cu}}{\varepsilon_{co}} = 78.55 - 303.26 \left( \frac{f_l}{f_{co}} \right) + 312.84 \left( \frac{f_l}{f_{co}} \right)^2 \quad \text{Equation 2-102}$$

### 2.6.2.2 Analytical Models

To the author's best knowledge, to date there has been no analytical model developed for SFRP-confined concrete.

### 2.6.2.3 Numerical Models

#### 2.6.2.3.1 Abdelrahman and El-Hacha (2014)

Abdelrahman and El-Hacha (2014) proposed a 3D FE model to simulate the behaviour of SFRP- and CFRP-confined concrete. They utilised the Concrete Damage Plasticity (CDP) material model to simulate the non-linear behaviour of confined concrete; the model parameters include the stress-strain response of concrete under compression and tension, yield surface criteria and

the plastic flow rule. The Hognestad (1951) concrete model, slightly modified to account for the unique characteristics of confined concrete was adopted for concrete under compression. The modified Hognestad compression stress-stain model takes the form of Equation 2-103 and is shown in Figure 2-22.

$$f_c(\varepsilon_c) = f'_{cc} \left[ 2 \frac{\varepsilon_c}{\varepsilon_{cc}} - \left( \frac{\varepsilon_c}{\varepsilon_{cc}} \right)^2 \right] \quad \text{Equation 2-103}$$

$$\varepsilon_c = 1.8 \frac{f'_c}{E_c}$$

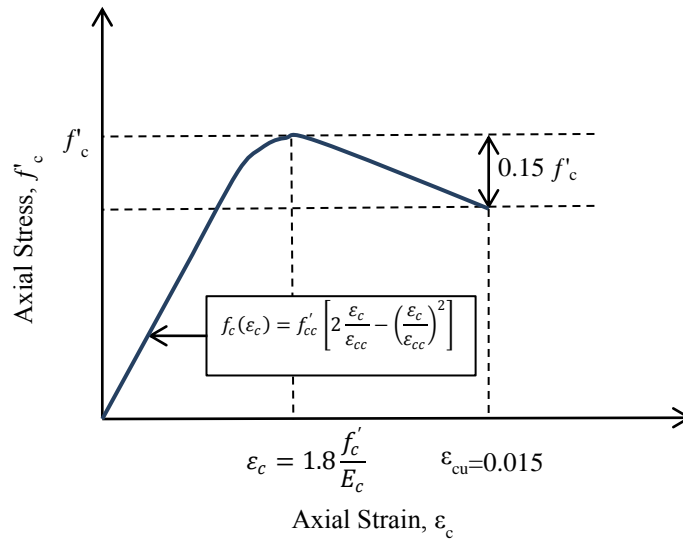


**Figure 2-22: Modified Hognestad compression stress-strain curve, Hognestad (1951)**

Using the fracture energy,  $G_t$ , as a material property, and assuming that a linear loss of tensile strength occurs after cracking, as shown Figure 2-23, the cracking displacement,  $u_t$ , at which tensile strength,  $\sigma_t$ , is completely lost is defined in Equation 2-104. The fracture energy, highly dependent on concrete unconfined compressive strength, was assumed in the range of 40 N/m and 120 N/m.

$$u_t = 2 \frac{G_t}{\sigma_t} \quad \text{Equation 2-104}$$

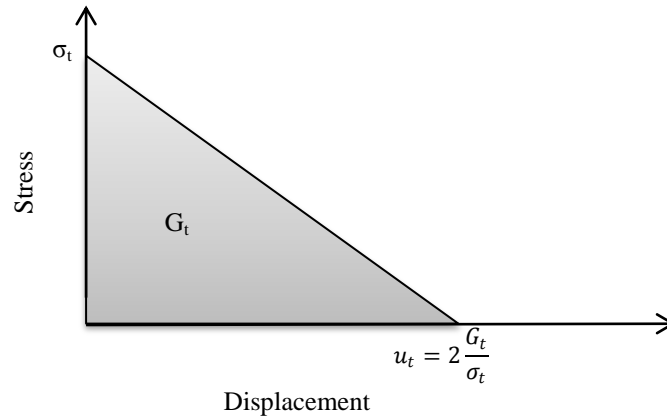


**Figure 2-23: Tensile stress-displacement model of confined concrete, ABAQUS (2009)**

Other parameters in Abdelrahman and El-Hacha model are summarized in Table 2-5.

**Table 2-5: Concrete Damage Plasticity (CDP) model parameter, Abdelrahman and El-Hacha (2014)**

Dilation angle	Eccentricity	$f_{b0}/f_{c0}$	$K_c$
30°	0.1	1.16	0.667

Elastic material model of nine engineering constants to model the linear elastic behaviour of FRP sheet was utilised in the model.

The general purpose FE software ABAQUS was used. The concrete was modeled using eight node linear brick element C3D8 and the FRP sheet was modeled using a four node general purpose shell S4. Boundary conditions include rotational and displacement degree of freedom (DOF) for nodes at the bottom while displacement control mode was applied to the opposite end of the cylinder. The interaction between the concrete surface and the FRP was modeled using a surface tie, assuming that good bond exists between the two surfaces until failure.

Abdelrahman and El-Hacha (2014) reported good agreement between the FE numerical predictions and the experimental results.

## **2.7 Summary**

This chapter presented a review of the existing literature knowledge relevant to concrete confined with SFRP jacket as well as other types of FRP jackets, such as CFRP. The review revealed that the amount of research conducted on SFRP-confined concrete is rather very limited. Furthermore, Despite the fact that numerous predictive empirical, analytical and FE models do exist nowadays to predict the ultimate stress, ultimate strain and the full stress-strain behaviour of GFRP-, CFRP- and AFRP-confined concrete, the validity of these models for SFRP-confined concrete has not yet been well established. It is therefore important to carry out more experimental investigations on SFRP-confined concrete as a first step into verifying the existing models or developing a more suitable analytical and numerical modeling technique to accurately simulate the behaviour of SFRP-confined concrete.

The next chapter presents the details of the experimental investigation conducted on small-scale unreinforced SFRP-and CFRP-confined concrete cylinders subjected to monotonic, concentric uniaxial compression.

## Chapter Three: **Experimental Program**

### **3.1 Introduction**

This chapter presents the experimental investigation conducted on small-scale unreinforced concrete cylinders confined with SFRP and CFRP jackets and subjected to monotonic concentric uniaxial compression loading. Following the experimental program overview, the material properties of concrete and the strengthening materials (CFRP, SFRP and epoxy), cylinders fabrication and FRP wrapping procedures, instrumentation techniques, test setup and testing procedures will be discussed in detail in the subsequent sections.

### **3.2 Experimental Program Overview**

The experimental program was designed mainly to investigate the compressive behaviour of SFRP-confined concrete cylinders subjected to monotonic concentric uniaxial compression loading and compare it to those exhibited by CFRP-confined concrete cylinders. The variables being considered were the concrete compressive strength, and the type and thickness of FRP jacket. The cylinders were divided into two groups based on the target unconfined concrete compressive strength. In each group, three unwrapped control cylinders were tested and represented a benchmark for the FRP confinement configurations in the group. For each FRP confinement configuration investigated, three nominally-identical specimens were prepared and tested for comparison purposes.

In total, 42 circular small-scale unreinforced concrete cylinders were prepared and tested, including 18 specimens wrapped with SFRP, 18 specimens wrapped with CFRP and 6 unwrapped control specimens. All specimens had an outer diameter of 150 mm and height of 300 mm. The specimens were cast in two batches with different concrete mix designs to produce two

different grades (specified concrete compressive strength) of 35.0 MPa to 45.0 MPa. Other details of the specimens are summarized in Table 3-1.

**Table 3-1: Summary of test specimens**

Concrete		Specimen ID	Number of Cylinders	Confinement Configuration	
Grade (MPa)	Batch			Fibre Type	Numbers of FRP Layers
35.0	1	C35.0-UW	3	-	-
		C35.0-SFRP1	3		1
		C35.0-SFRP2	3	SFRP	2
		C35.0-SFRP3	3		3
		C35.0-CFRP1	3		1
		C35.0-CFRP2	3	CFRP	2
		C35.0-CFRP3	3		3
45.0	2	C45.0-UW	3	-	-
		C45.0-SFRP1	3		1
		C45.0-SFRP2	3	SFRP	2
		C45.0-SFRP3	3		3
		C45.0-CFRP1	3		1
		C45.0-CFRP2	3	CFRP	2
		C45.0-CFRP3	3		3

Conventional foil strain gauges were used to obtain axial and lateral strain data. Independent axial and lateral displacement measurements were also obtained using Linear Strain Converters (LSCs) and the Digital Image Correlation (DIC) technique. Results were compared with those obtained from strain gauges measurements. Axial compressive loading was applied through a load control mechanism at a rate of 0.15 MPa/s – 0.35 MPa/s until complete failure.

A positive sign is assigned to indicate a compressive load, stress and strain and a negative sign to indicate a tensile stress and strain, unless otherwise specified. The metric unit system is used throughout the thesis.

### ***3.2.1 FRP Wrap Configuration Designation***

The designation system that has been assigned to cylinders and is referred to hereafter in all subsequent discussions and graphical plots is presented next. The designation system adopted allows useful information about concrete strength and FRP configuration to be deducted from; it takes the following general form:

$$C(F)\text{-FBR}(N)\text{-SP}\#(M)$$

where;

C = Cylinder;

F = Concrete 28-day specified compressive strength;

FBR = Fibre type;

N = Number of plies;

SP = Specimen number representation;

M = Specimen number ( $1 \leq M \leq 3$ )

It should be noted that when  $N=0$ , that is, when the specimen is unwrapped, the notation FBR(N) will be simply replaced by UW notation. It should also be noted that when it is referred to the group of FRP configuration rather than a particular specimen, the notation SP(M) will be discarded.

For example, when two plies of unidirectional carbon fibre composite is wrapped around a concrete cylinder that has a specified compressive strength of 35 MPa, and that the cylinder is specimen number 3 in that group, then the designation is written as C35.0-CFRP2-SP3.

### 3.3 Material Properties

#### 3.3.1 Concrete

Normal strength concrete was used throughout the experimental program. The concrete was produced in two batches; the first batch was a design-mix prepared in the civil engineering lab at the University of Calgary; the second batch was a ready-mixed concrete delivered by a local supplier, Lafarge, Canada. Details of the concrete mix designs for both batches are shown in Table 3-2. Three control specimens from each batch were tested at 28-day age to determine the unconfined concrete compressive strength.

**Table 3-2: Summary of concrete mix design**

Mix Design	Units	Batch	
		1	2
w/c	ratio	0.59	0.38
Portland Cement	kg/m <sup>3</sup>	315	545
Water	kg/m <sup>3</sup>	186	207
Coarse Aggregate	kg/m <sup>3</sup>	1085	1035
Fine Aggregate	kg/m <sup>3</sup>	870	516

#### 3.3.2 SFRP Sheets

SFRP sheet 3×2-20-12, manufactured by Hardwire LLC and shown in Figure 3-1, is a unidirectional steel wire cords fabric. The first two digits (3×2) defines the hardwire cord type; the 3×2 wire cord is made by twisting 5 individual filaments together – 3 straight filaments wrapped by 2 filaments at a high twist angle. The third digit (20) indicates the tape density, in this case 20 wires per inch (WPI). The last digit (12) indicates the width of shipped sheets in inches. Typical properties of single cord, SFRP sheet and SFRP composite are shown in Table 3-2, Table 3-3 and Table 3-4, respectively, as provided by the manufacturer.



**Figure 3-1: SFRP sheet**

**Table 3-3: Typical properties of single 3×2 roving (cord), HARDWIRE (2014)**

Properties	3×2 Cord
Filament Diameters (mm)	0.35
Break (kN)	1.54
Strain to Failure (%)	2.1
Length per kg (m)	54.19

**Table 3-4: Typical properties of SFRP sheet, HARDWIRE (2014)**

Properties	3×2-20
Sheet Density (wire/cm)	7.87
Sheet weight (kg/m <sup>2</sup> )	3.01
Ultimate Tensile Load (kg/cm)	10.9
Sheet Thickness (mm)	1.2

**Table 3-5: Typical properties of SFRP composite system, HARDWIRE (2014)**

Properties	3×2-20
Laminate Density (kg/m <sup>3</sup> )	3110
Laminate thickness (mm)	1.2
Ultimate Tensile stress (MPa)	985
Effective Modulus (GPa)	66.1

### **3.3.3 CFRP Sheets**

SikaWrap<sup>®</sup> Hex 230C, manufactured by Sika Canada Inc. and shown in Figure 3-2, is a unidirectional carbon fibre fabric.

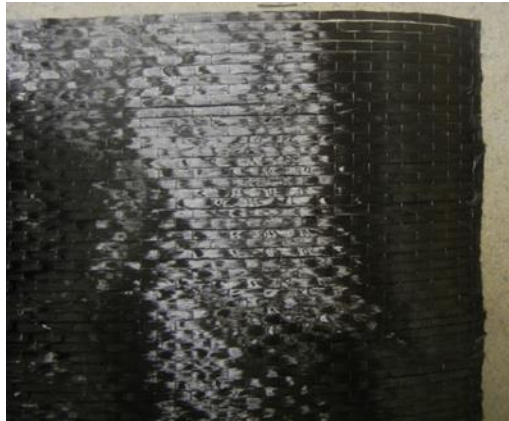


**Figure 3-2: CFRP sheet**

Typical properties of fibre and cured laminate with Sikadure 330 Epoxy are shown in Table 3-6 and Table 3-7, respectively, as provided by the manufacturer.

**Table 3-6: Typical properties of carbon fibre, SikaWrap® Hex 230C (2014)**

Properties	Carbon Fibre
Tensile Strength (MPa)	3450
Tensile Modulus (GPa)	230
Elongation (%)	1.5
Density (g/cc)	1.8

**Table 3-7: Typical properties of carbon cured laminate, SikaWrap® Hex 230C (2014)**

Properties	Value		ASTM Method Test
	Average	Design	
Tensile Strength (MPa)	894	715	D-3039
Tensile Modulus (GPa)	65.402	61.012	D-3039
Tensile Elongation (%)	1.33	1.09	D-3039
Compressive Strength (MPa)	779	668	D-695
Compressive Modulus (GPa)	67.003	63.597	D-695
Shear Strength (MPa)	63	56	D-3518
Shear Modulus (GPa)	2.902	2.8	D-3518
Laminate Thickness (mm)	0.381	0.381	-

While the material properties are typically given as averages, or the design values, as shown in the third column in Table 3-7, are also provided by the manufacturer. The design value is calculated as the average value minus 2 standard deviations and accounts for any reasonable

material property variation due to local effects such as environmental, preparation, application, curing and test methods, SikaWrap® Hex 230C (2014).

### 3.3.4 Epoxy Adhesive

Sikadure®-330, manufactured by Sika Canada Inc. and shown in Figure 3-3, is a two part epoxy impregnation resin conventionally used in field-laminated carbon and steel fibre fabrics to produce carbon or steel fibre reinforced polymers. The epoxy consists of two components; a resin, part A, and a hardener, part B with a mixing ratio of 4:1 by weight. The pot life of the epoxy mixture is 57 minutes at 35° C. Curing time was a minimum of 4-5 hours at room temperature.



**Figure 3-3: Sikadure®-330**

Typical mechanical properties of Sikadure®-330 are shown in Table 3-8 as provided by the manufacturer.

**Table 3-8: Typical mechanical/physical properties of Sikadure®-330, Sikadure®-330 (2014)**

Properties	Value	ASTM Method Test
Tensile Strength (MPa)	33.8	ASTM D-638
Flexure Elastic Modulus (GPa)	3.489	ASTM-D-790
Flexural Strength (MPa)	60.6	ASTM D-790
Elongation @ Break (%)	1.2	ASTM D-638

### **3.4 Cylinders Fabrication**

#### ***3.4.1 Concrete Casting Procedure***

Altogether, 42 concrete cylinders were cast in two batches. Each batch consisted of 21-150 mm × 300 mm cylinders. The procedures for concrete casting, finishing and curing were in accordance with CAN/CSA/A23.2-3C.

The plastic forms were cleaned, and the inner surface was sprayed with form oil. The pre-drilled hole at the bottom centre of each plastic form was filled with plasticine. The concrete was placed into the plastic forms in two layers and vibrated on a vibrator table until a dense, homogeneous and free of voids paste was achieved. After the final layer was vibrated, extra concrete on the top was removed and the top surface was leveled with the top edge of the form using a trowel. The forms were then carefully carried to another table and covered with a non-absorptive plastic sheet to prevent moisture loss.

The concrete was allowed to set for 24 hours before the forms were removed by applying compressed air through the form's bottom centre hole; after which additional curing regime was applied where the concrete cylinders were left at room temperature for 7 days before grinding the top and bottom ends of the concrete cylinders.

#### ***3.4.2 Cylinder's Ends Preparation***

The top and bottom ends of the concrete cylinders are usually neither smooth nor leveled.

Therefore, both end surfaces were ground until smooth, flat and perpendicular to the long axis of the cylinder, as shown in Figure 3-4. This will result in cylinder's top and bottom surfaces being in full contact with the steel platens of the loading machine while orthogonal to the loading axis so that the possibility of any accidental loading eccentricity is minimized. The grinding machine used to grind the cylinders is shown in Figure 3-5.

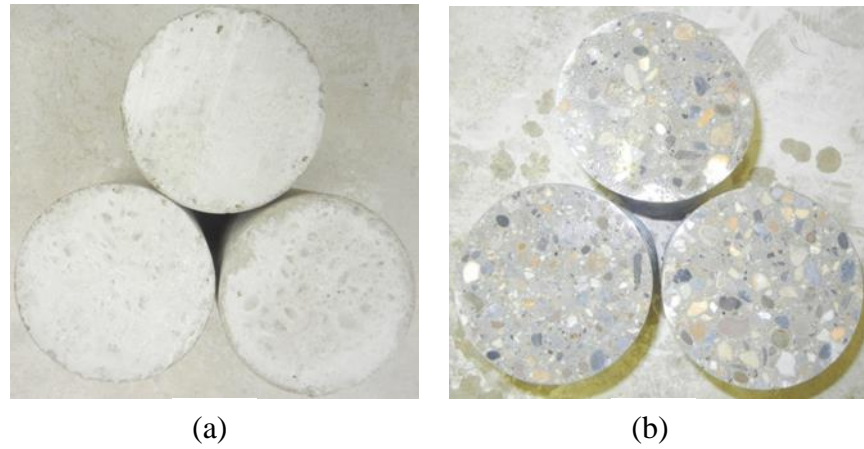


**Figure 3-4: Concrete cylinders end surfaces treatment: (a) Before grinding, (b) After grinding**

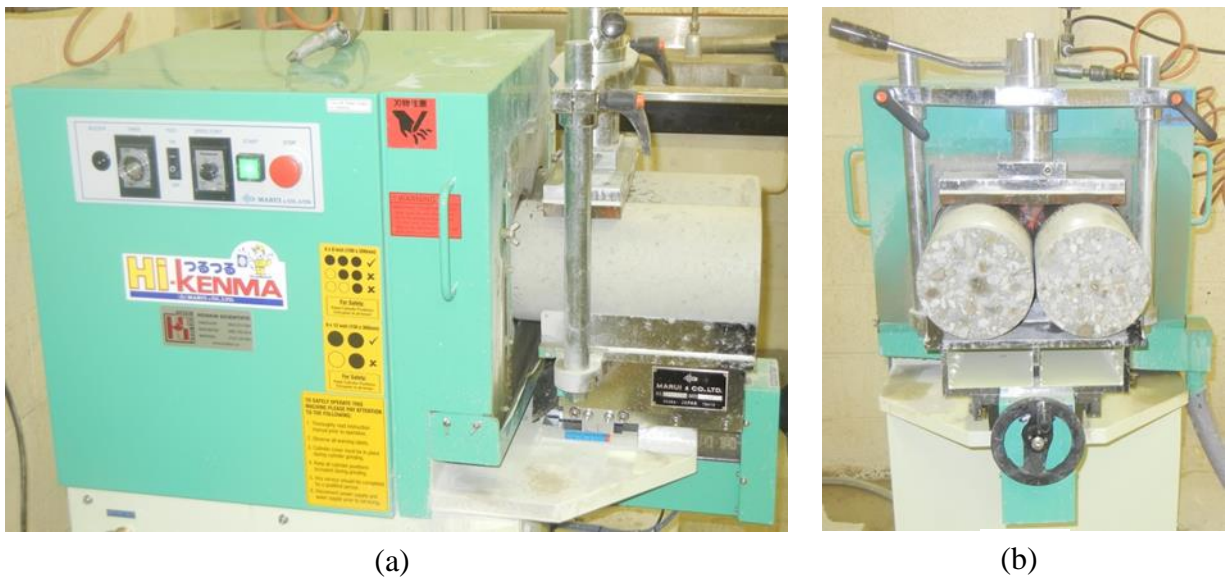


**Figure 3-5: Grinding machine: (a) Isometric view, (b) Front view**

### ***3.4.3 FRP System Installation Procedure***

#### ***3.4.3.1 Cylinder's Surface Preparation***

No special surface treatment is required for concrete substrates prior to FRP wrapping application except typical cleaning. The cylinders were washed and all dust and loose material

was completely removed. The cylinder surface should also be free from fins and any sharp edges. The concrete substrates should be completely dry and free from moisture at the time of wrapping. All specimens were blown clean by compressed air immediately prior to FRP fabric installation.

#### 3.4.3.2 Fabric and Epoxy Preparation

CFRP sheets were cut into desired lengths and widths using scissors while stiffer SFRP sheets were cut using a snipping tool. The sheet lengths were calculated based on 471 mm circumferential length for one layer in addition to 100 mm overlap. In the cases of two or three layers configuration, the former number was doubled or tripled, respectively while the latter number was kept constant for all confinement configurations.

Epoxy resin part A and hardener part B were mixed together at a ratio of 4:1 by weight and stirred at least 5 minutes to form a light gray soft brushable paste.

Prior to fabric saturation process, clean non-absorptive plastic sheets were always laid onto the working area to avoid any contamination of the composite system. Saturation of FRP sheets with the epoxy was achieved using a paint brush. As a general rule, a volumetric ratio of 10:8 (fibre-epoxy) was targeted for the composite system.

#### 3.4.3.3 FRP Fabric Installation

##### 3.4.3.3.1 CFRP Fabric Installation

The mixed epoxy was applied directly in a thin layer to the fabric and the concrete substrate using a brush. The cylinder was kept vertical and CFRP was carefully wrapped around it with a slight pressure using a hand roller to ensure that resin is squeezed out between and through the fibres strands and distributed evenly over the whole fabric surface. Additional thin layer of

epoxy is applied at overlap area to ensure good bonding. The procedures of wrapping the cylinders with CFRP sheets are shown in Figure 3-6.



**Figure 3-6: Procedures for wrapping cylinders with CFRP sheets**

#### 3.4.3.3.2 SFRP Fabric Installation

Stiff SFRP sheets, while wrapping around the cylinder circular surfaces, tend to open and detach from the concrete substrate. Hence, a day prior to SFRP fabric installation; duct tape was applied along the full width of the sheet, 20mm from the edge, and epoxy paste was applied along this 20mm strip. The cylinder was then placed onto the epoxy strip, and left for one day to cure.

At the time of SFRP fabric installation, the duct tape was removed; and the cylinder was placed horizontally, epoxy was applied in a thin layer to the concrete substrate and SFRP fabric using a paint brush. The cylinder was carefully rolled over the fabric with a slight constant pressure to ensure that the fibre sheet was flatly adhered to the concrete and no air pockets were trapped, and that the resin was squeezed out between and through the fibre strands and distributed evenly over the whole fabric surface. The orientation of fibres was checked with the naked eye.

The wrapped cylinders were then wrapped with a flexible plastic sheet and clamped to ensure complete contact between the concrete surface and the SFRP sheets, the specimens were left for one day to cure at room temperature before the clamps and plastic wrap were removed. The procedure of wrapping the cylinders with SFRP is shown in Figure 3-7.

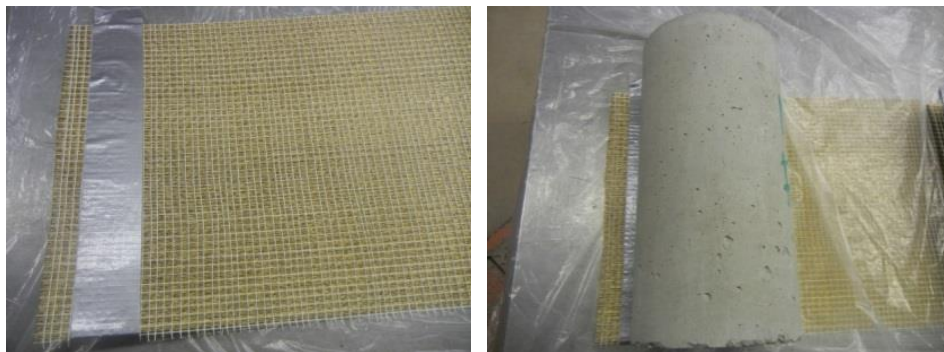




**Figure 3-7: Procedures for wrapping cylinders with SFRP sheet**

### ***3.4.4 Strain Gauge Installation Procedure***

#### ***3.4.4.1 Surface Preparation***

The surface preparation for strain gauge installation includes five basic operations; solvent degreasing, sanding, application of gauge layout lines, conditioning and neutralizing.

To develop a chemically clean surface appropriate for gauge installation, the gauging area was thoroughly cleaned and degreased from any dust, laitance and grease accumulated during composite curing and subsequent handling using isopropyl alcohol. It is also equally important to prevent recontamination of a once-cleaned surface. To achieve this, the surface preparation procedures, that will be discussed later, were applied to an area that is significantly larger than that occupied by the gauge to prevent dragging contaminants from the uncleaned area boundary. The gauze sponge and the cotton swap were never reused for another site and the surrounding

environment was always cleaned beforehand to prevent airborne contamination from dust on the work benches.

The surface texture of appropriate roughness for bonding was achieved by sanding the area using a 320 grit silicon carbide paper. The sanding residues were then removed and the area was cleaned with alcohol. Strain gauge layout lines for locating and orienting the strain gauges were marked on the surface at the point where the strain measurement is to be made. The surface was then cleaned with M-prep conditioner A, followed by M-prep Neutralizer 5A.

#### 3.4.4.2 Gauge Mounting

A plastic plate was chemically cleaned with M-prep conditioner A followed by M-prep Neutralizer 5A. The gauge was removed from its transparent envelope by grasping the edge of the gauge backing material using tweezers, and placing down on the pre-cleaned plastic plate. The solder terminal was positioned on the plate adjacent to the gauge approximately 1.6 mm apart. Gauge installation tape was used as a carrier to aid in positioning the strain gauge and terminal; one end of the tape was tacked to the plastic plate behind the gauge and terminal and was wiped forward onto the terminal and gauge. The tape was raised from the plastic plate carefully at a shallow angle bringing the gauge and terminal up with it. The gauge tape assembly was positioned so that the triangle marks on the gauge were over the layout lines on the specimen.

The end of the gauge tape assembly was then raised at a shallow angle until the gauge and terminal were free from the specimen surface, and lay flat with the bonding surface exposed, M-bond 200 catalyst was applied to the bonding surface and allow to dry for 1 minute under room temperature.

Holding the gauge tape assembly at the same position, one to two drops of M-bond 200 adhesive was applied at the fold formed by the junction of the tape and specimen surface. The tape was then rotated back to approximately 30 degree angle and with a piece of gauze, the gauge tape assembly was wiped forward bringing the gauge and terminal back over the alignment marks and producing a very thin uniform layer of adhesive.

#### 3.4.4.3 Curing

Firm thumb pressure was applied to the gauge and the terminal area for at least 1 minute as recommended by the manufacturer.

#### 3.4.4.4 Soldering

Soldering is the process of joining two metals together using a solder alloy. The 63/37 (tin/lead) type solder, most commonly used for hand soldering, was used. The Soldering machine used is shown in Figure 3-8.

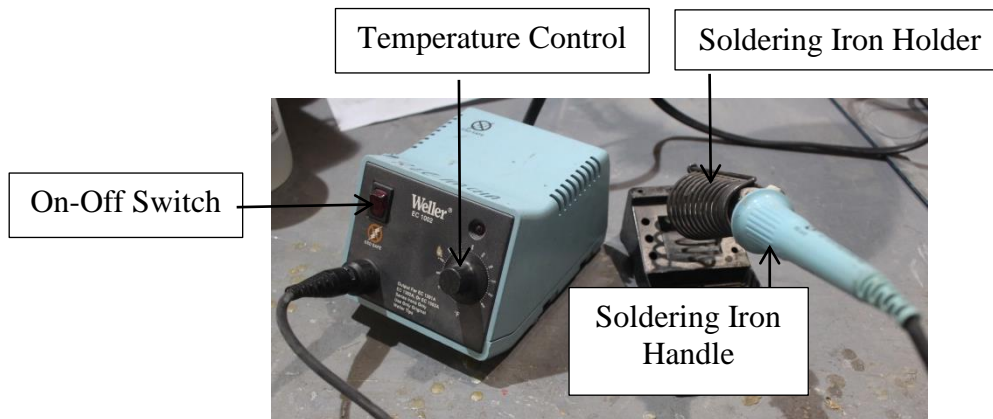


**Figure 3-8: Soldering machine**

The soldering station was set to 183°C, which was deemed appropriate for the solder in use. The soldering tip was allowed to heat and then tinned by feeding the heated tip with a generous amount of solder. Oxidation of the soldering tip hinders the soldering operation; hence, excess melted solder was ensured to remain on the soldering tip at all times.

A single strand of wire was used as a jumper between the terminal and the strain gauge solder tab; a single strand of wire was first separated out and trimmed short, wire ends were then slightly bent to form a spring like loop, and was firmly placed over the connection area. Holding the soldering pencil nearly horizontal and placing the solder wire on the gauge tabs, the hot soldering tip was pressed firmly onto the gauge tabs for about one to two seconds, then simultaneously both the soldering tip and solder wire was lift from the tab area. The same process was repeated to join the instrumentation cable to the terminal tabs.

#### 3.4.4.5 Verification

After the entire strain gauge installation process was completed, soldered joints were visually inspected for any peaks, jagged or non-uniform joint surfaces; circuit resistance-to-ground was also checked to ensure proper soldering. For a properly-installed circuit, the resistance across the strain gauge should be close to 120  $\Omega$ .

Electrical tape was applied on the top of strain gauge to protect it from dust, moisture and paint spray.

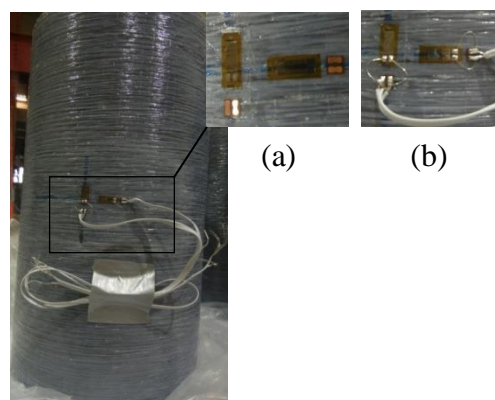


**Figure 3-9: Strain gauge installation: (a) After gauge mounting, (b) After Soldering**

### ***3.4.5 Cylinder's Surface Finishing Procedure***

All FRP-wrapped cylinders' surfaces were painted with a high contrast random pattern which consists of a white paint base followed by a sprayed black colour random speckle pattern to provide the required texture. The cylinders' interim white paint and the final paint pattern are shown in Figure 3-10.

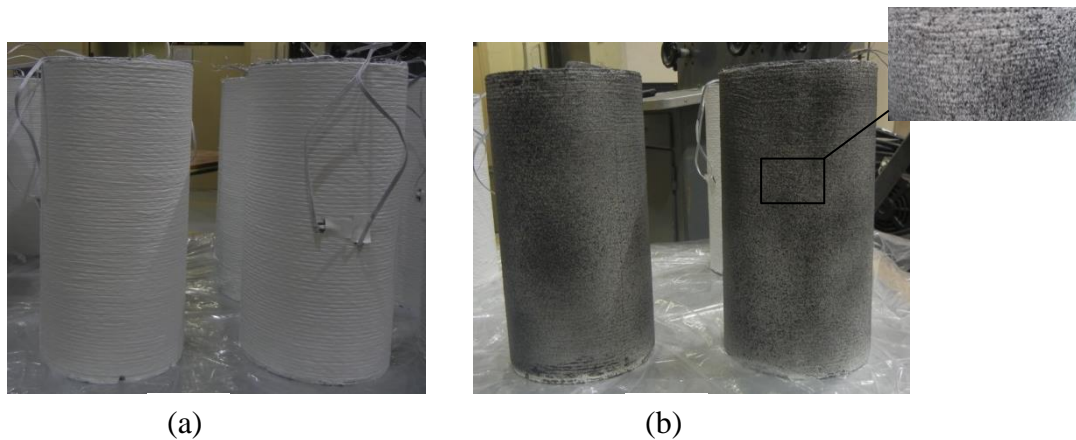


**Figure 3-10: Surface finish: (a) White paint, (b) Final finish**

## **3.5 Instrumentation**

### ***3.5.1 Strain Gauges***

General purpose foil strain gauges with a resistance of 120  $\Omega$  and a gauge length of 6.35 mm from Micro-Measurement were used. Unwrapped specimens were externally instrumented with four strain gauges installed in the vertical and radial direction at the mid height of the specimen and at opposite locations (180° apart). Wrapped specimens were externally instrumented with only two strain gauges, vertical and radial installed on one side of the specimen. Typical locations of the strain gauges are shown in Figure 3-11 for unconfined and confined configuration.

Conventional foil strain gauge construction involves a photo etched metal foil pattern mounted in a plastic backing as shown in Figure 3-12. The performance characteristics of a strain gauge are affected by several parameters such as strain-sensitive alloy; backing material; and gauge length. The selected strain gauge alloy and backing material were copper-nickel, commercially known as constantan, and flexible polyimide, respectively. The constantan alloy has adequate high strain sensitivity or gauge factor and high elongation capacity. The polyimide backing material is tough and extremely flexible and the high peel strength of the foil on the polyimide backing makes polyimide backed gauges less sensitive to mechanical damage during installation. Gauge length is very important factor in determining the gauge performance. A gauge length between 3 – 6 mm is preferable for general use. However, in strain measurement on nonhomogeneous materials, such as concrete, it is recommended to use a strain gauge length of at least 5 times the diameter of largest aggregate in the concrete so that sufficient gauge length spans several pieces of aggregate in order to measure representative average strain rather than local strain fluctuations at the interfaces between aggregate particles and the cement. Nevertheless, longer strain gauges were not available and 6.35 mm length strain gauges were used for control specimens as well.

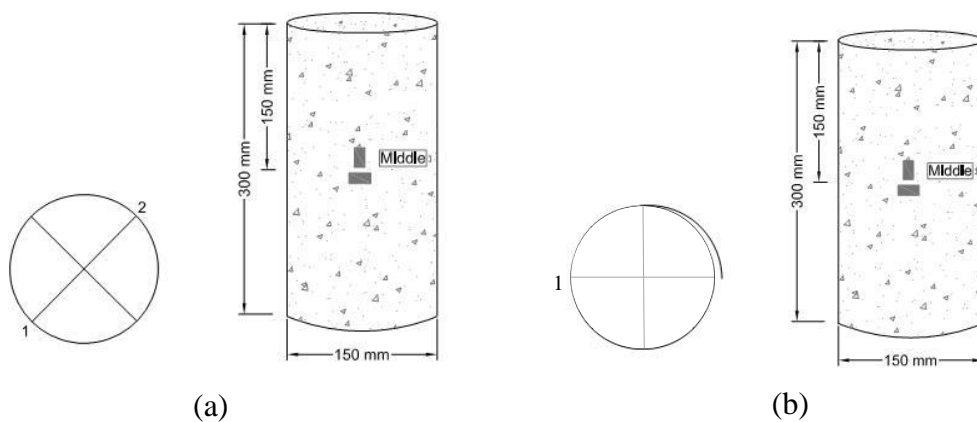


**Figure 3-11: Instrumentation of strain gauge: (a) Unconfined, (b) Confined cylinder**

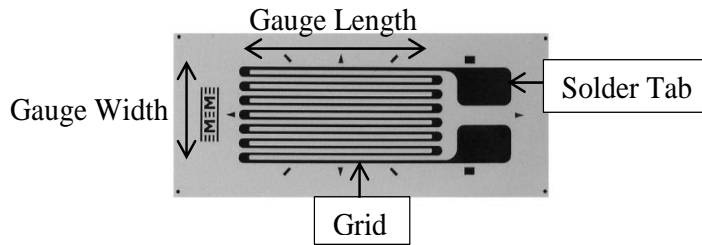


**Figure 3-12: Conventional foil strain gauge**

Strain gauge properties are displayed in Table 3-9.

**Table 3-9: Strain gauge properties, Micro-Measurement (2014)**

Properties	Steel Gauge
Series Designation	EA
Gauge Material	Constantan Alloy
Backing Material	Polyimide
Gauge Factor	2.085±0.5%
Transverse Sensitivity	(0.6±0.2)%
Resistance, Ω	120.0±0.15%
Strain Range	±5%
Gauge Length, mm	6.35
Grid Width	3.18

Adhesive is used to bond the gauge to the specimen surface. The adhesive becomes part of the gauge system and correspondingly affects the gauge performance. The adhesive chosen required 30 seconds thumb pressure for initial set and less than 5 minutes curing time. The strain limit of this adhesive is approximately 10% which well exceeds the failure strain expected.

### **3.5.2 Linear Strain Converter LSC**

Wenglor high-performance distance sensors were utilised. The sensor uses a laser light source and determines the object's distance using angular measurement. The sensor working range is between 40 to 160mm, which was deemed appropriate for the intended use. The measured value is output in voltage.

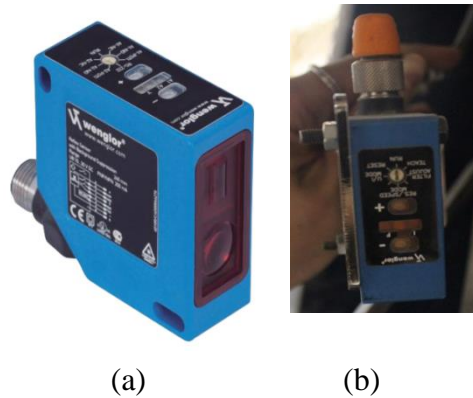


**Figure 3-13: Linear Strain Converter (LSC): (a) Isometric view (b) Top view**

### ***3.5.3 Digital Image Correlation (DIC) Technique***

For all FRP-confined columns, two high resolution (15.1 and 18 megapixel) cameras were used, each installed on one side of the cylinder in order to capture the strain behaviour over the entire height of the cylinder. To enable the DIC technique measurement, random speckle patterns were sprayed on all specimen surfaces.

The camera was placed in full zoom orientation and in sharp focus, whereas the automatic image stabilization and the auto focus of the lens was turned off.

The images and the data acquisition system were initiated at the same time to synchronise the images with the applied load. The images were captured every 5 seconds until the failure of the cylinder.

Each camera was connected to a computer with windows XP Pro operating system, in which the data are acquired and subsequently processed using the GeoPIV software through Matlab software.

### 3.6 Test Setup

Test set-up is shown in Figure 3-14. Two high resolution (15.1 and 18 megapixel) cameras were used; each camera was placed on a tripod in front of one side of the cylinder. The camera orientation was adjusted so that the camera line of sight is normal to the surface of the cylinder. Four portable work lights were installed to provide a well-lit environment and to maintain a consistent amount of light throughout the test.

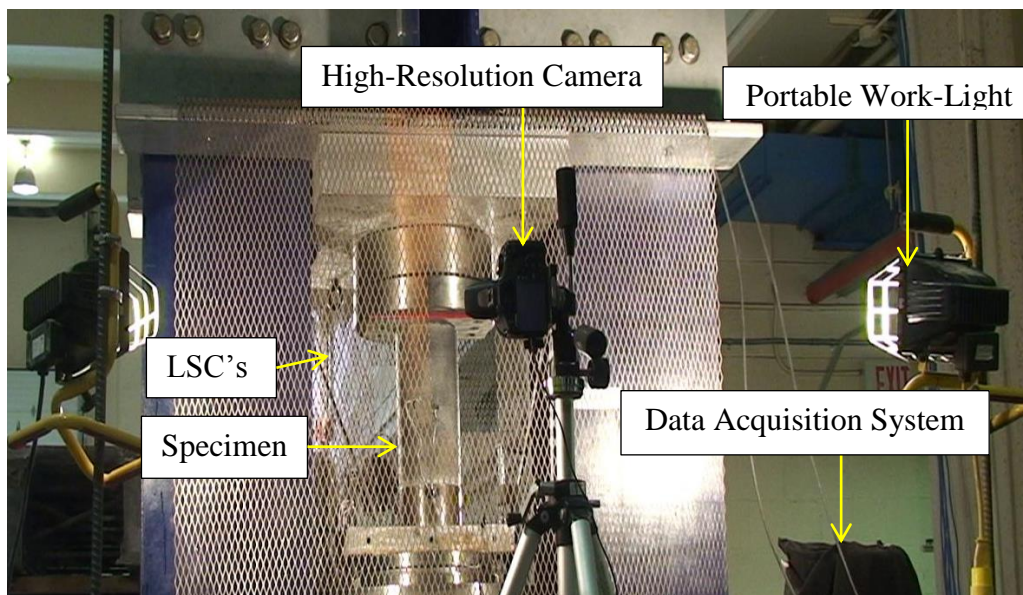


Figure 3-14: Test set-up - east side (west side similar)

### 3.7 Loading

A 9 MN loading frame as shown in Figure 3-15 was used to test all cylinders under monotonic concentric axial compression. It operates hydraulically and is manually controlled.

The welded wide-flange (WWF) crosshead is fixed while the platform moves upward according to the input loading rate. The steel platen affixed to the crosshead acts like swivel which adjust itself if any non-orthogonality exists.

Testing concrete cylinders were performed in accordance to CAN/CSA/A23.2-9C. Due to the machine constraints, load control rather than displacement control mechanism was used. During plastic deformation and prior to failure, axial displacement occurs at a much faster rate under the same load increment and so quickly that the cylinder's post failure behaviour could not be captured as clearly as in displacement control mechanism.

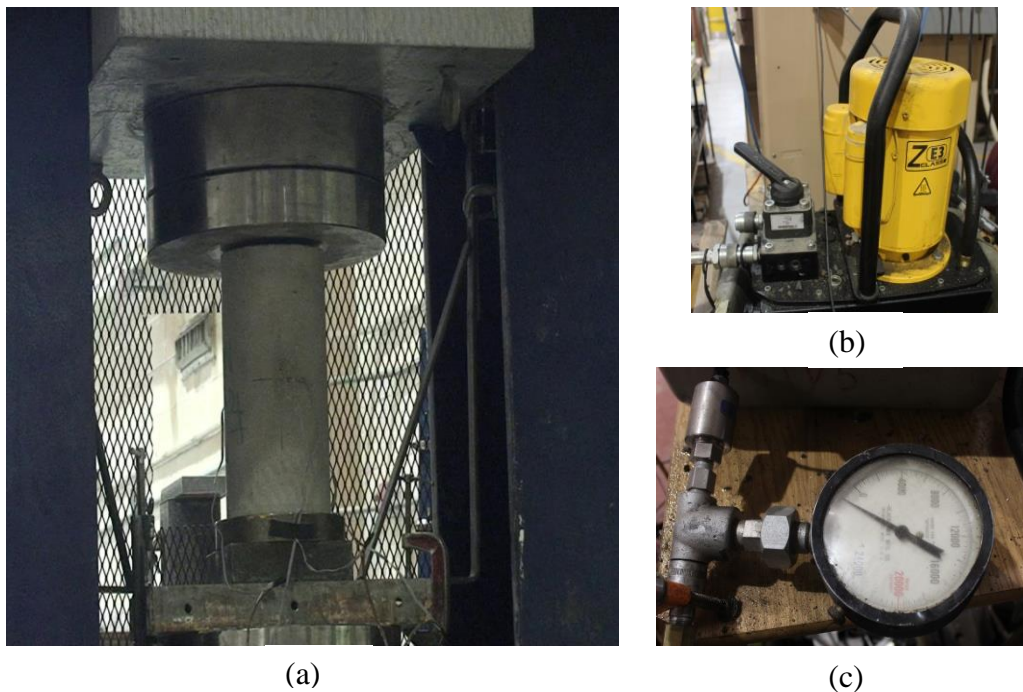


**Figure 3-15: Testing machine: (a) Loading frame (b) Hydraulic pump (c) Pressure transducer**

### 3.8 Summary

The current chapter presented the experimental program conducted on small scale unreinforced CFRP-and SFRP- confined concrete cylinders. Experiment test matrix, material properties, fabrication procedure, instrumentation, test setup and loading were discussed in detail throughout the chapter.

In the next chapter, the results from this experimental investigation will be analysed and the behaviour of the SFRP-confined concrete will be closely examined. The comparison of the compressive behaviour between the SFRP-and CFRP-confined concrete will also be presented. Furthermore, the data obtained from DIC technique will be first validated, and will subsequently be utilised in studying the axial and lateral strain variation across the full height of confined concrete cylinders.

## Chapter Four: **Compressive Behaviour of CFRP-and SFRP-Confined Concrete Cylinders**

### **4.1 Introduction**

The experimental results of concentric, monotonic, uniaxial compression tests that have been conducted on small- scale unreinforced confined concrete cylinders are interpreted, discussed and used in a systematic study on the compressive behaviour of CFRP- and SFRP-confined concrete cylinders. The main compressive behaviour aspects examined for both CFRP-and SFRP-confined cylinders include the failure mechanism; ultimate axial strength, ultimate lateral and axial strain, stress-strain behaviour, and axial and lateral strain distribution over the full height of the FRP jacket as well as the FRP strain efficiency utilising the DIC technique. The chapter closes with a performance comparison between CFRP-and SFRP-confined concrete by examining a series of parameters, including confinement effectiveness coefficient; and strain and energy ductility indices.

### **4.2 Ancillary Test Results**

#### ***4.2.1 Concrete***

As previously mentioned in Section 3.3.1, two different batches of concrete were mixed and cast. The target unconfined compressive concrete strengths were 35 and 45 MPa. Three standard size cylinders from each batch were tested at 28 days to determine the actual unconfined peak compressive strength and the corresponding axial and lateral strain. Results from the compression tests are summarized in Table 4-1.

**Table 4-1: Concrete ancillary test results**

Specimen Designation	Batch #	Compressive Strength		Ultimate Axial Strain		Ultimate Lateral Strain	
		Value (MPa)	Avg. $\pm$ SD (MPa)	Value ( $\mu\epsilon$ )	Avg. $\pm$ SD ( $\mu\epsilon$ )	Value ( $\mu\epsilon$ )	Avg. $\pm$ SD ( $\mu\epsilon$ )
C35.0-UW-SP#1	1	36.6	37.3 $\pm$ 0.7	868	1959 $\pm$ 1014	1038	1373 $\pm$ 669
C35.0-UW-SP#2		38.1		2873		2144	
C35.0-UW-SP#3		37.3		2135		938	
C45.0-UW-SP#1	2	44.1	42.4 $\pm$ 1.4	2750	1757 $\pm$ 892	910	1112 $\pm$ 227
C45.0-UW-SP#2		42.0		1495		1358	
C45.0-UW-SP#3		41.3		1024		1069	

As can be seen from Table 4-1, the actual average concrete strengths for both batches were different from the target values. Single factor Analysis of Variance (ANOVA) test using Microsoft Excel was conducted to determine whether the two concrete groups were statistically different or they belonged to the same concrete compressive strength category. ANOVA analysis examines the null hypothesis that the means of all groups are equal. The variability between groups (the scatter of the means) to the variability within the group (how much natural scatter is expected) is evaluated by calculating the F ratio. The F ratio is defined as the ratio of mean square (MS) between the groups to the MS within the group. If the F ratio is greater than F critical, the null hypothesis is rejected and the two groups are deemed statistically different. The results from the ANOVA analysis show that significant statistical differences do exist between the concrete cylinders from batch 1 and batch 2. The ANOVA test results are displayed in Table 4-2.

**Table 4-2: Summary of ANOVA analysis results for unconfined concrete cylinders**

Source of Variation	SS	df	MS	F ratio	P-value	F critical
Between Groups	39.234	1	39.234	30.032	0.0053	7.708
Within Groups	5.225	4	1.306			
Total	44.459	5				

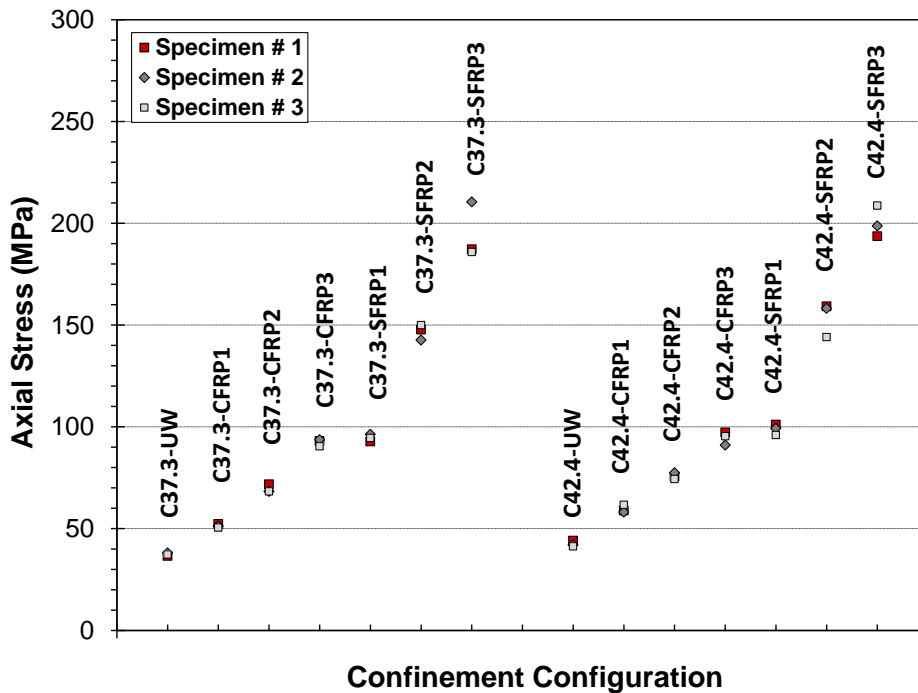
In Table 4-2, SS represents the sum of squared deviation from the mean, df represents groups degree of freedom; if n represents the number of groups and k represents the number of data

values per group, then, the between group degree of freedom is  $(n-1)$  and the within group degree of freedom is  $n(k-1)$ , MS represents the mean square and is calculated by dividing SS by the corresponding df. The P value represents the number that the test statistic must exceed to reject the null hypothesis.

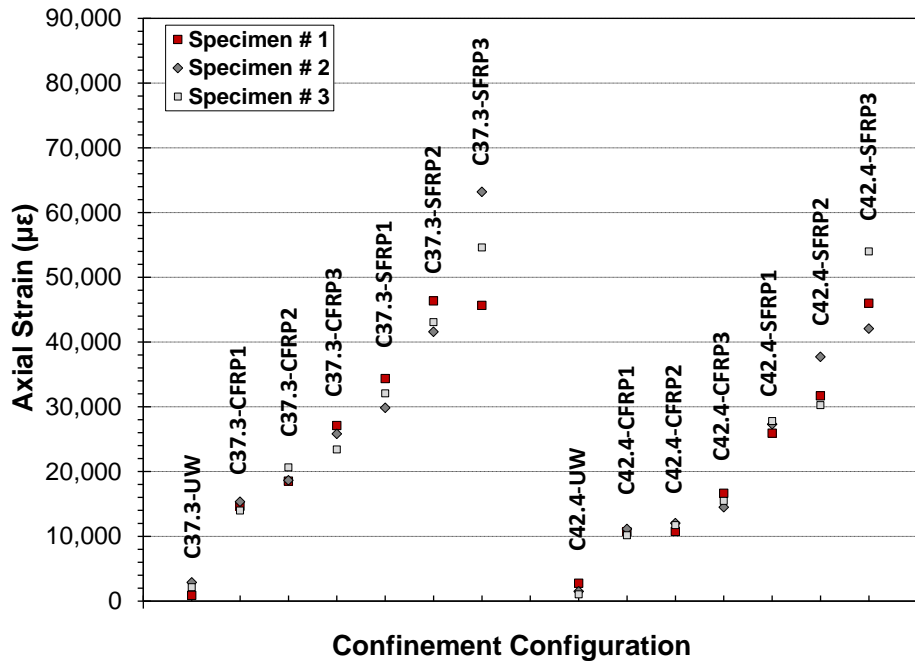
Since the target and the actual compressive strengths are different and to ensure clarity in all discussions that follow, the target concrete compressive strength in the first part of specimen designation will be replaced hereafter by the corresponding actual compressive strength obtained from the compression test.

### 4.3 Test Results Statistical Analysis

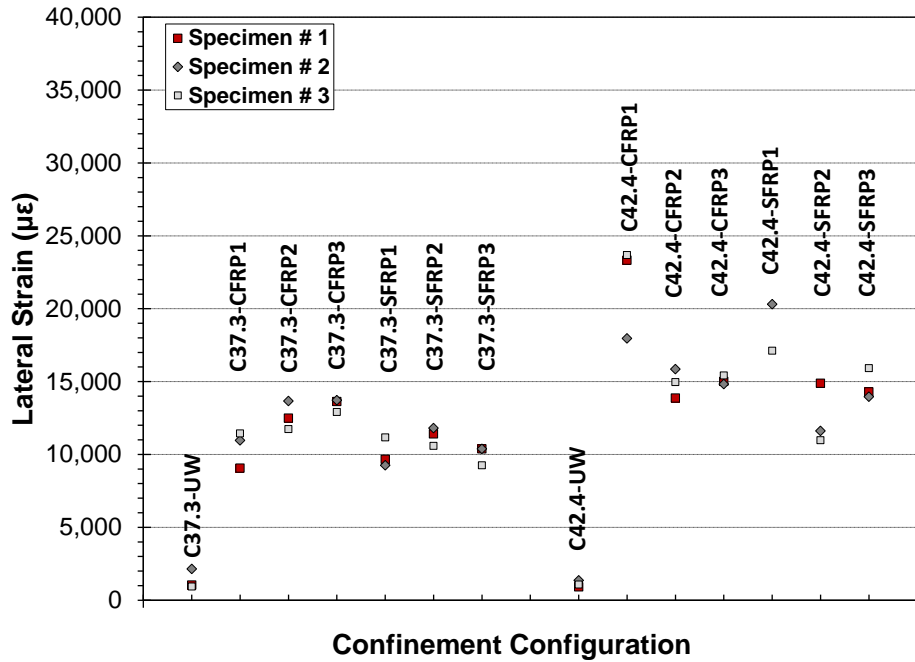
The experimental data results in terms of axial stress, axial strain and lateral strain for all confinement configurations are displayed in Figure 4-1.



(a)



(b)



(c)

Figure 4-1: Experiment results (a) Axial stress (b) Axial strain (c) Lateral strain for all confinement configurations

It should be noted that the terms lateral (radial) or circumferential strain are used interchangeably in all discussions hereafter when referring to circumferential (hoop) strain in the direction of FRP fibres. This is true for confined circular sections as explained next.

The change in the cylinder circumference due to circumferential strain,  $\varepsilon_h$  is

$$2\pi r\varepsilon_h \quad \text{Equation 4-1}$$

Hence, the new circumference is

$$2\pi r + 2\pi r\varepsilon_h = 2\pi r(1 + \varepsilon_h) \quad \text{Equation 4-2}$$

However, this is the circumference of a circle of a radius  $r$  that equals

$$r(1 + \varepsilon_h) \quad \text{Equation 4-3}$$

Hence, the change in radius is

$$r\varepsilon_h \quad \text{Equation 4-4}$$

Then, the radial (lateral) strain is calculated

$$\varepsilon_l = \frac{\Delta r}{r} = \frac{r\varepsilon_h}{r} = \varepsilon_h \quad \text{Equation 4-5}$$

ANOVA analysis was performed to examine the significance of FRP jacket thickness and type, and the unconfined concrete compressive strength parameters on the ultimate strength of FRP-confined concrete cylinders. ANOVA analysis results are summarized in Table 4-3, Table 4-4 and Table 4-5 for FRP jacket thickness, FRP jacket type and unconfined concrete strength parameters, respectively.

**Table 4-3: Summary of ANOVA analysis results of FRP jacket thickness parameter significance**

Group Designation	Source of Variation	SS	df	MS	F ratio	P-value	F critical
C37.3-CFRP	Between Groups	2532.291	2	1266.145	486.276	2.3E-07	5.143
	Within Groups	15.622	6	2.603			
	Total	2547.914	8				
C42.4-CFRP	Between Groups	1840.654	2	920.327	169.402	5.2E-06	5.143
	Within Groups	32.596	6	5.432			
	Total	1873.251	8				
C37.3-SFRP	Between Groups	15019.430	2	7509.72	108.153	2.0E-05	5.143
	Within Groups	416.617	6	69.436			
	Total	15436.047	8				
C42.4-SFRP	Between Groups	15512.385	2	7756.19	170.65	5.2E-06	5.143
	Within Groups	272.705	6	45.450			
	Total	15785.091	8				

**Table 4-4: Summary of ANOVA analysis results of FRP jacket type significance**

Group Designation	Source of Variation	SS	df	MS	F ratio	P-value	F critical
C37.3-xFRP1	Between Groups	2792.273	1	2792.273	1448.99	2.8E-06	7.708
	Within Groups	7.708	4	1.927			
	Total	2799.981	5				
C37.3-xFRP2	Between Groups	8971.899	1	8971.899	967.721	6.3E-06	7.708
	Within Groups	37.084	4	9.271			
	Total	9008.984	5				
C37.3-xFRP3	Between Groups	15662.349	1	15662.349	161.697	2.2E-04	7.708
	Within Groups	387.447	4	96.861			
	Total	16049.796	5				
C42.4-xFRP1	Between Groups	2308.480	1	2308.480	452.532	2.8E-05	7.708
	Within Groups	20.405	4	5.101			
	Total	2328.885	5				
C42.4-xFRP2	Between Groups	9138.268	1	9138.268	248.226	9.4E-05	7.708
	Within Groups	147.257	4	36.814			
	Total	9285.525	5				
C42.4-xFRP3	Between Groups	16791.172	1	16791.172	487.973	2.4E-05	7.708
	Within Groups	137.640	4	34.410			
	Total	16928.812	5				

**Table 4-5: Summary of ANOVA analysis results of concrete compressive strength significance**

Group Designation	Source of Variation	SS	df	MS	F ratio	P-value	F critical
CFRP1	Between Groups	1001.170	1	100.170	46.301	0.00243	7.708
	Within Groups	8.653	4	2.163			
	Total	108.824	5				
CFRP2	Between Groups	60.555	1	60.555	18.801	0.0122	7.708
	Within Groups	12.882	4	3.220			
	Total	73.438	5				
CFRP3	Between Groups	7.129	1	7.129	1.068	0.359	7.708
	Within Groups	26.682	4	6.670			
	Total	33.812	5				
SFRP1	Between Groups	27.177	1	27.177	5.586	0.077	7.708
	Within Groups	19.459	4	4.864			
	Total	46.637	5				
SFRP2	Between Groups	74.924	1	74.924	1.747	0.2566	7.708
	Within Groups	171.458	4	42.864			
	Total	246.383	5				
SFRP3	Between Groups	50.432	1	50.432	0.404	0.559	7.708
	Within Groups	498.405	4	124.601			
	Total	548.837	5				

Table 4-3 indicates that there is statistical significant difference among groups when groups of different FRP jacket thicknesses compared. Similarly, Table 4-4 indicates significant statistical differences do exist between groups of different FRP jacket type. On the other hand, different concrete compressive strengths are statistically significant for weakly confined concrete cylinders, i.e. concrete cylinders confined with one and two layers of CFRP sheets, while are not significant for moderately and highly confined concrete as shown in Table 4-5. The effect of FRP jacket thickness, type and concrete compressive strength on the ultimate strength of FRP confined concrete will be discussed in more detail in Section 4.4.3.

## 4.4 Compressive Behaviour of CFRP-and SFRP- Confined Cylinders

### 4.4.1 Failure Mechanism

#### 4.4.1.1 CFRP-Confined Concrete Cylinders

Failure of all cylinders confined with CFRP sheets exhibited a typical conical failure mode as shown in Figure 4-2; cylinders failed catastrophically in the middle third sections due to concrete crushing and fibre rupture. Fibre rupture consistently initiated at the beginning of the overlap region. Failure modes for individual cylinders are shown in Appendix A.



**Figure 4-2: Typical failure mode of CFRP-wrapped cylinders**

#### 4.4.1.2 SFRP-Confined Concrete Cylinders

All cylinders wrapped with one SFRP layer exhibited a typical conical failure mode; the middle section failed under concrete crushing and SFRP rupture. Two- and three layers SFRP-wrapped cylinders exhibited a similar failure mechanism; however, SFRP sheet failure was due either to a full de-bonding at the overlap or a combination of rupture and de-bonding. Typical failure modes for all confinement configurations are shown in Figure 4-3. Failure mode for each cylinder is shown in Appendix A.



(a)



(b)



(c)

**Figure 4-3: Typical failure mechanism: (a) SFRP rupture- (b) Full debonding- (c) Mixed failure modes**

Cracking sounds were heard during the initial to middle loading stages that were attributed to the micro-cracking of the concrete core and aggregate movement. Snapping sounds of SFRP layers were heard at the final loading stage. The failure was sudden and brittle as cylinders showed no

sign of physical distress or excessive deformation. Figure 4-4 presents three pictures that were taken consecutively at five seconds time intervals using the DIC technique, that illustrate the exemplary catastrophic nature of such a failure.

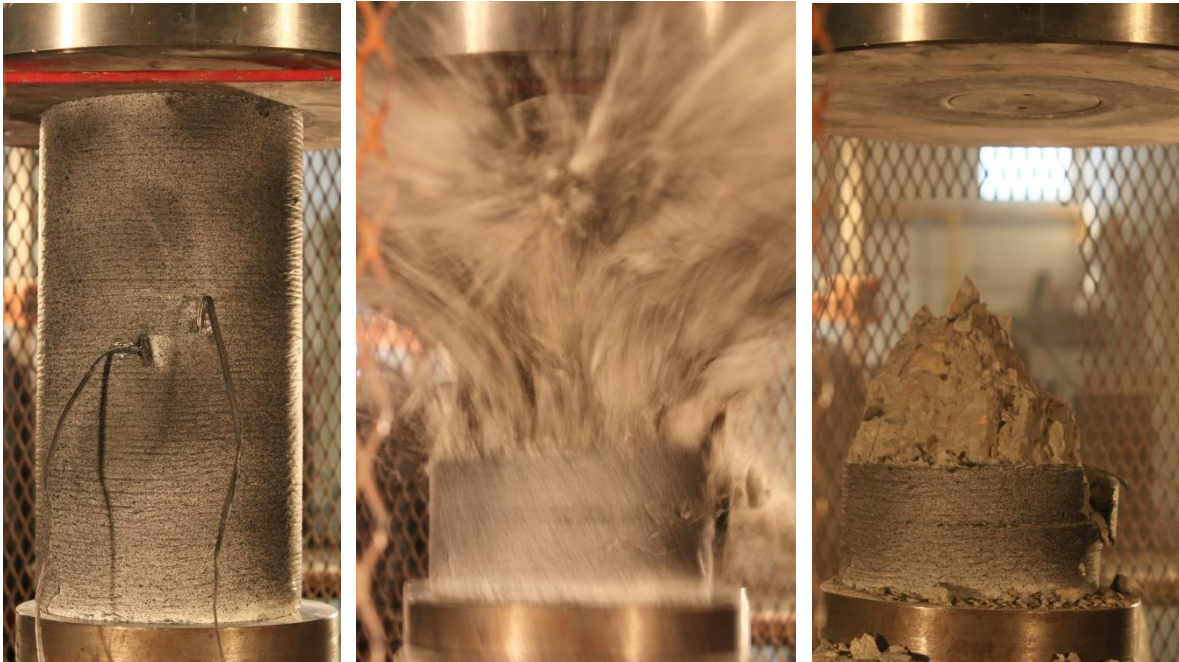


**Figure 4-4: Catastrophic failure of an SFRP-wrapped cylinder**

Good bonding between the concrete surface and FRP sheet was generally detected as the concrete-SFRP interface remained intact. Concrete chunks were still adhered to the inner face of ruptured SFRP wings, although the inner concrete was almost completely crushed, as can be seen in Figure 4-5.



**Figure 4-5: SFRP sheet – concrete interface**

## ***4.4.2 Ultimate Axial Strength***

### **4.4.2.1 CFRP-Confined Concrete Cylinders**

The key results of all 18 CFRP-confined cylinders are reported in Table 4-6. The ultimate axial strength averages for each confinement configuration are summarized in Table 4-7. It is found that wrapping cylinders with one, two and three layers of CFRP significantly enhanced the axial load capacity (by up to 2.5 and 2.2 times the unconfined concrete strength for C37.3 and C42.4 concrete, respectively). The percentage increase in strength for 1-, 2- and 3 layer-confinement configuration were 38, 86 and 147 % for C37.3 concrete, and 40, 79 and 123% for C42.4 concrete.

The average ultimate axial confined strengths are compared with respect to unconfined compressive concrete compressive strength and the number of layers of CFRP jacket in Figure 4-6 (a) and Figure 4-6 (b), respectively. The data presented include the error bar which calculated as the average  $\pm$  one standard deviation. It can be stated that for the same number of CFRP layers, the axial strength increases as concrete compressive strength increases. For the same concrete compressive strength, the ultimate axial strength increases as the number of CFRP layers increases. On the other hand, a higher percentage increase in ultimate strength was achieved for lower concrete compressive strength and thicker CFRP jacket as can be seen in Figure 4-7 (a) and Figure 4-7 (b), respectively.

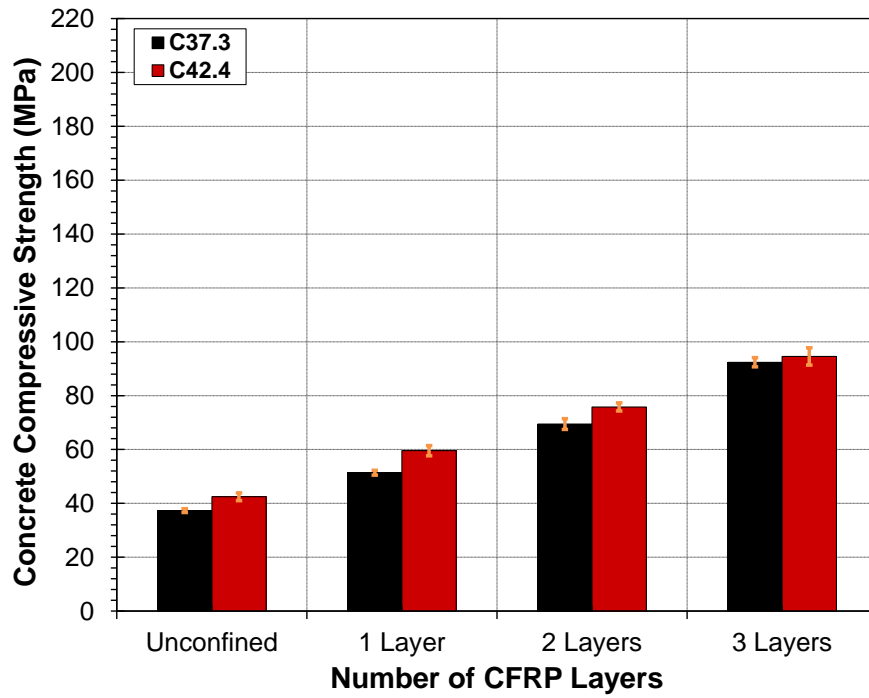
**Table 4-6: Key test results for CFRP-wrapped cylinders**

Specimen Designation	Ultimate Load (kN)	Ultimate Axial Strength (MPa)	Ultimate Axial Strain ( $\mu\epsilon$ )	Ultimate Lateral Strain ( $\mu\epsilon$ )	Axial Shortening	
					LSC#1 (mm)	LSC#2 (mm)
C37.3-CFRP1-SP#1	924	52.3	14641	-9060	4.66	4.06
C37.3-CFRP1-SP#2	907	51.3	15340	-10967	5.46	4.61
C37.3-CFRP1-SP#3	893	50.5	13976	-11446	*	*
C37.3-CFRP2-SP#1	1269	71.8	18523	-12494	5.20	6.78
C37.3-CFRP2-SP#2	1207	68.3	18642	-13668	6.34	5.92
C37.3-CFRP2-SP#3	1207	68.3	20630	-11733	6.66	6.49
C37.3-CFRP3-SP#1	1644	93.0	27108	-13633	9.33	8.22
C37.3-CFRP3-SP#2	1655	93.7	25811	-13715	9.03	7.89
C37.3-CFRP3-SP#3	1598	90.4	23400	-12909	7.18	9.10
C42.4-CFRP1-SP#1	1040	58.9	10690	-9660	3.14	3.05
C42.4-CFRP1-SP#2	1027	58.1	11130	-9250	2.90	2.71
C42.4-CFRP1-SP#3	1090	61.7	10158	-11163	3.25	3.02
C42.4-CFRP2-SP#1	1337	75.7	10731	-11409	3.93	3.96
C42.4-CFRP2-SP#2	1368	77.4	12018	-11807	4.59	3.76
C42.4-CFRP2-SP#3	1314	74.4	11723	-10589	3.47	3.95
C42.4-CFRP3-SP#1	1719	97.3	16631	-10382	3.98	6.64
C42.4-CFRP3-SP#2	1608	91.0	14480	-10386	5.53	5.19
C42.4-CFRP3-SP#3	1685	95.4	15464	-9259	6.18	6.42

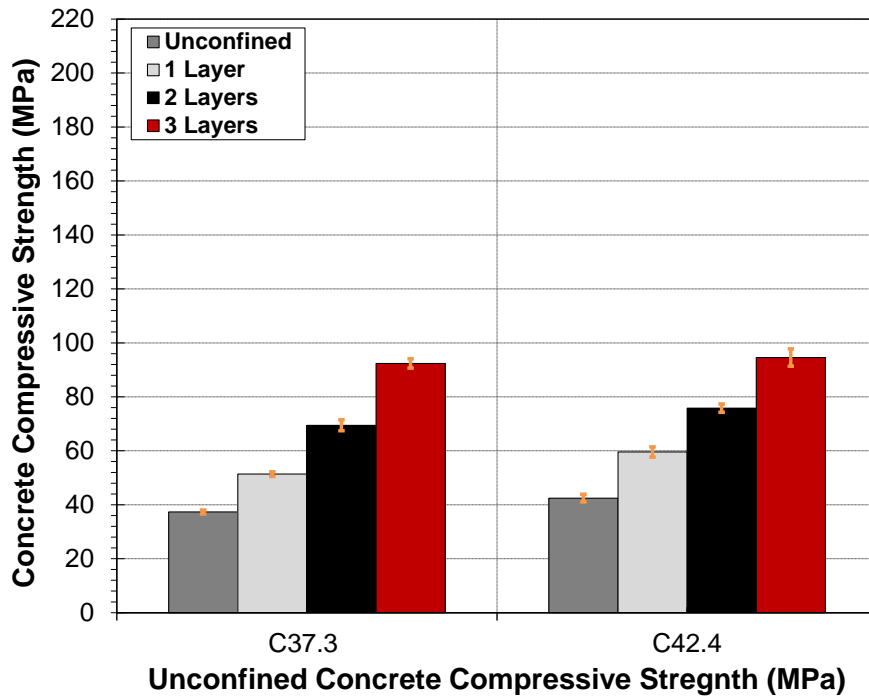
\* Data lost during testing

**Table 4-7: Summary of ultimate axial strength for CFRP-wrapped cylinders**

Configuration Designation	Ultimate Axial Strength			Strength Increase	
	Avg. (MPa)	SD (MPa)	COV (%)	$f'_{cu}/f'_{co}$	Percentage w.r.t unconfined (%)
C37.3-CFRP1	51.4	0.9	1.7	1.4	38
C37.3-CFRP2	69.5	2.0	2.9	1.9	86
C37.3-CFRP3	92.4	1.7	1.9	2.5	147
C42.4-CFRP1	59.6	1.9	3.2	1.4	40
C42.4-CFRP2	75.8	1.5	2.0	1.8	79
C42.4-CFRP3	94.6	3.2	3.4	2.2	123

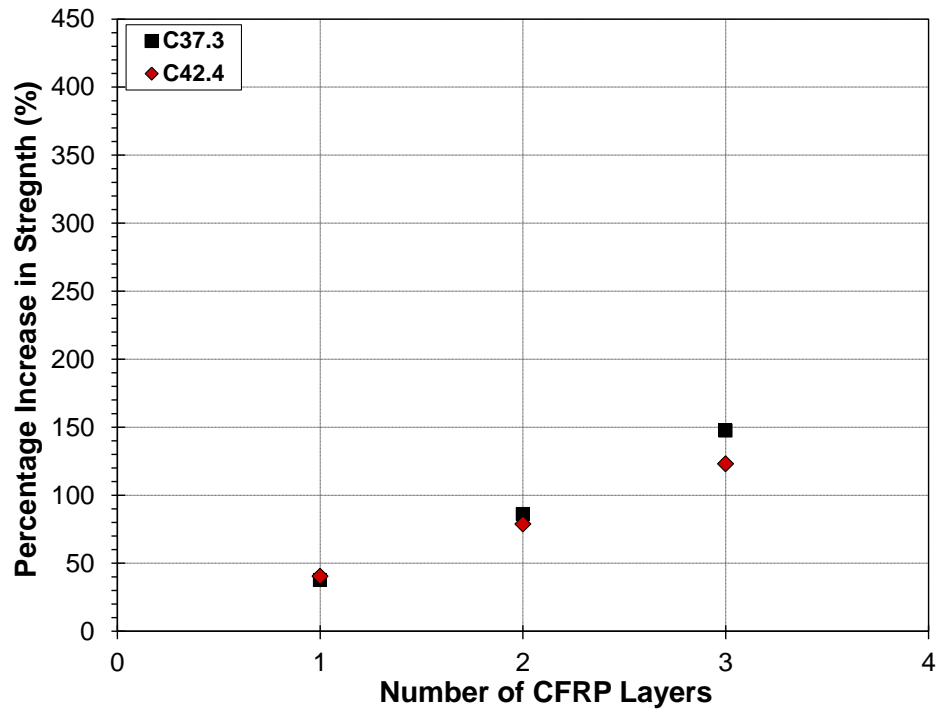


(a)

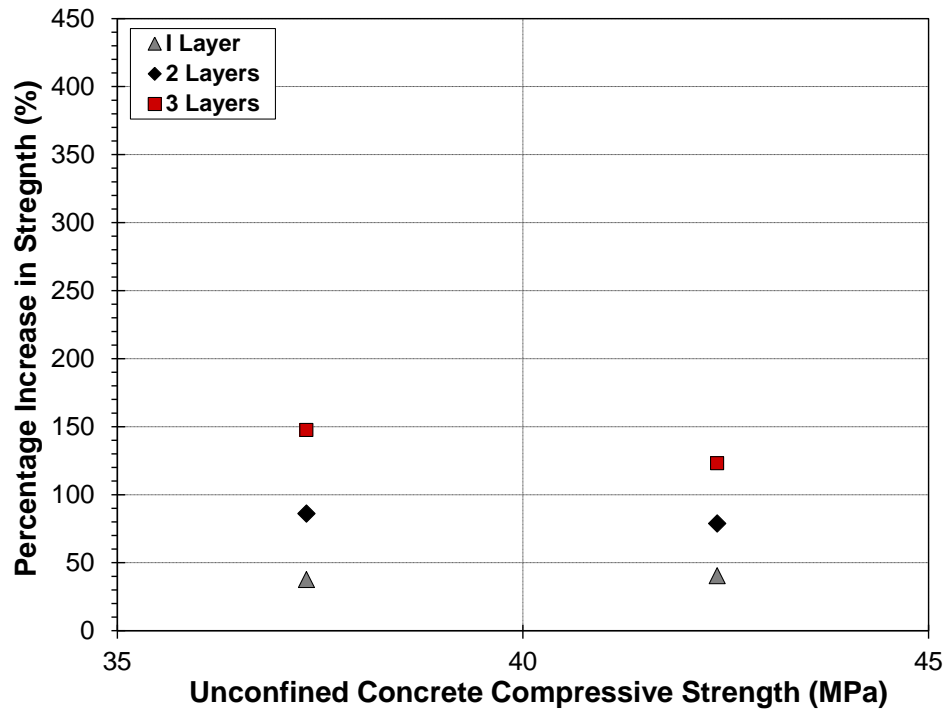


(b)

**Figure 4-6: Average ultimate axial strength for CFRP-wrapped cylinders with respect to: (a) Unconfined concrete strength (b) Number of CFRP layers**



(a)



(b)

**Figure 4-7: Percentage increase in axial strength for CFRP-wrapped cylinders with respect to: (a) Unconfined concrete strength (b) Number of CFRP layers**

#### 4.4.2.2 SFRP-Confined Concrete Cylinders

The key results of all 18 SFRP-wrapped cylinders are reported in Table 4-8. The ultimate axial compressive strength averages for each confinement configuration are summarized in Table 4-9, and are compared in Figure 4-8(a) and Figure 4-8(b) for different concrete compressive strength and different SFRP-jacket thicknesses, respectively. It can be observed that the provision of one, two and three layers of SFRP significantly enhanced the axial load capacity (by up to 5.2 and 4.7 times the unconfined concrete strength for C37.3 and C42.4 concrete, respectively). The percentage increase in strength was 153, 293 and 421 % of unconfined strength for C37.3 concrete, and 129, 263 and 373% of the unconfined strength for C42.4 concrete, as shown in Figure 4-9. However, this experimentally-observed linear relation between the thickness or number of wraps and the percentage increase in strength will not necessarily be maintained for higher number of wraps as thicker wraps may fail due to delamination at the overlap zone rather than fracture and the ultimate tensile strength of wraps will not be reached.

It is clear from Figure 4-9 that when all other parameters are the same, a thicker SFRP jacket leads to a greater percent increase in the ultimate load capacity. On the other hand, a higher concrete compressive strength resulted in reduction of the percent increase in strength, i.e., thicker jacket and lower concrete strength increase the efficiency of SFRP confinement.

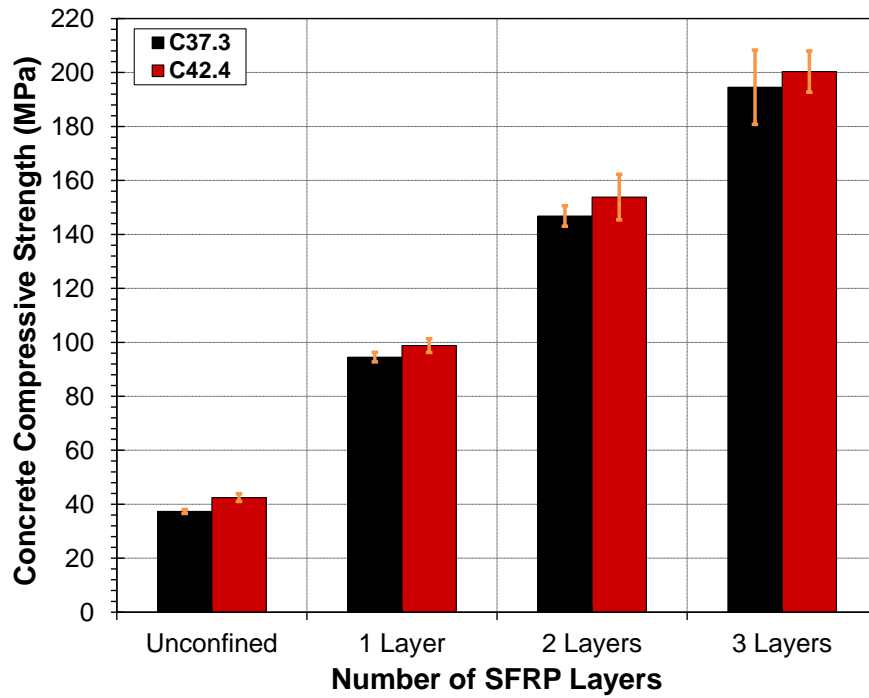
**Table 4-8: Key test results for SFRP-wrapped cylinders**

Specimen Designation	Ultimate Load (kN)	Ultimate Axial Strength (MPa)	Ultimate Axial Strain ( $\mu\epsilon$ )	Ultimate Lateral Strain ( $\mu\epsilon$ )	Axial Shortening	
					LSC#1 (mm)	LSC#2 (mm)
C37.3-SFRP1-SP#1	1640	92.8	34346	-23326	12.3	9.9
C37.3-SFRP1-SP#2	1702	96.3	29837	-17957	10.6	10.5
C37.3-SFRP1-SP#3	1670	94.5	32080	-23681	8.5	13.5
C37.3-SFRP2-SP#1	2611	147.8	46361	-13873	17.0	13.8
C37.3-SFRP2-SP#2	2520	142.6	41587	-15857	*	*
C37.3-SFRP2-SP#3	2651	150.0	43073	-14958	16.9	15.2
C37.3-SFRP3-SP#1	3310	187.3	45676	-15012	18.0	14.3
C37.3-SFRP3-SP#2	3720	210.5	63198	-14827	20.7	15.8
C37.3-SFRP3-SP#3	3285	185.9	54611	-15415	17.8	17.4
C42.4-SFRP1-SP#1	1787	101.1	25925	*	8.6	8.7
C42.4-SFRP1-SP#2	1753	99.2	27311	-20308	8.6	8.4
C42.4-SFRP1-SP#3	1697	96.0	27785	-17120	9.6	9.1
C42.4-SFRP2-SP#1	2814	159.2	31691	-14882	13.9	11.1
C42.4-SFRP2-SP#2	2796	158.2	37727	-11617	12.5	11.7
C42.4-SFRP2-SP#3	2547	144.1	30262	-10975	15.6	11.9
C42.4-SFRP3-SP#1	3423	193.7	46007	-14292	14.0	15.5
C42.4-SFRP3-SP#2	3511	198.7	42083	-13959	13.4	15.0
C42.4-SFRP3-SP#3	3688	208.7	53992	-15916	17.2	12.7

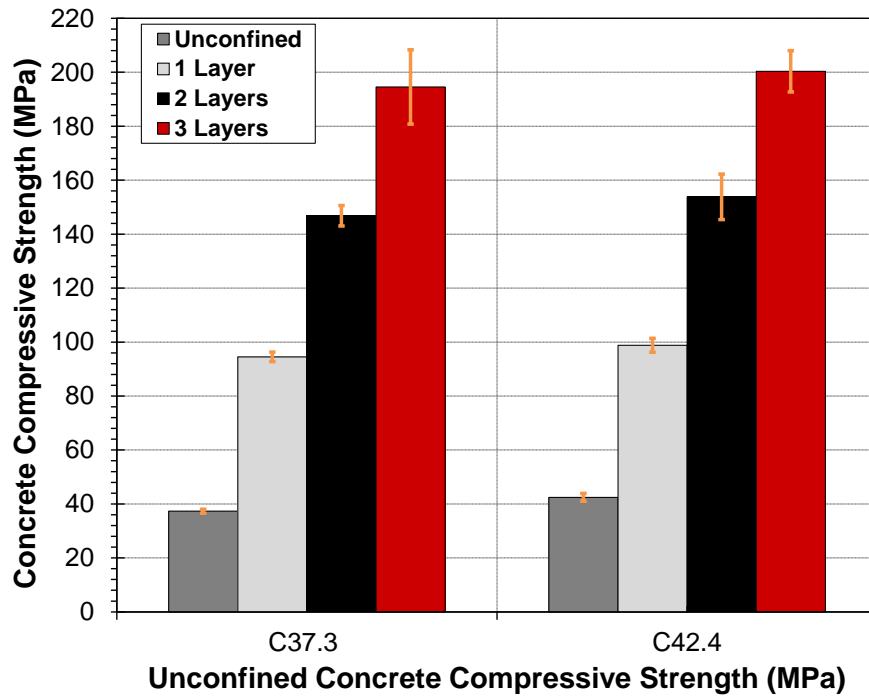
\* Data lost during testing

**Table 4-9: Summary of ultimate axial strength for SFRP-wrapped cylinders**

Configuration Designation	Ultimate Axial Strength			Strength Enhancement	
	Avg. (MPa)	SD (MPa)	COV (%)	$f'_{cu}/f'_{co}$	Percentage w.r.t unconfined (%)
C37.3-SFRP1	94.5	1.8	1.9	2.5	153
C37.3-SFRP2	146.8	3.8	2.6	3.9	293
C37.3-SFRP3	194.6	13.8	7.1	5.2	421
C42.4-SFRP1	98.8	2.6	2.6	2.3	133
C42.4-SFRP2	153.9	8.4	5.5	3.6	263
C42.4-SFRP3	200.4	7.6	3.8	4.7	373

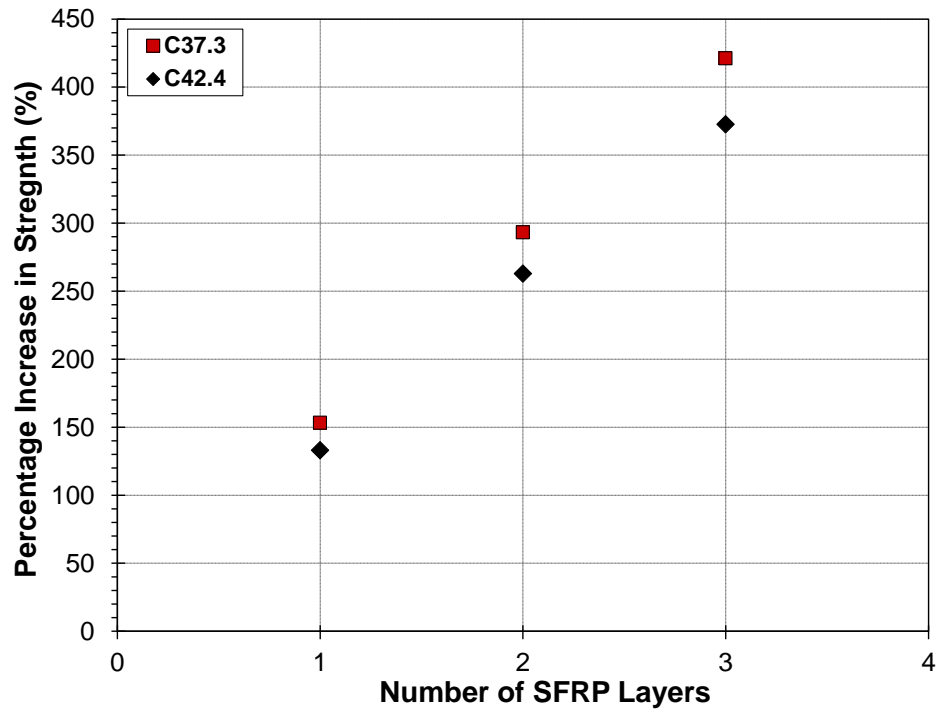


(a)

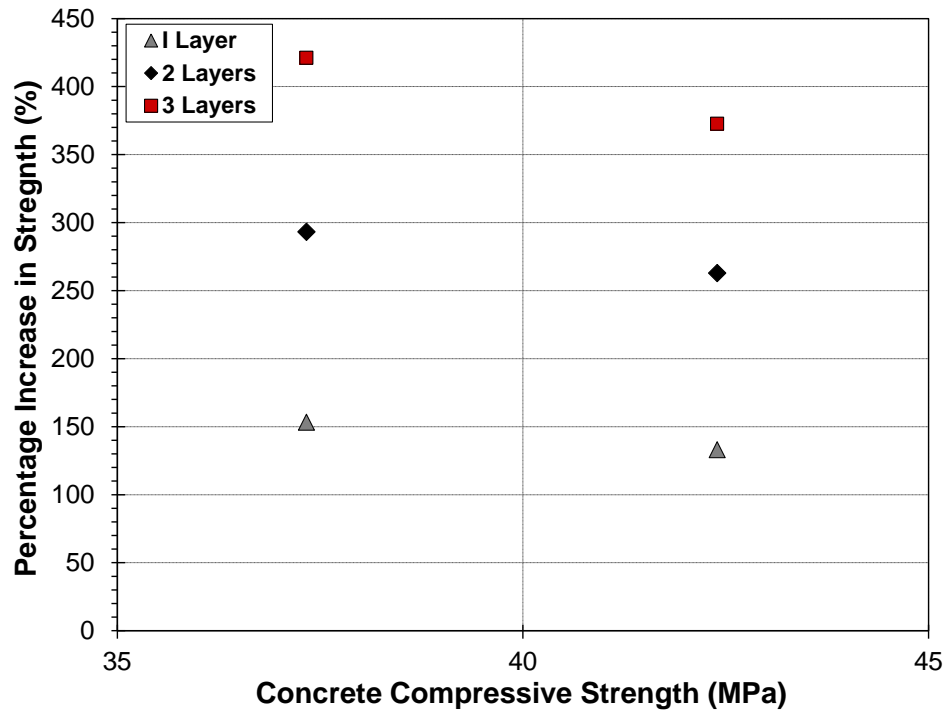


(b)

**Figure 4-8: Average ultimate axial strength for SFRP-wrapped cylinders with respect to: (a) Unconfined compressive strength (b) Number of SFRP layers**



(a)



(b)

**Figure 4-9: Percentage increase in axial strength of SFRP-wrapped cylinders with respect to: (a) Unconfined compressive strength (b) Number of SFRP layers**

### ***4.4.3 Ultimate Axial Strain***

#### **4.4.3.1 CFRP-Confined Concrete Cylinders**

Average ultimate axial strain measured from strain gauges installed at mid height of the cylinder and ultimate axial strain calculated from the average measurement of the two vertical LSC's devices for each three nominally identical tested cylinders are summarized in Table 4-10.

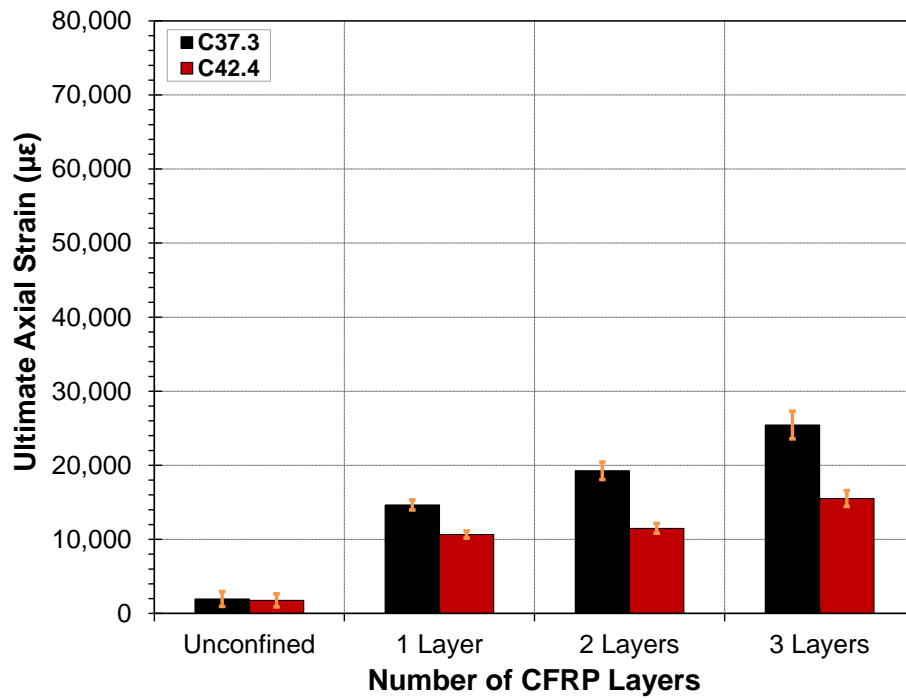
All cylinders featured a substantial increase in ultimate axial strain compared to axial strain at peak of unconfined concrete strength, with the largest value of the former being 13.0 and 8.8 times the latter for C37.3 and C42.4 concrete, respectively. The percentage increase in axial strain was 648, 884, 1199 and 507, 554 and 784 for C37.3 and C42.4 concrete respectively.

The average ultimate axial strains are compared with respect to concrete compressive strength and thickness of CFRP layers in Figure 4-10 (a) and Figure 4-10 (b), respectively. It is shown that for the same number of CFRP layers, the average ultimate axial strain decreases as the concrete compressive strength increases. For the same concrete compressive strength, the average axial strain increases as the number of CFRP layers, i.e. thickness of CFRP, increases.

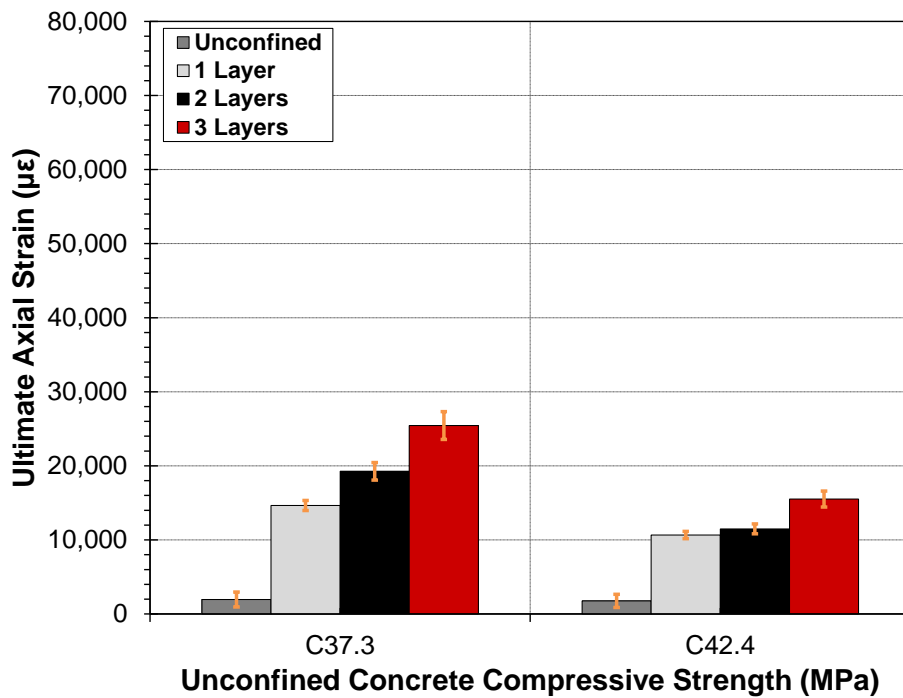
It can be concluded from Figure 4-11 (a) and Figure 4-11 (b) that increasing the number of CFRP wraps and lowering the compressive strength of concrete increase the percentage increase in axial strain.

From the comparison between the axial strain data from strain gauge installed at the mid height of the wrapped cylinders and axial strain data obtained from the average measurement of the two vertical LSCs devices shown in Table 4-10, it is clear that that the foil strain gauges grossly underestimate the strain up to 17.7%. This is due, as will be discussed in detail in Section 4.4.7.3, to the localized regions of high strain that will be developed in the FRP jackets where jacket crosses a splitting cracks. Unless the foil strain gauge is located within one of these highly

strained regions, the failure strain is most probably not captured by the foil strain gauge and the strain reading from the foil strain gauge is less than the actual failure strain. On the other hand, measurements from the LSCs devices capture the average global shortening behaviour along the full height of the loaded cylinder.

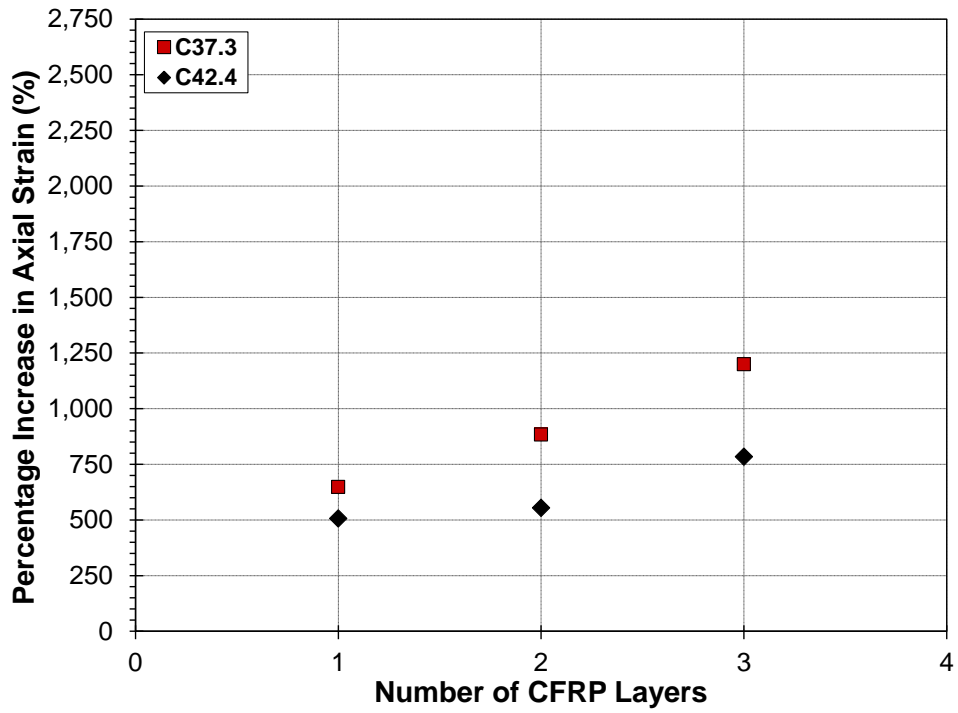


(a)

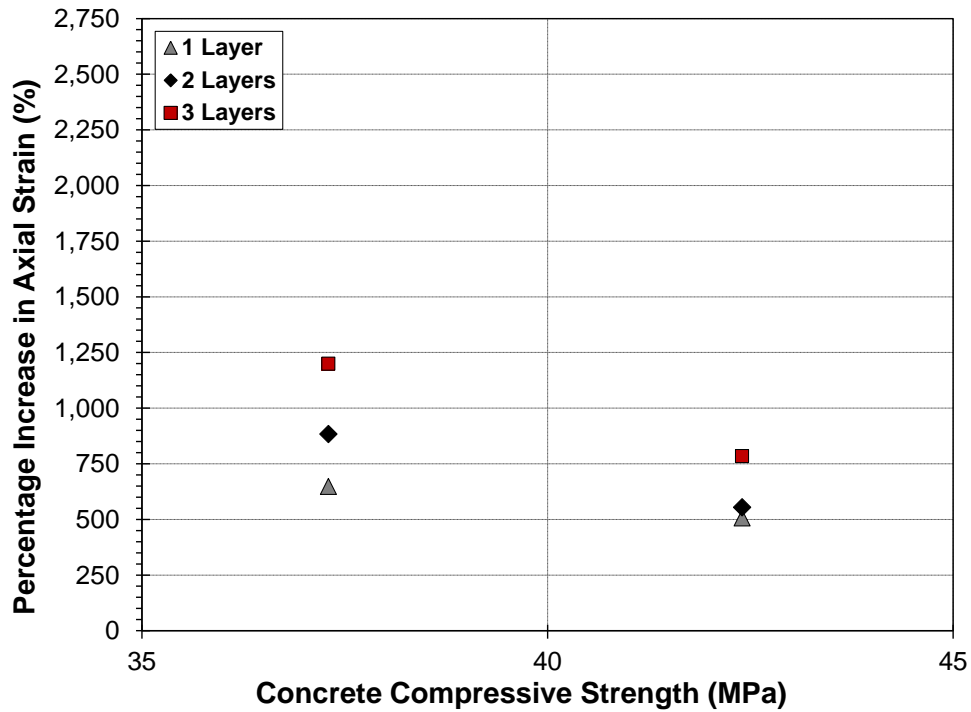


(b)

**Figure 4-10: Ultimate axial strain for CFRP-wrapped cylinders with respect to: (a) Unconfined compressive strength (b) Number of CFRP layers**



(a)



(b)

**Figure 4-11: Percentage increase in axial strain of CFRP-wrapped cylinders with respect to (a) Unconfined compressive strength (b) Number of CFRP layers**

#### 4.4.3.2 SFRP-Confined Concrete Cylinders

The average ultimate axial strain measured from strain gauges installed at mid height of the cylinder and the average ultimate axial strain calculated from axial shortening for each three nominally identical tested cylinders are reported and compared in Table 4-11.

It is evident that all 18 cylinders show a substantial increase in ultimate axial strain compared to axial strain at peak of unconfined concrete, with the largest value of the former being 27.8 and 27.0 times the latter for C37.3 and C42.4 concrete, respectively.

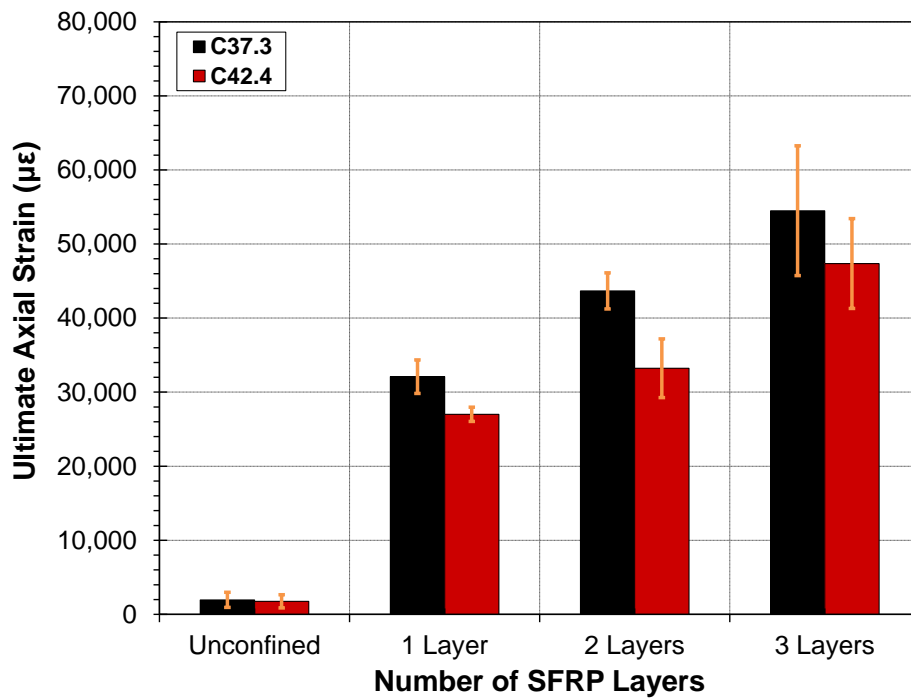
The average ultimate axial strains are compared with respect to concrete compressive strength and thickness of SFRP layers in Figure 4-12(a) and Figure 4-12(b), respectively. It can be stated that for the same number of SFRP layers, the average ultimate axial strain decreases as the concrete compressive strength increases. For the same concrete compressive strength, the average axial strain increases as the number of SFRP layers.

The percentage increase in strain was 1538, 2130 and 2682 % and 1437, 1791 and 2596 % of the axial strain at peak of unconfined concrete for C37.3 and C42.4 concrete, respectively.

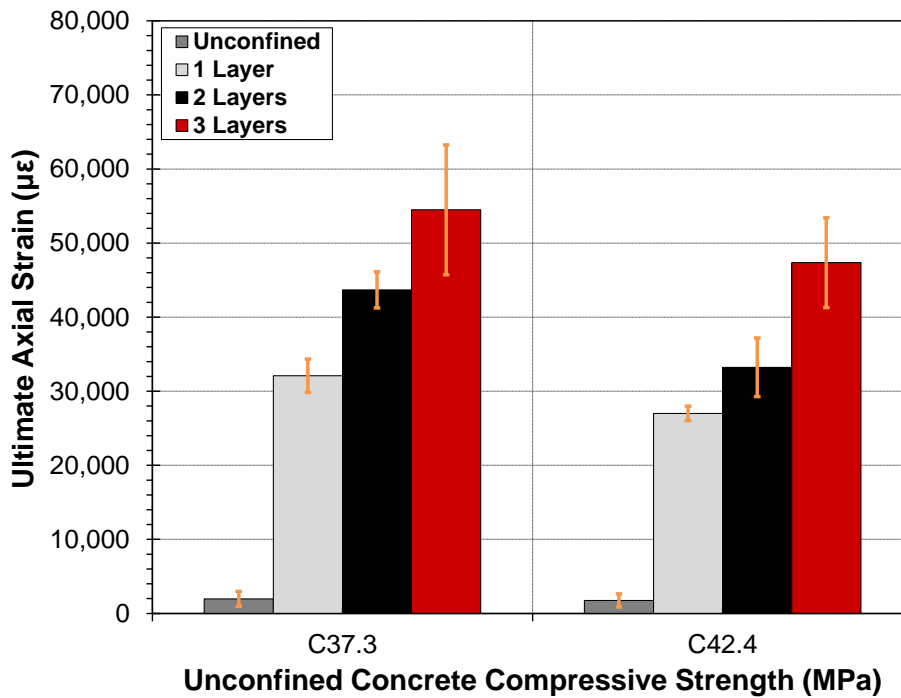
It is clear from Figure 4-13 (a) and Figure 4-13 (b) that when all other parameters are the same, a thicker SFRP wrap and a lower concrete compressive strength resulted in higher increase percentage in the ultimate axial strain for SFRP wrapped cylinders.

Comparing the axial strain data from strain gauge installed at the mid height wrapped cylinders with the axial strain data obtained from the average measurements of the two vertical LSCs devices revealed that the foil strain gauges grossly underestimate the strain up to 22%. As will be discussed in detail in Section 4.4.7.3, local regions of high strain developed in the FRP jacket where jacket crosses splitting cracks. If the strain gauge location is not at the exact location of these highly strained regions, the measured strain will be lower than the actual FRP rupture

strain. On the other hand, measurements from the LSCs devices capture the average global shortening behaviour of the loaded cylinder.

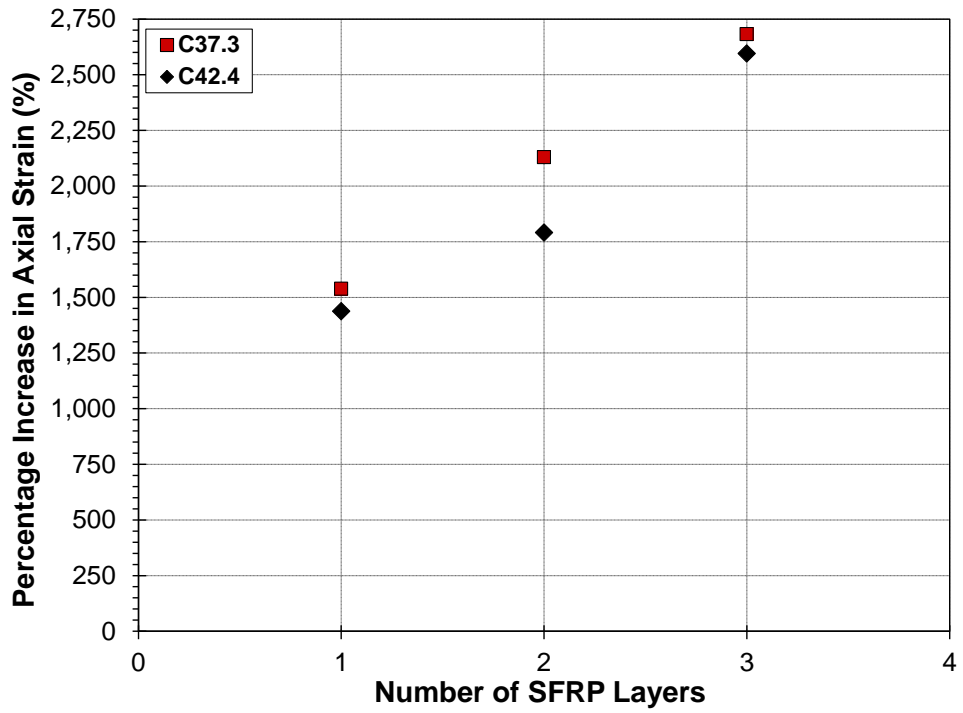


(a)

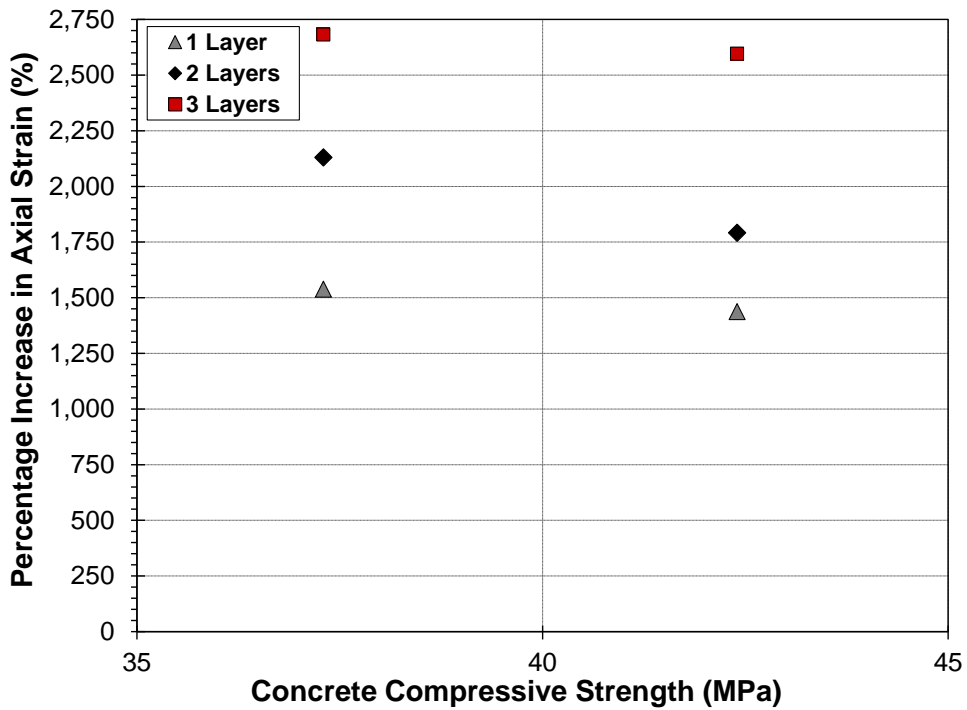


(b)

**Figure 4-12: Ultimate axial strain for SFRP-wrapped cylinders with respect to: (a) Unconfined compressive strength (b) Number of SFRP layers**



(a)



(b)

**Figure 4-13: Percentage increase in axial strain of SFRP-wrapped cylinders with respect to: (a) Unconfined compressive strength (b) Number of SFRP layers**

**Table 4-10: Summary of ultimate axial strain for CFRP-wrapped cylinders**

Configuration Designation	Ultimate Axial Strain										Diff (%)
	From Strain Gauge					From Axial Shortening					
	Avg. ( $\mu\epsilon$ )	SD ( $\mu\epsilon$ )	COV (%)	$\epsilon_{cu}/\epsilon_o$	% w.r.t unconfined (%)	Avg. ( $\mu\epsilon$ )	SD ( $\mu\epsilon$ )	COV (%)	$\epsilon_{cu}/\epsilon_o$	% w.r.t unconfined (%)	
C37.3-CFRP1	14652	682	4.7	7.5	648	15665	1120	7.2	8.0	700	6.5
C37.3-CFRP2	19265	1184	6.1	9.8	884	20768	830	4.0	10.6	960	7.2
C37.3-CFRP3	25440	1882	7.4	13.0	1199	28193	869	3.1	14.4	1339	9.2
C42.4-CFRP1	10659	487	4.6	6.1	507	11073	743	6.7	6.3	530	3.7
C42.4-CFRP2	11491	674	5.9	6.5	554	13147	632	4.8	7.5	648	12.6
C42.4-CFRP3	15525	1077	6.9	8.8	784	18855	1520	8.1	10.7	973	17.7

**Table 4-11: Summary of ultimate axial strain for SFRP-wrapped cylinders**

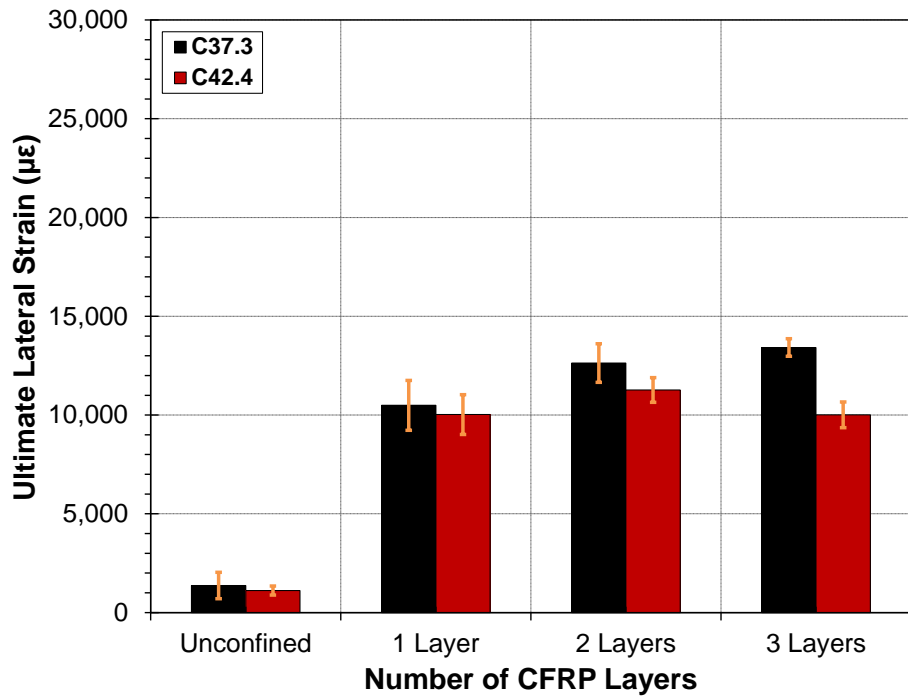
Configuration Designation	Ultimate Axial Strain										Diff (%)
	From Strain Gauge					From Axial Shortening					
	Avg. ( $\mu\epsilon$ )	SD ( $\mu\epsilon$ )	COV (%)	$\epsilon_{cu}/\epsilon_o$	Increase w.r.t unconfined (%)	Avg. ( $\mu\epsilon$ )	SD ( $\mu\epsilon$ )	COV (%)	$\epsilon_{cu}/\epsilon_o$	Increase w.r.t unconfined (%)	
C37.3-SFRP1	32088	2254	7.0	16.4	1538	36258	790	2.2	18.5	1751	11.5
C37.3-SFRP2	43674	2443	5.6	22.3	2130	52457	1113	2.1	26.8	2578	16.7
C37.3-SFRP3	54495	8762	16.1	27.8	2682	57832	2947	5.1	29.5	2852	5.8
C42.4-SFRP1	27007	967	3.6	15.4	1437	29397	1238	4.2	16.7	1573	8.1
C42.4-SFRP2	33227	3962	11.9	18.9	1791	42588	2271	5.3	24.2	2324	22.0
C42.4-SFRP3	47361	6069	12.8	27.0	2596	48748	1133	2.3	27.7	2675	2.8

#### ***4.4.4 Ultimate Lateral Strain***

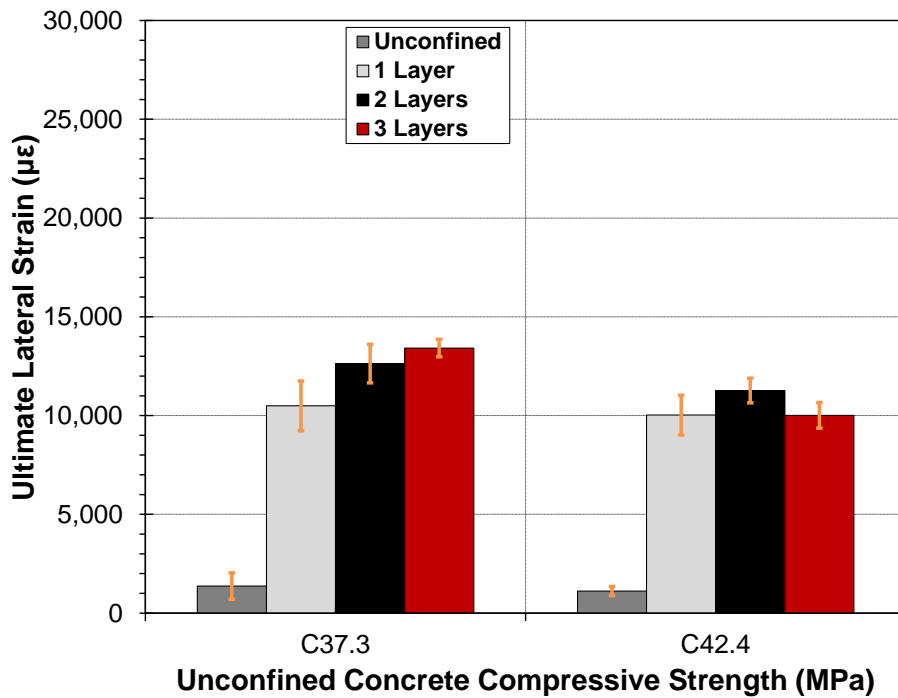
##### **4.4.4.1 CFRP-Confined Concrete Cylinders**

CFRP-wrapped cylinders achieved a much larger ultimate lateral strain than the lateral strain at peak of unconfined concrete; with the largest value of the former being 9.8 and 10.1 times the latter for C37.3 and C42.4 concrete, respectively.

Figure 4-14 (a) and Figure 4-14 (b) show that for the same number of CFRP layers, the average ultimate lateral strain decreases as concrete compressive strength increases and that for the same concrete compressive strength, the average measured lateral strain increases as number of FRP layers increases for C37.3 concrete while remains approximately the same for C42.4.



(a)



(b)

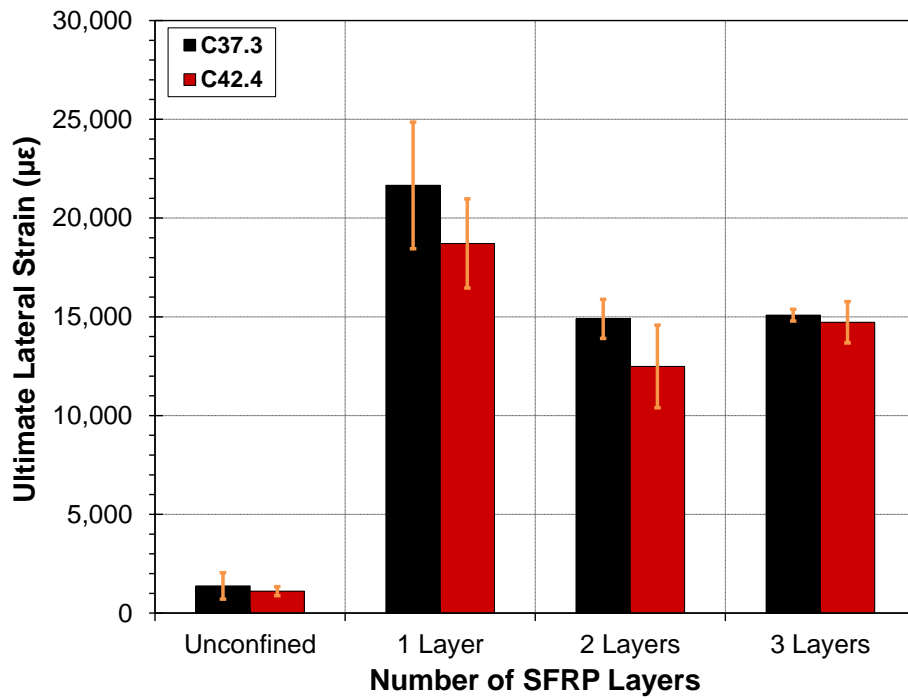
**Figure 4-14: Lateral strain for CFRP-wrapped cylinders with respect to: (a) Unconfined compressive strength (b) Number of CFRP layers**

#### 4.4.4.2 SFRP-Confined Concrete Cylinders

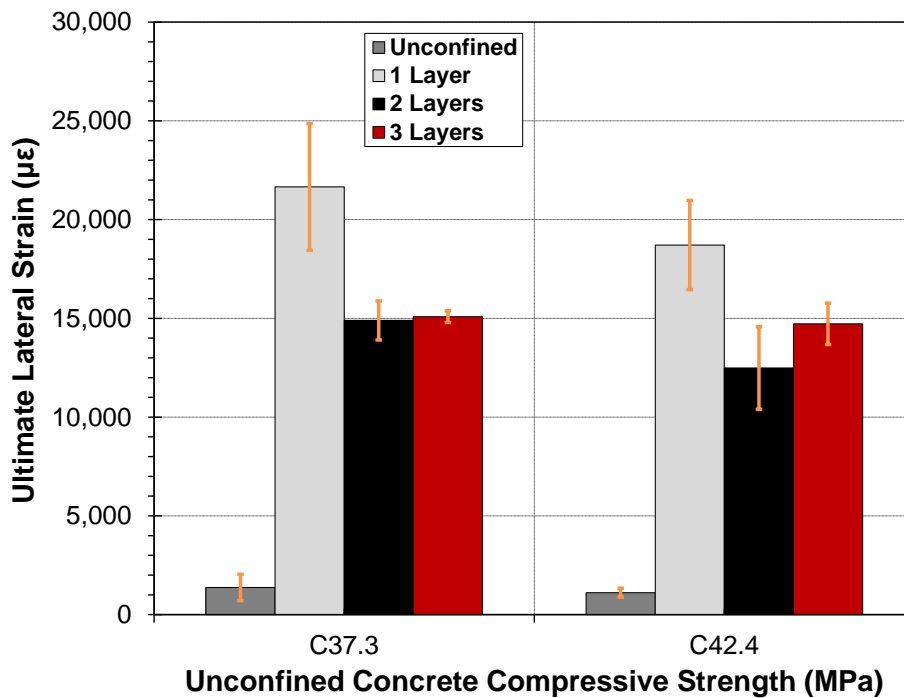
Similarly, all SFRP-wrapped cylinders achieved a much larger ultimate lateral strain than the lateral strain at peak of unconfined concrete; with the largest ultimate lateral strain for wrapped cylinders being 15.8 and 16.8 times lateral strain at peak of unconfined concrete for C37.3 and C42.4, respectively.

Figure 4-15 (a) and Figure 4-15 (b) show that for the same number of SFRP layers, the average ultimate lateral strain decreases as concrete compressive strength increases and that for the same concrete compressive strength, the average measured lateral strain decreases as number of FRP layers increases. The decrease, in general, was more noticeable between 1 and 2 layers while negligible between 2 and 3 layers.

The above mentioned observation should be interpreted while keeping in mind that the strains were measured from strain gauges and that depending on the strain gauge location proximity to the local highly-strained region, the results may vary widely. This will be discussed in more detail when reviewing the failure mechanism of FRP sheets in Section 4.4.7.3.



(a)



(b)

**Figure 4-15: Ultimate lateral strain for SFRP-confined cylinders with respect to: (a) Unconfined compressive strength (b) Number of SFRP layers**

**Table 4-12: Summary of lateral strain for CFRP-wrapped cylinders**

Configuration Designation	Ultimate Lateral Strain				
	From Foil Strain Gauge			$\varepsilon/\varepsilon_0$	Increase w.r.t unconfined
	Avg.	SD	COV		
( $\mu\varepsilon$ )	( $\mu\varepsilon$ )	(%)	(%)		
C37.3-CFRP1	-10491	1262	12.0	7.6	664
C37.3-CFRP2	-12632	975	7.7	9.2	820
C37.3-CFRP3	-13419	444	3.3	9.8	878
C42.4-CFRP1	-10024	1007	10.0	9.0	801
C42.4-CFRP2	-11268	621	5.5	10.1	913
C42.4-CFRP3	-10009	650	6.5	9.0	800

**Table 4-13: Summary of lateral strain for SFRP-wrapped cylinders**

Configuration Designation	Ultimate Lateral Strain				
	From Foil Strain Gauge			$\varepsilon/\varepsilon_0$	Increase w.r.t unconfined
	Avg.	SD	COV		
( $\mu\varepsilon$ )	( $\mu\varepsilon$ )	(%)	(%)		
C37.3-SFRP1	-21655	3207	14.8	15.8	1478
C37.3-SFRP2	-14896	993	6.7	10.9	985
C37.3-SFRP3	-15085	301	2.0	11.0	999
C42.4-SFRP1	-18714	2254	12.0	16.8	1583
C42.4-SFRP2	-12491	2095	16.8	11.2	1023
C42.4-SFRP3	-14722	1047	7.1	13.2	1224

#### 4.4.5 Load-Deformation Behaviour

Load-deformation behaviour in terms of stress-strain behaviour and dilation behaviour is examined next. The stress-strain behaviour is examined by looking at the axial stress-axial strain and axial stress-lateral strain plots; dilation behaviour is examined by looking at two distinct behavioural representation plots; axial strain-lateral strain and axial stress-volumetric strain. Since some scattering exists within the same confinement configuration, direct interpretation or comparison of peak values from the plots is not recommended and average values reported in the designated tables should always be consulted.

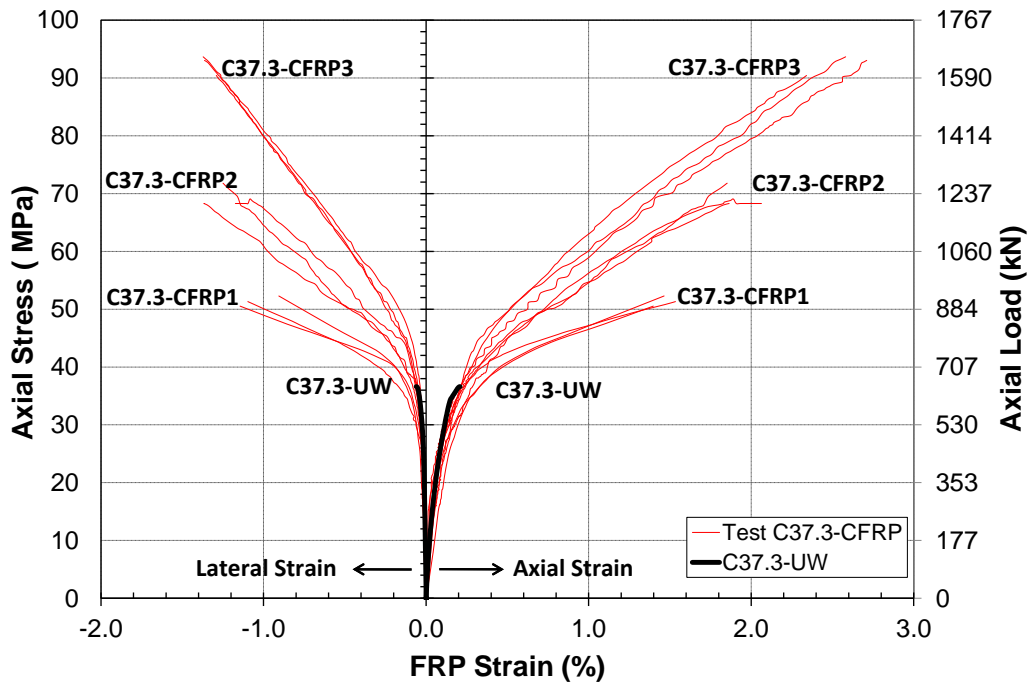
#### 4.4.5.1 Stress-Strain Behaviour

Axial stress data used for plotting stress-strain curves were calculated from dividing load results obtained from the data acquisition system over the cylinder cross section area, axial strain and lateral strain data were obtained from readings from foil strain gauges installed at the mid height of each cylinder. Curves to the right represent the axial stress-axial strain relation, while curves to the left represent the axial stress-lateral strain relation. Individual stress-strain plots are shown in Appendix B.

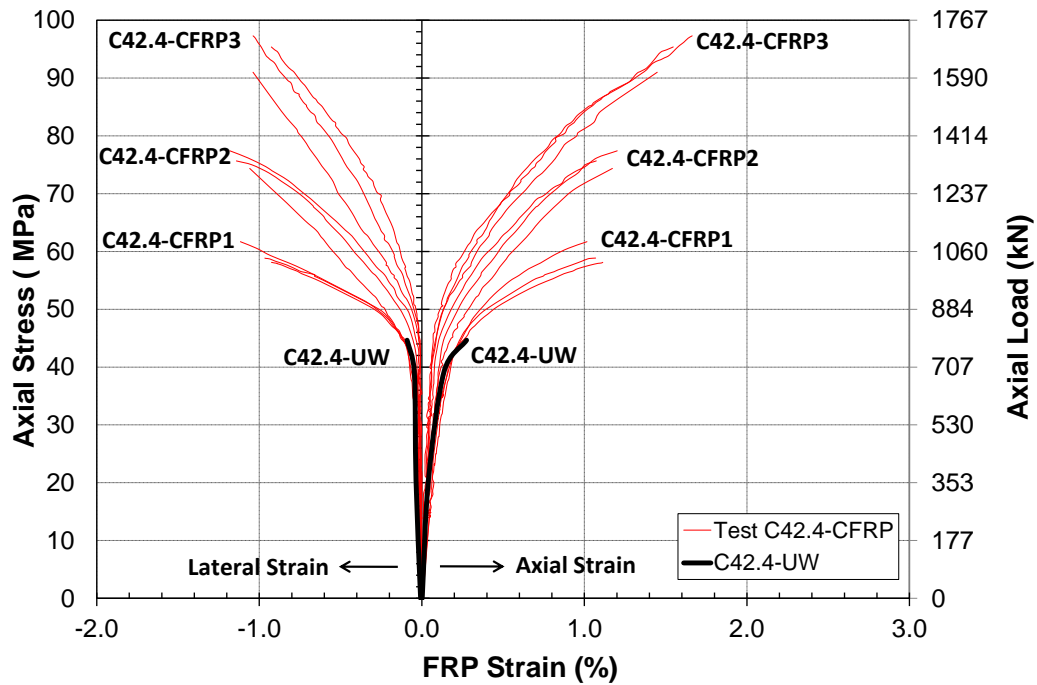
##### 4.4.5.1.1 CFRP-Confined Concrete Cylinders

Stress-strain curves for CFRP-confined concrete cylinders from each confinement configuration are plotted in Figure 4-17 (a) and Figure 4-17 (b) for C37.3 and C42.4, respectively. The stress-strain curves for the corresponding unconfined concrete are also shown for comparison purposes. As can be seen from Figure 4-16, the stress-strain curves for all CFRP-wrapped cylinders exhibit a bilinear ascending stress-strain behaviour until the CFRP ruptures.

CFRP-confined cylinders stress-strain response comprises three distinct regions. The first region, in which the lateral expansion of concrete core is still negligible and CFRP jacket is not yet activated, follows closely that of unconfined concrete, followed quickly by a transition zone as micro cracks in the concrete core start rapidly growing. Finally, in the third region, the concrete is fully cracked and the CFRP jacket is fully activated. The response is then linear up to failure and the response is mainly dependent on the lateral stiffness and strength of the CFRP jacket. It is also observed that the point at which the slope changes occurs at a stress level that is proportional to the confinement strength.



(a)



(b)

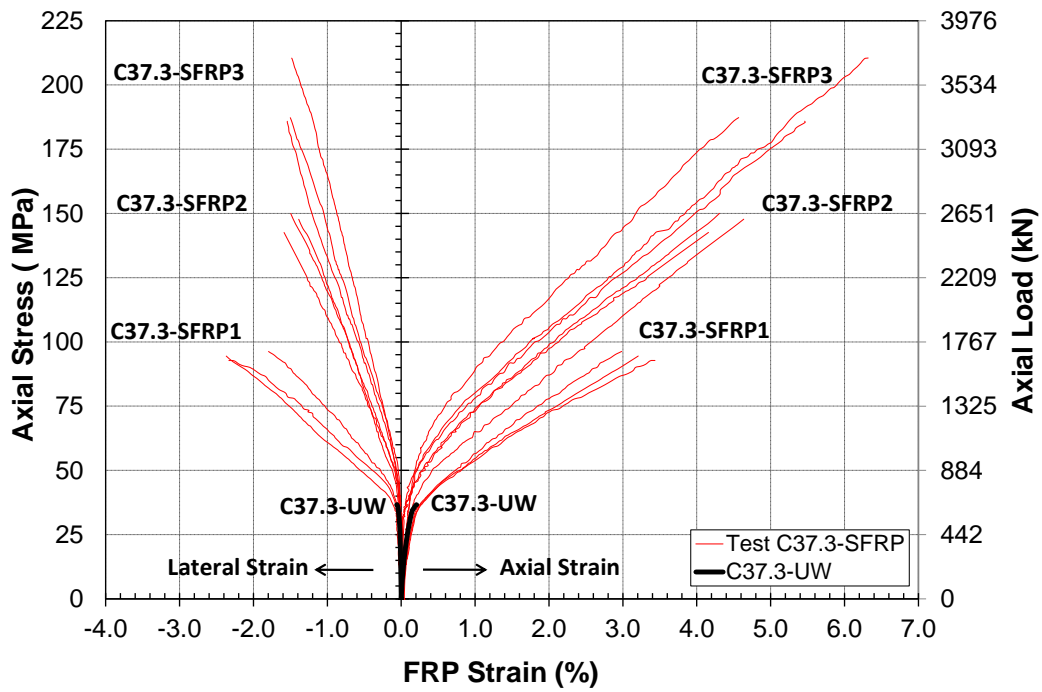
Figure 4-16: Stress-strain curve of CFRP-confined cylinders for: (a) C37.3 (b) C42.4

#### 4.4.5.1.2 SFRP-Confined Concrete Cylinders

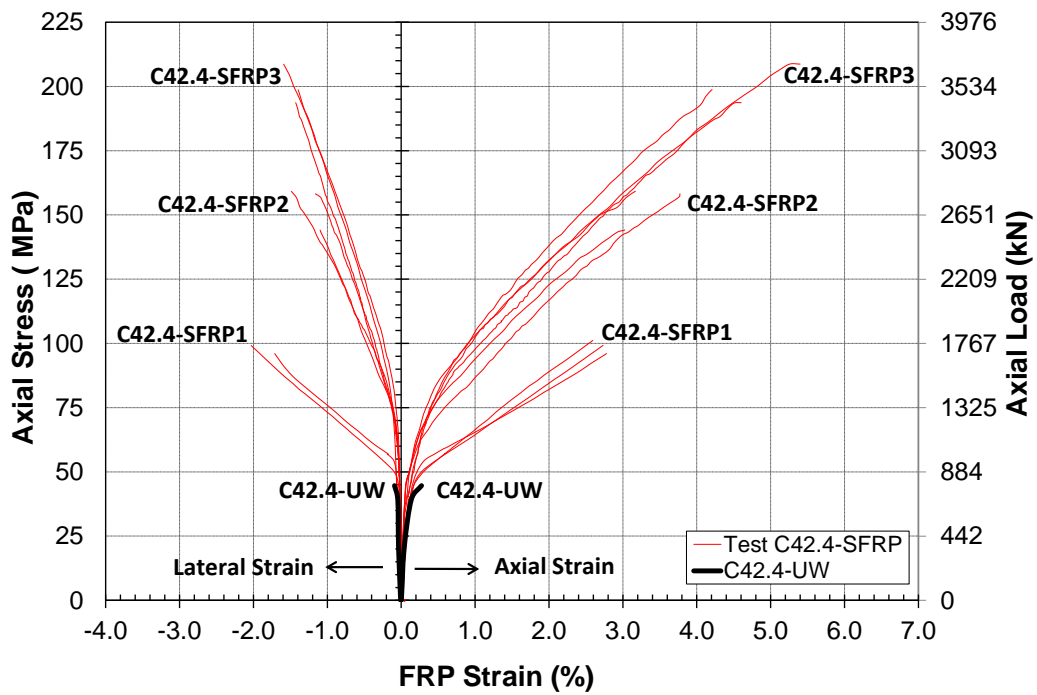
Stress-strain curves for SFRP-confined cylinders for each confinement configuration are plotted in Figure 4-17 (a) and Figure 4-17 (b) for C37.3 and C42.4, respectively. The stress-strain curves for the corresponding unconfined concrete are also shown for comparison purposes.

Reviewing the stress-strain curves indicates that all SFRP-wrapped cylinders exhibit a bilinear ascending stress-strain curve until SFRP failure.

Similar to CFRP-confined cylinders, the stress-strain response of SFRP wrapped cylinders comprises three distinct regions. The first region features behaviour that is similar to that of unconfined concrete, which indicates that the lateral expansion of concrete core is insignificant and SFRP warps are not yet activated. As micro cracks in concrete core grow rapidly, the response softens and a nonlinear transition zone is entered where the SFRP wraps exerts a confining pressure on concrete core to counteract its increasingly lateral expansion. Finally, in the third region, the concrete is fully cracked and the SFRP is fully activated. The response is then linear up to failure and the response is mainly dependent on the lateral stiffness and strength of the SFRP wraps. Furthermore, the point at which the bilinear curve changes slope shift upward as ultimate load increases. Studies by Mashrik (2011); Abdelrahman (2011) and Napoli and Realfonzo (2013) have shown a similar bilinear trend for SFRP-wrapped cylinders.



(a)



(b)

Figure 4-17: Stress-strain curves of SFRP-confined cylinders for: (a) C37.3 (b) C42.4

#### 4.4.5.2 Dilation Behaviour

Axial stress data used for plotting axial stress-volumetric strain curves were calculated from dividing the load results obtained from data acquisition system in the cylinder cross section area. Volumetric strain,  $\varepsilon_v$ , which is defined as the volume change per unit volume (Chen 1982) , is calculated from Equation 4-6 using axial strain,  $\varepsilon_c$  and lateral strain,  $\varepsilon_l$  collected from readings from of the foil strain gauges installed at the mid height of each cylinder.

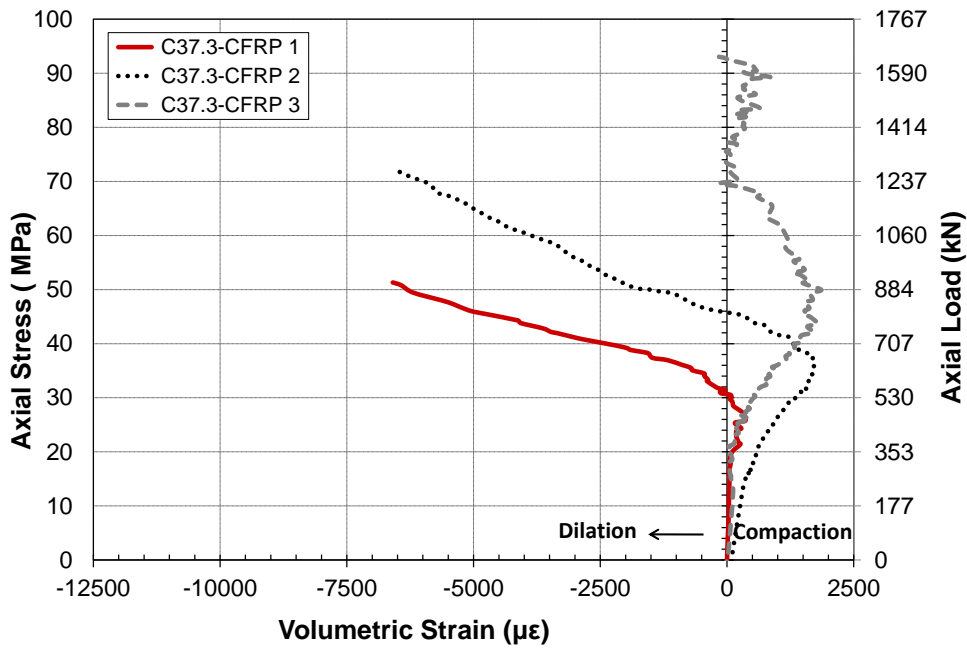
$$\varepsilon_v = \frac{\Delta V}{V} = \varepsilon_c + 2\varepsilon_l \quad \text{Equation 4-6}$$

where  $\Delta V$  is the change of volume, and  $V$  is the volume.

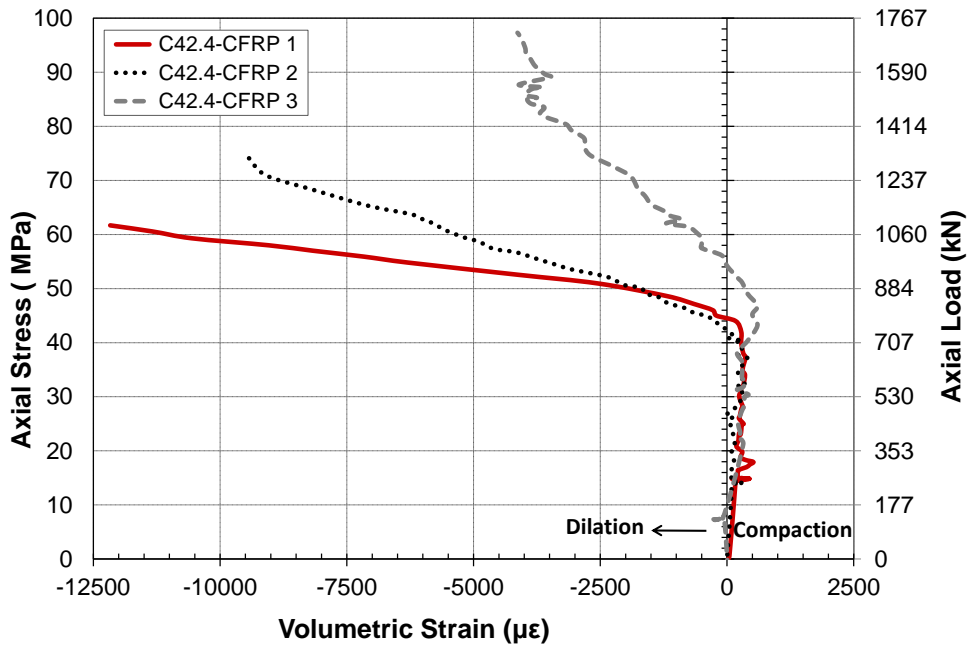
In the following axial stress-volumetric strain plots, positive volumetric strain represents volumetric compaction, whereas negative volumetric strain represents volumetric dilation

##### 4.4.5.2.1 CFRP-Confined Concrete Cylinders

The axial stress - volumetric strain plots for different CFRP jacket thicknesses are shown in Figure 4-18 (a) and Figure 4-18 (b) for C37.3 and C42.4, respectively. For C37.3, one and two CFRP wraps were eventually unable to curtail the dilation of concrete. However, three wraps effectively curtailed the concrete dilation until failure. , On the other hand, for C42.4, although the CFRP jacket was able to prevent concrete dilation at the initial loading stage, the concrete eventually expands laterally at loading close to failure, regardless the number of the wraps of the CFRP jacket. Hence, the dilation behaviour of CFRP-confined concrete depends not only on the FRP jacket stiffness, but also on the FRP jacket stiffness ratio.



(a)



(b)

**Figure 4-18: Dilation behaviour of CFRP-confined cylinders for: (a) C37.3 (b) C42.4**

The axial strain – lateral strain plots for all CFRP confinement configurations for both C37.3 and C42.4 are shown in Figure 4-19. The slope of each of these curves represents the dilation rate.

Dilation rate is defined as the rate of change of lateral strain with respect to the change in the axial strain. As can be seen from the figure, the dilation rate decreases as the stiffness of the confining jacket increases

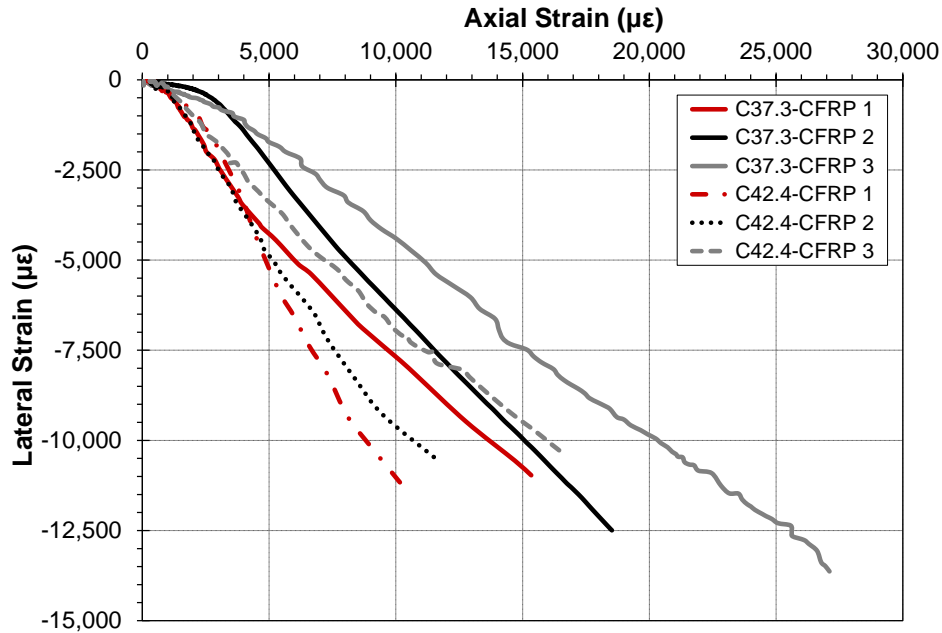


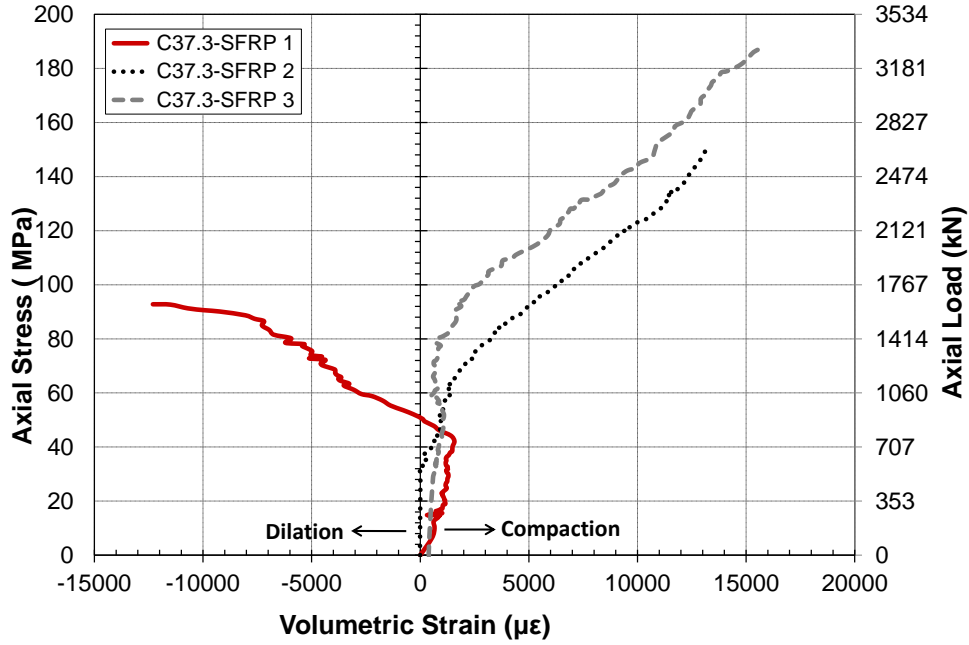
**Figure 4-19: Axial strain-lateral strain plots for CFRP-confined cylinders**

#### 4.4.5.2.2 SFRP-Confined Concrete Cylinders

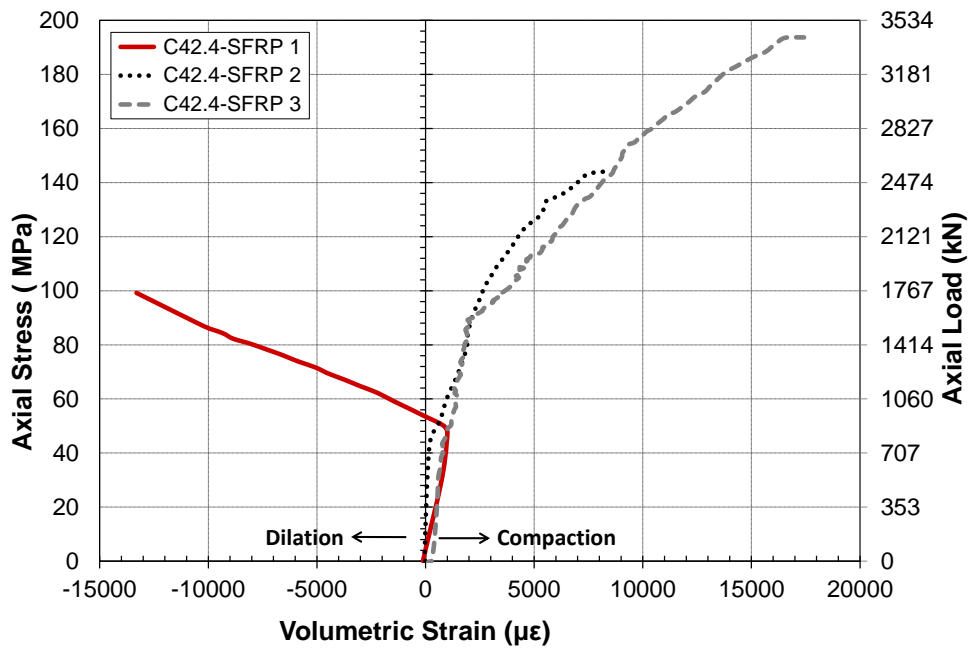
To examine the unique volumetric strain response of SFRP-confined cylinders, plots of axial stress - volumetric strain for C37.3 and C42.4 are shown in Figure 4-20 (a) and Figure 4-20 (b), respectively for different SFRP jacket thicknesses.

As shown in Figure 4-20 (a) and Figure 4-20 (b) for C37.3 and C42.4, respectively, despite some volume reduction beyond the critical stress of unconfined concrete, one SFRP wrap was eventually unable to curtail the volume expansion of concrete. However, two and three wraps of SFRP maintained volumetric reduction until failure. It is clear that volumetric strain behaviour is

affected by the SFRP jacket stiffness as the lateral expansion can be effectively curtailed as SFRP wrap thickness increases.



(a)



(b)

Figure 4-20: Dilation behaviour of SFRP-wrapped cylinders (a) C37.3 (b) C42.4

This characteristic can be further investigated by plotting the lateral strain-axial strain curve for all SFRP confinement configurations for both C37.3 and C42.4 as shown in Figure 4-21. The slope of each of these curves represents the dilation rate. It can be seen from Figure 4-21 that as the SFRP jacket lateral stiffness increases, the dilation rate decreases.

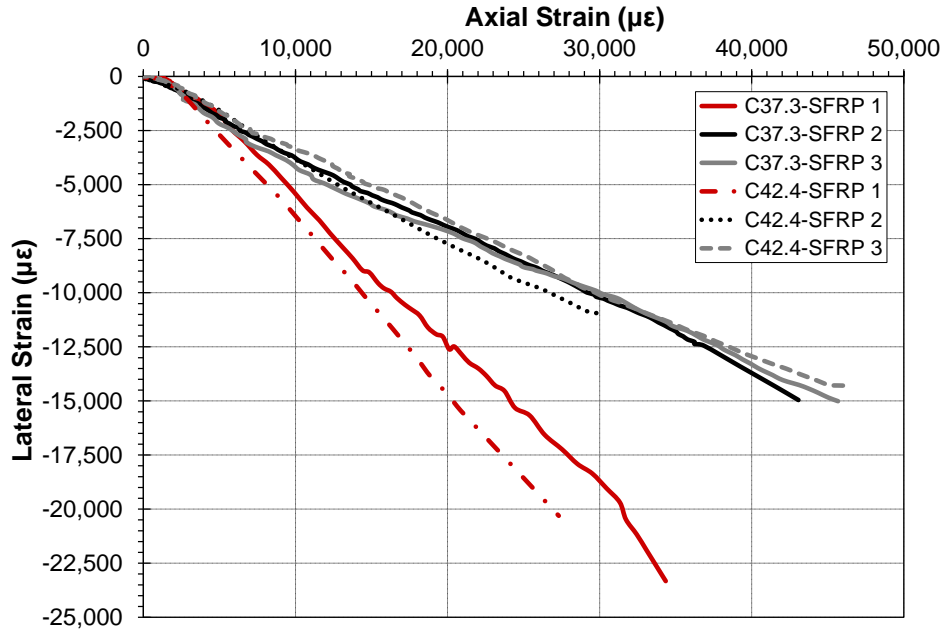


**Figure 4-21: lateral strain-axial strain curve of SFRP-wrapped cylinders**

#### ***4.4.6 Axial and Lateral Strain Variation over FRP-Confined Cylinder's Surface***

As mentioned previously in Section 3.5.3, multiple high resolution Canon Digital Rebel cameras were used to capture digital images of cylinder's front and rear view every five seconds as each cylinder was loaded until failure. These digital images were further processed using the normalised cross-correlation technique by implementing the geoPIV code; square batches of 64x64 pixels were defined in the first image and were tracked through subsequent images. Axial and horizontal strain profile between each of these patches can be then directly calculated from measured axial and lateral deformation of each of these data points.

The length of the axial virtual strain gauge was approximately 25 mm, while the length of the lateral virtual strain gauge was almost 70 mm. It should be noted that top and bottom 50 mm were excluded from analysis to eliminate any effect from the artificial confinement arising from loading platens' frictional lateral strain. Figure 4-22 (a) shows the two digital cameras field of view, Figure 4-22 (b) shows the typical conventional foil strain gauge instrumentation for confined cylinder, and Figure 4-22 (c) Figure 4-22 (d) show axial and lateral virtual strain gauges typical distribution over the height of each tested cylinders.

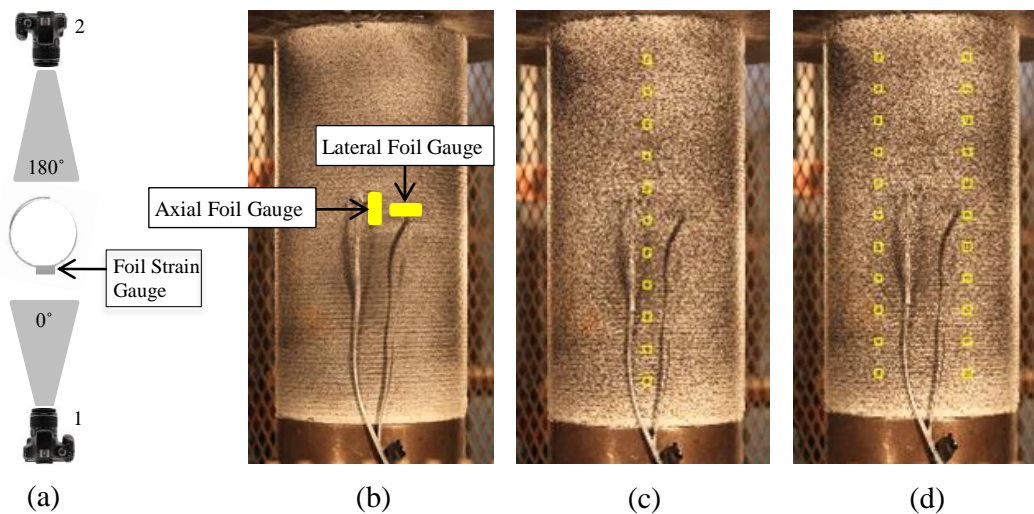


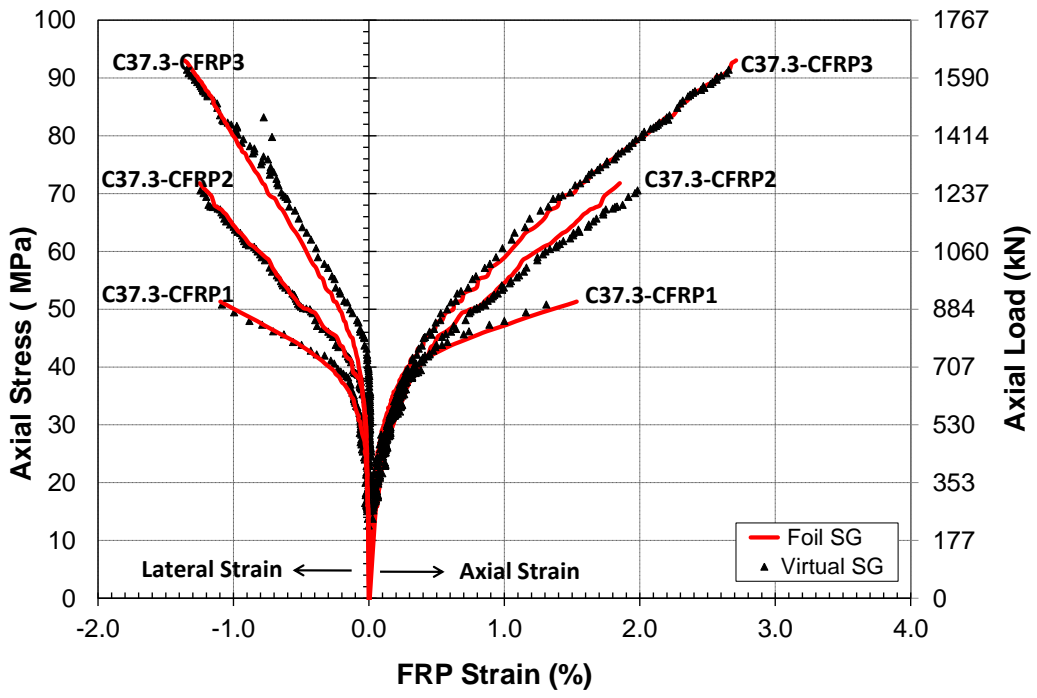
**Figure 4-22: Typical instrumentation: (a) DICT setup (b) Conventional strain gauges (c) vertical strain patches (d) Horizontal strain patches**

#### 4.4.6.1 Validation of the DIC Technique

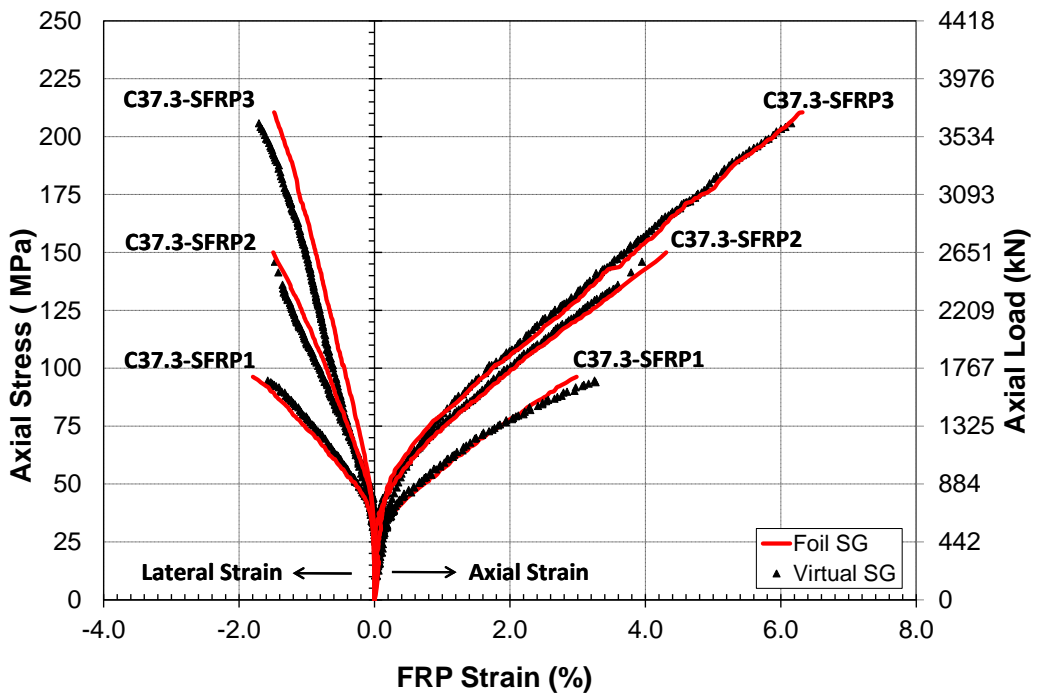
DIC technique validation results are shown in Figure 4-23 (a), (b), (c) and (d) by presenting a comparison of the axial and the lateral strains measured at the mid-height of the cylinder using both conventional and virtual strain gauges. It is clear from figures that the agreement between the stains from conventional and foil gauges is excellent in terms of trend and magnitude, however, readings from virtual strain gauges at initial loading stage were slightly scattered. At the initial loading stage, before the unconfined concrete strength is reached and the FRP jacket is

still inactivated, the strain deformation over the full surface of the jacket is very small; hence, it was extremely difficult to be captured accurately by the DIC technique.

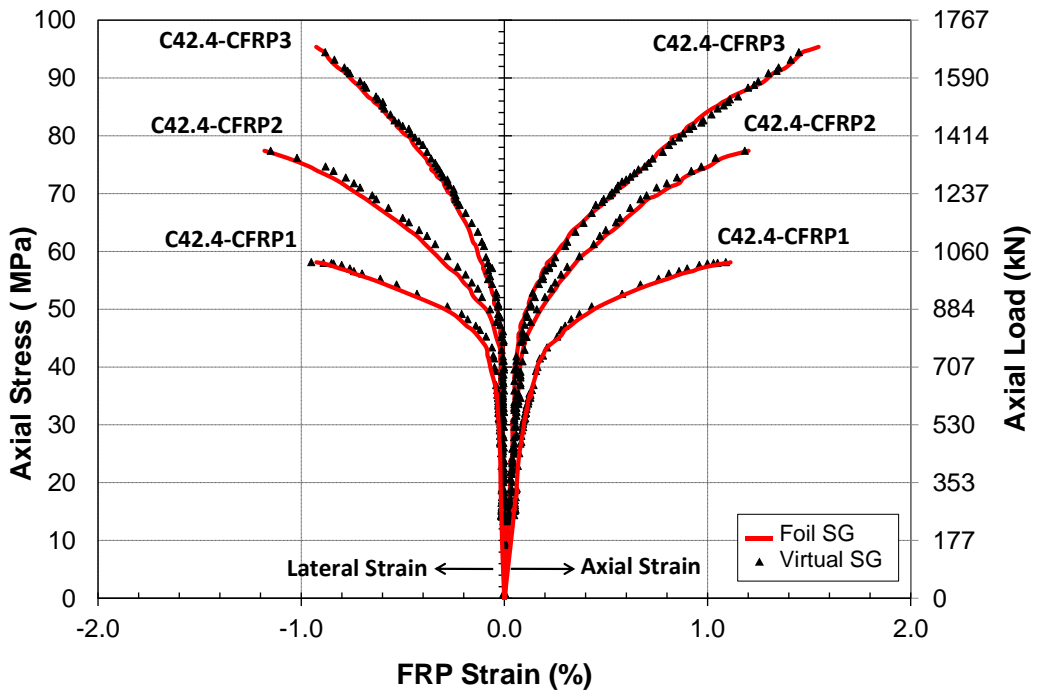
Furthermore, the axial and lateral strain at failure measured at mid-height of the cylinders using both conventional and virtual strain gauges are compared in Table 4-14 and Table 4-15 for CFRP-and SFRP-confined cylinders, respectively. It is clear from the tables that, in most cases, the differences between both readings are marginal with a percentage difference less than 5%, however, in some cases, the maximum axial and lateral strains were not accurately captured by the virtual strain gauges, and the percentage difference was in the range of 20%. This is due to the fact that photos were taken at 5 second intervals during testing while conventional strain readings were recorded at 0.1 second intervals (10 Hz). If a cylinder fails almost five seconds from the last photo taken, the measured strain, from the last photo, and the actual strain, at the end of the five seconds interval, may differ considerably as the strain rate, at loading close to failure, is high. Despite this drawback, which can be overcome by using higher frame rate, the technique is still considered a very powerful tool and is used, as will be explained in the next section, for quantifying the axial and lateral strain distribution over the full surface of the FRP jacket.



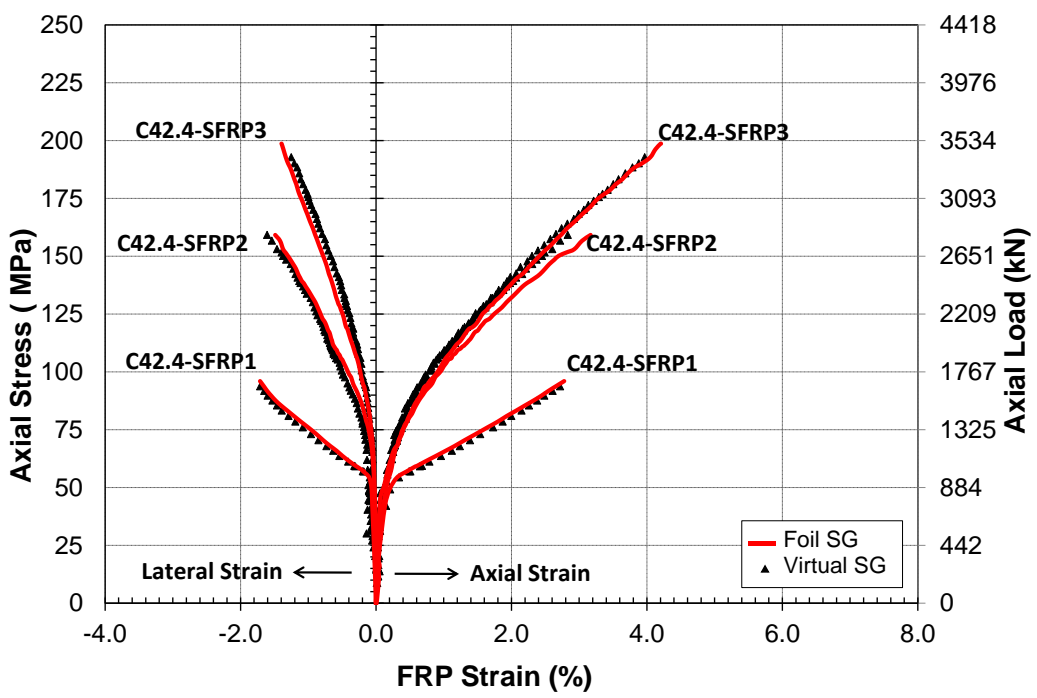
(a)



(b)



(c)



(d)

Figure 4-23: Comparison between foil and virtual strain gauges at mid height of confined cylinders for: (a) C37.3-CFRP (b) C37.3-SFRP (c) C42.4-CFRP (d) C42.4-SFRP

**Table 4-14: Ultimate axial and lateral strain readings from foil and virtual gauges for CFRP-confined cylinders**

Configuration Designation	Ultimate Axial and Lateral Strain					
	Foil Strain Gauge		Virtual Strain Gauges		Percentage Difference	
	Axial Strain	Lateral Strain	Axial Strain	Lateral Strain	Axial	Lateral
	Avg. (%)	Avg. (%)	Avg. (%)	Avg. (%)	(%)	(%)
C37.3-CFRP1-SP#1	1.46	-0.91	1.48	-1.09	1	21
C37.3-CFRP1-SP#2	1.53	-1.10	1.31	-1.09	15	1
C37.3-CFRP1-SP#3	1.40	-1.15	1.32	-1.29	6	13
C37.3-CFRP2-SP#1	1.85	-1.25	1.98	-1.24	7	0
C37.3-CFRP2-SP#2	1.86	-1.37	2.09	-1.16	12	15
C37.3-CFRP2-SP#3	2.06	-1.17	1.92	-1.15	7	2
C37.3-CFRP3-SP#1	2.71	-1.36	2.67	-1.34	1	2
C37.3-CFRP3-SP#2	2.58	-1.37	2.35	-1.25	9	9
C37.3-CFRP3-SP#3	2.34	-1.29	2.33	-1.26	0	2
C42.4-CFRP1-SP#1	1.07	-0.97	1.06	-1.02	1	6
C42.4-CFRP1-SP#2	1.11	-0.93	1.09	-0.95	2	3
C42.4-CFRP1-SP#3	1.02	-1.12	0.98	-1.05	4	6
C42.4-CFRP2-SP#1	1.07	-1.14	1.07	-1.10	1	4
C42.4-CFRP2-SP#2	1.20	-1.18	1.18	-1.15	1	3
C42.4-CFRP2-SP#3	1.17	-1.06	*	*		
C42.4-CFRP3-SP#1	1.66	-1.04	1.72	-1.00	3	4
C42.4-CFRP3-SP#2	1.45	-1.04	1.43	-1.02	1	2
C42.4-CFRP3-SP#3	1.51	-0.91	1.45	-0.88	4	3

\* data lost during testing

**Table 4-15: Ultimate axial and lateral strain readings from foil and virtual gauges for SFRP-confined cylinders**

Configuration Designation	Ultimate Axial and Lateral Strain					
	Foil Strain Gauge		Virtual Strain Gauges		Percentage Difference	
	Axial Strain	Lateral Strain	Axial Strain	Lateral Strain	Axial	Lateral
	Avg. (%)	Avg. (%)	Avg. (%)	Avg. (%)	(%)	(%)
C37.3-SFRP1-SP#1	3.44	-2.33	3.22	-1.95	6	16
C37.3-SFRP1-SP#2	2.98	-1.80	2.84	-1.69	5	6
C37.3-SFRP1-SP#3	3.21	-2.37	3.37	-1.96	5	17
C37.3-SFRP2-SP#1	4.64	-1.39	4.70	-1.48	1	7
C37.3-SFRP2-SP#2	4.16	-1.59	*	*		
C37.3-SFRP2-SP#3	4.31	-1.50	3.95	-1.47	8	2
C37.3-SFRP3-SP#1	4.57	-1.50	4.42	-1.39	3	8
C37.3-SFRP3-SP#2	6.32	-1.48	6.15	-1.67	3	13
C37.3-SFRP3-SP#3	5.46	-1.54	5.30	-1.53	3	1
C42.4-SFRP1-SP#1	2.59	*	2.22	-1.48	15	
C42.4-SFRP1-SP#2	2.73	-2.03	2.78	-1.99	2	2
C42.4-SFRP1-SP#3	2.78	-1.71	2.72	-1.71	2	0
C42.4-SFRP2-SP#1	3.17	-1.49	2.83	-1.61	11	8
C42.4-SFRP2-SP#2	3.77	-1.16	3.42	-1.53	9	31
C42.4-SFRP2-SP#3	3.03	-1.10	2.71	-1.09	10	1
C42.4-SFRP3-SP#1	4.60	-1.43	4.28	-1.36	7	5
C42.4-SFRP3-SP#2	4.21	-1.40	3.97	-1.33	6	5
C42.4-SFRP3-SP#3	5.40	-1.59	5.00	-1.52	7	4

\* data lost during testing

#### 4.4.6.2 Axial and Lateral Strain Variation in CFRP-Confined Concrete Cylinders

The evolution of the virtual lateral strain profile over cylinder full height as cylinder loaded to failure is shown in Figure 4-24 and Figure 4-25 for each confinement configuration. In each plot, curves to the left are from camera 1 location while curves to the right are from camera 2.

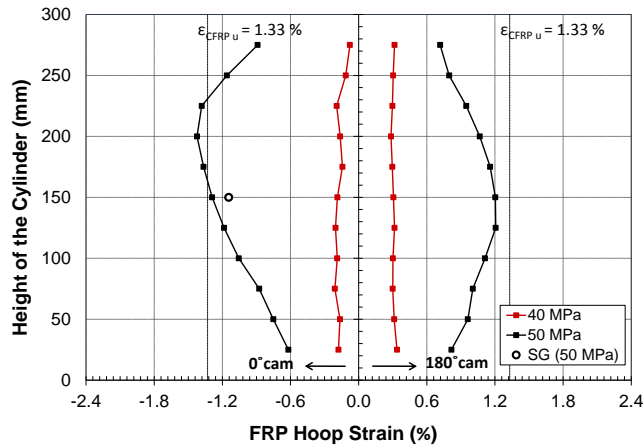
Discrete lateral strain readings from conventional strain gauge at the corresponding loading level are also shown for comparison. As previously discussed, the agreement between strain readings from conventional and virtual strain gauges over the full range of loading is apparent in all figures. Furthermore, the trend of how the lateral strain profile developed as compression loading increases looks similar, irrespective of the FRP jacket thickness or concrete unconfined strength. As expected, at load levels close to the unconfined concrete strength, lateral strain is negligible,

after which it starts to increase rapidly as the concrete dilates and the lateral strain profile develops consistently at all subsequent load levels forming a bell shaped curve as the maximum lateral strain occurs at or close to the mid height of the cylinder.

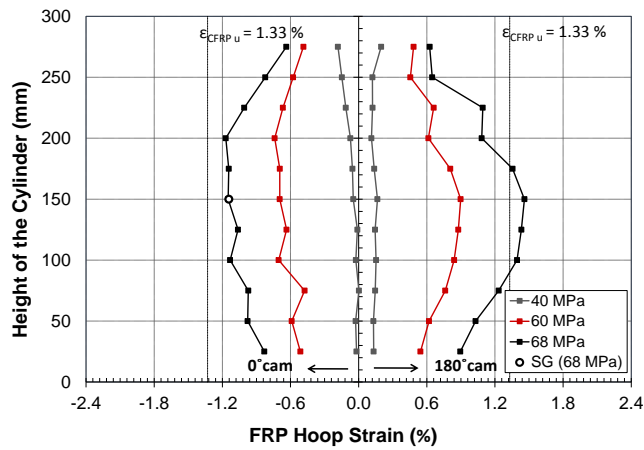
Individual plots of lateral strain evolution for each cylinder are shown in Appendix C.

The virtual axial and lateral strain profiles at failure for each confinement configuration are shown in Figure 4-26 and Figure 4-27. In each plot, curves to the right represent the virtual axial strain profiles at failure and curves to the left represent the virtual lateral strain profile at failure.

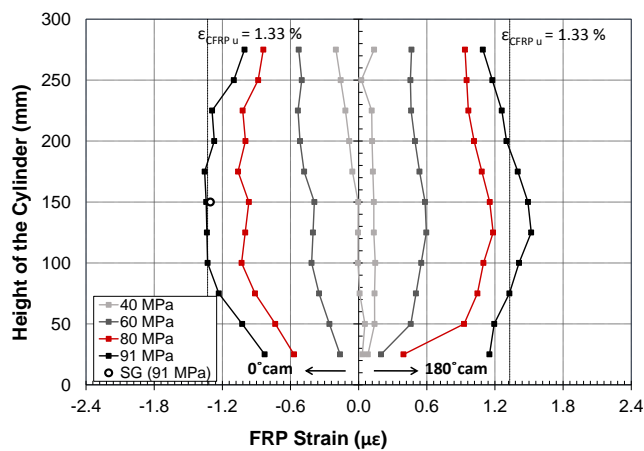
The lateral strain profiles, as mentioned previously, exhibit a bell-shaped curve due to friction restraint from loading platens, however, the axial strain profiles are somehow random. It is also clear that there are significant lateral and axial strain variations at failure over the height of the cylinder in all cases.



(a)

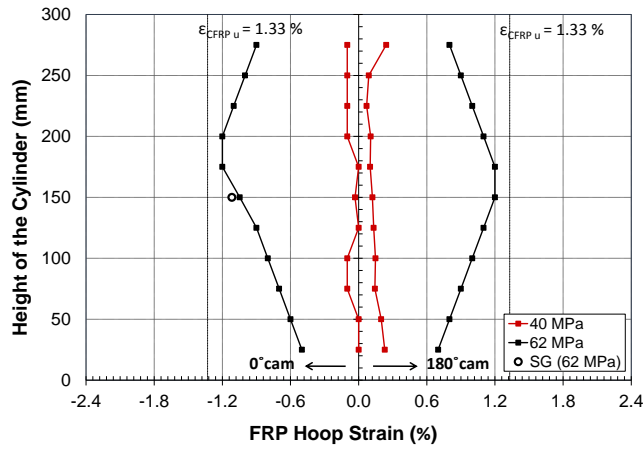


(b)

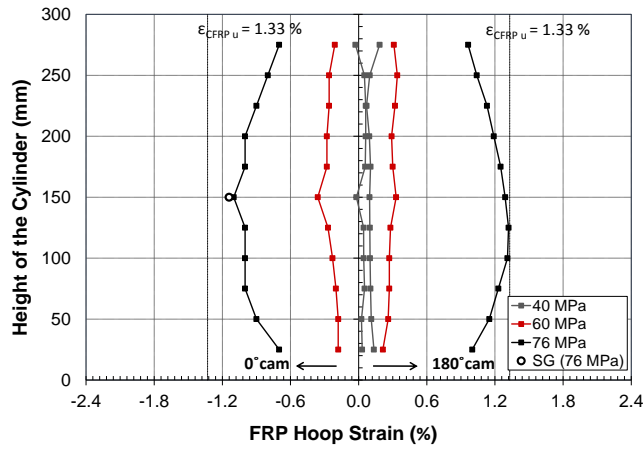


(c)

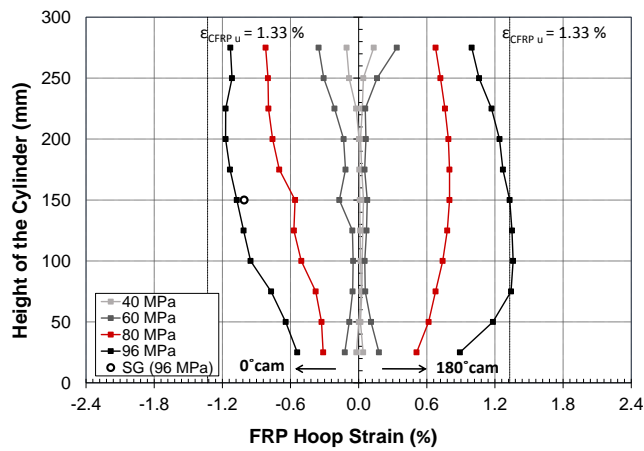
Figure 4-24: Lateral strain profile evolution for: (a) C37.3-CFRP1 (b) C37.3-CFRP2 (c) C37.3-CFRP3



(a)

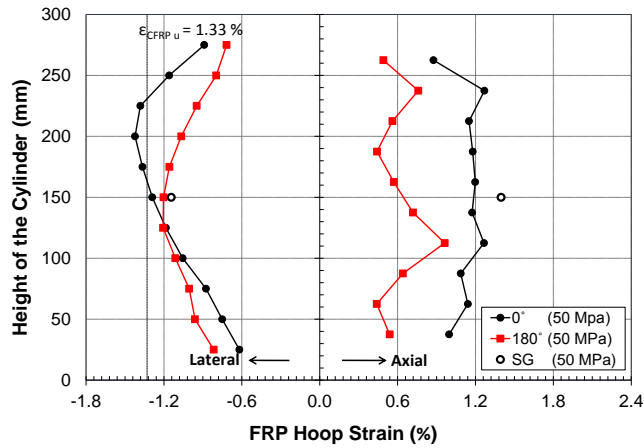


(b)

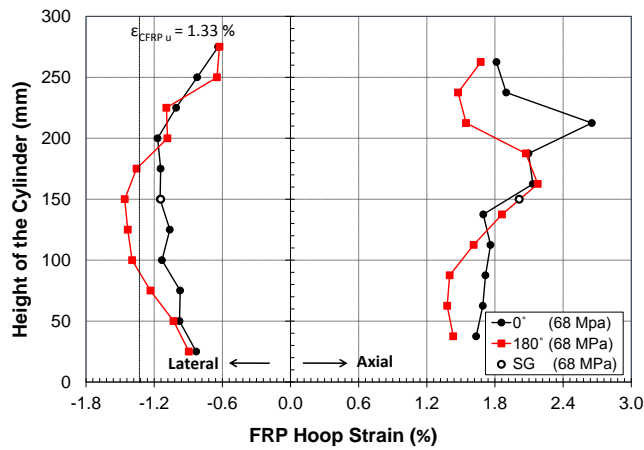


(c)

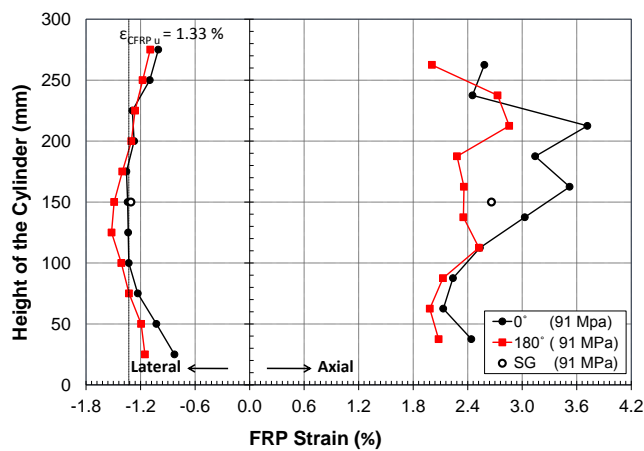
Figure 4-25: Lateral strain profile evolution for: (a) C42.4-CFRP1 (b) C42.4-CFRP2 (c) C42.4-CFRP3



(a)

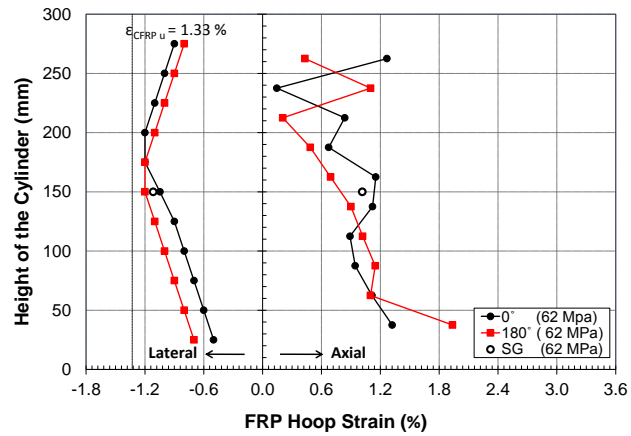


(b)

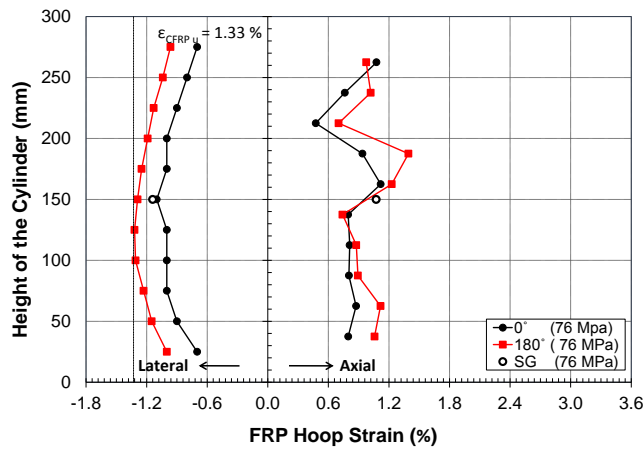


(c)

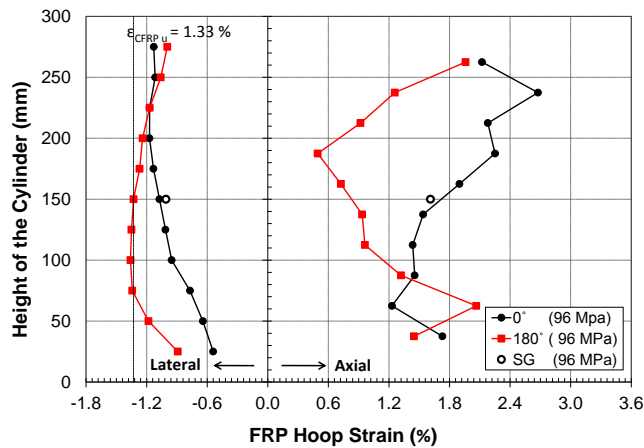
**Figure 4-26: Axial and lateral strain distribution at failure for: (a) C37.3-CFRP1 (b) C37.3-CFRP2 (c) C37.3-CFRP3**



(a)



(b)



(c)

Figure 4-27: Lateral strain profile evolution for: (a) C42.4-CFRP1 (b) C42.4-CFRP2 (c) C42.4-CFRP3

To obtain a more detailed quantification of the axial and lateral strain variation at failure, the results of the statistical analysis of the virtual strain readings obtained from camera 1 and camera 2 for the three nominally identical cylinders from each confinement configuration are reported in Table 4-16. The results presented include the mean, the maximum and minimum of all virtual strain data points within the middle 200 mm of each cylinder. Strain variation is calculated by taking the difference between the maximum and minimum virtual strain readings. It was found that the average lateral strain variation for CFRP-confined cylinders was around 5000  $\mu\epsilon$  while the axial strain variation was more pronounced and in order of 12500  $\mu\epsilon$ .

This strain variation clearly shows that the accuracy of strain measurement obtained using isolated discrete foil strain gauges is questionable in terms of presenting the actual lateral FRP strain at failure and provides partially an explanation of the wide scatter in the FRP strain efficiency reported in the literature. Bearing that in mind, the majority of confinement models that have been developed or calibrated based on these discrete strain measurements should be interpreted and used with caution.

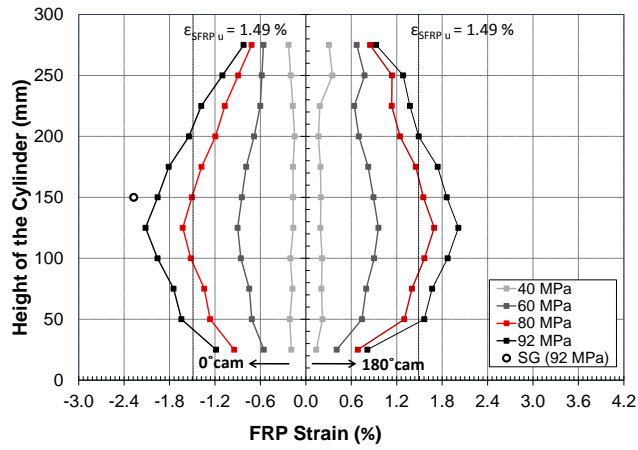
**Table 4-16: Axial and lateral strain variation at failure for CFRP-confined cylinders**

Configuration Designation	Axial and Lateral Strain Variation							
	Virtual Axial Strain				Virtual Lateral Strain			
	Mean	Max.	Min.	Variation	Mean	Max.	Min.	Variation
	(%)	(%)	(%)	(%)	(%)	(%)	(%)	(%)
C37.3-CFRP1	0.92	1.30	0.51	0.79	-1.01	-1.35	-0.73	0.62
C37.3-CFRP2	1.76	2.46	1.29	1.17	-1.18	-1.39	-0.96	0.43
C37.3-CFRP3	2.48	3.10	1.98	1.12	-1.30	-1.54	-1.06	0.48
C42.4-CFRP1	0.83	1.30	0.24	1.07	-1.03	-1.23	-0.67	0.56
C42.4-CFRP2	0.85	1.96	0.28	1.68	-1.15	-1.32	-1.00	0.32
C42.4-CFRP3	1.33	2.27	0.58	1.69	-1.08	-1.25	-0.80	0.45

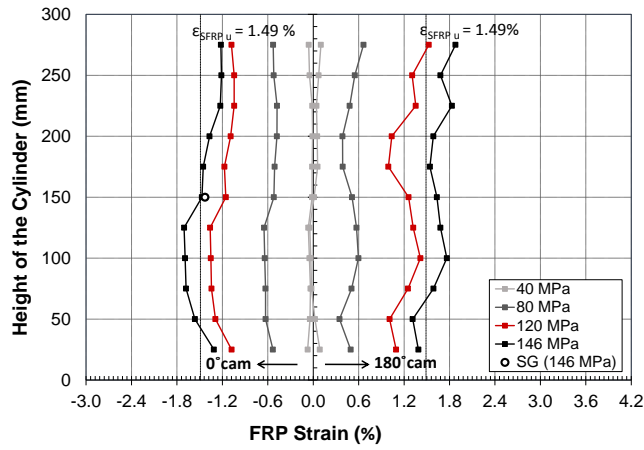
#### 4.4.6.3 Axial and Lateral Strain Variation in SFRP-Confined Concrete Cylinders

The evolution of the virtual lateral strain profile over the full height of the cylinder as the cylinders were loaded to failure is shown in Figure 4-28 and Figure 4-29. In each plot, curves to the left are from camera 1 location while curves to the right are from camera 2. Discrete lateral strain readings from conventional strain gauges at the corresponding loading level are also shown for comparison. As discussed previously, the agreement between strain readings from conventional and virtual strain gauges over the full range of loading is apparent in all figures. Furthermore, the trend of how lateral strain profile developed as compression loading increases looks similar, irrespective of the FRP jacket thickness or concrete unconfined strength. As expected, at load levels close to the unconfined concrete strength, lateral strain is negligible, after which it starts to increase rapidly as the concrete dilates and the lateral strain profile develops consistently at all subsequent load levels forming a bell shaped curve as the maximum lateral strain occurs at or close to the mid height of the cylinder.

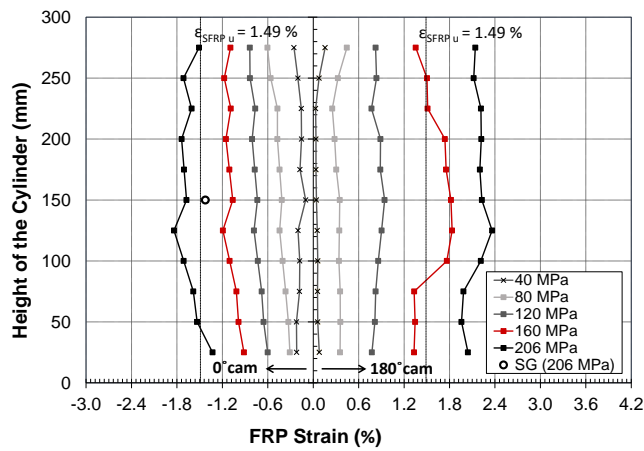
The virtual axial and lateral strain profiles at failure for each confinement configuration are shown in Figure 4-30 and Figure 4-31. Plots to the right represent the virtual axial strain profile at failure and plots to the left represent the virtual lateral strain profile at failure. The lateral strain profiles, as mentioned previously, exhibit a bell-shaped curve due to friction restraint from loading platens, however, the axial strain profiles are somehow random. It is also clear that there is significant lateral and axial strain variation over the height of the cylinder in all cases. The maximum lateral strain is generally at or close to the mid-height of cylinder while the maximum axial strain at failure is somehow arbitrary and there is no apparent correlation between the location of the maximum axial and lateral strain at failure.



(a)

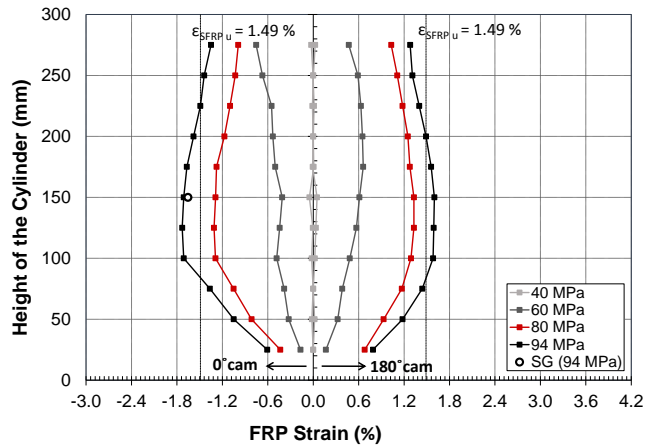


(b)

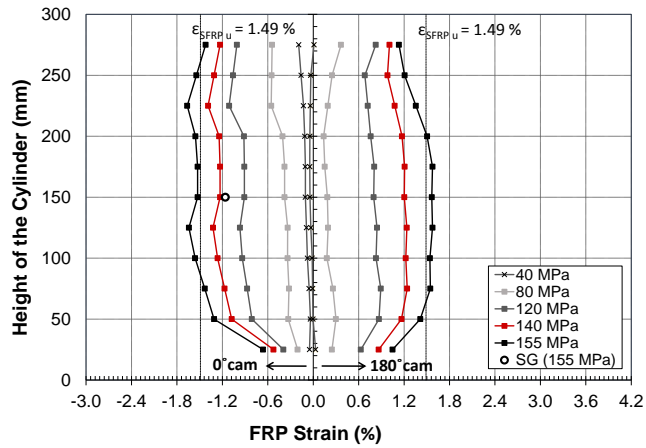


(c)

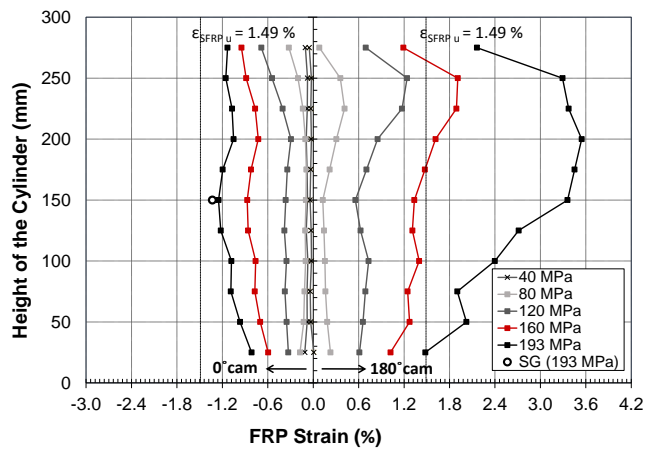
Figure 4-28: Lateral strain profile evolution for: (a) C37.3-SFRP1 (b) C37.3-SFRP2 (c) C37.3-SFRP3



(a)

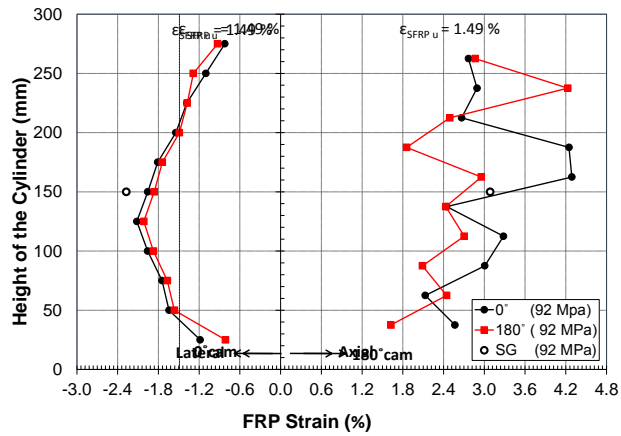


(b)

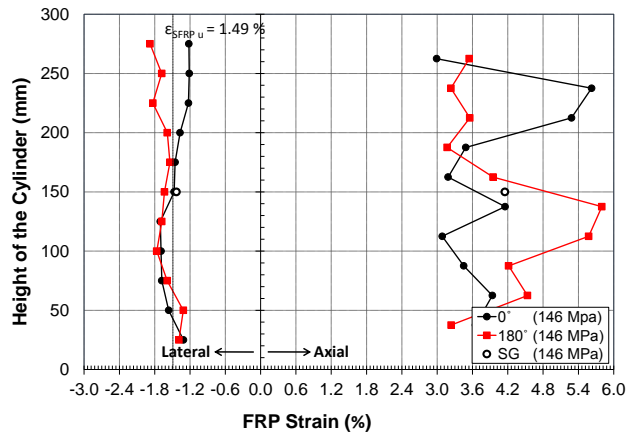


(c)

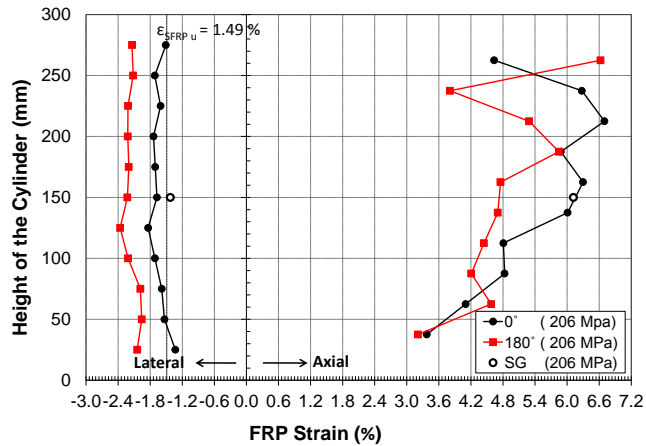
Figure 4-29: Lateral strain profile evolution for: (a) C42.4-SFRP1 (b) C42.4-SFRP2 (c) C42.4-SFRP3



(a)

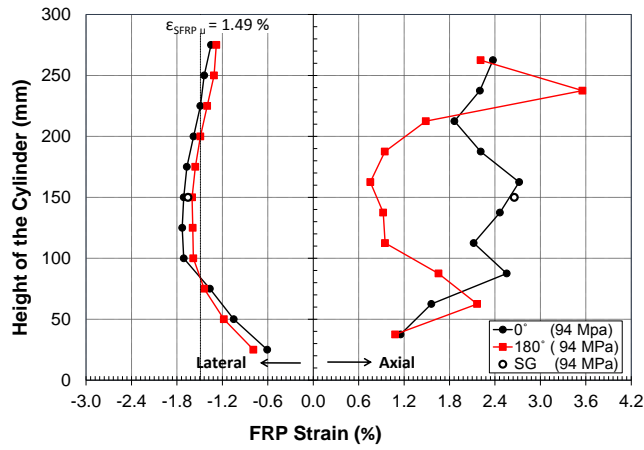


(b)

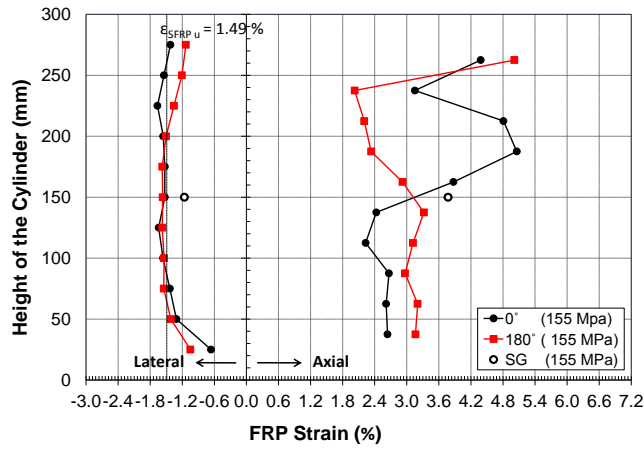


(c)

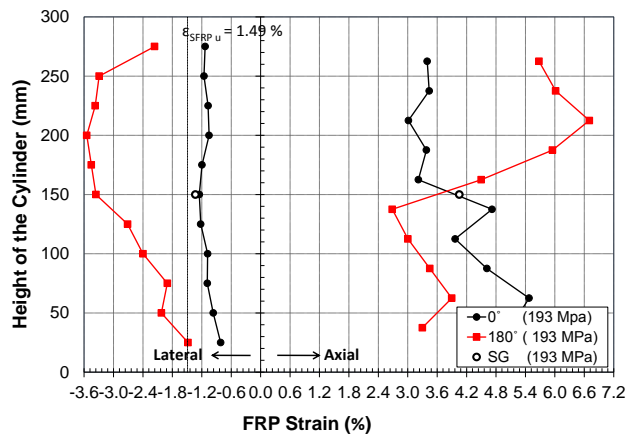
Figure 4-30: Lateral strain profile evolution for: (a) C37.3-SFRP1 (b) C37.3-SFRP2 (c) C37.3-SFRP3



(a)



(b)



(c)

**Figure 4-31: Lateral strain profile evolution for: (a) C42.4-SFRP1 (b) C42.4-SFRP2 (c) C42.4-SFRP3**

To obtain a more detailed quantification of the axial and lateral strain variation, the results of the statistical analysis of the virtual strain readings obtained from camera 1 and camera 2 for each CFRP-confined cylinder are reported in Table 4-17. The results presented include the mean, maximum and minimum of all virtual strain data points within the middle 200 mm of each cylinder. Strain variation is calculated by taking the difference between the maximum and minimum virtual strain readings. The average lateral strain variation for SFRP-confined concrete cylinders was in the order of 8200  $\mu\epsilon$  while the average axial strain variation was more pronounced and in the order of 25500  $\mu\epsilon$ .

**Table 4-17: Axial and lateral strain variation at failure for SFRP-confined cylinders**

Configuration Designation	Axial and Lateral Strain Variation							
	Virtual Axial Strain				Virtual Lateral Strain			
	Mean (%)	Max. (%)	Min. (%)	Variation (%)	Mean (%)	Max. (%)	Min. (%)	Variation (%)
C37.3-SFRP1	2.96	4.30	1.90	2.40	-1.51	-1.93	-1.03	0.90
C37.3-SFRP2	4.09	5.17	3.26	1.91	-1.44	-1.67	-1.07	0.61
C37.3-SFRP3	4.89	6.18	3.46	2.72	-1.840	-2.36	-1.38	0.98
C42.4-SFRP1	1.70	2.77	0.65	2.12	-1.46	-1.73	-1.23	0.50
C42.4-SFRP2	3.05	4.81	2.19	2.62	-1.46	-1.72	-1.23	0.49
C42.4-SFRP3	4.22	6.13	2.63	3.50	-1.73	-2.56	-1.10	1.46

#### 4.4.7 FRP Strain Efficiency

The FRP efficiency factor,  $\eta_{frp}$ , is defined as the ratio of the actual FRP lateral tensile strain at failure,  $\epsilon_{frp,a}$ , over the FRP rupture strain reported by the manufacturer or obtained from flat coupon tests,  $\epsilon_{frp}$ . The efficiency factor is calculated from the following equation

$$\eta_{frp} = \frac{\epsilon_{frp,a}}{\epsilon_{frp}} \quad \text{Equation 4-7}$$

##### 4.4.7.1 CFRP Sheet Strain Efficiency

CFRP strain efficiency for each confinement configuration calculated from the ultimate lateral strain obtained from the discrete conventional strain gauge that was installed at the mid height of

each cylinder and the corresponding strain efficiency calculated from the mean value of all virtual strain gauges distributed over the full height of the tested cylinder are compared in Table 4-18 for CFRP-confined cylinders. Two values of strain efficiency for each are reported in the table, the first is based on the CFRP rupture strain reported by the manufacturer while the second is based on the CFRP rupture strain obtained from flat coupon test. It has been found that the CFRP strain efficiency from discrete strain gauge for C37.3-CFRP, and C42.4-CFRP confinement configuration, respectively, are 0.92 and 0.78 based on the manufacturer's rupture strain and 1.09 and 0.93 based on the flat coupon test. On the other hand, the CFRP strain efficiency from the DIC technique for the aforementioned two confinement configuration are 0.85 and 0.79 based on the manufacturer's rupture strain and 1.04 and 0.97 based on the flat coupon test value.

**Table 4-18: CFRP strain efficiency**

Configuration Designation	CFRP Strain Efficiency				Diff. (%)
	From Discrete Strain Gauge		From DIC Technique		
	Manuf. (%)	Coupon (%)	Manuf. (%)	Coupon (%)	
C37.3-CFRP1	0.79	0.94	0.74	0.90	3.7
C37.3-CFRP2	0.95	1.13	0.86	1.06	6.4
C37.3-CFRP3	1.01	1.20	0.95	1.16	3.0
C42.4-CFRP1	0.75	0.90	0.74	0.91	-1.3
C42.4-CFRP2	0.85	1.01	0.84	1.03	-2.1
C42.4-CFRP3	0.75	0.89	0.80	0.97	-8.8

#### 4.4.7.2 SFRP Sheet Strain Efficiency

SFRP strain efficiency for each confinement configuration calculated from the ultimate lateral strain obtained from the discrete conventional strain gauge that was installed at the mid height of the cylinder and the corresponding strain efficiency calculated from the mean value of all virtual strain gauges distributed over the full height of the tested cylinder are compared in Table 4-19 for SFRP-confined cylinders. Two values of strain efficiency for each are reported in the table,

the first is based on the FRP rupture strain reported by the manufacturer while the second is based on the FRP rupture strain obtained from the flat coupon test. It has been found that the SFRP strain efficiency from discrete strain gauge for C37.3-SFRP, and C42.4-SFRP confinement configuration, respectively, are 1.16 and 1.03 based on the manufacturer's rupture strain and 1.25 and 1.11 based on the flat coupon test. On the other hand, the SFRP strain efficiency from the DIC technique for the former two confinement configurations are 1.07 and 1.04 based on the manufacturer's rupture strain and 1.16 and 1.12 based on the flat coupon test value.

**Table 4-19: SFRP sheet strain efficiency**

Configuration Designation	SFRP Strain Efficiency				
	From Discrete Strain Gauge		From DIC Technique		Diff. (%)
	Manuf. (%)	Coupon (%)	Manuf. (%)	Coupon (%)	
C37.3-SFRP1	1.45	1.57	1.01	1.10	30.2
C37.3-SFRP2	1.00	1.08	0.97	1.05	3.1
C37.3-SFRP3	1.01	1.09	1.23	1.33	-21.7
C42.4-SFRP1	1.26	1.36	0.98	1.06	21.9
C42.4-SFRP2	0.84	0.91	0.98	1.05	-16.4
C42.4-SFRP3	0.99	1.07	1.16	1.25	-17.4

This long-observed discrepancy between the FRP rupture strain determined from tensile coupon tests and those obtained from strain gauge reading at failure has been the centre of research focus for decades, and several theories have been suggested in the literature to explain this observation, two of which are discussed in detail in the following section.

#### 4.4.7.3 Failure Theories of FRP Wraps

When concrete is subjected to a uniaxial compression, multiple visible cracks propagate parallel to the direction of the applied load, Wang and Shrive (1995). Once the cracks are developed, there are mainly two suggested failure mechanisms of the FRP wraps; the first stated that the FRP sheets are not bonded to the concrete and the interface is frictionless, hence, shear forces are not transferred across the interface between the jacket and the concrete, and uniform strain around

the perimeter of the jacket is developed as shown in Figure 4-32 (a). In this case, the difference between the experimentally-obtained FRP strain at failure and the FRP rupture strain determined from tensile coupon test is attributed to many factors such as: misalignment, damage, or uneven tension in the jacket fibre during handling and layup process, flaws in concrete substrate, or the cumulative flaws in the FRP materials when compared to the much smaller FRP tensile coupons. Pessiki et al. (2001). However, the above theory is not in line with the observed significant axial and lateral strain variations along the full surface of the confined cylinders that have been quantified from DIC technique and have been discussed in Section 4.4.6.2 and Section 4.4.6.3 which confirm that FRP jacket is not uniformly strained neither around the cylinder perimeter nor along the cylinder height.

Another theory on the FRP failure mechanism, which aligns with the herein experimental observation, suggested that if there is a good bond between FRP sheets and the concrete core, shear forces can transfer from jacket to concrete reducing the average strain in the jacket but localising the strain in local regions where jacket crosses splitting cracks as shown in Figure 4-32 (b). Unless the strain gauge measurements are taken exactly at these localized region of high strain, the measured strain at rupture are lower than the actual jacket strain at rupture. Pessiki et al. (2001).

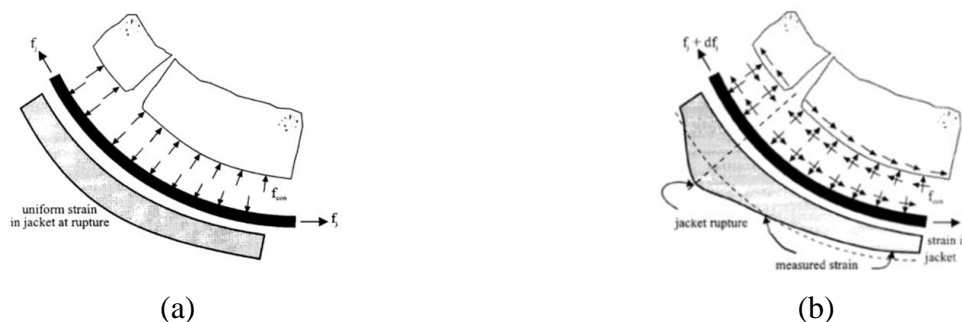


**Figure 4-32: FRP failure mechanism theory (a) Uniform (b) Localized strain failure, Pessiki et al. (2001)**

## 4.5 Performance Comparison between CFRP- and SFRP-Confined Cylinders

The performance of SFRP-confined cylinders are analyzed and compared to that exhibited by corresponding CFRP-confined cylinders based on a series of parameters. These parameters include confinement effectiveness coefficient,  $k_l$ , strain ductility index,  $\mu_{cu}$ , and energy ductility index,  $\omega_{cu}$ . The aforementioned parameters are calculated based on the current test data and are reported for all CFRP-and SFRP-confined cylinders in Table 4-20 and Table 4-21, respectively.

### 4.5.1 Performance Parameters

#### 4.5.1.1 Confinement Effectiveness Coefficients ( $k_l$ )

Experimental confinement effectiveness coefficient,  $k_l$ , is calculated utilising the formula originally developed by Richart et al. (1928) as shown below

$$k_l = \frac{(f'_{cu} - f'_{co})}{f_{lu}} \quad \text{Equation 4-8}$$

where  $f'_{cu}$  is the ultimate confined concrete strength,  $f'_{co}$  is the unconfined concrete strength at peak and  $f_{lu}$  is the ultimate lateral confining pressure.

#### 4.5.1.2 Strain Ductility Index, ( $\mu_{cu}$ )

The strain ductility factor,  $\mu_{cu}$ , measures the ability of a structural member to undergo large inelastic deformation without significant loss in strength. It is defined as the ratio of the FRP ultimate axial strain at rupture,  $\varepsilon_{cu}$  over the axial strain corresponding to unconfined concrete at peak,  $\varepsilon_{co}$ . It is calculated as per the following equation:

$$\mu_{cu} = \frac{\varepsilon_{cu}}{\varepsilon_{co}} \quad \text{Equation 4-9}$$

#### 4.5.1.3 Energy Ductility Index, ( $\omega_{cu}$ )

The energy ductility index,  $\omega_{cu}$ , is defined as the area under the stress-strain curve up to the failure of FRP jacket over the area under the stress stress-strain curve corresponding to the unconfined state. It expresses the ability of the structural member to dissipate energy during inelastic deformation.

$$\omega_{cu} = \frac{Area_1}{Area_2} \quad \text{Equation 4-10}$$

Different parameters of ductility indices for bilinear stress-strain response are illustrated in Figure 4-33.

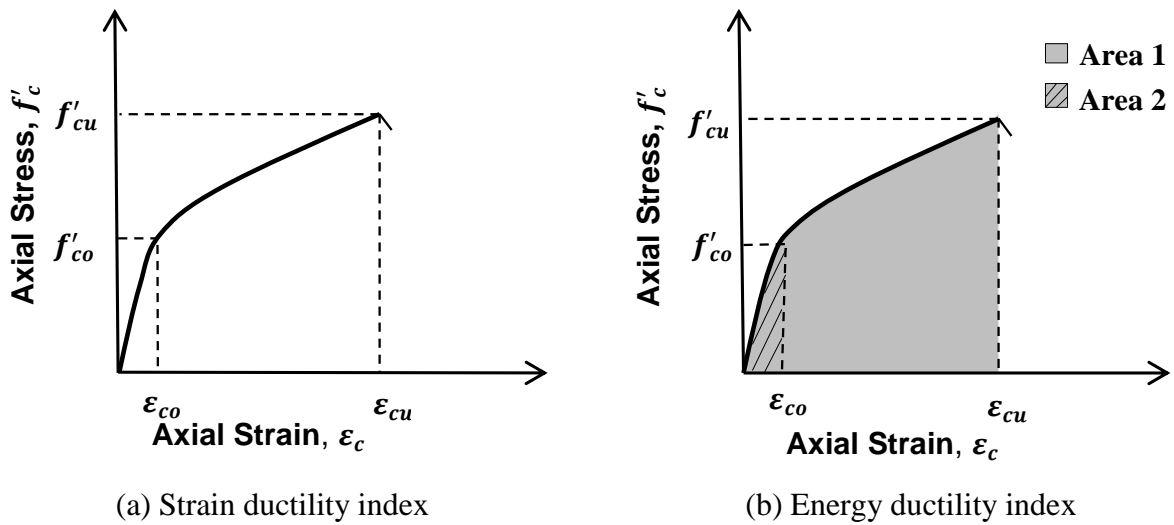


**Figure 4-33: Definition of ductility indices: (a) Strain ductility index (b) Energy ductility index**

**Table 4-20: Summary of performance parameters for CFRP-confined cylinders**

Configuration Designation	Confinement Effectiveness Coefficient					Ductility Indices		
	Lateral Confinement Pressure $f_l$ (MPa)	Confinement Ratio $f_l/f'_{co}$	Strengthening Ratio $f'_{cu}/f'_{co}$	Lateral Stiffness $(2Et/D)$ (MPa)	Lateral Stiffness Ratio $(2Et/Df'_{co})$	Confinement Effectiveness Coefficient $k_l$	Strain Ductility Index $\mu_{cu}$	Energy Ductility Index $\omega_{cu}$
C37.3-CFRP1-SP#1							7.5	9.4
C37.3-CFRP1-SP#2	4.54	0.12	1.38	332	8.9	3.10	7.8	10.4
C37.3-CFRP1-SP#3							7.1	9.0
C37.3-CFRP2-SP#1							9.5	14.9
C37.3-CFRP2-SP#2	9.08	0.24	1.86	664	17.8	3.54	9.5	15.1
C37.3-CFRP2-SP#3							10.5	17.5
C37.3-CFRP3-SP#1							13.8	27.8
C37.3-CFRP3-SP#2	13.62	0.37	2.48	997	26.7	4.04	13.2	26.5
C37.3-CFRP3-SP#3							11.9	23.7
C42.4-CFRP1-SP#1							6.2	11.0
C42.4-CFRP1-SP#2	4.54	0.11	1.36	332	7.8	3.40	6.3	11.3
C42.4-CFRP1-SP#3							5.8	10.6
C42.4-CFRP2-SP#1							6.1	13.3
C42.4-CFRP2-SP#2	9.08	0.21	1.79	664	15.7	3.68	6.8	15.9
C42.4-CFRP2-SP#3							6.7	14.3
C42.4-CFRP3-SP#1							9.5	26.6
C42.4-CFRP3-SP#2	13.62	0.32	2.23	997	23.5	3.83	8.2	21.6
C42.4-CFRP3-SP#3							8.8	24.33

**Table 4-21: Summary of performance parameters for SFRP-confined cylinders**

Configuration Designation	Confinement Effectiveness Coefficient						Ductility Indices	
	Lateral Confinement Pressure	Confinement Ratio	Strengthening Ratio	Lateral Stiffness	Lateral Stiffness Ratio	Confinement Effectiveness Ratio	Strain Ductility Index	Energy Ductility Index
	$f_l$ (MPa)	$f_l/f'_{co}$	$f'_{cu}/f'_{co}$	$(2Et/D)$ (MPa)	$(2Et/Df'_{co})$	$k_l$	$\mu_{cu}$	$\omega_{cu}$
C37.3-SFRP1-SP#1							17.5	35.1
C37.3-SFRP1-SP#2	15.78	0.42	2.53	1058	28.4	3.63	15.2	30.7
C37.3-SFRP1-SP#3							16.4	32.5
C37.3-SFRP2-SP#1							23.7	68.6
C37.3-SFRP2-SP#2	31.55	0.85	3.94	2115	56.7	3.47	21.2	63.4
C37.3-SFRP2-SP#3							22.0	67.9
C37.3-SFRP3-SP#1							23.3	88.5
C37.3-SFRP3-SP#2	47.33	1.27	5.22	3173	85.1	3.32	32.3	132.2
C37.3-SFRP3-SP#3							27.9	102.9
C42.4-SFRP1-SP#1							14.8	39.4
C42.4-SFRP1-SP#2	15.78	0.37	2.33	1058	24.9	3.57	15.5	40.8
C42.4-SFRP1-SP#3							15.8	41.6
C42.4-SFRP2-SP#1							18.0	77.4
C42.4-SFRP2-SP#2	31.55	0.74	3.63	2115	49.9	3.53	21.5	88.1
C42.4-SFRP2-SP#3							17.2	67.6
C42.4-SFRP3-SP#1							26.2	129.3
C42.4-SFRP3-SP#2	47.33	1.12	4.73	3173	74.8	3.34	24.0	120.9
C42.4-SFRP3-SP#3							30.7	166.9

## ***4.5.2 Effect of Different Parameters***

### **4.5.2.1 Effect of FRP Jacket Thickness**

The thickness of FRP jacket, i.e. the number of FRP layers, plays a significant role in improving the concrete behaviour in terms of strength and ductility. As mentioned earlier, strength and ductility increased as thickness of FRP jacket increases. However, the thickness of FRP jacket has a more pronounced effect on ductility than on strength. For example, concrete cylinders of 37.3 MPa unconfined strength and wrapped with one to three layers of CFRP sheets exhibited an increase in strength of 38% - 147% over unconfined strength while the axial strain increased by 648% - 1199% of the axial strain at peak for unconfined concrete. Concrete cylinders from the same group but wrapped with one to three layers of SFRP sheets exhibited an increase in strength by 153% - 421 % of the unconfined strength, while the axial strain, for the same group, increased by 1538% - 2682% of axial strain at peak stress for unconfined concrete. The same trend has been observed for CFRP-and SFRP-confined concrete cylinders of 42.4 MPa unconfined strength.

On the other hand, the degree of strength and ductility enhancement reduces as the thickness of FRP jacket increases. For example, CFRP-confined cylinders strength improved 38% when wrapped with one layer, 35% when wraps increase from 1 layer to two layer and only 33% from when wraps increase from two layers to three layers. The same trend was more prominent in SFRP-confined cylinder as strength increased by 153% when unconfined cylinders were wrapped with one layer of SFRP sheet, by 55% when the wraps were increased from one layer to two and only 33% when the wraps were increased from two layers to three layers. The same observations can be made for cylinders having 42.4 MPa unconfined compressive strength.

Irrespective of the unconfined concrete strength, as the thickness of the CFRP jacket increases, confinement effectiveness,  $k_l$ , increases. This is expected as increasing the CFRP jacket directly increase the jacket lateral stiffness and hence increase the effectiveness of confinement in restraining concrete expansion. However, SFRP confined cylinders did not show the same trend and the confinement effectiveness,  $k_l$ , marginally reduces as FRP jacket thickness increases. This comes as no surprise bearing in mind that SFRP-confined cylinders with two and three layers fails by partial or full debonding and the SFRP sheets were not fully utilised. The effect of FRP jacket thickness on  $k_l$  is shown in Figure 4-34 (a) and Figure 4-34 (b) for CFRP- and SFRP-confined concrete, respectively.

Increasing the thickness of FRP jacket enhances the ductility as indicated by strain ductility indices for both CFRP-and SFRP-confined cylinders as shown in Figure 4-35 (a) and Figure 4-35 (b), respectively. The strain ductility index for cylinders of concrete strength of 37.3 MPa confined with CFRP sheets improved by 31% when CFRP jacket thickness doubled and improved by 74% when jacket thickness tripled. The same observed for cylinders of concrete strength of 42.4 MPa as strain ductility index enhances by 8% and 46% when CFRP jacket doubled and tripled, respectively.

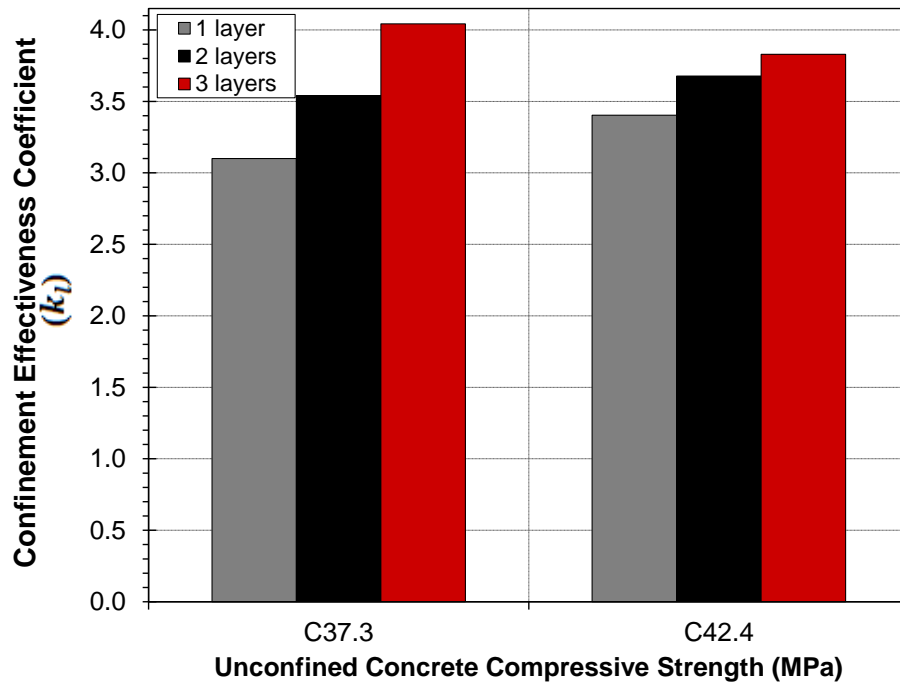
The same trend has been observed for SFRP-confined concrete. Test results showed that for cylinders of concrete strength of 37.3 MPa, the strain ductility index increased by 36% and 70% when the SFRP jacket thickness doubled and tripled, respectively, while for cylinders of concrete strength of 42.4 MPa, the strain ductility index was increased by 23% and 75% when SFRP jacket thickness doubles and tripled, respectively.

Energy absorption capacity improved significantly due to the increase in FRP jacket thickness.

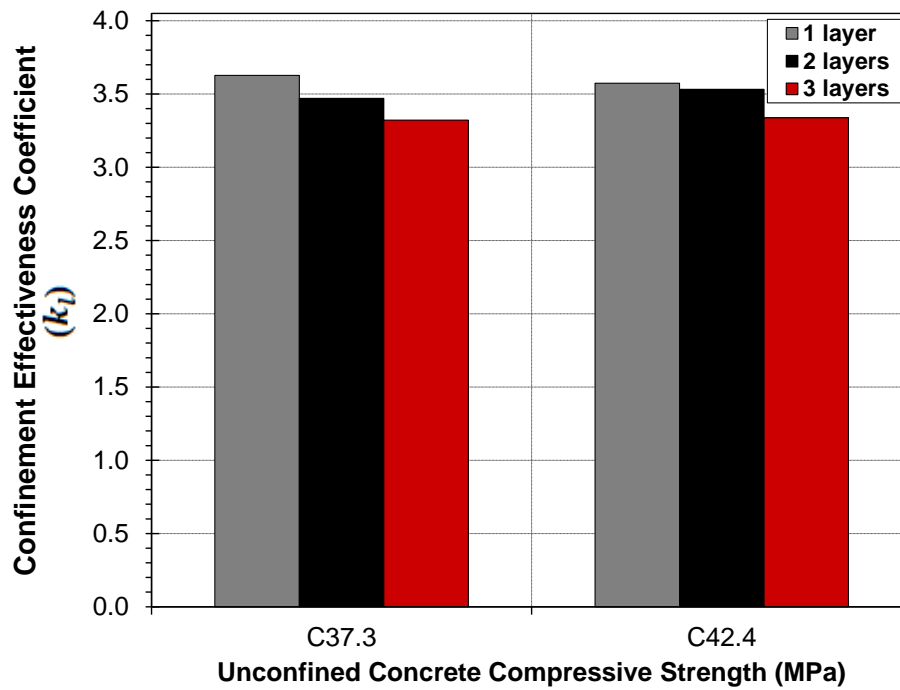
For example, CFRP-confined cylinders of concrete compressive strength of 37.3 MPa and

wrapped with one, two and three layers has energy ductility indices of 9.6, 15.8 and 26.0 implying increase of 65% and 171 % increase in ductility when CFRP jacket thickness doubled and tripled. The energy ductility index, for CFRP-confined cylinders of concrete strength of 42.4 MPa enhanced by 32% and 121% when CFRP jacket doubled and tripled, respectively.

A similar trend is observed for SFRP-confined cylinders; the energy ductility index, when concrete compressive strength is the same, improved significantly due to the increase of the SFRP jacket thickness. For cylinders of concrete strength of 37.3 MPa, the calculated energy ductility index for SFRP-wrapped cylinders with one, two and three layers were 33, 67 and 108, respectively. This means that the energy ductility index has increased by 103% and 229% when SFRP jacket thickness has been doubled and tripled, respectively. For cylinders of concrete strength of 42.4 MPa, the calculated energy ductility index for one, two and three layers were 41, 78 and 139, respectively, i.e., the energy ductility index has increased by 91% and 242% when SFRP jacket thickness has been doubled and tripled, respectively.

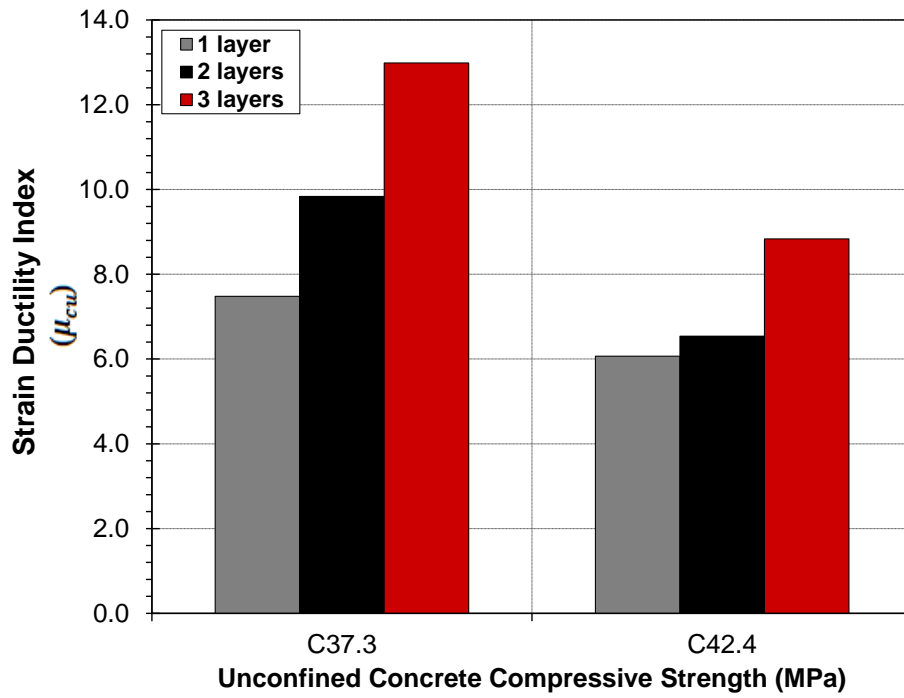


(a)

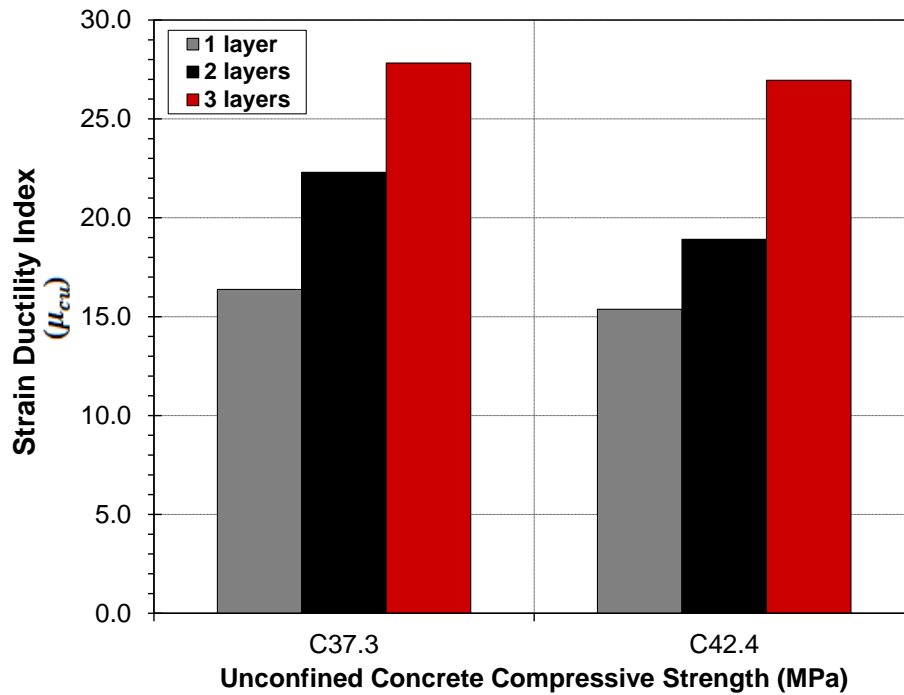


(b)

Figure 4-34: Effect of FRP jacket thickness on confinement effectiveness coefficient for: (a) CFRP- (b) SFRP-confined cylinders

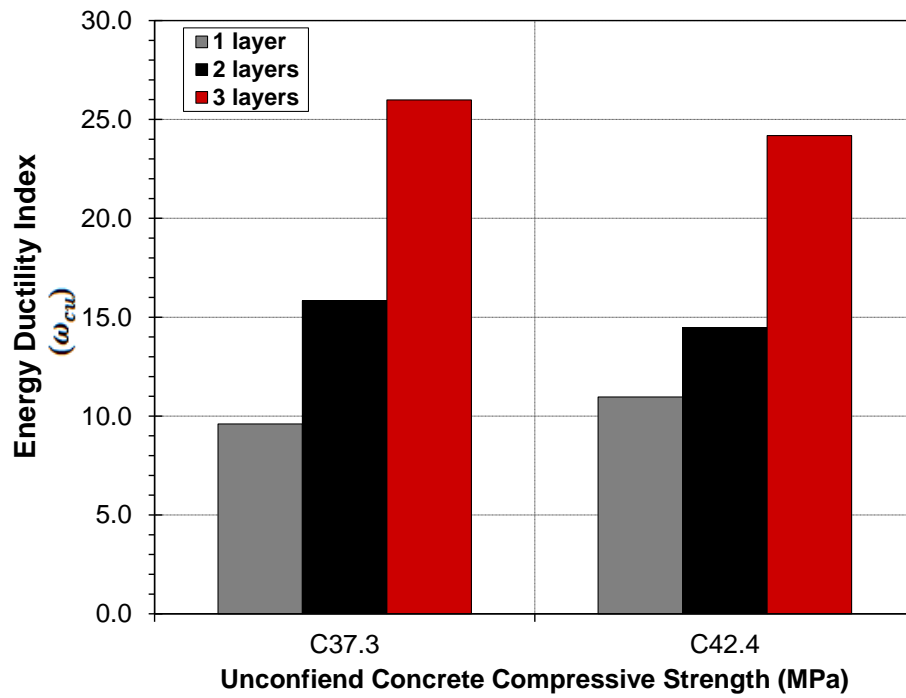


(a)

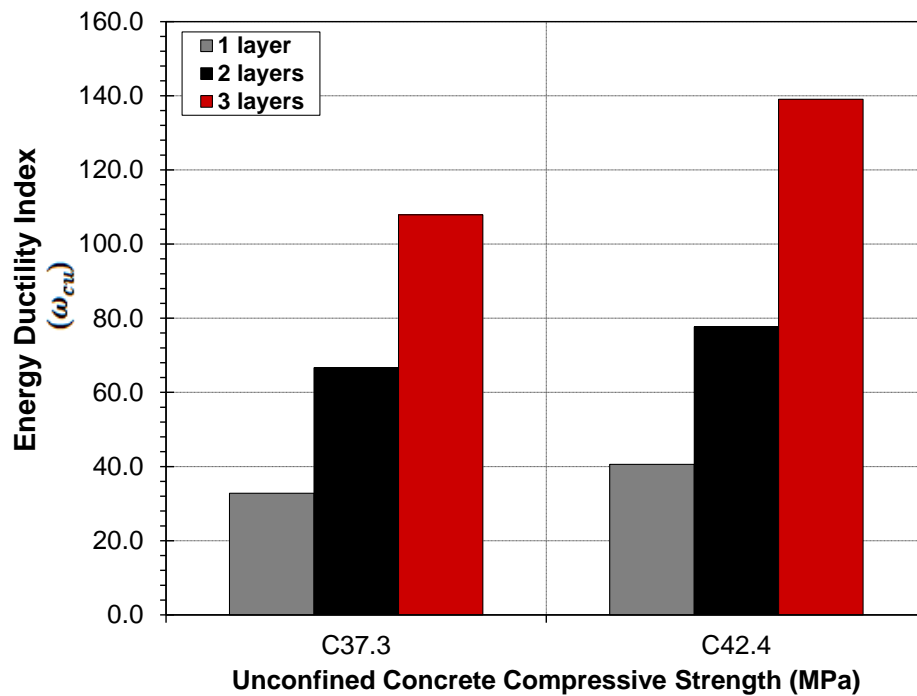


(b)

**Figure 4-35: Effect of FRP jacket thickness on strain ductility index for: (a) CFRP- (b) SFRP-confined cylinders**



(a)

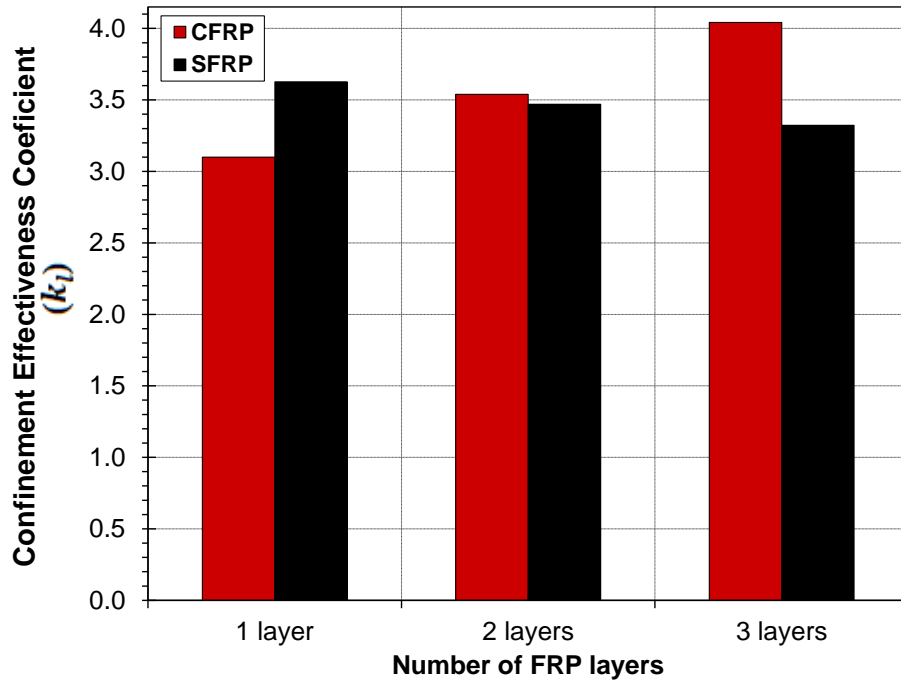


(b)

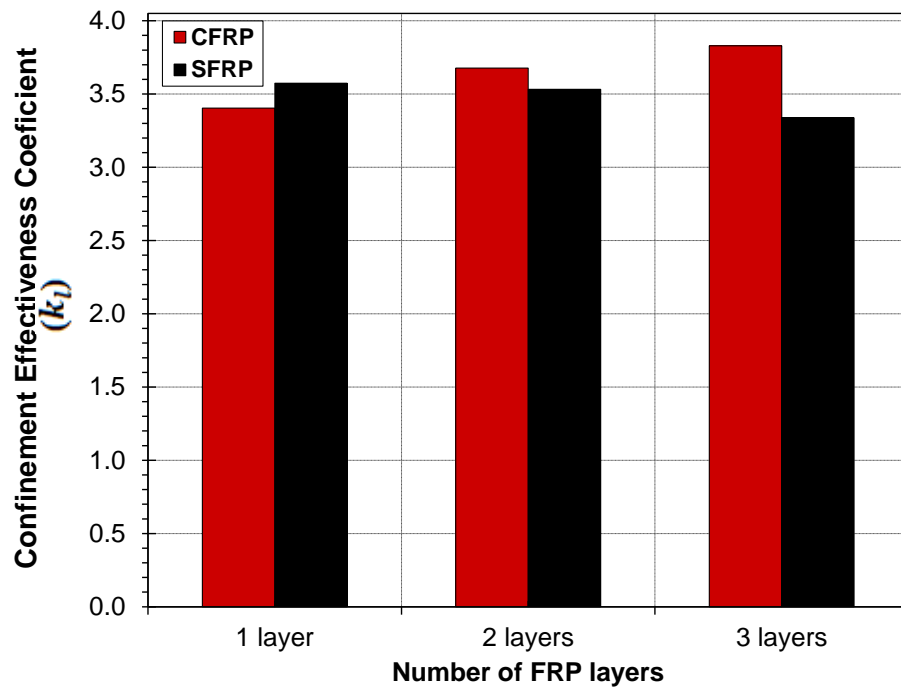
Figure 4-36: Effect of FRP jacket thickness on energy ductility index for: (a) CFRP- (b) SFRP-confined cylinders

#### 4.5.2.2 Effect of FRP Type

Irrespective of the unconfined concrete strength, SFRP jacket of one layer was more effective in concrete confinement than corresponding CFRP jacket; however, for two and three layers jackets, CFRP jacket shows superior confinement effectiveness than corresponding SFRP jacket. This comes as no surprise bearing in mind that SFRP-confined cylinders with two and three layers fails by partial or full debonding and the SFRP sheets were not fully utilised. A comparison of confinement effectiveness between various jacket layers for CFRP and SFRP is shown in Figure 4-37(a) and Figure 4-37(b) for C37.3 and C42.4 concrete grade, respectively. SFRP-confined cylinders, when the unconfined concrete strength and the number of wraps parameters are the same, exhibited far superior performance than corresponding CFRP in terms of strain ductility and energy absorption capacity, despite the fact that SFRP confined cylinders with two layers and three layers FRP jackets failed by partial or full debonding rather than FRP rupture that witnessed in all CFRP confined cylinders.

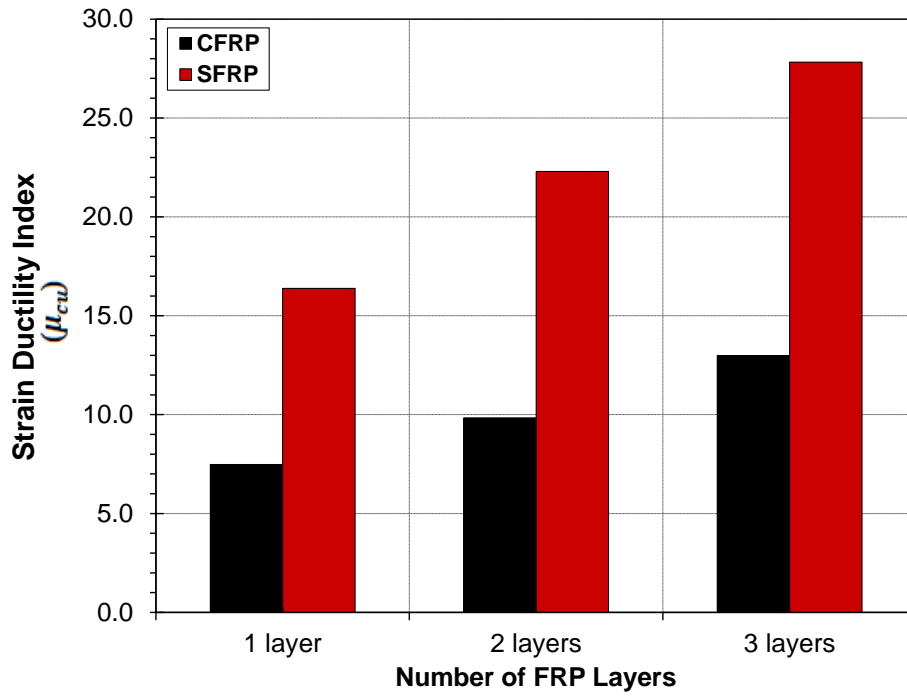


(a)

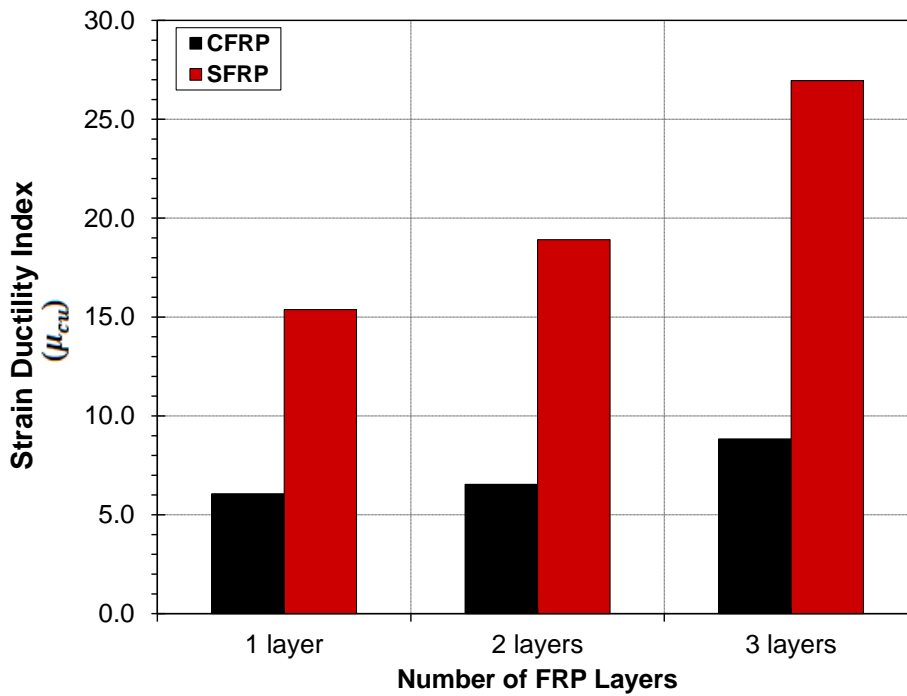


(b)

Figure 4-37: Effect of FRP type on confinement effectiveness for: (a) C37.3 (b) C42.4

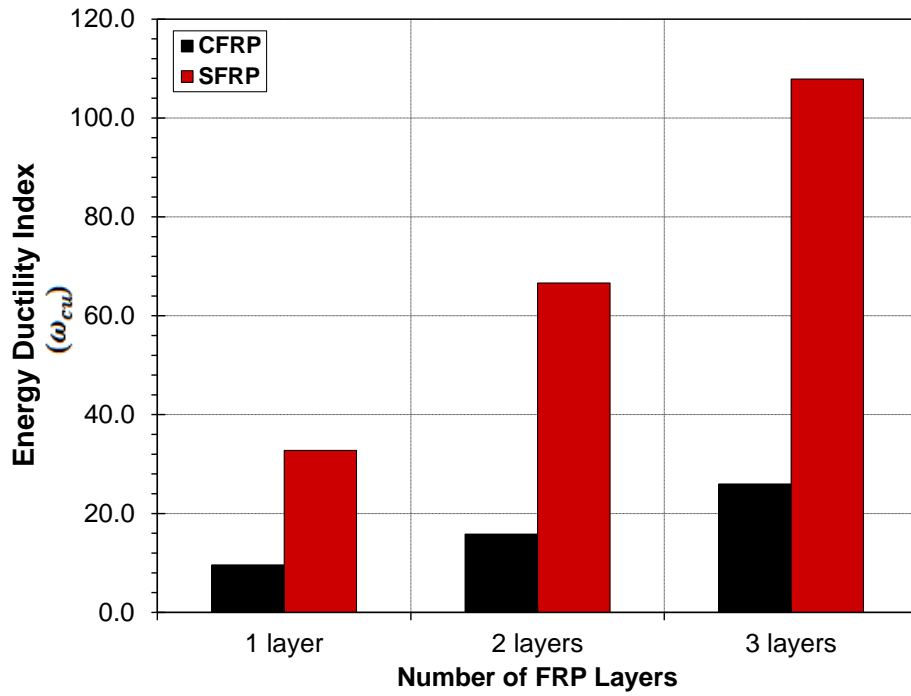


(a)

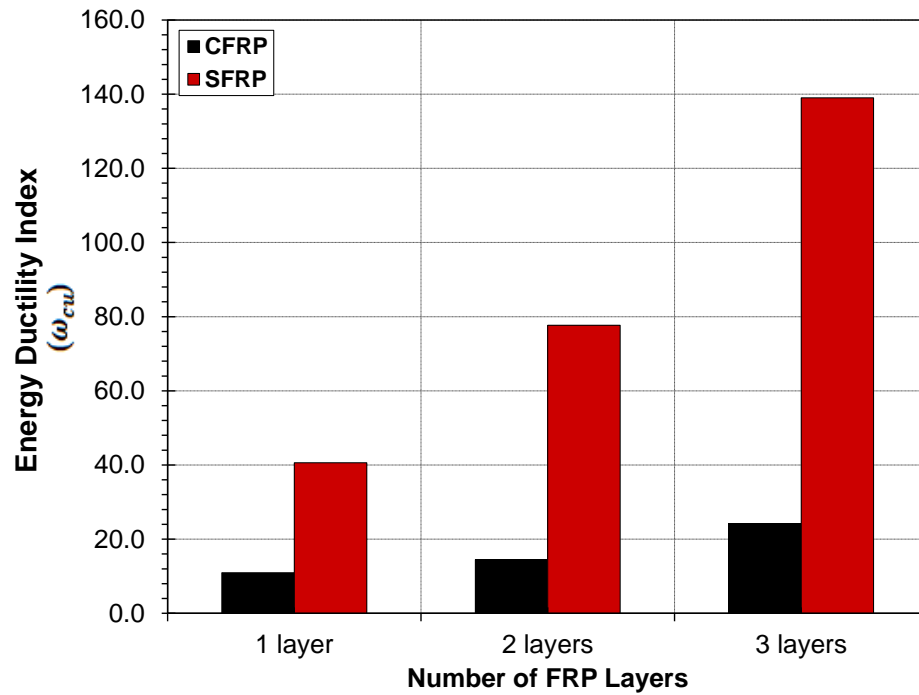


(b)

**Figure 4-38: Effect of FRP type on strain ductility index for: (a) C37.3 (b) C42.4**



(a)



(b)

Figure 4-39: Effect of FRP type on energy ductility index for: (a) C37.3 (b) C42.4

The difference in the structural performance between CFRP and SFRP sheets can be mainly attributed to two factors, FRP lateral stiffness and FRP ultimate confinement pressure. FRP lateral stiffness is defined as the ratio of confinement pressure increment and lateral strain increment, this can be defined as

$$E_l = \frac{2nt_{frp}E_{frp}}{D} \quad \text{Equation 4-11}$$

where  $n$  is the number of FRP wraps,  $t_{frp}$  and  $E_{frp}$  are the thickness and elastic modulus of FRP jacket,  $D$  is the cylinder diameter.

The ultimate confinement pressure exerted by FRP jacket is attained when the lateral strain in The FRP reaches its ultimate strain,  $\varepsilon_{frpu}$  corresponding to its ultimate tensile strength,  $f_{lu}$  as defined

$$f_{lu} = E_l \varepsilon_{frpu} \quad \text{Equation 4-12}$$

where  $E_l$  is the FRP lateral stiffness.

To examine the effect of both FRP lateral stiffness and ultimate confinement pressure on the FRP-confined concrete ultimate conditions, mainly the ultimate axial compressive stress and ultimate axial strain, two groups from current tests data were selected. Each group comprises two test sets, of which one is confined with CFRP and the other is confined with SFRP, however, the design lateral stiffness were approximately the same, 1058, 997, respectively. The details of these groups are summarized in Table 4-22. It is clear that when the ultimate confinement pressure were comparable, 15.78 and 13.62, the achieved ultimate strength was almost identical, and that the higher the ultimate confinement pressure, the higher the ultimate axial confined strength achieved. Other researchers, Fahmy and Wu (2010) reported similar conclusions.

It is well known that the ultimate axial strain of FRP confined concrete highly depends on the confinement ratio and the lateral strain capacity of FRP at rupture. This can be understood by examining the strain at ultimate,  $\varepsilon_{cu}$  formula derived from the constitutive model proposed by Ottosen (1979) for concrete under triaxial state of stress for FRP-confined concrete.

$$\varepsilon_{cu} = \frac{\varepsilon_{frp}}{v_{secu}} + \frac{\varepsilon_{co}(1 - v_{secu} - 2v_{secu}^2)}{v_{secu}} \frac{f_{lu}}{f'_{co}} \left[ 1 + 4 \left( \frac{k_l - 1}{\sqrt{3}} \right) \frac{f_{lu}}{f'_{co}} \right] \quad \text{Equation 4-13}$$

where  $v_{secu}$  is the secant Poisson's ratio of confined concrete at the ultimate conditions,  $f_{lu}$  is the ultimate lateral confining pressure,  $f'_{co}$  and  $\varepsilon_{co}$  are the unconfined concrete strength at peak and the corresponding strain,  $k_l$  is the confinement effectiveness coefficient,  $\varepsilon_{frp}$  is the rupture strain of FRP jacket

Hence, it would be expected that based on the above equation, for different types of FRP, and given that the lateral confinement ratio for all is the same, the FRP type with higher rupture strain will attain a higher ultimate axial strain. This aligns very well with the test data reported for the two-selected groups in Table 4-22.

**Table 4-22: Effect of FRP lateral stiffness and FRP ultimate confinement pressure**

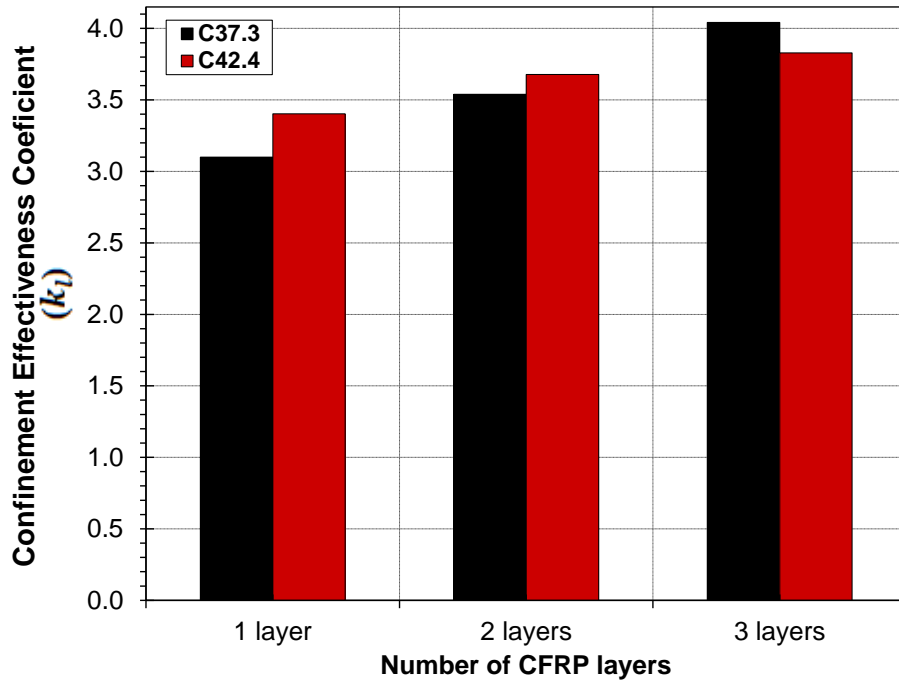
Group	Specimen Designation	$f'_{co}$ (MPa)	$nt_{frp}$ (mm)	Fibre Type	$f_l$ (MPa)	$E_l$ (MPa)	Axial Results	
							$f'_{cu}$ (MPa)	$\varepsilon_{cu}$ ( $\mu\varepsilon$ )
I	C37.3-SFRP1-SP#1	37.3	1.200	SFRP	15.78	1058	94.5	32088
	C37.3-SFRP1-SP#2							
	C37.3-SFRP1-SP#3							
	C37.3-CFRP3-SP#1	37.3	1.143	CFRP	13.62	997	92.4	25440
	C37.3-CFRP3-SP#2							
	C37.3-CFRP3-SP#3							
II	C42.4-SFRP1-SP#1	42.4	1.200	SFRP	15.78	1058	98.8	27007
	C42.4-SFRP1-SP#2							
	C42.4-SFRP1-SP#3							
	C42.4-CFRP3-SP#1	42.4	1.143	CFRP	13.62	997	94.6	15525
	C42.4-CFRP3-SP#2							
	C42.4-CFRP3-SP#3							

#### 4.5.2.3 Effect of Unconfined Concrete Compressive Strength

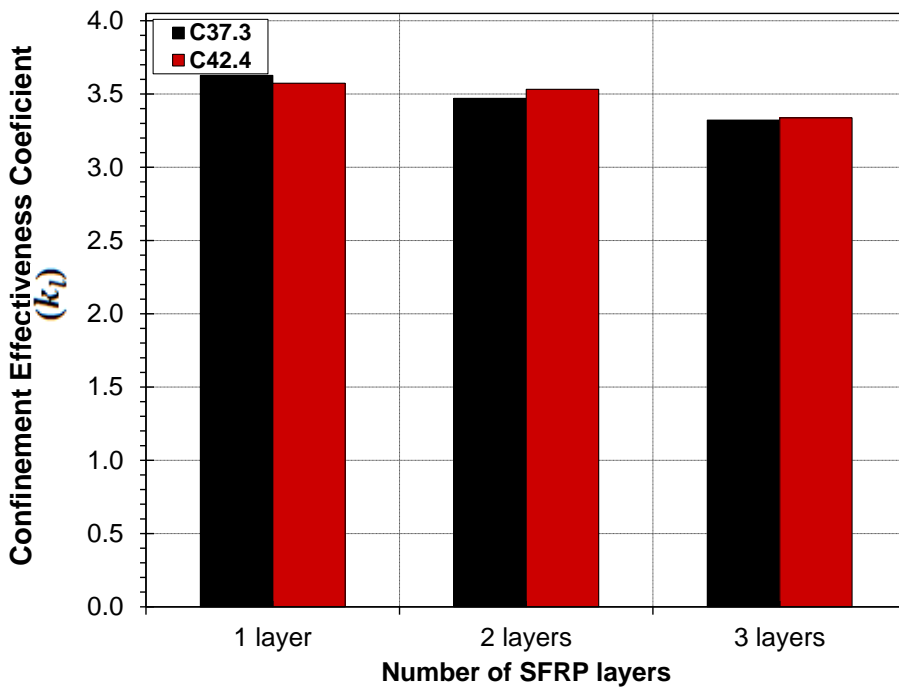
Test results show that an increase in  $f'_{co}$  resulted in an increase in the effectiveness of CFRP jacket confinement for cylinders wrapped with one and two layers, but a reduction in the confinement effectiveness for cylinders wrapped with three layers as shown in Figure 4-40 (a). On the other hand, the confinement effectiveness coefficient shows no dependency on  $f'_{co}$  for SFRP-confined cylinders as illustrated in Figure 4-40 (b).

An increase in  $f'_{co}$  has an adverse effect on the ductility of CFRP-confined cylinders in terms of strain and energy ductility as can be clearly seen in Figure 4-41 (a) and Figure 4-42 (a). Strain ductility indices reduced by 42%, 34% and 29% and energy ductility indices reduced by 17%, 4% and 12%, respectively for 1-, 2- and 3-CFRP confinement configuration when unconfined concrete strength increased from 37.3 MPa to 42.4 MPa.

Figure 4-41 (b) and Figure 4-42 (b) show that for SFRP-confined cylinders, an increase in  $f'_{co}$  results in a reduction in strain ductility indices; however, it results in an increase in energy ductility indices. Concrete cylinders confined with one, two and three layers of SFRP sheets exhibited reductions in strain ductility index by 7%, 18% and 3%, but at the same time, exhibited an increase in energy ductility indices by 24%, 17%, and 29% when  $f'_{co}$  increased from 37.3 MPa to 42.4 MPa.

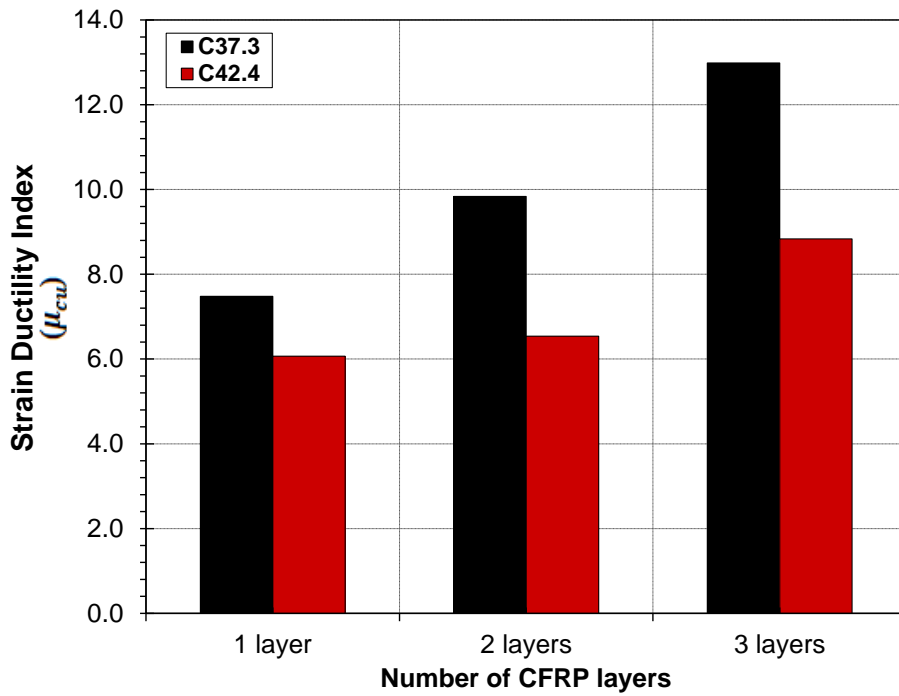


(a)

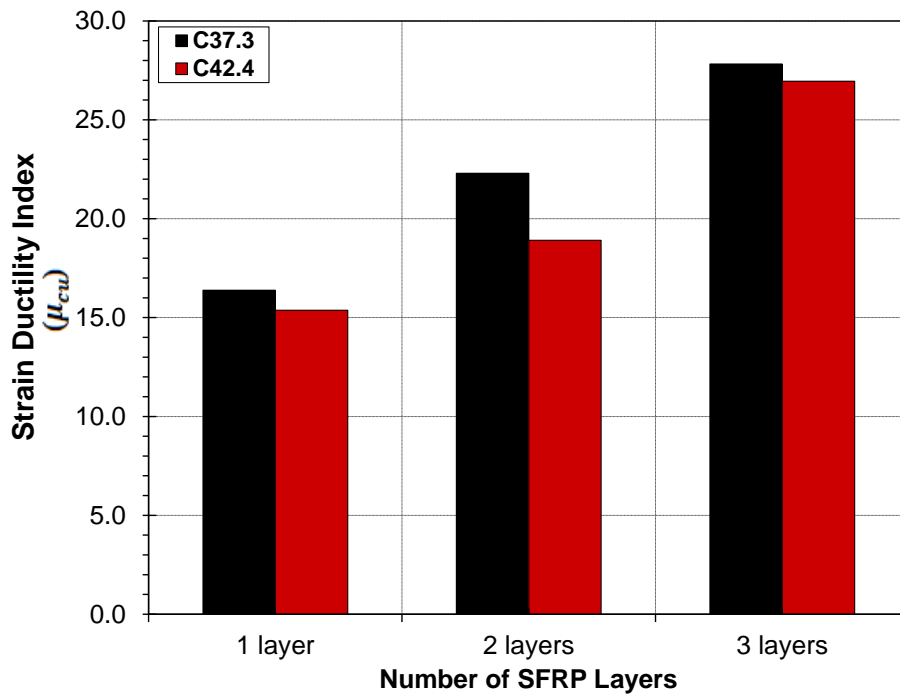


(b)

Figure 4-40: Effect of concrete strength on confinement effectiveness for: (a) CFRP- (b) SFRP-confined cylinders

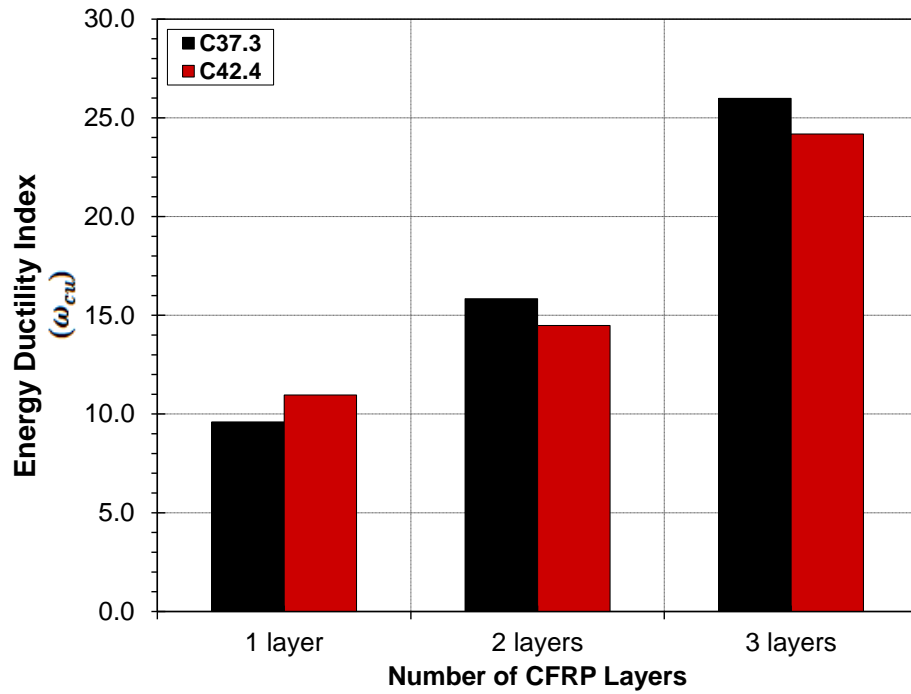


(a)

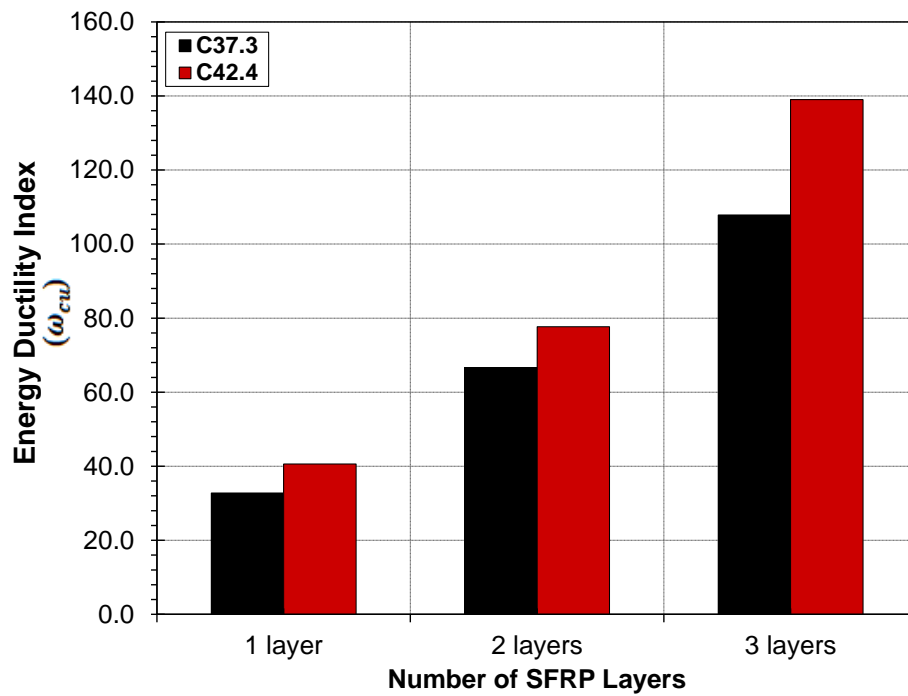


(b)

**Figure 4-41: Effect of concrete strength on strain ductility index for: (a) CFRP- (b) SFRP-confined cylinders**



(a)



(b)

**Figure 4-42: Effect of concrete strength on energy ductility index for: (a) CFRP- (b) SFRP- confined cylinders**

## 4.6 Summary

This chapter has presented and interpreted the results from uniaxial compression tests that have been conducted on a large number of small- scale plain concrete cylinders confined with different thicknesses of CFRP or SFRP jacket. Confined concrete behaviour was examined in terms of ultimate axial strength, ultimate axial strain, ultimate lateral strain, stress-strain response, dilation behaviour and ductility behaviour.

The DIC technique was implemented to study and quantify the axial and lateral strain variation over the full surface of the FRP jacket. It was found that a significant variation of the axial and lateral strain at failure exists over the surface of the FRP jacket. The magnitude of the variation, both axial and lateral, however, was independent on the FRP jacket thickness or the unconfined concrete strength.

Performance comparison between CFRP-and SFRP-confined concrete was also presented. It was found that SFRP-confined cylinders, when the unconfined concrete strength and number of wraps parameters are the same, exhibit far superior performance in terms of strength, strain ductility and energy absorption than the corresponding CFRP-confined cylinders. On the other hand, CFRP-and SFRP-confined cylinders of the same lateral stiffness ratio achieved comparable ultimate axial strength. However, the ultimate axial strain at failure was higher for SFRP-confined cylinders

In the next chapter, the performance of various confinement models available in the literature will be examined to evaluate their capability of accurate predictions of the strength and deformability of CFRP-and SFRP-confined cylinders. A new analytical confinement model for FRP-confined concrete will also be presented.

## Chapter Five: **Analytical Modeling of FRP-Confined Concrete Cylinders**

### **5.1 Introduction**

Various confinement models have been developed for FRP-confined concrete over the last few decades, a few of which were introduced in Chapter 2, Section 2.5.2. In this chapter, the performance of each of these models is closely examined by comparing the theoretical predictions from these models against the 12 sets of experimental results obtained from the experimental program described in Chapter 3. The performance analysis focus is on three main parameters, namely, the ultimate axial strength, the ultimate axial strain and the overall axial stress-strain response.

An overview of the confinement models under consideration in this chapter is first given in which the model's theoretical bases, key assumptions and approaches are highlighted. The performance of each of these models is then reviewed. Finally, a new analytical model which is simply a modification to the existing Spoelstra and Monti analytical model is developed, and the accuracy of the new model is assessed.

### **5.2 FRP Confinement Models Overview**

#### ***5.2.1 Empirical/ Analytical Confinement models***

The performance of the empirical/ analytical confinement models reviewed in Chapter 3 are analysed in this section to assess their accuracy in predicting the ultimate axial strength, ultimate axial strain and the stress-strain behaviour of CFRP- and SFRP-confined concrete cylinders. The confinement models under investigation are summarized below in Table 5.1. Each model is assigned a unique model designation as shown in the second column of Table 5-1 and will be used hereafter when referring to these models in any discussion that follows.

**Table 5-1: Summary of empirical/ analytical confinement models**

Models	Model Designation	Theoretical $f'_{cu}$	Theoretical $\varepsilon_{cu}$
Fardis and Khalili (1982), (Richart)	FK-R	$f'_{cu} = f'_{co} \left[ 1 + 4.1 \frac{f_{lu}}{f'_{co}} \right]$	$\varepsilon_{cu} = 0.002 + 0.001 \frac{E_{frp} t_{frp}}{D f'_{co}}$
Fardis and Khalili (1982), (Newman)	FK-N	$f'_{cu} = f'_{co} \left[ 1 + 3.7 \left[ \frac{f_{lu}}{f'_{co}} \right]^{0.86} \right]$	$\varepsilon_{cu} = 0.002 + 0.001 \frac{E_{frp} t_{frp}}{D f'_{co}}$
Toutanji (1999)	TTJ	$f'_{cu} = f'_{co} \left[ 1 + 3.5 \left( \frac{f_{lu}}{f'_{co}} \right)^{0.85} \right]$	$\varepsilon_{cu} = \varepsilon_{co} \left[ 1 + (310.57 \varepsilon_{frp} + 1.9) \left( \frac{f'_{cu}}{f'_{co}} - 1 \right) \right]$
Lam and Teng (2003)	LT	$\frac{f'_{cu}}{f'_{co}} = 1 + 3.3 \frac{f_{lu,a}}{f'_{co}}$	$\frac{\varepsilon_{cu}}{\varepsilon_{co}} = 1.75 + 12 \left[ \frac{f_{lu,a}}{f'_{co}} \right] \left[ \frac{\varepsilon_{frp,a}}{\varepsilon_{co}} \right]^{0.45}$
Berthet et al. (2005)	BFH	$f'_{cu} = f'_{co} + k_l f_{lu}$ $k_l = 3.45, 20 \leq f'_{co} \leq 50 \text{ MPa}$ $k_l = \frac{9.5}{(f'_{co})^{1/4}}, 50 \leq f'_{co} \leq 200 \text{ MPa}$	$\varepsilon_{cu} = \varepsilon_{co} + \frac{(\varepsilon_{frp} - v_c \varepsilon_{co})}{\gamma}$
Fahmy and Wu (2010)	FW	$f'_{cu} = f'_{co} + k_l f_{lu}$ $k_l = 4.5 f_{lu}^{-0.3}, f'_{co} \leq 40 \text{ MPa}$ $k_l = 3.75 f_{lu}^{-0.3}, f'_{co} > 40 \text{ MPa}$	$\varepsilon_{cu} = \frac{f'_{co} - f_o}{E_2}$ $E_2 = m_2(245.61 f'_{co} m_1 + 0.6728 E_l)$ $m_1 = 0.5, m_2 = 0.83 \text{ if } f'_{co} \leq 40 \text{ MPa}$ $m_1 = 0.2, m_2 = 1.73 \text{ if } f'_{co} > 40 \text{ MPa}$
Spoelstra and Monti, Exact (1999)	SM-E	$f'_{cu} = E_{sec,u} \varepsilon_{cu}$	$\varepsilon_{cu} = \varepsilon_{cc} \left[ \frac{E_{sec} [E_{co} - E_{sec,u}]}{E_{sec,u} [E_{co} - E_{sec}]} \right]^{1 - \frac{E_{sec}}{E_{co}}}$
Spoelstra and Monti, Approx. (1999)	SM-A	$\frac{f'_{cu}}{f'_{co}} = 0.2 + 3.0 \left( \frac{f_{lu}}{f'_{co}} \right)^{0.5}$	$\frac{\varepsilon_{cuc}}{\varepsilon_{co}} = 2 + 1.25 \frac{E_c}{f'_{co}} \left( \frac{f_{lu}}{f'_{co}} \right) \varepsilon_{lu}^{0.5}$
Teng et al. (2007)	THY	$\frac{f'_{cuc}}{f'_{co}} = 1 + 3.5 \frac{f_l}{f'_{co}}$	$\frac{\varepsilon_{cuc}}{\varepsilon_{co}} = 1 + 17.5 \frac{f_l}{f'_{co}}$

As previously discussed in Chapter 2, all the aforementioned confinement models, except SM and THY, are empirical models in which the ultimate axial strength and ultimate axial strain prediction expressions were derived based on their author's own experimental data sets.

Furthermore, only four of these models have expressions to predict the entire axial stress-axial and lateral strain curve. These four models are TTJ, BFH, SM and THY models. The rest propose expressions for the axial stress-axial strain curve only.

The two models of FK are the only models, out of the nine, which was developed based on models developed for steel-confined concrete. SM and THY models were based on an actively-confined concrete model by Popovics. TTJ and BFH utilised a model originally developed by Sargin and modified by Ahmad and Shah for concrete confined by steel spiral while LT based their model on the four parameter curve by Richard and Abbot (1975).

Of the nine confinement models reviewed in this section, five models, namely, FK-R, LT, BFH, FW, and THY models have an ultimate strength expression that is based on an expression originally proposed by Richart et al. (1928). The strength enhancement coefficients,  $k_1$  used in the models are summarized in Table 5-2.

**Table 5-2: Strength enhancement coefficient,  $k_l$ , for FRP-confined concrete**

Confinement Effectiveness Coefficient	
Model	$k_l$
Fardis and khalili (1982), (Richart)	4.1
Farids and Khalili (1982), (Newman)	$3.7 \left( \frac{f_{lu}}{f'_{co}} \right)^{-0.14}$
Toutanji (1999)	$3.5 \left( \frac{f_l}{f'_{co}} \right)^{-0.15}$
Lam and Teng (2003)	3.3
Berthet et al. (2005)	$k_l = 3.45, 20 \leq f'_{co} \leq 50 \text{ MPa}$ $k_l = \frac{9.5}{(f'_{co})^{1/4}}, 50 \leq f'_{co} \leq 200 \text{ MPa}$
Fahmy and Wu (2010)	$k_l = 4.5 f_{lu}^{-0.3}, f'_{co} \leq 40 \text{ MPa}$ $k_l = 3.75 f_{lu}^{-0.3}, f'_{co} > 40 \text{ MPa}$
Teng et al. (2007)	3.5

### 5.2.2 Confinement Models Adopted by the Canadian Design Codes

The two FRP confinement models adopted by the building and bridge Canadian codes are summarized in Table 5-3. As previously mentioned in Section 2.5.2.4, both models are based on a model originally developed by Richart et al. (1928), however, CAN/CSA S806-12 adopted the modified version of the model that was proposed by Saatcioglu and Razvi (1992). Neither code has yet adopted any model for ultimate axial strain prediction.

**Table 5-3: Summary of the Canadian codes confinement models**

Models	Theoretical $f'_{cu}$	Theoretical $\varepsilon_{cu}$
CAN/CSA S806-12	$f'_{cu} = 0.85f'_{co} + k_l k_c f_{lu}$ $k_l = 6.7(k_c f_{lu})^{-0.17}$ $f_{lu} = \frac{2t_{frp}\phi_{frp}f_{frp}}{D} \leq \frac{2t_{frp}0.006E_{frp}}{D}$	-
CAN/CSA S6-14	$f'_{cu} = f'_{co} + 2f_{lu}$ $f_{lu} = \frac{2\phi_{frp}t_{frp}f_{frp}}{D}$	-

### 5.3 Performance Analysis of Confinement Models

The experimental results versus the theoretical predictions of the various confinement models are first summarized and tabulated for each confinement configuration. The performance of each of these models is then evaluated graphically by plotting the experimental results versus the corresponding theoretical values with the 45° reference line representing exact match between experiment and theory is also plotted for comparison. Points falling above the 45° line imply that the theoretical predictions are lower than the experimental values and hence, indicate conservative predictions while points falling below the line imply that the theoretical predictions are higher than the experimental values and hence indicate unconservative predictions.

Linear regression analysis of experimental versus theoretical values is also performed and the regression line is plotted in each graph along with the corresponding 95% confidence band, Devore (2000). The way the regression line deviates from the 45° reference line provides visual information on the tendency of the models to overestimate or underestimate experimental results. A 45° reference line which is completely within the 95% confidence band indicates very good agreement between the experiment and the theoretical model, Lorenzis and Tepfers (2003).

The accuracy of each empirical/analytical model is then quantified by computing the model's percent error in evaluating  $f'_{cu}$  or  $\varepsilon_{cu}$  for each experimental data set. The average value, standard

deviation and coefficient of variation of the absolute percent errors for each model are then reported.

### ***5.3.1 Models' Performance in Prediction of $f'_{cu}$***

The experimental results versus the theoretical predictions of the ultimate axial strength,  $f'_{cu}$  for empirical and analytical confinement models are reported respectively in Table 5-4 and Table 5-5. The experimental results versus the theoretical predictions of the ultimate axial strength,  $f'_{cu}$  for building and bridge Canadian design codes are reported in Table 5-6. The percent error in the theoretical prediction with respect to the experimental averages which used as a bench mark is also reported. A negative percent error value indicates a conservative prediction while positive percent error value indicates unconservative prediction.

**Table 5-4: Empirical models prediction of  $f'_{cu}$**

Confinement Designation	Exp. (avg.) (MPa)	FK-R		FK-N		TTJ		LT		BHF		FW	
		$f'_{cu}$ (MPa)	Error (%)										
C37.3-CFRP1	51.4	55.4	8	59.3	15	58.6	14	51.9	1	52.5	2	50.0	-3
C37.3-CFRP2	69.5	73.5	6	77.3	11	75.7	9	66.5	-4	67.8	-2	58.0	-17
C37.3-CFRP3	92.4	91.7	-1	94.0	2	91.5	-1	81.0	-12	83.0	-10	64.8	-30
C37.3-SFRP1	94.5	102.3	8	103.5	9	100.4	6	89.7	-5	92.0	-3	68.5	-28
C37.3-SFRP2	146.8	167.4	14	157.4	7	151.1	3	142.0	-3	146.8	0	87.9	-40
C37.3-SFRP3	194.6	232.4	19	207.5	7	197.9	2	194.4	0	201.5	4	104.5	-46
C42.4-CFRP1	59.6	60.5	2	64.8	9	64.1	8	57.0	-4	57.6	-3	53.0	-11
C42.4-CFRP2	75.8	78.6	4	83.1	10	81.5	8	71.6	-6	72.9	-4	59.6	-21
C42.4-CFRP3	94.6	96.8	2	100.1	6	97.6	3	86.1	-9	88.1	-7	65.3	-31
C42.4-SFRP1	98.8	107.4	9	109.8	11	106.7	8	94.8	-4	97.1	-2	68.4	-31
C42.4-SFRP2	153.9	172.5	12	164.7	7	158.4	3	147.1	-4	151.9	-1	84.6	-45
C42.4-SFRP3	200.4	237.5	19	215.7	8	206.1	3	199.5	0	206.6	3	98.4	-51

**Table 5-5: Analytical models prediction of  $f'_{cu}$**

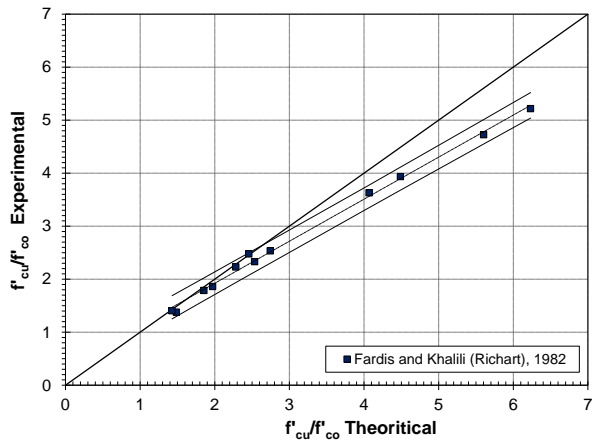
Confinement Designation	Exp. (avg.) (MPa)	SM-E		SM-A		THY	
		$f'_{cu}$ (MPa)	Error (%)	$f'_{cu}$ (MPa)	Error (%)	$f'_{cu}$ (MPa)	Error (%)
C37.3-CFRP1	51.4	57.7	12	46.0	-11	49.0	-5
C37.3-CFRP2	69.5	75.8	9	61.9	-11	65.9	-5
C37.3-CFRP3	92.4	89.1	-3	74.2	-20	81.8	-11
C37.3-SFRP1	94.5	94.8	0	80.4	-15	90.4	-4
C37.3-SFRP2	146.8	121.7	-17	110.7	-25	145.8	-1
C37.3-SFRP3	194.6	136.5	-30	133.9	-31	201.0	3
C42.4-CFRP1	59.6	64.3	8	49.5	-17	50.1	-16
C42.4-CFRP2	75.8	83.7	10	66.6	-12	68.5	-10
C42.4-CFRP3	94.6	98.0	4	79.6	-16	84.8	-10
C42.4-SFRP1	98.8	104.5	6	86.3	-13	93.2	-6
C42.4-SFRP2	153.9	134.6	-13	118.5	-23	148.6	-3
C42.4-SFRP3	200.4	152.2	-24	143.2	-29	203.5	-2

**Table 5-6: Design codes confinement models prediction of  $f'_{cu}$** 

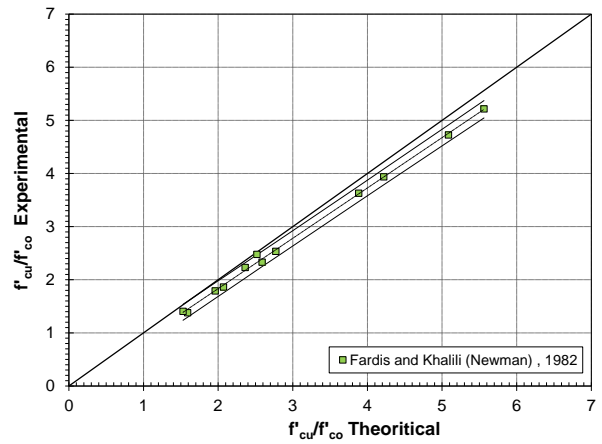
Confinement Designation	Exp. (avg.) (MPa)	CAN/CSA S806-12		CAN/CSAS6-14	
		$f'_{cu}$ (MPa)	Error (%)	$f'_{cu}$ (MPa)	Error (%)
C37.3-CFRP1	51.4	43.6	-15	44.4	-14
C37.3-CFRP2	69.5	52.8	-24	51.4	-26
C37.3-CFRP3	92.4	61.3	-34	58.5	-37
C37.3-SFRP1	94.5	62.8	-34	*	*
C37.3-SFRP2	146.8	86.9	-41	*	*
C37.3-SFRP3	194.6	109.0	-44	*	*
C42.4-CFRP1	59.6	47.9	-20	49.5	-17
C42.4-CFRP2	75.8	57.2	-25	56.5	-25
C42.4-CFRP3	94.6	65.6	-31	63.6	-33
C42.4-SFRP1	98.8	67.1	-32	*	*
C42.4-SFRP2	153.9	91.2	-41	*	*
C42.4-SFRP3	200.4	113.3	-43	*	*

\* Resistance reduction factor for SFRP material is not provided by the code

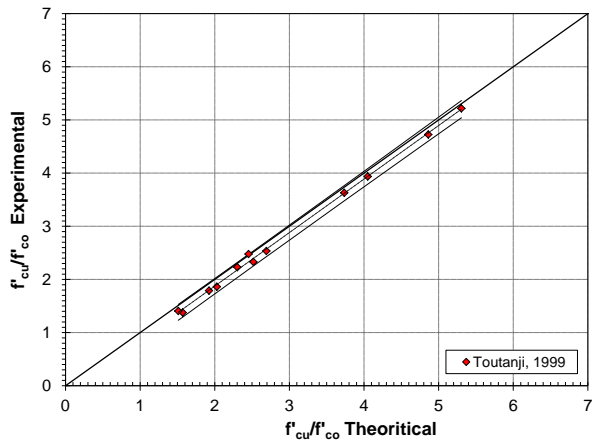
The experimental and theoretical ultimate axial strength are normalized by being divided by their respective cylinders unconfined concrete strength values and are compared respectively for empirical and analytical models in Figure 5-1 and Figure 5-2 and for design codes confinement models in Figure 5-3.



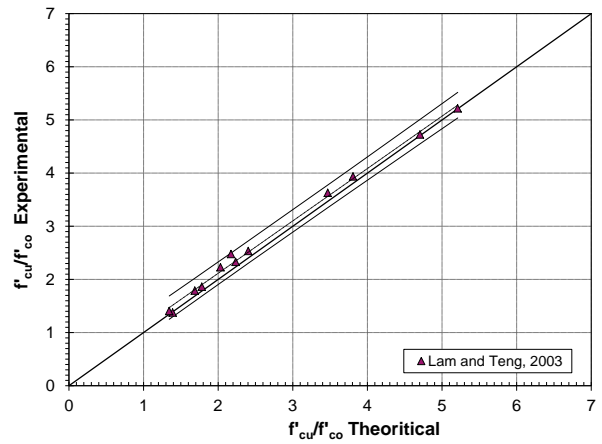
Fardis and Khalili, 1982 (Richart)



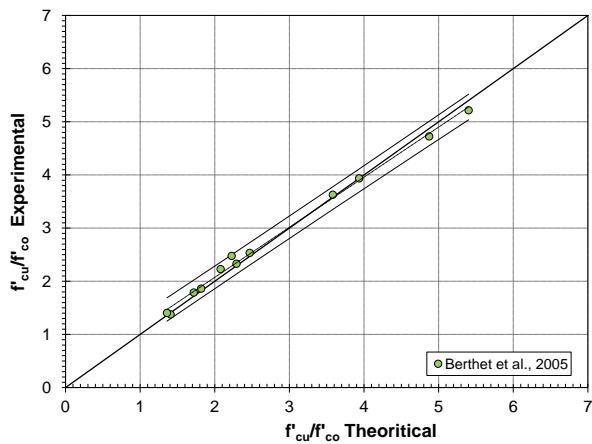
Fardis and Khalili, 1982 (Newman)



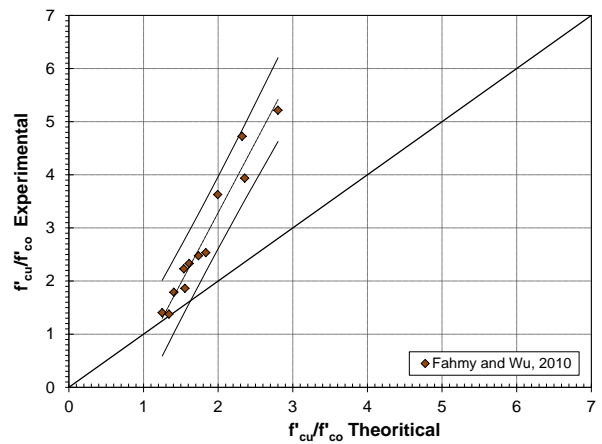
Toutanji, 1999



Lam and Teng, 2003

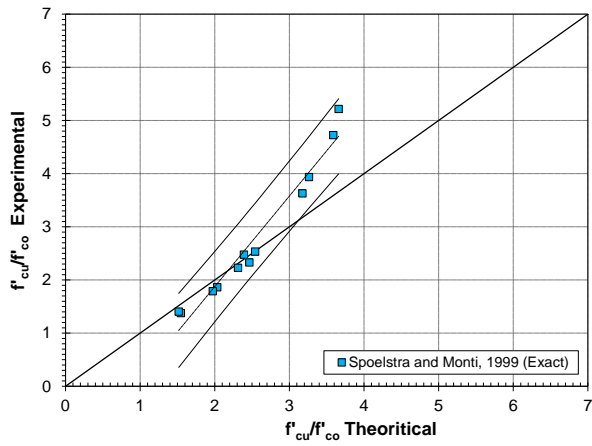


Berthet et al., 2005

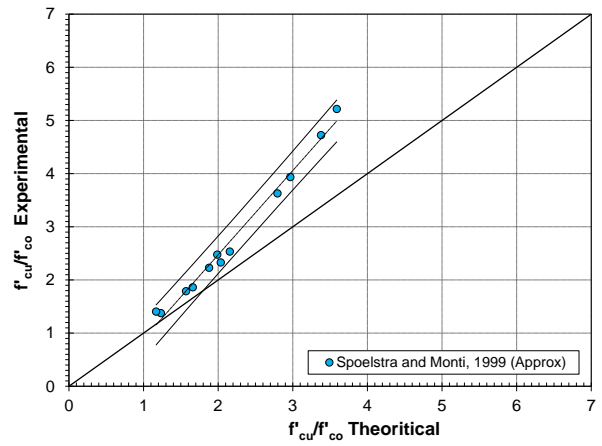


Fahmy and Wu, 2010

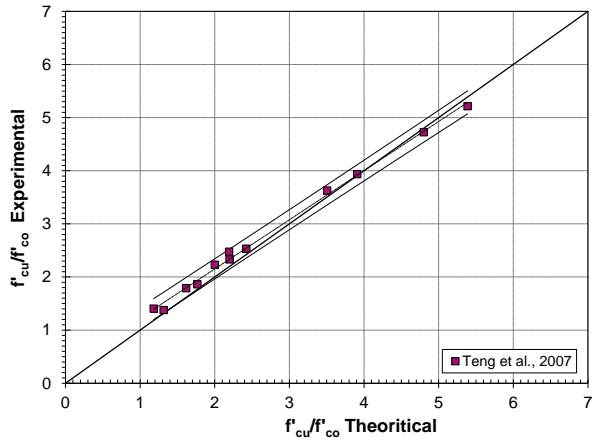
**Figure 5-1: Empirical models' performance in the prediction of  $f'_{cu}/f'_{co}$**



Spolstra and Monti, 1999 (Exact)

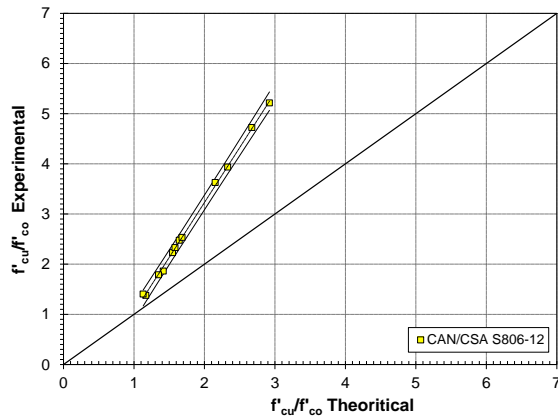


Spolstra and Monti, 1999 (Approx.)

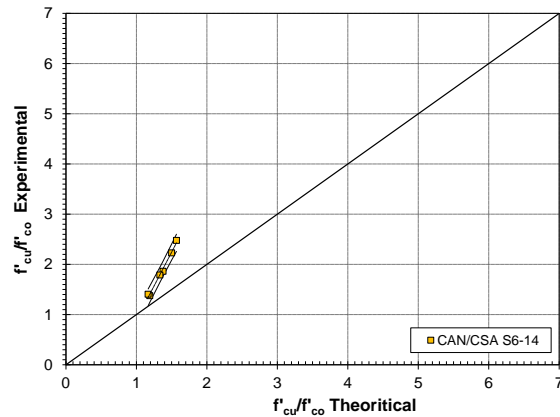


Teng et al., 2007

**Figure 5-2: Analytical models' performance in the prediction of  $f'_{cu}/f'_{co}$**



CAN/CSA S806-12



CAN/CSA S6-14

**Figure 5-3: Canadian codes confinement models' performance in the prediction of  $f'_{cu}/f'_{co}$**

It can be noted that both models by FK largely overestimate the axial ultimate strength, however,

the prediction was less accurate for cylinders with higher lateral confinement pressure ratio,  $\frac{f'_{lu}}{f'_{co}}$ .

This is specifically true for FK-R model due to the use of high confinement effectiveness ratio of 4.1, which is more suitable for actively confined concrete but not for FRP-confined concrete which is expected to have lower confinement effectiveness ratio in the range of 3.5, Jiang and Wu (2012). In general FK-N performs better than FK-R in the prediction of  $f'_{cu}$ .

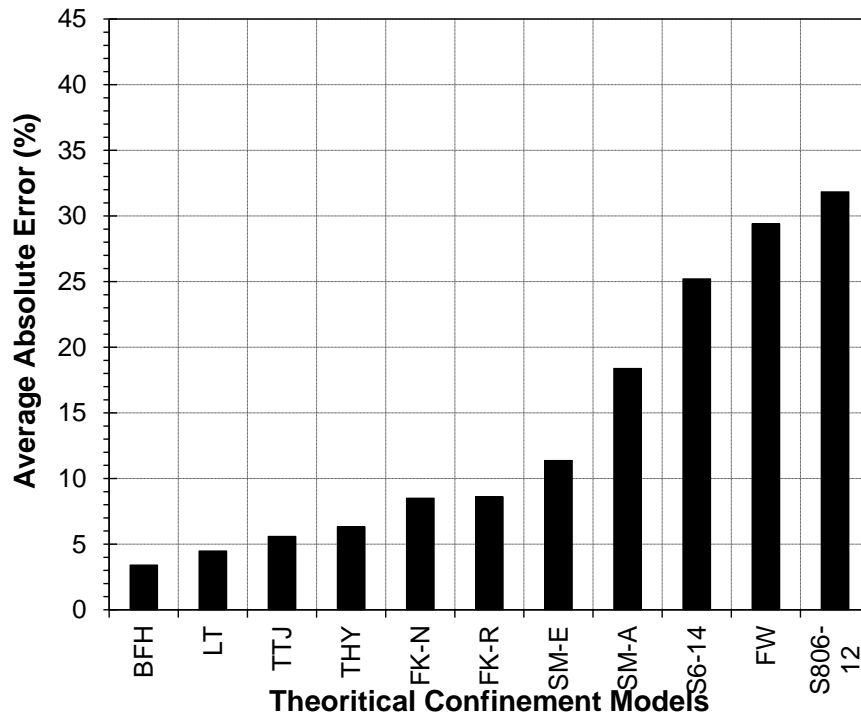
Models by TTJ, LT, BFH and THY perform equally well while FW and SM-A models tend to significantly underestimate the ultimate axial strength of FRP-confined concrete cylinders. SM-E model performs quite well in predicting the ultimate axial strength for weakly and moderately confined cylinders; however, the error in the prediction was high for highly confined cylinders, as opposed to THY model which accurately predicted the ultimate axial strength for highly confined cylinders while slightly overestimate the ultimate axial strength for weakly and moderately confined cylinders.

The overall accuracy of the empirical, analytical and adopted by design codes confinement models in the prediction of the ultimate axial strength is summarized in Table 5-7 and plotted in Figure 5-4. The average, standard deviation and coefficient of variation of the absolute average error in the prediction of  $f'_{cu}$  are shown for the whole experimental set and for the two distinctive sets of CFRP- and SFRP-confined concrete cylinders.

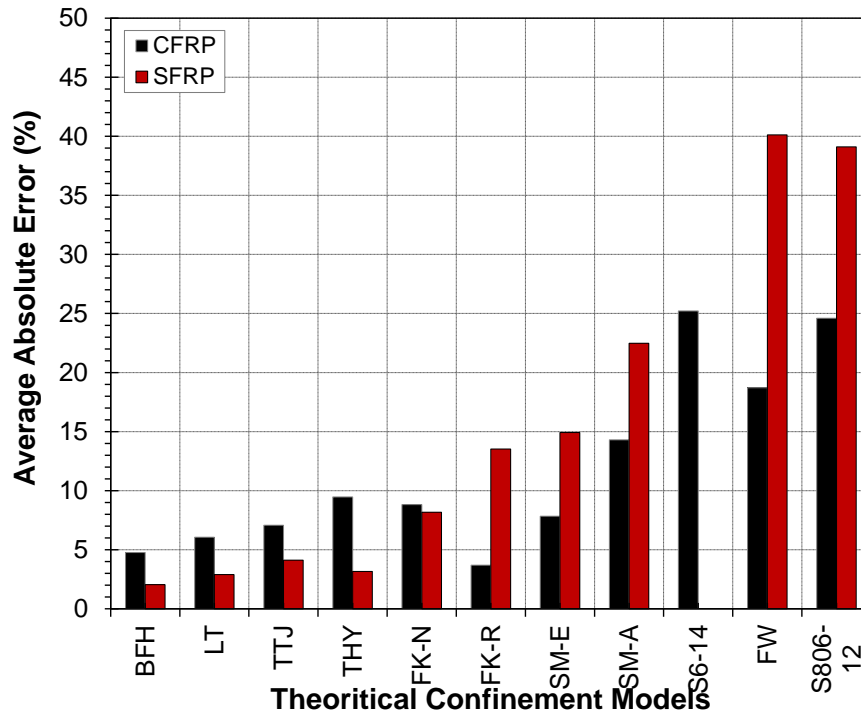
**Table 5-7: Confinement models accuracy in the prediction of  $f'_{cu}$**

Confinement Model	Predictions of $f'_{cu}$ (whole set)			Predictions of $f'_{cu}$ (CFRP)			Predictions of $f'_{cu}$ (SFRP)		
	Avg. (%)	SD (%)	COV (%)	Avg. (%)	SD (%)	COV (%)	Avg. (%)	SD (%)	COV (%)
FK-R	8.6	6.2	72.4	3.7	2.8	76.4	13.5	4.3	32.1
FK-N	8.5	3.2	38.1	8.8	4.3	48.5	8.2	1.6	19.4
TTJ	5.6	3.9	69.6	7.1	4.7	66.1	4.1	2.2	54.4
LT	4.5	3.5	78.4	6.1	4.1	68.0	2.9	1.9	66.9
BFH	3.4	3.8	111.7	4.8	3.8	80.2	2.1	2.4	115.5
FW	29.4	14.1	48.1	18.7	10.0	53.7	40.1	8.4	20.9
SM-E	11.4	13.7	120.8	7.8	5.3	67.0	14.9	12.6	84.4
SM-A	18.4	6.7	36.5	14.3	3.4	23.6	22.5	6.7	29.9
THY	6.3	5.3	84.3	9.5	3.8	40.6	3.2	3.2	102.0
CAN/CSA S806-12	31.8	9.1	28.6	24.6	6.2	25.4	39.1	4.6	11.8
CAN/CSA S6-14	25.2	8.1	32.0	25.2	8.1	32.0	*	*	*

\* Resistance reduction factor for SFRP sheet is not provided by code



(a)



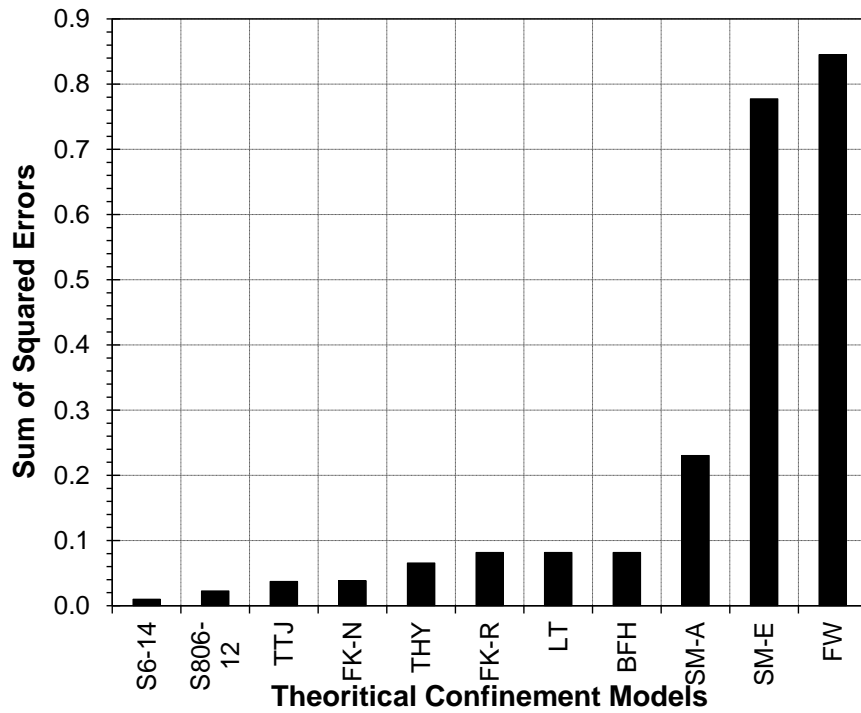
(b)

Figure 5-4: Confinement models accuracy in the prediction of  $f'_{cu}$  for: (a) the whole experimental set (b) CFRP and SFRP experimental sets

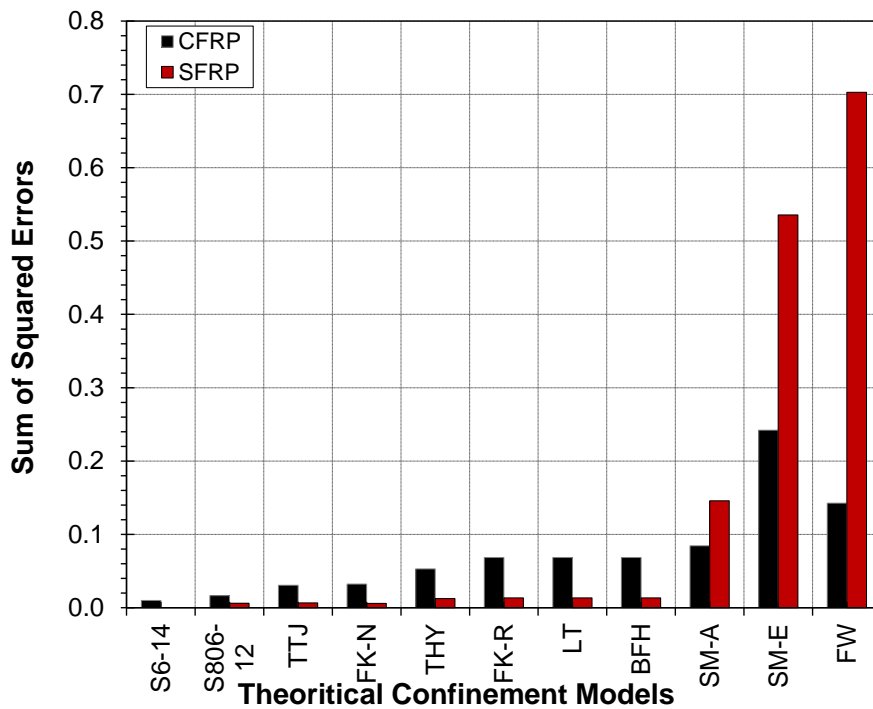
The three most accurate models in predicting the ultimate axial strength are BFH, LT and TTJ, the average absolute errors for the whole set of cylinders are 3.4%, 4.5% and 5.6%, respectively. It is interesting to note that models by BFH, LT, TTJ, THY were more accurate for the prediction of the ultimate axial strength of the SFRP-confined cylinders while models by FK-R, SM-E, SM-A and FW were more accurate for CFRP-confined concrete cylinders. In fact, the models that show a considerable difference in accuracy between CFRP-and SFRP confined concrete are the models that are most sensitive to the value of the lateral confinement ratio.

Both building and bridge Canadian design codes significantly underestimate the ultimate axial strength with the bridge design code CAN/CSA S6-14 performing slightly better than the building design code CAN/CSA S806-12. However, the bridge design code CAN/CSA S6-14 does not include a material resistance reduction factor for SFRP sheets, and hence the strength capacity of SFRP-confined concrete cylinders cannot be predicted in accordance with this code. The prediction error was higher for SFRP-confined concrete cylinders by the building design code CAN/CSA S806-12, mainly because the original model was calibrated based on experimental databases for CFRP, GFRP and AFRP. Clearly, both models require refinement and/or revision to accommodate and/or improve the strength prediction of SFRP-confined concrete cylinders.

The sum of squares due to errors, SSE, in the prediction of  $f'_{cu}$  for all confinement models under consideration is shown in Figure 5-4. SSE measures the total deviation of the model prediction values from the fit of the model prediction values. A Model of SSE close to zero indicates that the model has less random error components and that the fit is more useful for prediction.



(a)



(b)

**Figure 5-5: Confinement models SSE in the prediction of  $f'_{cu}$  for: (a) the whole experimental set (b) CFRP and SFRP experimental sets**

### ***5.3.2 Models' Performance in Prediction of $\epsilon_{cu}$***

The experimental results versus the theoretical predictions of the ultimate axial strain,  $\epsilon_{cu}$  for empirical and analytical confinement models are reported respectively in Table 5-8 and Table 5-9. The percent error in the theoretical prediction with respect to the experimental averages is also reported for each confinement configuration.

**Table 5-8: Empirical models prediction of  $\epsilon_{cu}$**

Confinement Designation	Exp. (avg.)	FK-R		FK-N		TTJ		LT		BHF		FW	
		$\epsilon_{cu}$	Error (%)										
C37.3-CFRP1	0.0147	0.0065	-56	0.0065	-56	0.0089	14	0.0066	-55	0.0090	-38	0.0089	-39
C37.3-CFRP2	0.0193	0.0109	-43	0.0109	-43	0.0144	9	0.0096	-50	0.0131	-32	0.0128	-34
C37.3-CFRP3	0.0254	0.0154	-40	0.0154	-40	0.0195	-1	0.0127	-50	0.0166	-35	0.0152	-40
C37.3-SFRP1	0.0321	0.0162	-50	0.0162	-50	0.0242	6	0.0151	-53	0.0192	-40	0.0170	-47
C37.3-SFRP2	0.0437	0.0304	-30	0.0304	-30	0.0420	3	0.0268	-39	0.0293	-33	0.0209	-52
C37.3-SFRP3	0.0545	0.0445	-18	0.0445	-18	0.0585	2	0.0384	-29	0.0378	-31	0.0223	-59
C42.4-CFRP1	0.0107	0.0059	-44	0.0059	-44	0.0072	8	0.0056	-48	0.0077	-28	0.0083	-23
C42.4-CFRP2	0.0115	0.0098	-14	0.0098	-14	0.0115	8	0.0081	-30	0.0112	-3	0.0103	-10
C42.4-CFRP3	0.0155	0.0138	-11	0.0138	-11	0.0155	3	0.0106	-32	0.0141	-9	0.0111	-28
C42.4-SFRP1	0.0270	0.0145	-46	0.0145	-46	0.0192	8	0.0126	-53	0.0163	-40	0.0122	-55
C42.4-SFRP2	0.0332	0.0269	-19	0.0269	-19	0.0331	3	0.0221	-33	0.0248	-25	0.0125	-62
C42.4-SFRP3	0.0474	0.0394	-17	0.0394	-17	0.0460	3	0.0316	-33	0.0320	-32	0.0122	-74

**Table 5-9: Analytical models prediction of  $\epsilon_{cu}$**

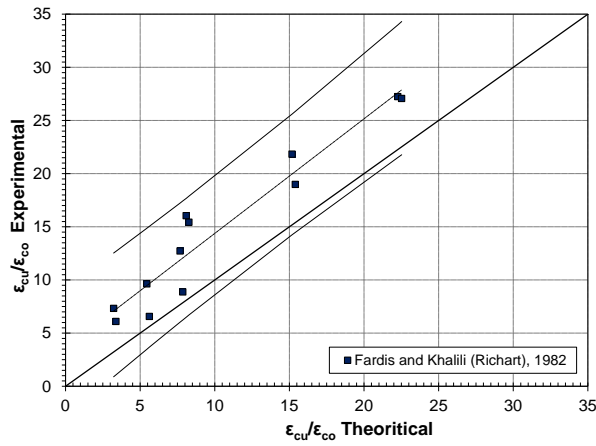
Confinement Designation	Exp. (avg.)	SM-E		SA		THY	
		$\epsilon_{cu}$	Error (%)	$\epsilon_{cu}$	Error (%)	$\epsilon_{cu}$	Error (%)
C37.3-CFRP1	0.0147	0.0167	14	0.0093	-37	0.0116	-5
C37.3-CFRP2	0.0193	0.0219	14	0.0130	-33	0.0172	-5
C37.3-CFRP3	0.0254	0.0258	1	0.0158	-38	0.0229	-11
C37.3-SFRP1	0.0321	0.0305	-5	0.0194	-39	0.0281	-4
C37.3-SFRP2	0.0437	0.0392	-10	0.0273	-37	0.0498	-1
C37.3-SFRP3	0.0545	0.0439	-19	0.0333	-39	0.0716	3
C42.4-CFRP1	0.0107	0.0108	2	0.0072	-32	0.0103	-16
C42.4-CFRP2	0.0115	0.0141	23	0.0100	-13	0.0150	-10
C42.4-CFRP3	0.0155	0.0165	6	0.0122	-21	0.0197	-10
C42.4-SFRP1	0.0270	0.0194	-28	0.0150	-44	0.0242	-6
C42.4-SFRP2	0.0332	0.0250	-25	0.0211	-37	0.0423	-3
C42.4-SFRP3	0.0474	0.0282	-40	0.0257	-46	0.0604	2

The experimental and theoretical ultimate axial strain are normalized by being divided by their respective cylinders unconfined concrete strain at peak values and are compared respectively for empirical and analytical models in Figure 5-6 and Figure 5-7.

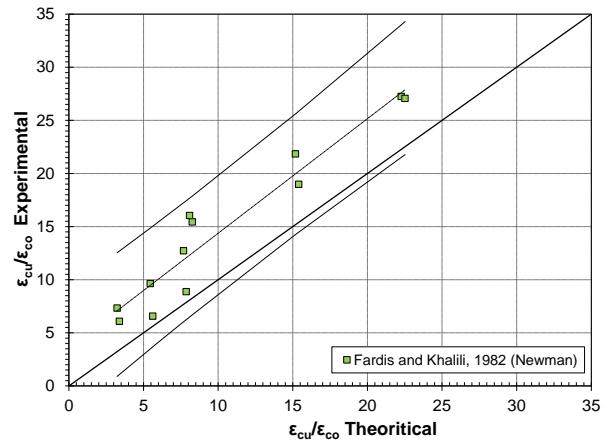
It can be observed that the errors in the predictions of  $\varepsilon_{cu}$  are much larger than those in the predictions of  $f'_{cu}$ , which is in line with the previous observations from other researchers, Lorenzis and Tepfers (2003); Teng and Lam (2004) and Bisby et al. (2005).

Out of the nine models under investigation, SM-E and THY models perform very well in predicting the ultimate axial strain for weakly and moderately confined concrete cylinders; however, SM-E underestimates the ultimate axial strain as opposed to THY model which overestimates the ultimate axial strain for highly confined concrete cylinders. The TTJ model performs very well in predicting the ultimate axial strain for highly confined concrete cylinders; however, the model underestimates the ultimate axial strain for weakly and moderately confined concrete cylinders. Other models perform quite poorly and tend to underestimate the ultimate axial strain.

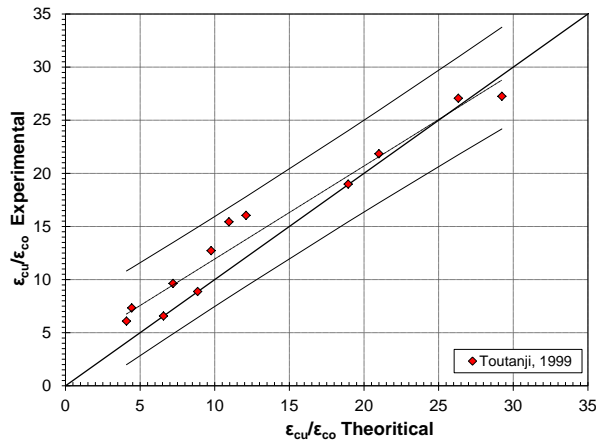
The overall accuracy of the empirical/analytical confinement models in the prediction of the ultimate axial strain is summarized in Table 5-10 and plotted in Figure 5-8. The average, standard deviation and coefficient of variation of the absolute average error in the prediction of  $\varepsilon_{cu}$  are shown for the whole experimental set and for two distinctive sets of CFRP- and SFRP-confined concrete cylinders.



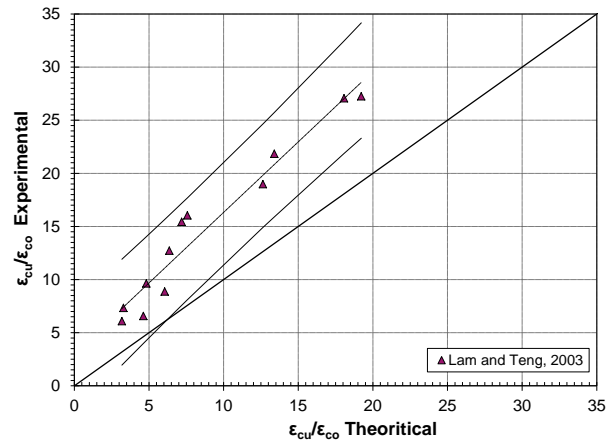
Fardis and Khalili (Richart), 1982



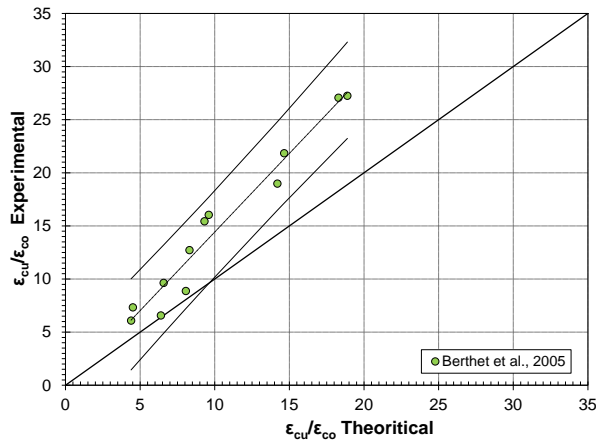
Fardis and Khalili (Newman), 1982



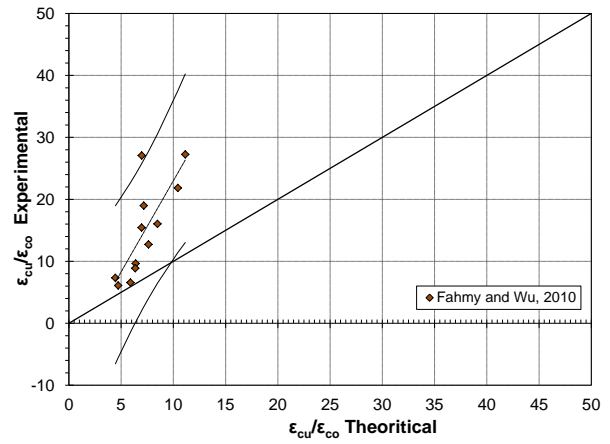
Toutanji, 1999



Lam and Teng, 2003

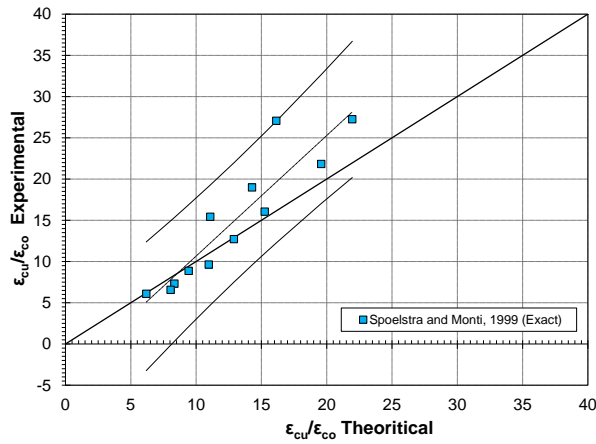


Berthet et al., 2005

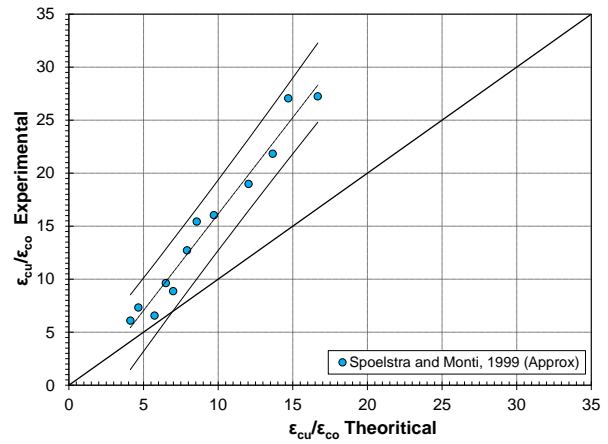


Fahmy and Wu, 2010

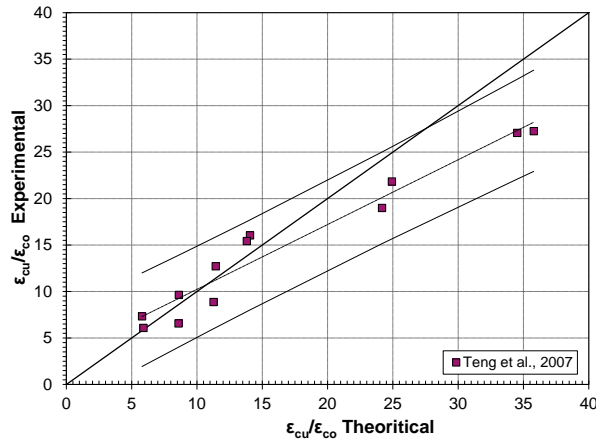
**Figure 5-6: Empirical models' performance in the prediction  $\epsilon_{cu}/\epsilon_{co}$**



Spolstra and Monti, 1999 (Exact)



Spolstra and Monti, 1999 (Approx.)

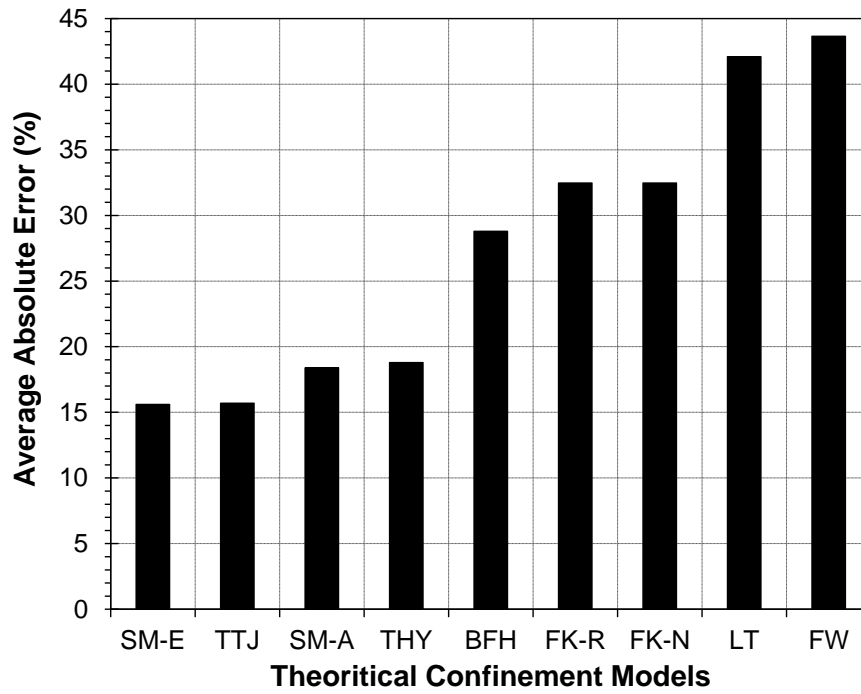


Teng et al., 2007

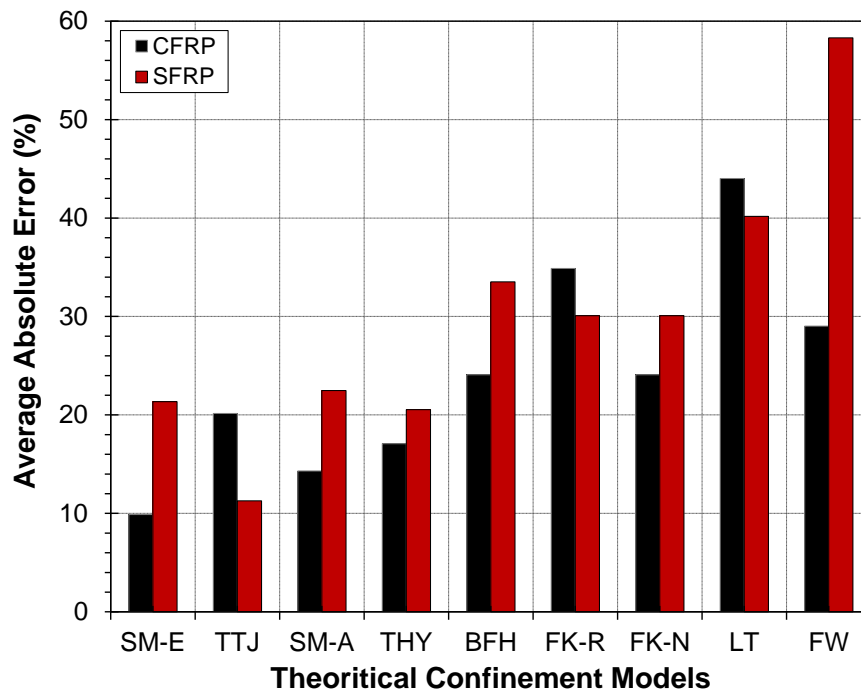
Figure 5-7: Analytical models' performance in the prediction of  $\epsilon_{cu}/\epsilon_{co}$

Table 5-10: Confinement models accuracy in the prediction of  $\epsilon_{cu}$

Confinement Model	Predictions of $\epsilon_{cu}$ (whole set)			Predictions of $\epsilon_{cu}$ (CFRP)			Predictions of $\epsilon_{cu}$ (SFRP)		
	Avg. (%)	SD (%)	COV (%)	Avg. (%)	SD (%)	COV (%)	Avg. (%)	SD (%)	COV (%)
FK-R	32.5	15.2	46.7	34.9	16.3	46.8	30.1	13.5	44.8
FK-N	32.5	15.2	46.7	34.9	16.3	46.8	30.1	13.5	44.8
TTJ	15.7	15.3	97.3	20.1	15.1	75.1	11.3	13.2	117.4
LT	42.1	9.8	23.3	44.0	9.7	22.1	40.2	9.5	23.7
BFH	28.8	11.2	38.8	24.1	13.4	55.5	33.5	5.2	15.4
FW	43.7	17.5	40.0	29.0	10.3	35.6	58.3	8.6	14.8
SM-E	15.6	18.5	118.2	9.9	7.6	77.1	21.3	11.6	54.6
SM-A	34.7	8.9	25.8	28.9	9.0	31.2	40.4	3.4	8.5
THY	18.8	19.6	104.2	17.1	19.6	114.8	20.5	18.0	87.8



(a)

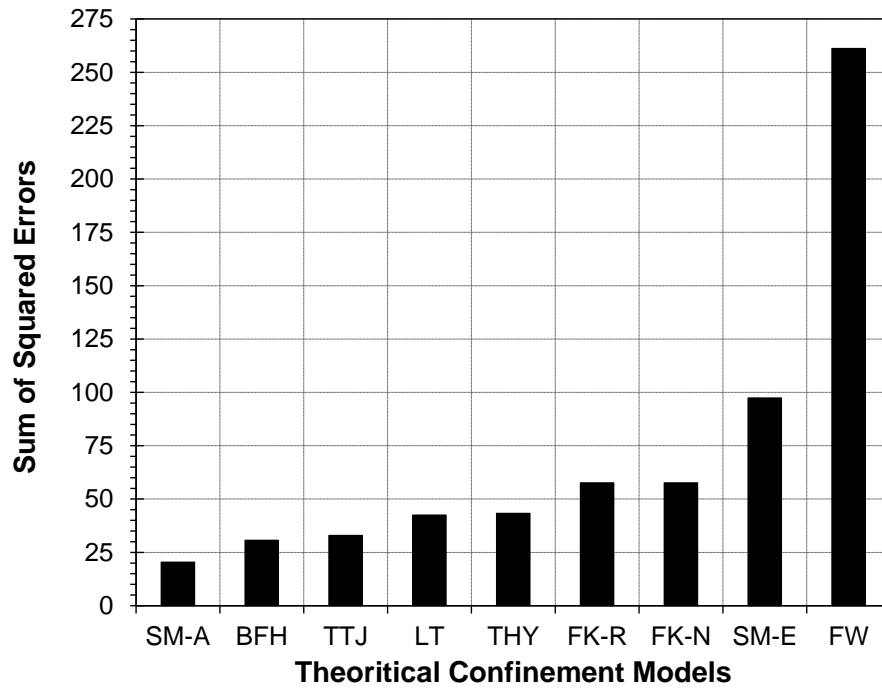


(b)

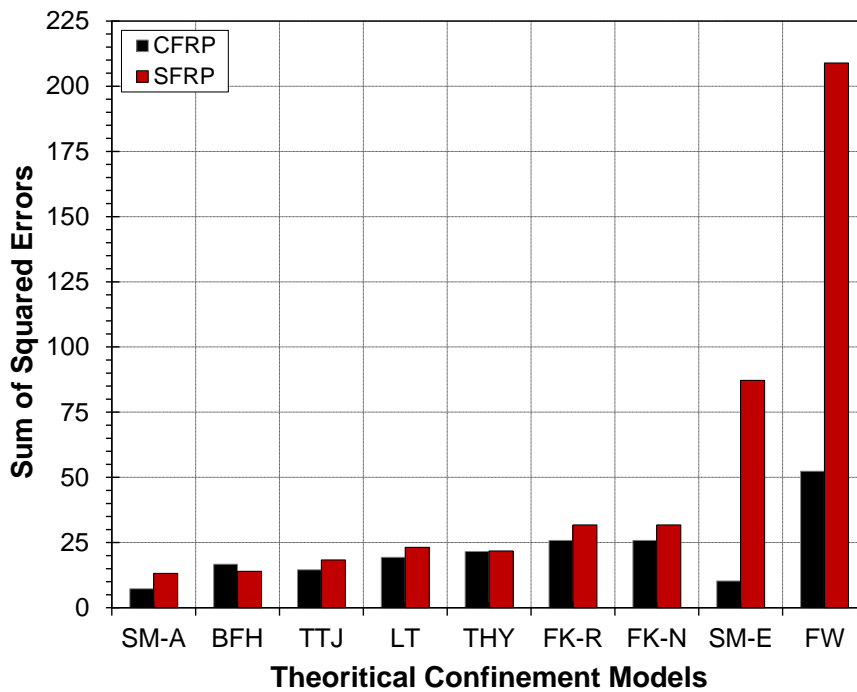
**Figure 5-8: Confinement models accuracy in  $\epsilon_{cu}$  predictions for: (a) the whole experimental set (b) CFRP and SFRP experimental sets**

It can be concluded that the models that exhibit superior performance when it comes to  $\varepsilon_{cu}$  prediction are SM-E, TTJ and SM-A which have average absolute errors respectively of 15.6%, 18.8% and 34%. It seems that all models fail in predicting the ultimate axial strain with reasonable accuracy.

The sum of squares due to errors, SSE, in the prediction of  $\varepsilon_{cu}$  for all confinement models under consideration is shown in Figure 5-9. SSE measures the total deviation of the model prediction values from the fit of the model prediction values. A Model of SSE close to zero indicates that the model has less random error components and that the fit is more useful for prediction.



(a)



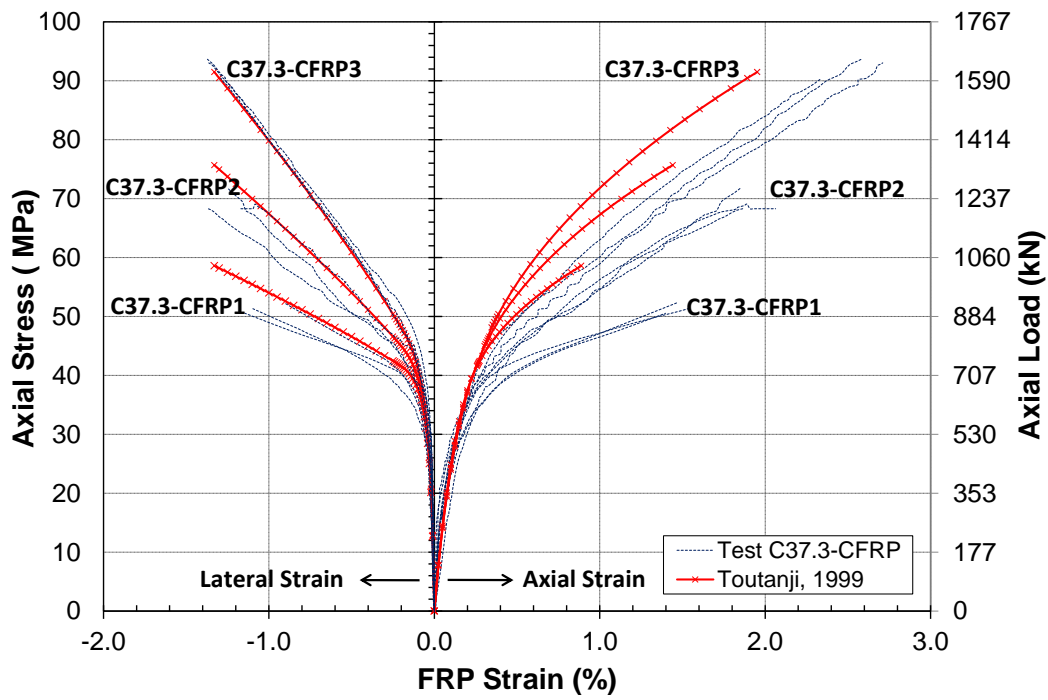
(b)

**Figure 5-9: Confinement models SSE in  $\epsilon_{cu}$  predictions for: (a) the whole experimental set (b) CFRP and SFRP experimental sets**

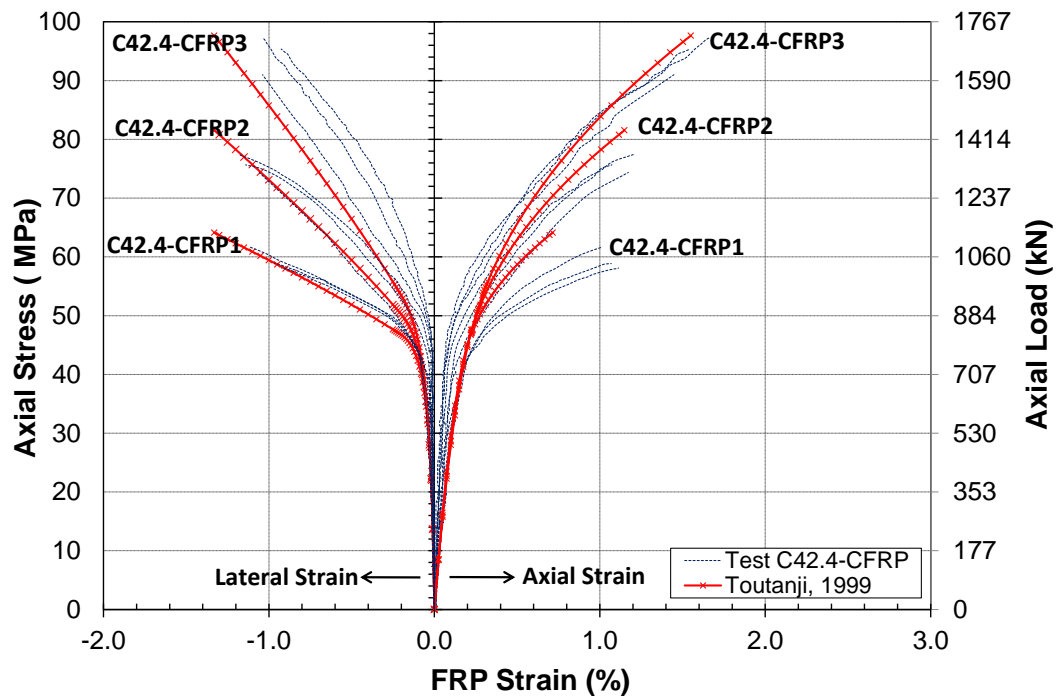
### ***5.3.3 Axial Stress-Strain Behaviour Prediction***

The performance of two empirical models, namely, TTJ and BFH and two analytical models, namely; SM-E, THY in predicting the entire stress - strain response of FRP-confined cylinders is examined in this section. As previously noted, these four models out of the nine models under consideration are the only models which provide predictions for the entire axial stress-axial strain and axial stress - lateral strain behaviour. The rest give predictions to the axial stress - axial strain response only and hence will not be further discussed.

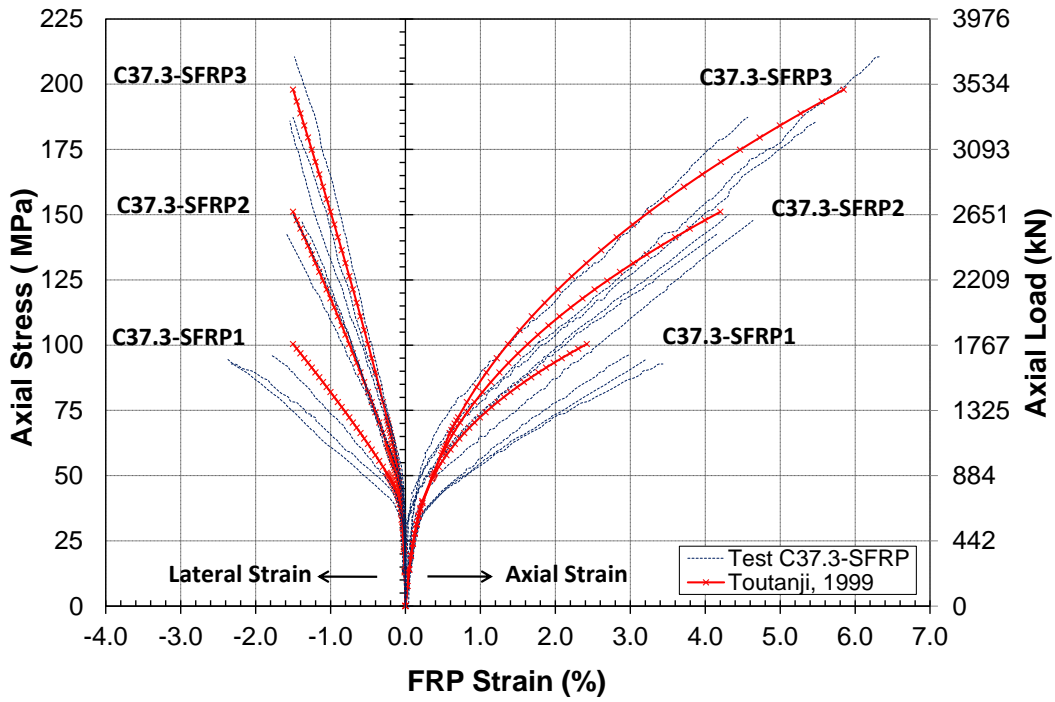
The theoretical prediction of the stress – strain response from TTJ, BFH, SM-E and THY models are shown respectively in Figure 5-10 through Figure 5-13 for various confinement configurations. The corresponding experimental stress-strain curves are shown as well for comparison purposes. Stress – strain curve aspects such as the transition point, initial and final slope, and the ultimate stress and ultimate strain predictions are the focus of the comparison and the discussion that follow.



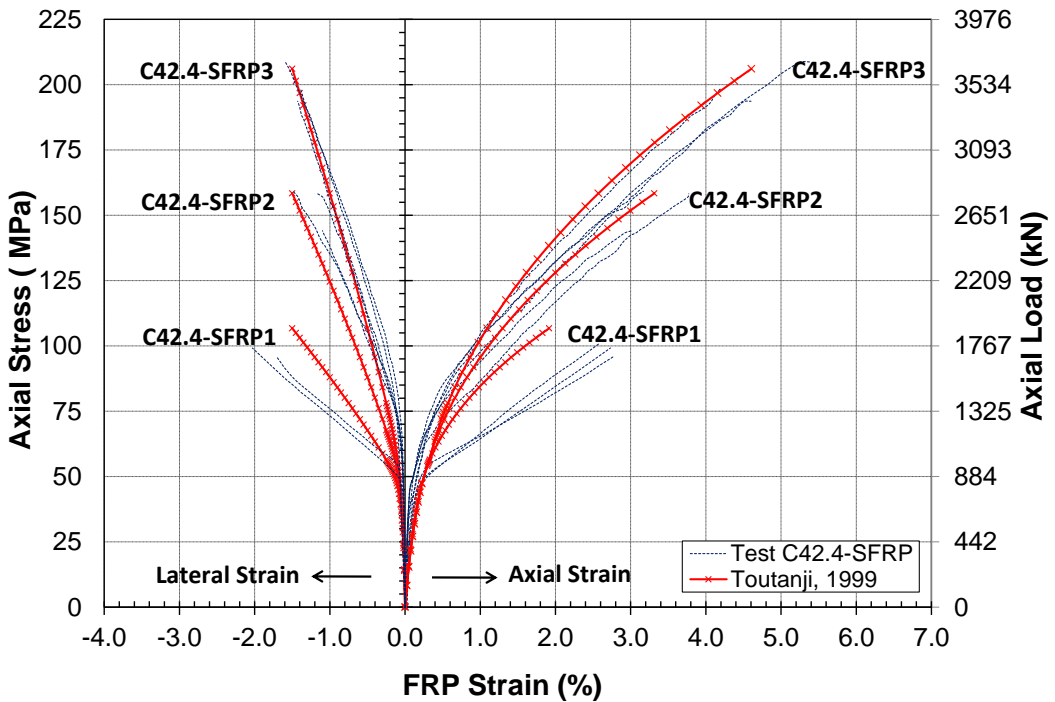
(a)



(b)

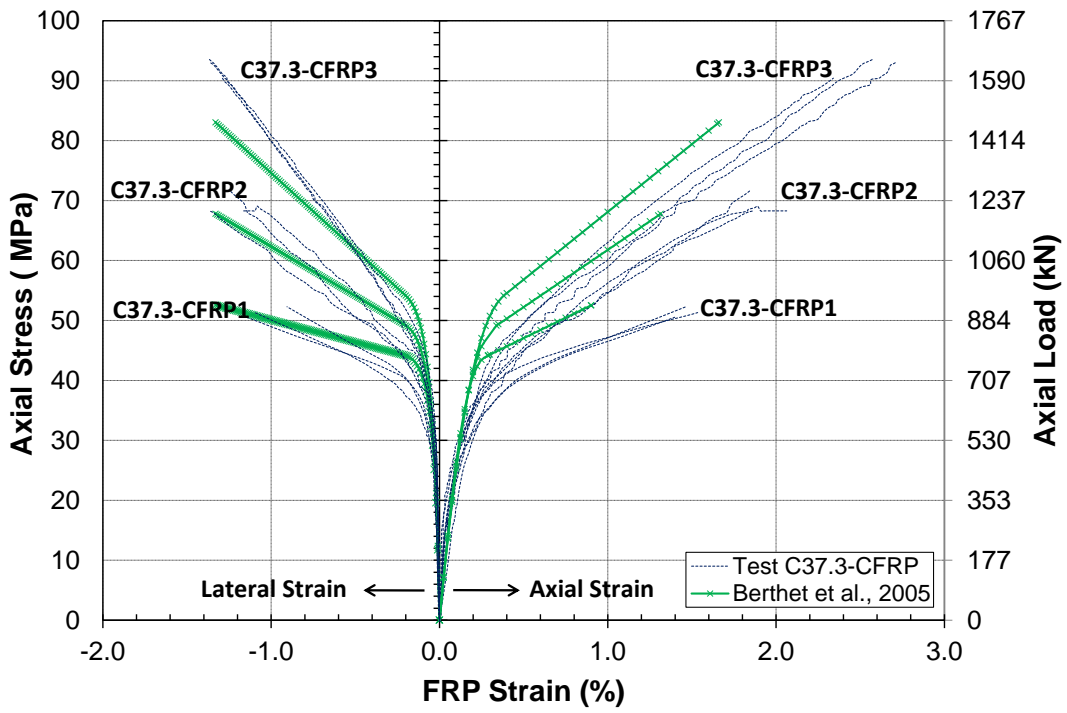


(c)

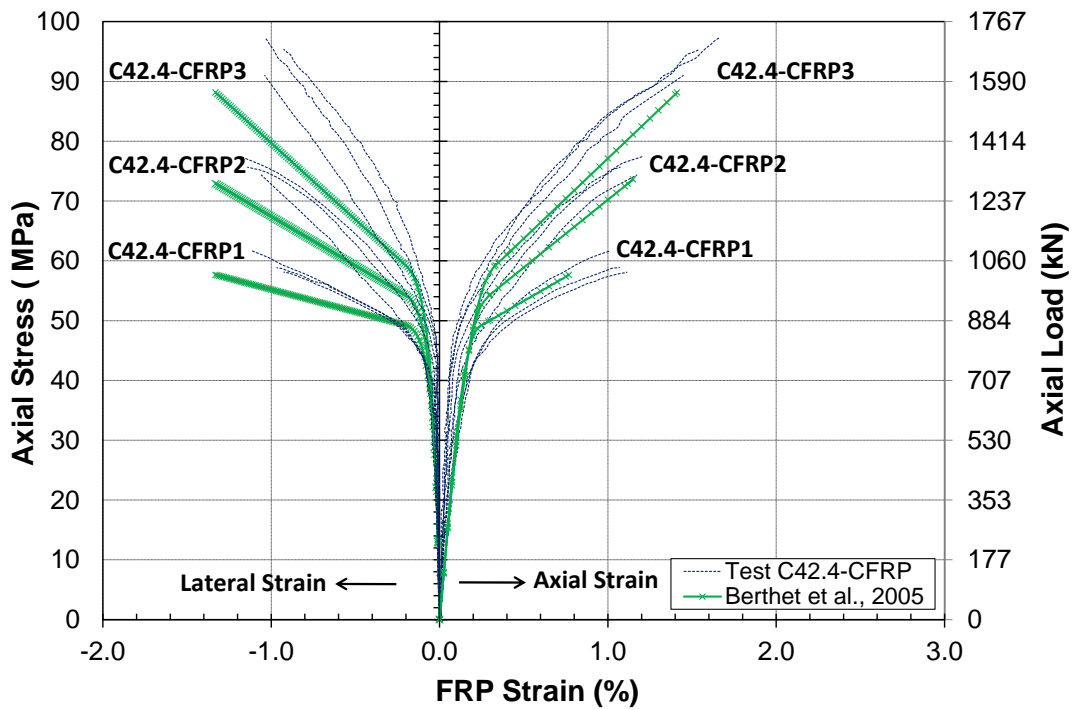


(d)

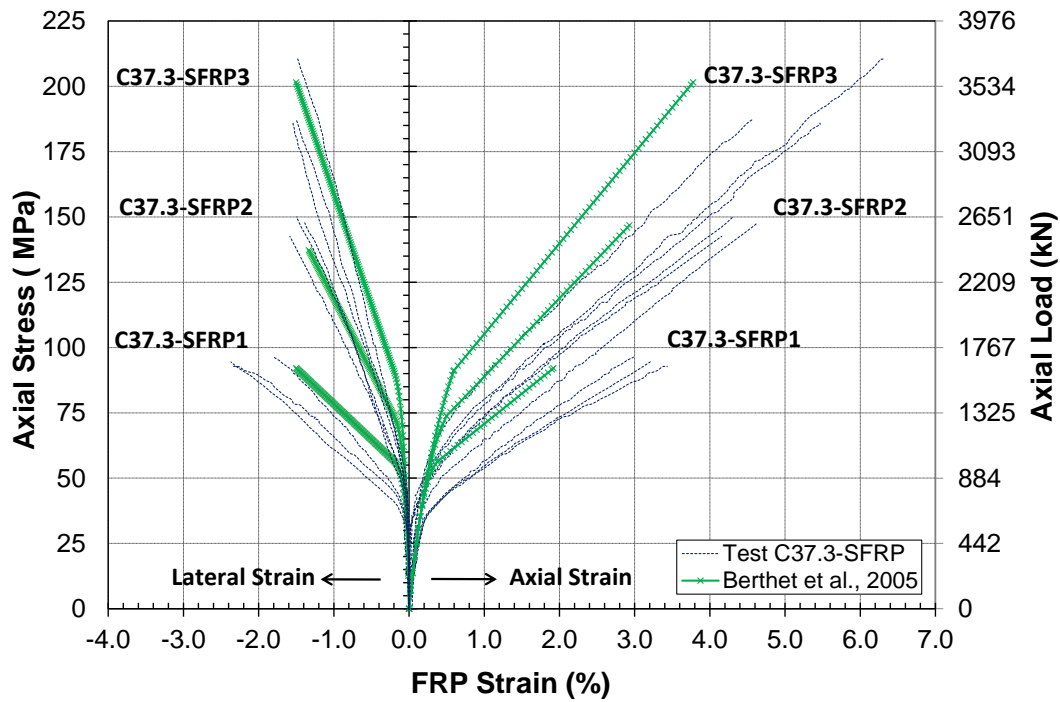
Figure 5-10: Comparison of Toutanji, 1999 Empirical model with experimental results of: (a) C37.3-CFRP (b) C42.4-CFRP (c) C37.3-SFRP (d) C42.4-SFRP



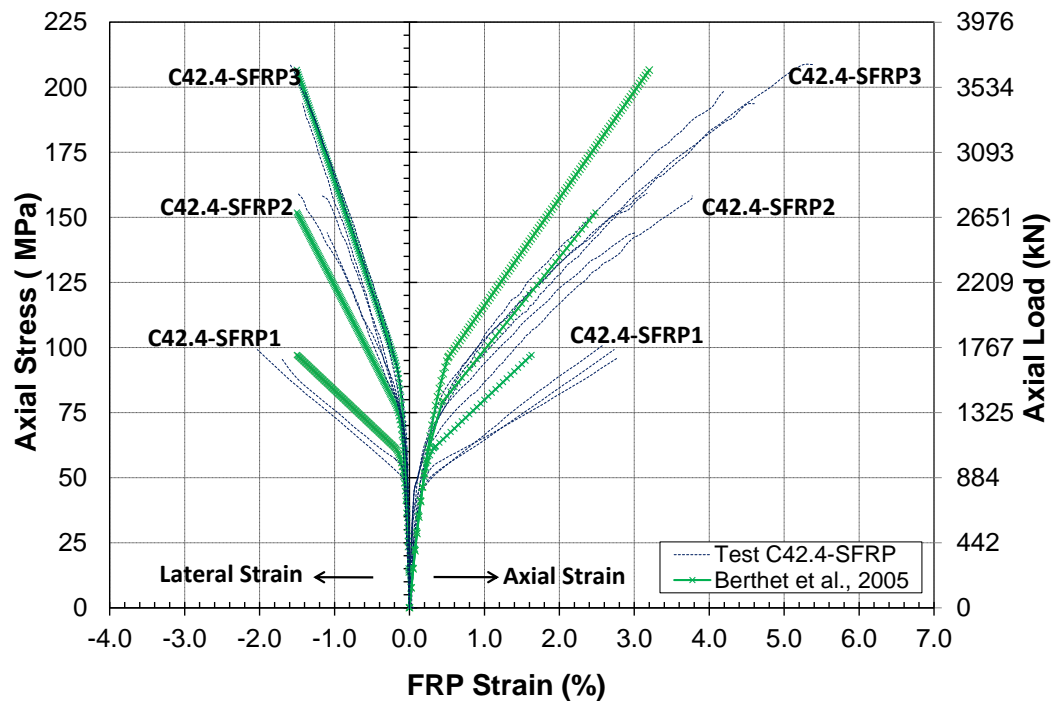
(a)



(b)

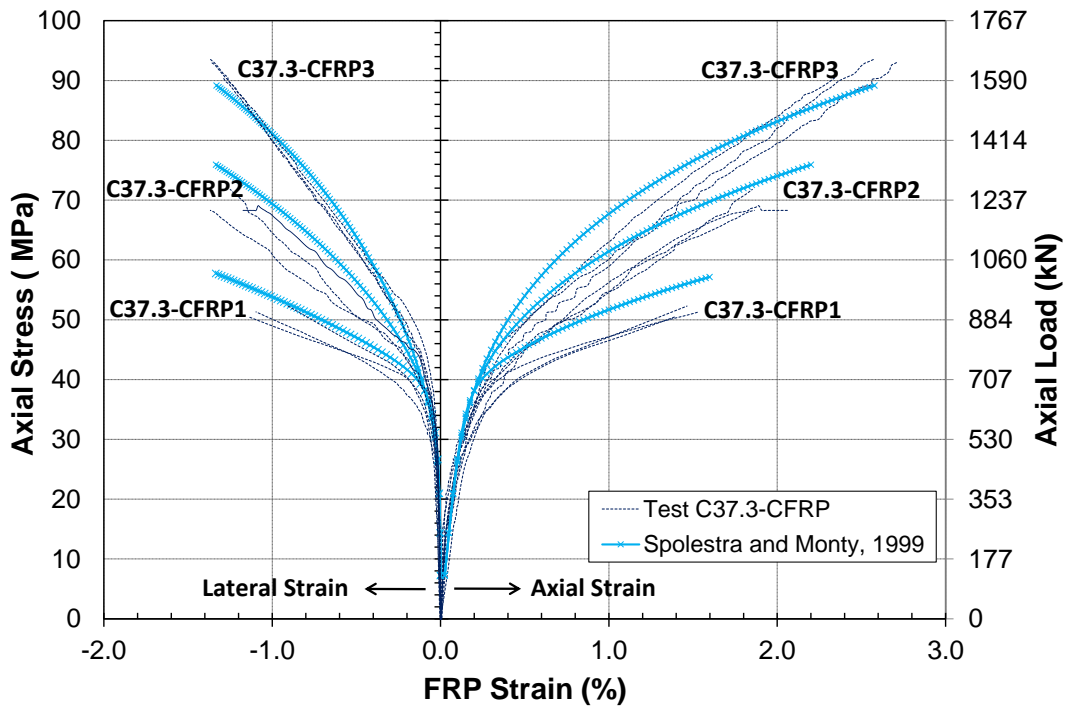


(c)

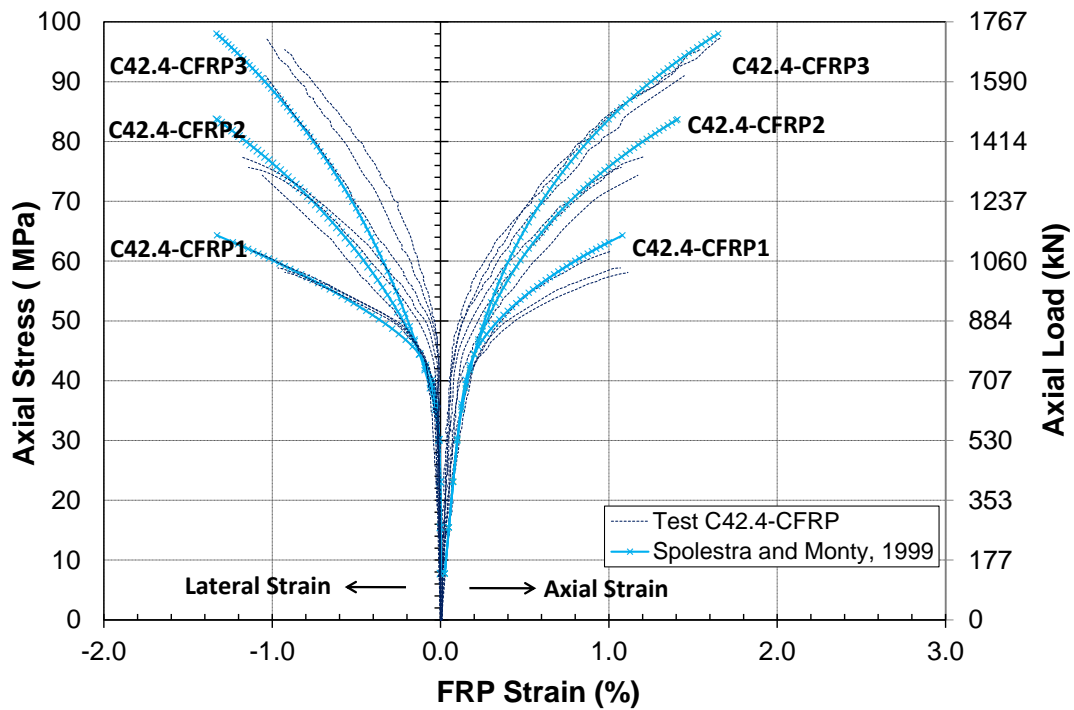


(d)

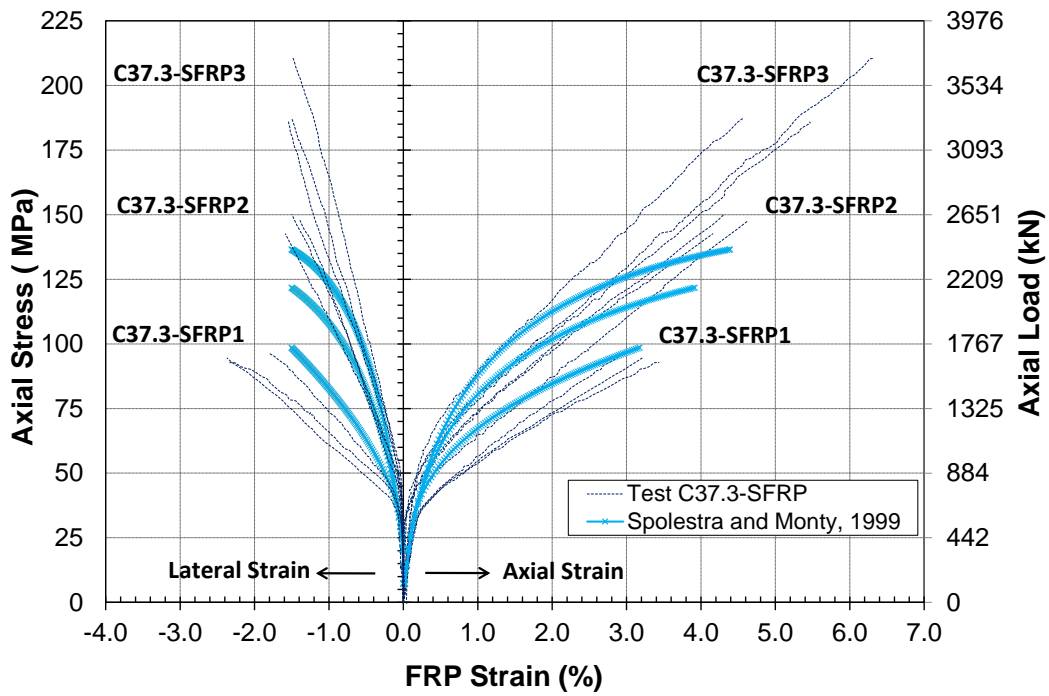
**Figure 5-11: Comparison of Berthet et al., 2005 Empirical models with experimental results of: (a) C37.3-CFRP (b) C42.4-CFRP (c) C37.3-SFRP (d) C42.4-SFRP**



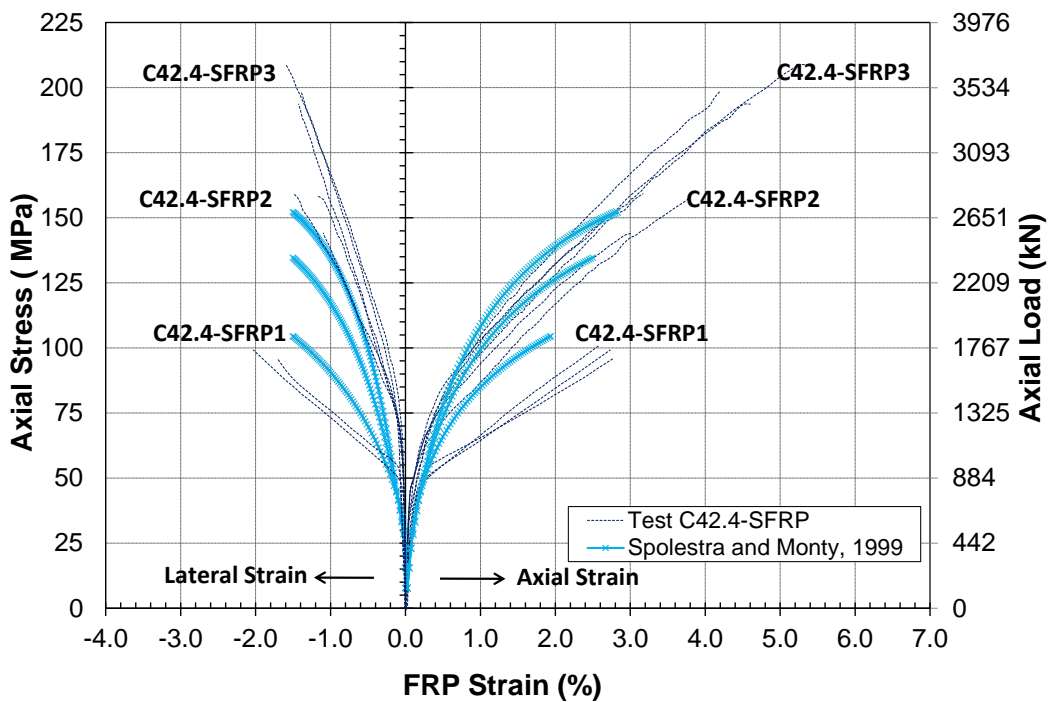
(a)



(b)

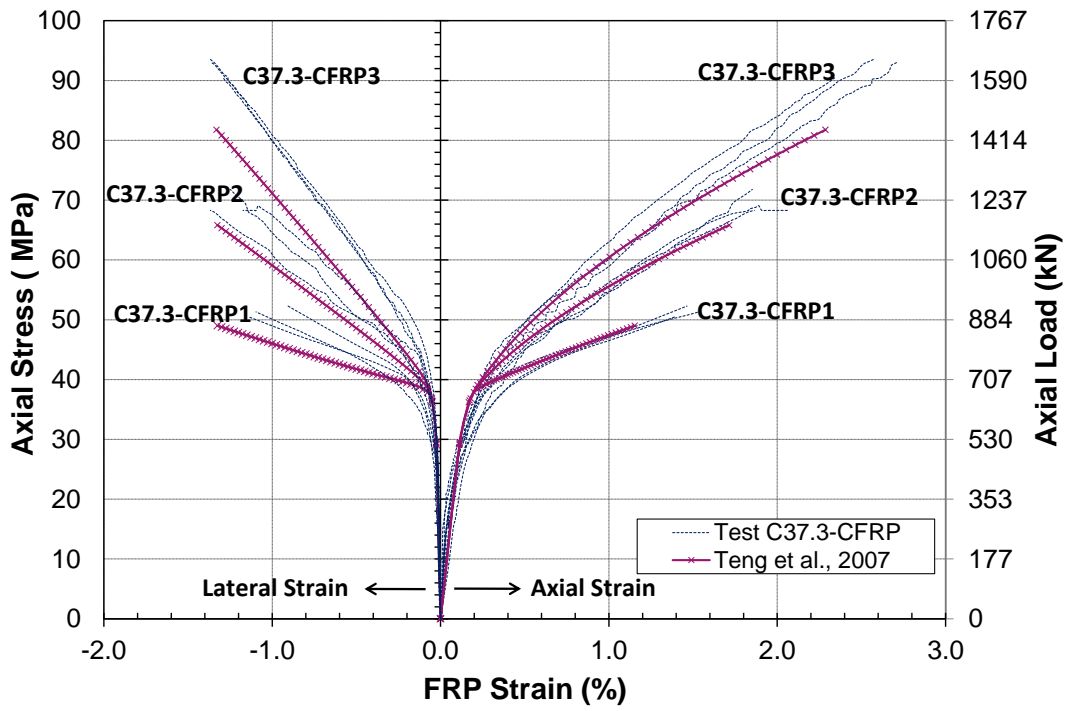


(c)

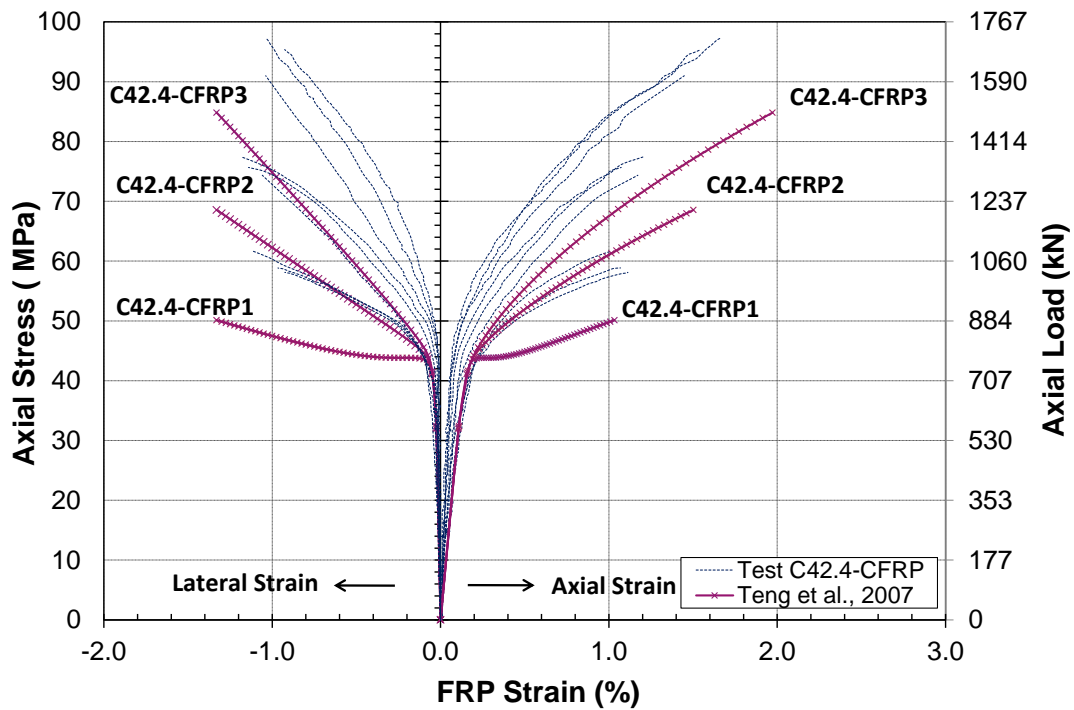


(d)

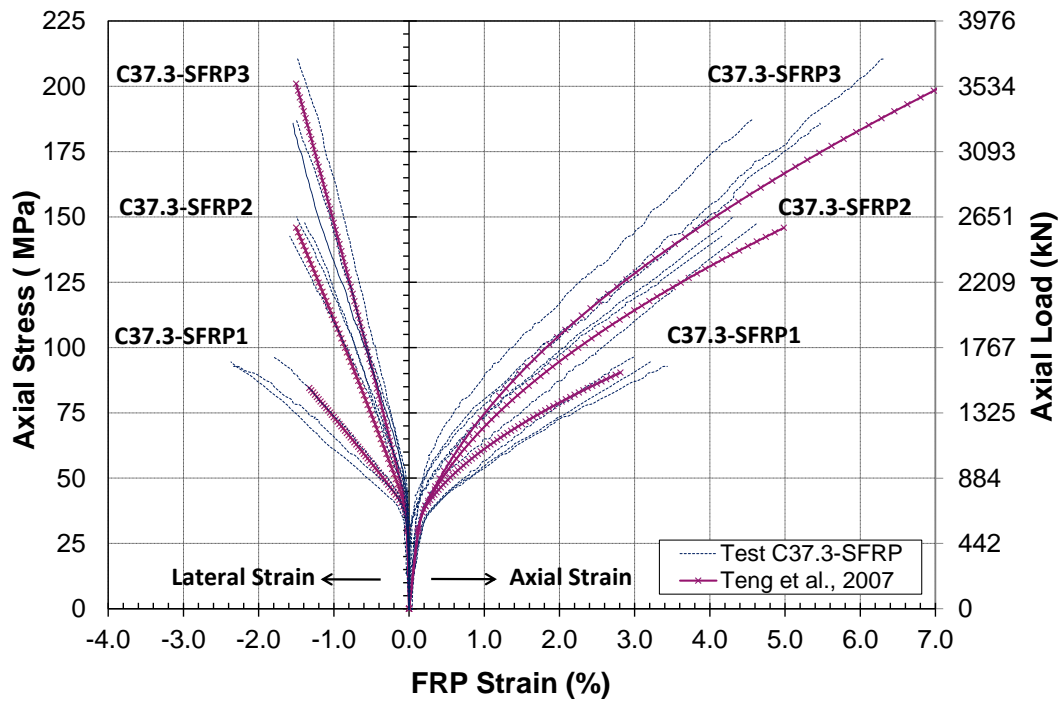
**Figure 5-12: Comparison of Spoelstra and Monti, 1999 analytical model with experimental stress-strain curve of: (a) C37.3-CFRP (b) C42.4-CFRP (c) C437.3-SFRP (d) C42.4-SFRP**



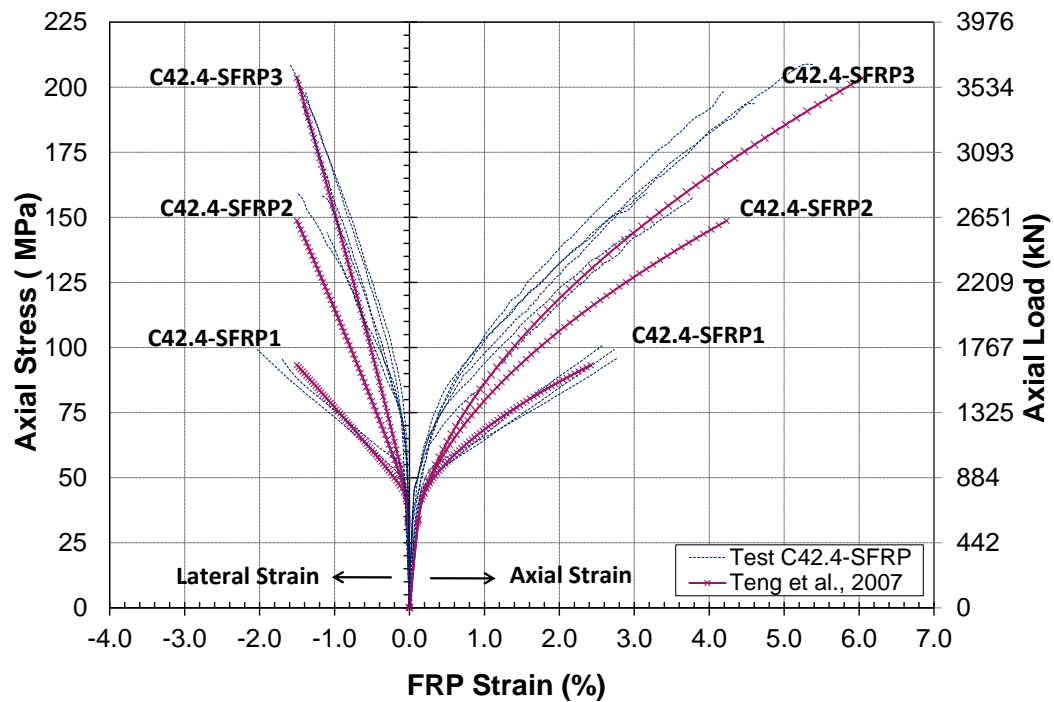
(a)



(b)



(c)



(d)

**Figure 5-13: Comparison of Teng et al., 2007 Analytical models with experimental results of: (a) C37.3-CFRP (b) C42.4-CFRP (c) C37.3-SFRP (d) C42.4-SFRP**

The TTJ model predicts the main characteristics of the transition point of the axial stress – lateral strain very accurately in terms of the stress level and the radius of curvature at which the axial stress – lateral strain changes slope for all confinement configurations. However, the model gives an inaccurate presentation of the axial stress – axial strain response due to overestimation of the radius of curvature at the kinking point and an underestimation to the ultimate axial strain.

The BFH model captures the upward-shift tendency of the transition point as the FRP lateral stiffness increase, a behaviour that has been observed experimentally. However, the model overall presents an overestimation of the axial stress – axial strain response due to an overestimation of the stress at which the transition point occurs: this is specifically true for highly confined concrete cylinders. The model also exhibited the smallest radius of curvature at the kinking point among the four models examined, which can be accurate for the weakly to moderately confined cylinders but not the highly confined cylinders.

Among all curves, the SM-E model seems to be the most successful model in accurately predicting all the characteristic of the stress – strain response in terms of the stress level at which the transition point occurs, the radius of curvature of the transition point, initial and final slope and the ultimate stress and ultimate strain for weakly and moderately confined concrete.

However, the model significantly underestimates the overall stress – strain behaviour of highly confined concrete.

The THY model did not capture the upward-shift tendency of the transition point as the FRP jacket lateral stiffness increases and the model assumes that the transition point occurs at stress close to the unconfined concrete. However, the model accurately captures the increase of radius of curvature at the kinking point as the lateral stiffness increases. The overall performance of THY model in predicting the stress – strain response was reasonably accurate.

## 5.4 Proposed Analytical Confinement Model

The performance analysis of nine of the major existing confinement models presented in the previous sections revealed that no model is capable of predicting accurately the ultimate strength, ultimate strain and the entire stress-strain behaviour that have been experimentally observed for the FRP confined cylinders and as such, an effort is made to develop a new predictive model that fits better with the current experimental database.

The models by SM-E and THY which generally show superior overall performance in the prediction of the compressive behaviour of the FRP confined concrete adopted the active confinement model originally proposed by Popovics (1973) as the base model. Hence, it is also adopted for the proposed model. The Popovics axial stress-strain model takes the form:

$$f_c(f'_{cc}) = \frac{f'_{cc}(f_l) \cdot x \cdot r}{r - 1 + x^r} \quad \text{Equation 5-1}$$

$$x = \frac{\varepsilon_c}{\varepsilon_{cc}} \quad \text{Equation 5-2}$$

$$r = \frac{E_{co}}{E_{co} - E_{sec}} \quad \text{Equation 5-3}$$

$$E_{sec} = f'_{cc}/\varepsilon_{cc} \quad \text{Equation 5-4}$$

where  $f'_{cc}$  and  $\varepsilon_{cc}$  are the confined strength at peak and the corresponding strain,  $E_{co}$  is the elastic modulus of unconfined concrete,  $E_{sec}$  is the secant elastic modulus and  $r$  is constant and accounts for the brittleness of concrete.

A key parameter in any analytical model, in addition to the active confinement base model, is the failure surface model by which the peak stress at specific lateral confining pressure level is predicted. Spoelstra and Monti adopted the Mander et al. (1988) model which was originally proposed by Willam and Warnke (1975) to define the peak axial stress under a specific confining

pressure. Teng et al. (2007) adopted a linear relationship between the confining pressure and the peak stress. The former appears to perform very well for weakly to moderately confined cylinders while the latter appears to perform better for highly confined cylinders. Examining the existing failure surface models in the literature, it was found that the Leon-Pramono failure surface, if tensile strength of concrete is taken 0.1 of compressive strength lies at the boundary of the two aforementioned models.

Therefore, it is suggested that in the proposed model, the Leon-Pramono (Pramono and Willam 1989) model is adopted to define the failure surface of actively confined concrete. The Leon-Pramono failure surface model takes the form:

$$\frac{f'_{cc}(f_l)}{f'_{co}} = \sqrt{1 + 9.9 \frac{f_l}{f'_{co}} + \frac{f_l}{f'_{co}}} \quad \text{Equation 5-5}$$

where  $f'_{cc}(f_l)$  is the confined strength at peak at any lateral confining pressure,  $f'_{co}$  is the unconfined concrete strength at peak, and  $f_l$  is the lateral confining pressure.

The axial strain at peak stress relationship,  $\varepsilon_c(f'_{cc})$  originally proposed by Richart et al. (1928) and adopted in the analytical models by SM-E and THY is also adopted for the present model and takes the form:

$$\varepsilon_c(f'_{cc}) = \varepsilon_{co} \left[ 1 + 5 \left[ \frac{f'_{cc}}{f'_{co}} - 1 \right] \right] \quad \text{Equation 5-6}$$

where  $\varepsilon_{co}$  is the axial strain corresponding to the unconfined strength at peak.

Now, the axial stress-axial strain and axial stress-lateral strain curve can be generated using the same iterative procedure that has been adopted by Spoelstra and Monti, 1999.

#### 5.4.1 Performance of the Proposed Stress-Strain Model

The proposed model theoretical predictions of the ultimate axial strength,  $f_{cu}$  and the ultimate axial strain,  $\epsilon_{cu}$  for each confinement configuration are reported in Table 5-11. The percent error in the theoretical prediction with respect to the experimental averages is also reported.

**Table 5-11: Proposed model prediction of  $f'_{cu}$  and  $\epsilon_{cu}$**

Confinement Designation	Ultimate Axial Strength			Ultimate Axial Strain		
	Exp. (avg.)	$f_{cu}$	Error	Exp. (avg.)	$\epsilon_{cu}$	Error
	(MPa)	(MPa)	(%)			(%)
C37.3-CFRP1	51.4	55.3	8	0.0147	0.0160	9
C37.3-CFRP2	69.5	74.6	7	0.0193	0.0216	12
C37.3-CFRP3	92.4	90.7	-2	0.0254	0.0262	3
C37.3-SFRP1	94.5	98.6	4	0.0321	0.0318	-1
C37.3-SFRP2	146.8	144.4	-2	0.0437	0.0465	6
C37.3-SFRP3	194.6	184.0	-5	0.0545	0.0595	9
C42.4-CFRP1	59.6	61.6	3	0.0107	0.0104	-3
C42.4-CFRP2	75.8	81.8	7	0.0115	0.0135	7
C42.4-CFRP3	94.6	98.4	4	0.0155	0.0166	7
C42.4-SFRP1	98.8	103.7	5	0.0270	0.0265	-2
C42.4-SFRP2	153.9	152.8	-1	0.0332	0.0346	4
C42.4-SFRP3	200.4	193.6	-3	0.0474	0.0438	-7

The overall accuracy of the proposed models in the prediction of the ultimate axial stress and ultimate axial strain is summarized respectively in Table 5-12 and Table 5-13. The average, standard deviation and coefficient of variation of the absolute average error in the theoretical prediction are shown for the whole experimental set and for two distinctive sets of CFRP- and SFRP-confined concrete cylinders.

**Table 5-12: The proposed model accuracy in the prediction of  $f'_{cu}$**

Confinement Model	Predictions of $f'_{cu}$ (whole set)			Predictions of $f'_{cu}$ (CFRP)			Predictions of $f'_{cu}$ (SFRP)		
	Avg. (%)	SD (%)	COV (%)	Ave (%)	SD (%)	COV (%)	Ave (%)	SD (%)	COV (%)
	Proposed Model	4.3	4.3	100.5	5.3	3.3	63.5	3.4	3.8

**Table 5-13: The proposed model accuracy in the prediction of  $\epsilon_{cu}$**

Confinement Model	Predictions of $\epsilon_{cu}/\epsilon_{co}$ (whole set)			Predictions of $\epsilon_{cu}/\epsilon_{co}$ (CFRP)			Predictions of $\epsilon_{cu}/\epsilon_{co}$ (SFRP)		
	Avg. (%)	SD (%)	COV (%)	Avg. (%)	SD (%)	COV (%)	Avg. (%)	SD (%)	COV (%)
	Proposed Model	6.8	6.7	99.7	8.5	6.4	75.7	5.0	5.6

The experimental and theoretical ultimate axial stress are normalized by being divided by their respective cylinders unconfined concrete strength and are compared for the proposed model in Figure 5-14. Similarly, the experimental and theoretical ultimate axial strain are normalized by being divided by their respective cylinders unconfined concrete strain at peak values and are compared for the proposed model in Figure 5-15. Furthermore, the proposed model prediction of the entire stress – strain response is displayed in Figure 5-16.

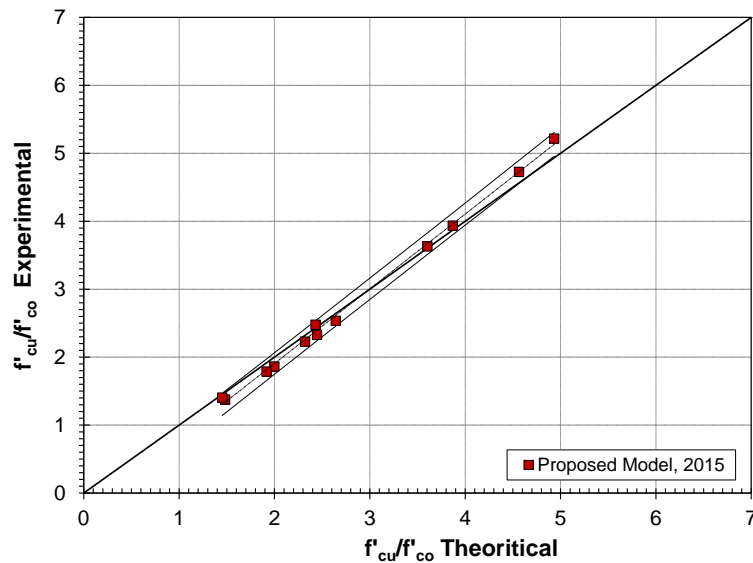


**Figure 5-14: Proposed models’ performance in the prediction of  $f'_{cu}/f'_{co}$**

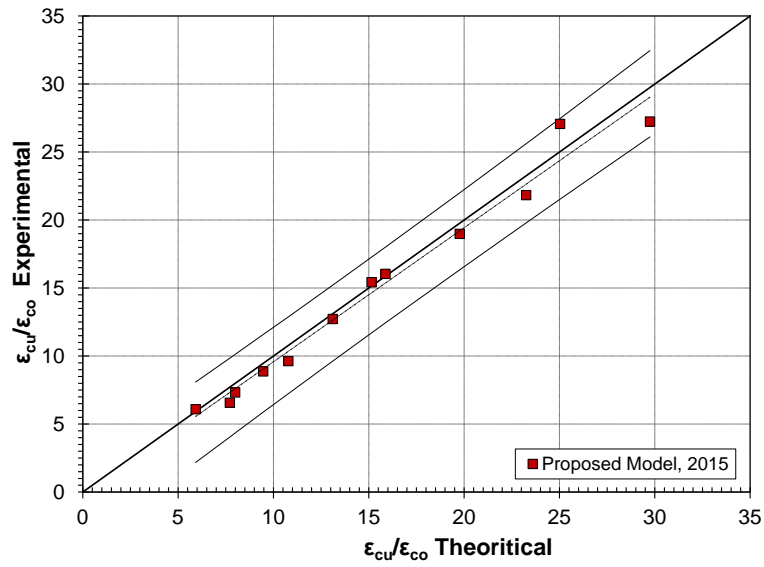
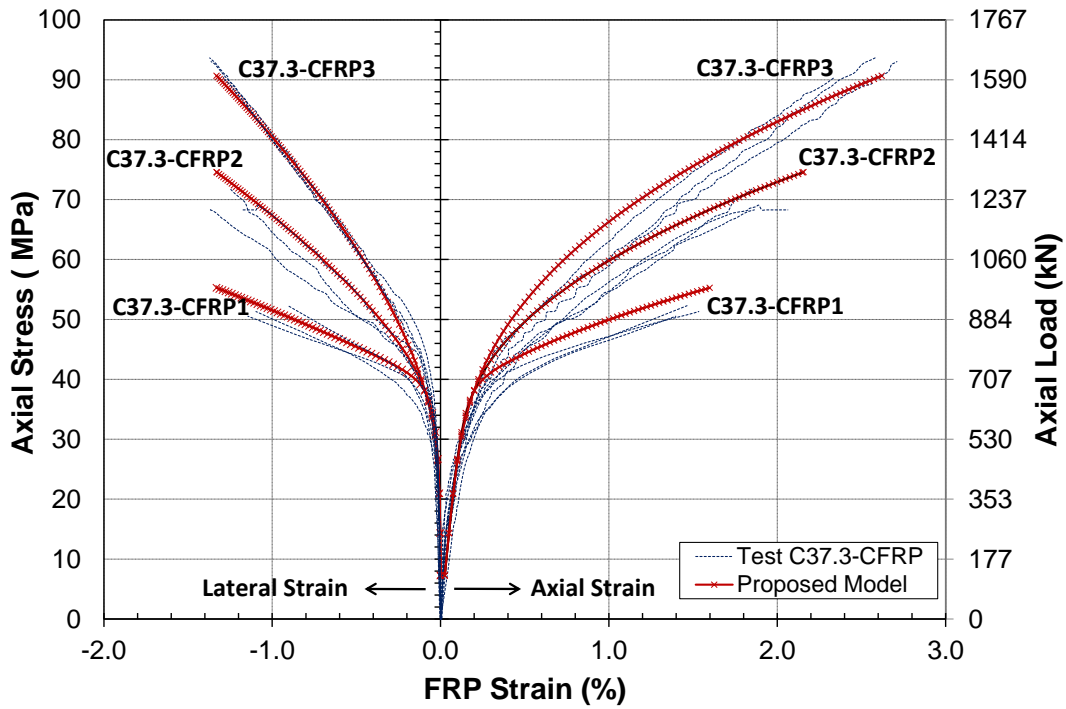
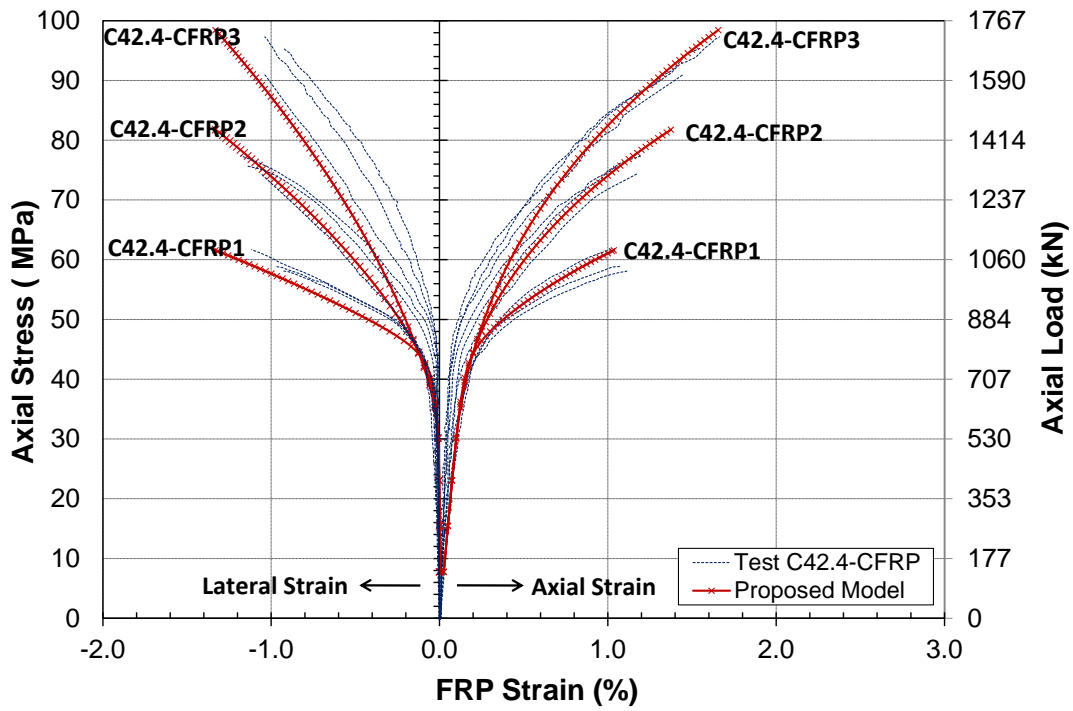


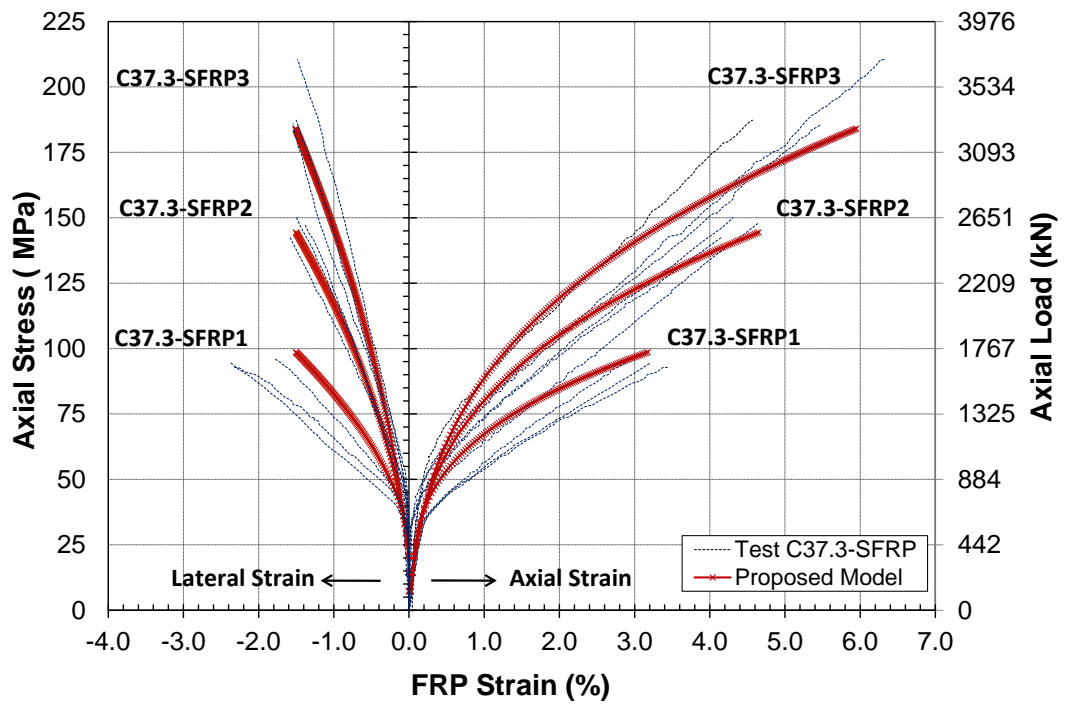
Figure 5-15: Proposed models' performance in the prediction of  $\epsilon_{cu}/\epsilon_{co}$



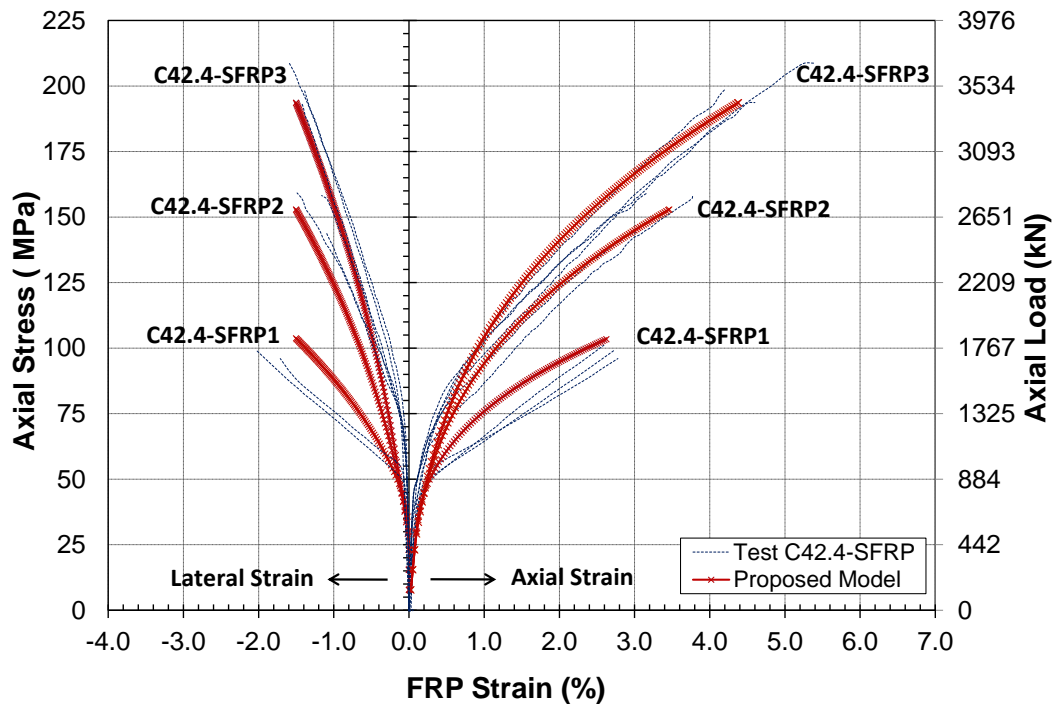
(a)



(b)



(c)



(d)

**Figure 5-16: Comparison of the proposed analytical model with experimental results for: (a) C37.3-CFRP (b) C42.4-CFRP (c) C37.3-SFRP (d) C42.4-SFRP**

It can be noted from the above that the peak stress and the corresponding strain as well as the stress-strain curve fit quite well with the experimental results and that the proposed model exhibits superior capability in predicting equally accurately the ultimate axial strength and ultimate axial strain, a feature that has not been exhibited by any of the nine models that has been examined in the herein investigation.

### 5.5 Summary

This chapter presented a systematic assessment of the performance of nine of the major existing empirical/analytical models for concrete cylinders confined with FRP sheets. It has been remarked that the ultimate strength of confined cylinders was rather accurately predicted by some of the existing models such as Berthet et al. (2005), and Lam and Teng (2003) with an

average absolute errors of 3.4% for the former and 4.5% for the latter. On the other hand, the errors, when it comes to the prediction of the ultimate strain, were significantly larger with a minimum average absolute error of 15.6%.

A new analytical model was proposed to predict the entire stress-strain response. The proposed model is in a better agreement with the current experimental database.

Numerical FE modeling for the FRP-confined concrete cylinders is presented in the next chapter.

## Chapter Six: **Finite Element Modeling of FRP-Confined Concrete Cylinders**

### **6.1 Introduction**

The FE modeling of FRP-confined concrete column cylinders under compressive loading is presented in this chapter. Concrete plasticity is first discussed as a basis for developing insights into the general form used in the plasticity-based model formulation. A constitutive model for concrete in the framework of the DP plasticity model is then introduced and the model's parameters that define the yield criterion, hardening/softening rule and flow rule are thoroughly discussed and derived based on regression analysis of the existing test data. The detail of the FE model implemented in ABAQUS is given next. The model is then validated by comparing the numerical results from the FE analysis against the experimental data obtained from the current research in addition to three independent experimental investigations by other researchers. The comparison focuses on the ultimate strength, ultimate strain and the stress-strain behaviour. The chapter closes with parametric study using the validated model to quantify the effect of FRP jacket thickness and type on the strength and deformability of FRP-confined concrete.

### **6.2 Concrete Plasticity**

It is well known that the concrete core in FRP-confined concrete cylinders is subjected to a tri-axial stress state due to the confining pressure in the circumferential direction and the axial compression in the loading direction. Due to the complex and highly nonlinear response of concrete when subjected to such a multi-axial stress state, the development of a generally accepted constitutive model for the concrete material is far from complete. However, it is generally believed that the basic characteristics of concrete behaviour can be adequately captured by constitutive models based on the plasticity theory, Pekau et al. (1992) and Jiang and Wu (2012).

A plasticity model is generally described by three main parameters which include yield criterion (including initial and subsequent yield criterion), hardening-softening rule and flow rule.

Yield criterion defines the limit of elastic behaviour and the beginning of plastic deformation, it represents a surface in principal stress space, which is called a yield surface. Different yield criteria for concrete can be found in the literature; ranging from a simple one-parameter criterion, Von Mises (1913), or two-parameter criterion, Drucker-Prager (1952), to a more refined five-parameter criterion, Willam and Warnke (1975), Chen (1982).

The hardening rule describes the behaviour of concrete after initial yielding and is governed by a hardening function which defines how the yield surface evolves with plastic deformation in principal stress space. These evolved surfaces are called subsequent or loading surfaces; if the hardening function is constant, subsequent surfaces remains on initial yielding surfaces as plastic deformation occurs until ultimate strain is reached, and the post-yielding behaviour is described as perfectly plastic. If the hardening function depends on the plastic strain increment, subsequent surfaces evolve with plastic strain deformation, and the post-yielding behaviour is described as work-hardening or work-softening behaviour.

The flow rule defines the direction of the plastic deformation increment in stress space and thus the dilation behaviour. The flow rule is governed by the so-called potential function. When the potential function is set equal to the yield function, the flow rule is called an associative flow rule; otherwise, the flow rule is called a non-associative flow rule.

In the framework of DP type plasticity models, the yield criteria and the hardening/softening rules for confined concrete can be defined by parameters related to friction angle and cohesion, while the flow rule is defined by parameters related to plastic dilation (Karabinis and Rousakis , 2002). Closed-form formulas for these parameters are derived later in this chapter through a

regression analysis of the experimental results of the current investigation so that these parameters are directly implemented in FE models for FRP-confined concrete.

### 6.3 Concrete Constitutive Model

The concrete plasticity model used to simulate the behaviour of confined concrete in this study is based on the linear extended DP built-in model in the general purposes commercial FE software ABAQUS.

#### 6.3.1 Extended Linear Drucker-Prager Plasticity Model

The Drucker-Prager (DP) model was proposed by Drucker and Prager in 1952 . It can accurately capture the behaviour of frictional material that exhibits pressure-dependent yield such as rock and concrete as is capable of predicting the increase in shear strength when hydrostatic pressure increases. The extended linear DP model in ABAQUS is a DP type plasticity model with a modified yield criterion that includes the effect of the third deviatoric stress invariant. Similar to other plasticity models, there are three main criteria that control the framework of the extended DP model. The details, in case of uniaxial compression with uniform confinement, are discussed in the following sections. In the subsequent sections, compression is considered negative, and tension is considered positive, unless otherwise specified.

##### 6.3.1.1 Yield criterion and Hardening-Softening Rule

The yield criterion for extended linear DP plasticity model takes the following form:

$$f = t - p \tan \varphi - k = 0 \quad \text{Equation 6-1}$$

where

$$t = \frac{1}{2} q \left[ 1 + \frac{1}{K} - \left( 1 - \frac{1}{K} \right) \left( \frac{r}{q} \right)^3 \right] \quad \text{Equation 6-2}$$

$p$  is the equivalent hydrostatic pressure:,

$$p = \frac{-I_1}{3} \quad \text{Equation 6-3}$$

$I_1$  is the first stress invariant:

$$I_1 = (\sigma_1 + \sigma_2 + \sigma_3) \quad \text{Equation 6-4}$$

where  $\sigma_1$ ,  $\sigma_2$  and  $\sigma_3$  are the principal stresses in the 1, 2 and 3 directions.

$q$  is the Von Misses equivalent stress:

$$q = \sqrt{3J_2} \quad \text{Equation 6-5}$$

$J_2$  is the second deviatoric stress invariant:,

$$J_2 = \frac{1}{6} [(\sigma_1 - \sigma_2)^2 + (\sigma_2 - \sigma_3)^2 + (\sigma_3 - \sigma_1)^2] \quad \text{Equation 6-6}$$

$r$  is third invariant of deviatoric shear:

$$r = \sqrt[3]{2J_3} \quad \text{Equation 6-7}$$

The function  $f$  in Equation 6-1 represents initial and subsequent yield surfaces;  $f < 0$  represents an elastic behaviour, while  $f = 0$  represents yield state.  $K$  is the ratio of the yield stress in tri-axial tension to that in tri-axial compression; it determines the shape of the yielding function in the deviatoric plane.  $\varphi$  is a material property, commonly referred to as the friction angle, which describes the material sensitivity to the hydrostatic pressure and determines the slope of the yield surface in the meridian space.  $k$  is the hardening-softening function.

The DP failure surface in the deviatoric plane and in the meridian plane p-t is displayed in Figure 6-1, when  $K = 1$ , the yield surface in the deviatoric plane is circular and the yield stresses in tri-axial tension and tri-axial compression are the same. When  $K < 1$  the shape of the yield

surface in the deviatoric plane is changed and is no longer circular. In the extended DP model in ABAQUS, the value of  $K$  is limited between 0.778 and 1 to ensure that yield surface remains convex.

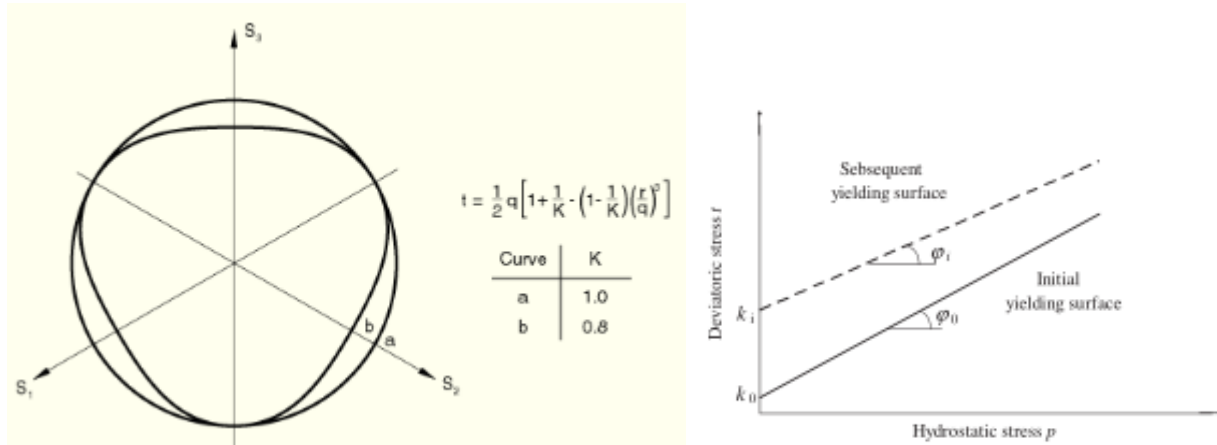


**Figure 6-1: Failure surface of extended DP model in ABAQUS: (a) in the deviatoric plane (b) in the meridian  $p$ - $t$  plane (ABAQUS 6.9)**

#### 6.3.1.1.1 Friction Angle, $\varphi$

The DP plasticity model parameter, friction angle,  $\varphi$ , can be related to the more-common Mohr-Coulomb (MC) material parameter, internal friction angle  $\phi$  if the DP failure surface is adjusted so that the DP cone circumscribes the MC hexagonal pyramid, Chen (1982) as shown in Figure 6-2. The friction angle,  $\varphi$  is then defined as shown in Equation 6-8. As such, the friction angle has been typically considered as a material constant that is a function of concrete strength and is not affected by the current stress state. However, Vermeer and de Borst (1984) reported that concrete behaviour cannot be well simulated using a constant friction angle. Indeed, recent research by Jiang et al. (2011), as previously reviewed in Chapter 2, have demonstrated that the friction angle is related to the state of the internal damage and that the friction angle slightly decreases with the increase of the equivalent plastic strain.

$$\tan \phi = \frac{6 \sin \phi}{3 - \sin \phi} \quad \text{Equation 6-8}$$

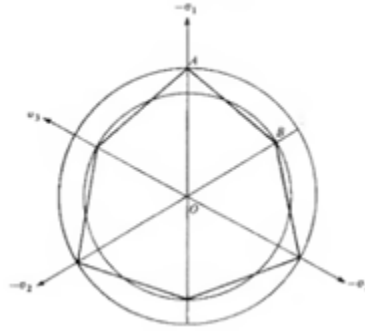


**Figure 6-2: Mohr-Coulomb and DP failure surfaces in the deviatoric plane, Chen (1982)**

The friction angle is further investigated here using the available test data from the current research, the friction angle can be calculated following the procedures outlined next:

- For a particular loading level on a tested cylinder, the deviatoric stress,  $t$ , and the equivalent pressure,  $p$ , is calculated using Equation 6-2 and Equation 6-3, respectively.

The lateral stress is calculated from the measured FRP lateral strain.

- The corresponding axial and plastic strains are calculated

$$\varepsilon_c^p = \varepsilon_c - \frac{1}{E_{co}} (\sigma_c - 2\nu\sigma_l) \quad \text{Equation 6-9}$$

$$\varepsilon_l^p = \varepsilon_l - \frac{1}{E_{co}} [(1 - \nu)\sigma_l - \nu\sigma_c] \quad \text{Equation 6-10}$$

where  $\varepsilon_c$  and  $\varepsilon_l$  are the current axial and lateral strain,  $\varepsilon_c^p$  and  $\varepsilon_l^p$  are the axial and lateral plastic strain,  $\sigma_c$  and  $\sigma_l$  are the axial and lateral stress,  $E_{co}$  is the elastic modulus of unconfined concrete, and  $\nu$  is the Poisson's ratio of concrete.

The elastic modulus  $E_{co}$  is calculated using Equation 6-11, and the Poisson's ratio is set to 0.2.

$$E_{co} = 4734\sqrt{f'_{co}} \quad \text{Equation 6-11}$$

- The equivalent principal plastic strain,  $\tilde{\epsilon}_p$ , is calculated by Equation 6-12.

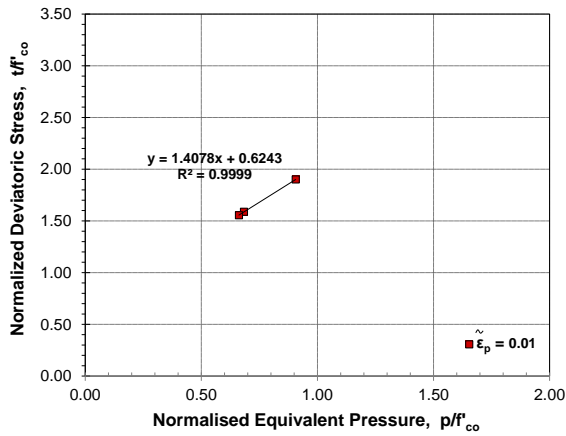
$$\tilde{\epsilon}_p = \int \sqrt{d\epsilon_i^p d\epsilon_i^p} \quad \text{Equation 6-12}$$

where  $d\epsilon_i^p$  is the plastic strain increment in the  $i^{\text{th}}$  direction.

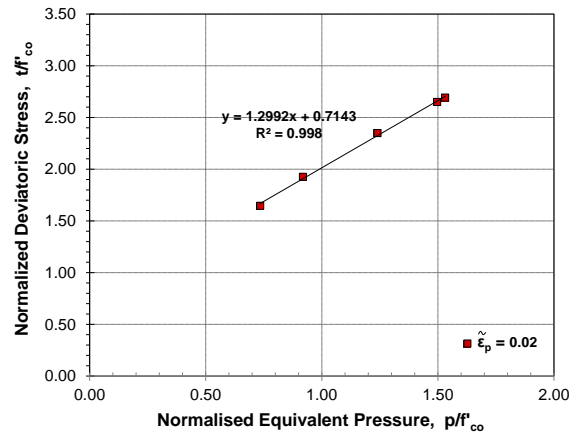
- The previous steps are repeated for all the axial loading level recorded for one tested cylinder.
- The same procedures are followed for all the tested cylinders in the current test database.
- For the same equivalent principal plastic strain, the deviatoric stress,  $t$ , and the equivalent pressure,  $p$ , is normalized and plotted as shown in Figure 6-3. The points in one figure are from different tested cylinders. The slope of the line in each figure represents the friction angle that corresponds to the specific equivalent plastic strain.
- The friction angle and its corresponding equivalent plastic strain from each figure in Figure 6-3 is plotted as a single point in Figure 6-4, resulting in a series of points as shown in Figure 6-4. The trend line equation of these points represents the experimentally derived friction angle model. It takes the form:

$$\varphi = 56.84^\circ - 223.32 \tilde{\epsilon}_p \quad \text{Equation 6-13}$$

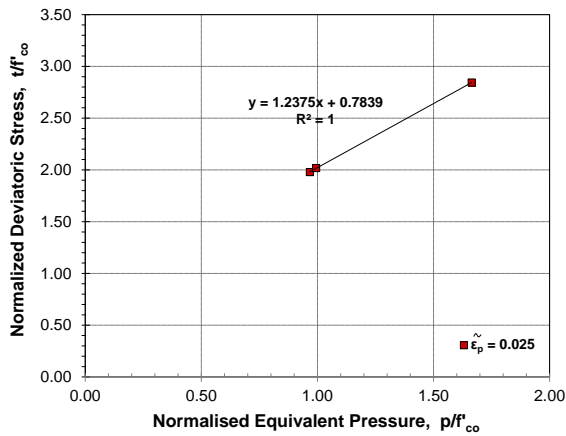
where  $\tilde{\epsilon}_p$  is the equivalent plastic strain.



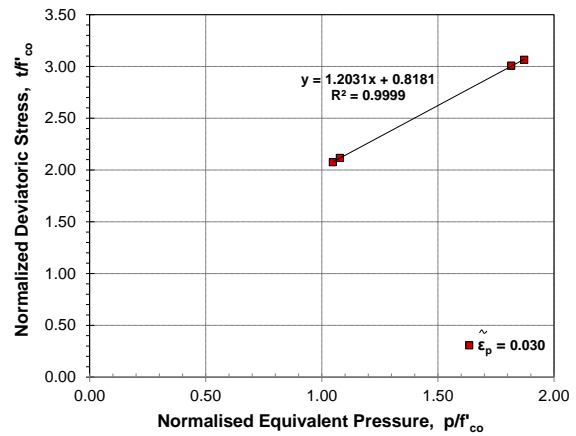
(a)



(b)



(c)



(d)

**Figure 6-3: Experimental friction angle at different equivalent plastic strain: (a)  $\epsilon_p=0.010$  (b)  $\epsilon_p=0.020$  (c)  $\epsilon_p=0.025$  (d)  $\epsilon_p=0.030$**

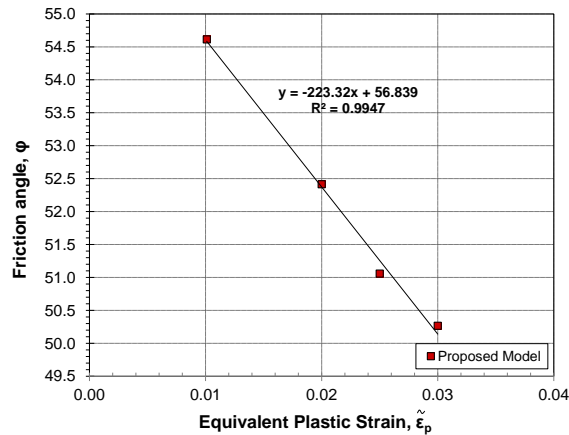


**Figure 6-4: Proposed friction angle model**

#### 6.3.1.1.2 Hardening/Softening Rule, k

The Hardening/softening rule in a plasticity model governs the development of the subsequent yielding surfaces. Earlier researchers adopted an elastic-perfectly plastic model for confined concrete Mirmiran et al. (2000); Shahawy et al. (2000) which is inconsistent with the long-observed hardening-softening behaviour of confined concrete in experiments, Chen (1982). Some researchers such as Mahfouz and Sarkani (2001) adopted a classical hardening rule that depends only on plastic deformation. However, researchers such as Karabinis and Kiousis (1996); Lan (1998); Oh (2002) pointed out that such a hardening rule cannot lead to an accurate prediction of the behaviour of confined concrete and that the confinement level should be taken as another parameter. Karabinis and Kiousis (1996), based on their work on actively confined concrete, proposed a modified hardening rule that depends on plastic strain and confining pressure with 8 parameters. Oh (2002) proposed a hardening /softening model for actively confined concrete that depends on plastic strain and confining pressure with 13 parameters. Yu et al. (2010) used the empirical stress-strain model of Teng et al. (2007) to calculate a hardening-softening function that depends on the plastic strain and confinement level. Jiang and Wu (2012) through analytical study of FRP confined concrete test results, developed a hardening-softening explicit model that is governed by the plastic strain and the FRP lateral stiffness ratio.

The hardening/softening rule is further examined here using the available experimental database from the current research. The softening-hardening values for each confinement configuration is calculated using Equation 6-1; the deviatoric stress,  $t$ , and the equivalent pressure,  $p$ , is calculated using Equation 6-2 and Equation 6-3, respectively, the friction angle is calculated using the proposed model in Equation 6-13. This yielded a series of experimentally-derived hardening/softening curves.

Performing a regression analysis on these derived curves gives the proposed hardening and softening rule which takes the form

$$k(\tilde{\varepsilon}_p, \rho) = f'_{co} \left[ \frac{1}{8} + \frac{2583.15\tilde{\varepsilon}_p}{1 + 4417.42\tilde{\varepsilon}_p} + p_1(\rho)\sqrt{\tilde{\varepsilon}_p} + p_2(\rho)\tilde{\varepsilon}_p + p_3(\rho)\tilde{\varepsilon}_p^2 \right] \quad \text{Equation 6-14}$$

where  $p_1$ ,  $p_2$  and  $p_3$  are functions of  $\rho$  and are determined by the following equations:

$$p_1 = \frac{0.06\rho + 0.13}{0.0033\rho + 0.715} \quad \text{Equation 6-15}$$

$$p_2 = \frac{318.77 - 12.78\rho}{\rho - 24.93} \quad \text{Equation 6-16}$$

$$p_3 = \frac{8.92\rho - 1.37 - 0.45\rho^2}{-30.39 - 1.08\rho + 11.38\sqrt{\rho}} \quad \text{Equation 6-17}$$

### 6.3.1.2 Flow Rule

The plastic potential function,  $G$ , that governs the flow rule in the extended DP model is shown in Figure 6-5, and is mathematically expressed by the following expression:

$$G = t - p \tan \beta + \text{constant} \quad \text{Equation 6-18}$$

Increments of the plastic strain,  $d\varepsilon_{ij}^p$ , can be defined by:

$$d\varepsilon_{ij}^p = \lambda \frac{\partial G}{\partial \sigma_{ij}} \quad \text{Equation 6-19}$$

In the case of uniformly confined cylinder,  $\sigma_1 = \sigma_c$  and  $\sigma_2 = \sigma_3 = \sigma_1$ , hence

$$d\varepsilon_1^p = \frac{\partial G}{\partial \sigma_1} = \lambda \left( \frac{1}{2\sqrt{3}J_2} 2(\sigma_1 - \sigma_3) + \frac{\tan \beta}{3} \right) \quad \text{Equation 6-20}$$

$$d\varepsilon_2^p = \frac{\partial G}{\partial \sigma_2} = \lambda \left( \frac{1}{2\sqrt{3}J_2} (\sigma_3 - \sigma_1) + \frac{\tan \beta}{3} \right) \quad \text{Equation 6-21}$$

$$d\varepsilon_3^p = \frac{\partial G}{\partial \sigma_3} = \lambda \left( \frac{1}{2\sqrt{3}J_2} (\sigma_3 - \sigma_1) + \frac{\tan \beta}{3} \right) \quad \text{Equation 6-22}$$

$$d\varepsilon_v^p = d\varepsilon_1^p + 2d\varepsilon_3^p \quad \text{Equation 6-23}$$

$$d\varepsilon_s^p = d\varepsilon_1^p - d\varepsilon_3^p \quad \text{Equation 6-24}$$

$$\frac{\partial G}{\partial \sigma_1} + 2 \frac{\partial G}{\partial \sigma_3} = \lambda \tan \beta \quad \text{Equation 6-25}$$

For uniformly confined cylinders,

$$\sqrt{3J_2} = (\sigma_1 - \sigma_3) \quad \text{Equation 6-26}$$

Then,

$$\frac{\partial G}{\partial \sigma_1} - \frac{\partial G}{\partial \sigma_3} = \lambda \frac{1}{2\sqrt{3}J_2} 3(\sigma_1 - \sigma_3) = \lambda \frac{3}{2} \quad \text{Equation 6-27}$$

Therefore,

$$\frac{d\varepsilon_v^p}{d\varepsilon_s^p} = \frac{2}{3} \tan \beta \quad \text{Equation 6-28}$$

$$\tan \beta = \frac{3}{2} \frac{d\varepsilon_v^p}{d\varepsilon_s^p} = \frac{\sqrt{3}}{2} \alpha \quad \text{Equation 6-29}$$

It can be seen from Equation 6-29 that  $\beta$  and  $\alpha$  define the relationship between the volumetric plastic strain increment and the deviatoric plastic strain increment. Under the current sign convention,  $\beta < 0$  indicates volumetric compaction, while  $\beta > 0$  indicates volumetric dilation, when  $\beta = 0$ , it indicates that plastic strains are deviatoric and no volume changes occur.

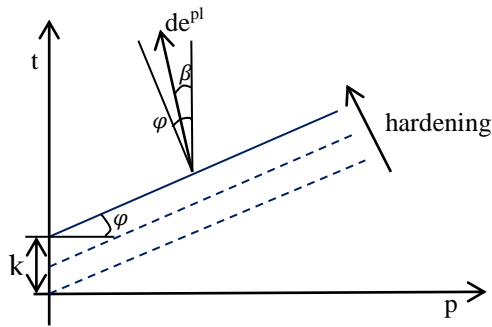


**Figure 6-5: Linear DP yield surface and flow direction in the meridian plane**

#### 6.3.1.2.1 Plastic Dilation Angle, $\beta$

Earlier research on the plastic dilation of FRP-confined concrete adopted a constant dilation angle. Mirmiran et al. (2000) adopted a non-associated flow rule with a zero plastic dilation rate for modeling confined concrete, although they reported that the model was capable of reasonably predicting the stress-strain behaviour of confined concrete, they pointed out that constant plastic dilation rate may not truly represent the true dilation behaviour of confined concrete. Karabinis and Rousakis (2002) developed an asymptotic function that is related to the axial plastic strain to model the plastic dilation tendency of confined concrete. The plastic dilation angle decreases from  $-27.4^\circ$  ( $\alpha = -0.6$ ) to  $-56.3^\circ$  ( $\alpha = -\sqrt{3}$ ). Oh (2002) proposed an asymptotic function that is related to the plastic strain and the confining pressure. The plastic dilation angle increases from  $-40.9^\circ$  ( $\alpha = -0.866$ ) to  $56.3^\circ$  ( $\alpha = -\sqrt{3}$ ). Rousakis, et al. (2008) later adopted a constant dilation rate that depends on concrete strength and the modulus of confinement. Yu et al. (2010) proposed a procedure to calculate the variation of plastic dilation angle based on the empirical model of Teng et al. (2007). Most recently, as previously mentioned in chapter 2, an explicit model for the plastic dilation of FRP-confined concrete was provided by Jiang and Wu (2012) in

which the plastic dilation angle,  $\beta$ , is governed by the plastic deformation and the lateral stiffness ratio. The latter is also adopted here. However, the model is modified based on a regression analysis of the herein test database, it takes the form:

$$\beta(\varepsilon_c^p) = \frac{-37 + (52242 - 37\lambda_1)\varepsilon_c^p + \lambda_2\beta_u(\varepsilon_c^p)^2}{1 + \lambda_1\varepsilon_c^p + \lambda_2(\varepsilon_c^p)^2} \quad \text{Equation 6-30}$$

$$\lambda_1 = 2\rho - 3 \quad \text{Equation 6-31}$$

$$\lambda_2 = 1154\rho + 172584 \quad \text{Equation 6-32}$$

$$\beta_u = 96.70 \exp(-0.05\rho) - 36.68 \quad \text{Equation 6-33}$$

### 6.3.1.3 Implementation in ABAQUS

The material properties in ABAQUS can be made dependent on the so-called solution dependent field variables SDFV using the user defined subroutine USDFLD. A SDFV can represent any independent variable that is calculated by ABAQUS at the nodes as a function of time during the analysis process such as the displacements and stresses. This feature allows the material models in ABAQUS to account for additional material parameters that are not integrated into the original model.

In the current FE model, two field variables were defined in the USDFLD subroutine, namely, axial plastic strain and the lateral stiffness ratio. The input material properties were produced in a tabular format and imported to ABAQUS using the SDFV feature in ABAQUS so that the variation of the material properties during the loading process can be appropriately modeled.

## 6.4 Modeling of FRP-Confined Concrete Cylinders

The general purposes commercial FE software ABAQUS (version 6.11) is utilised to model the 150 mm x300 mm concrete cylinders with different amount of confinement and different concrete strengths. The detail of the FE model is described next.

### 6.4.1 Model Geometry

Considering the symmetry of tested cylinders in loading and geometry, only 1/8 of the cylinder is modeled, as shown in Figure 6-6.

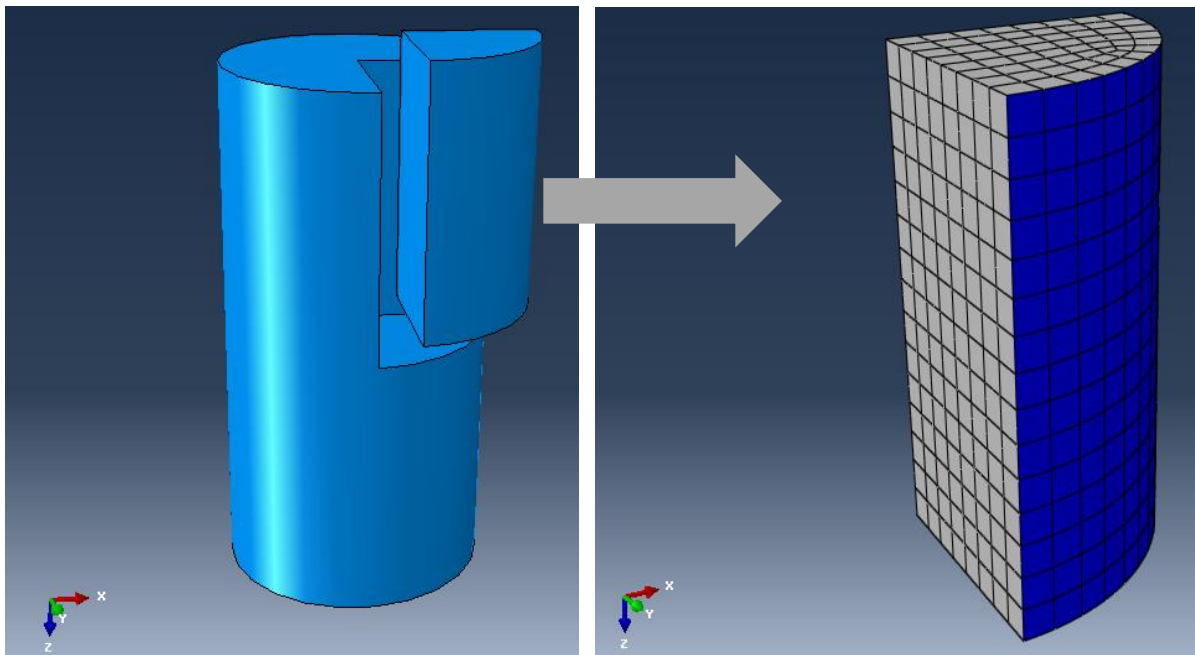


**Figure 6-6: FE modeling of FRP-confined concrete cylinders - model geometry**

### 6.4.2 Material Properties

#### 6.4.2.1 FRP

The FRP sheet is generally assumed to have a linear elastic behaviour until rupture; hence an elastic laminar material model is used for the FRP sheet. The unidirectional laminar has three mutually orthogonal planes of material properties (1, 2 and n) which are referred to as the principal material coordinates. The 1 direction is aligned with the direction of fibres while n is

normal to the FRP sheet plane. Input data for the FRP sheet in the FE model are: thickness of each layer, orientation of the fibre in each layer, Elastic modulus in two directions ( $E_1$  and  $E_2$ ), shear modulus in three directions ( $G_{12}$ ,  $G_{13}$  and  $G_{23}$ ) and Poisson's ratio ( $\nu_{12}$ ).

#### 6.4.2.2 Concrete

The initial linear elastic behaviour of concrete follows Hooke's law, while the nonlinear behaviour follows the extended DP type plasticity model. The extended DP plasticity model was modified as previously discussed in section 6.3 so that the friction angle and the hardening-softening parameters depend on the equivalent plastic strain and lateral stiffness modulus ratio, and the dilation angle depends on the axial plastic strain and the lateral stiffness modulus ratio. The friction angle, the hardening-softening function and the dilation angle are imported to ABAQUS in a tabular format through the SDFV option.

#### **6.4.3 Element Types**

Concrete is modeled using an 8-node linear brick, reduced integration element C3D8R. The FRP jacket is modeled using a 4-node doubly curved thick shell, reduced integration element, S4R.

#### **6.4.4 Boundary Conditions and Loading Control**

In the current model, the z-axis of the coordinate system corresponds to the axis of the cylinder, the x and y axes represent the radial and lateral directions of the cylinder, respectively.

Symmetric boundary conditions are applied to the three cut surfaces parallel to the xy, xz and yz planes in which nodes on each plane of symmetry are free to move within that plane while fixed in the direction normal to it. The interaction between the concrete and the FRP was modeled using surface tie constraints. This constraint ties the nodes on one surface to the corresponding nodes in the contact surfaces and maintained the same displacement such that no relative

slippage between the two contact surfaces occur. The loading was simulated by applying a downward displacement to the top surface of concrete, no direct loading is applied to the FRP.

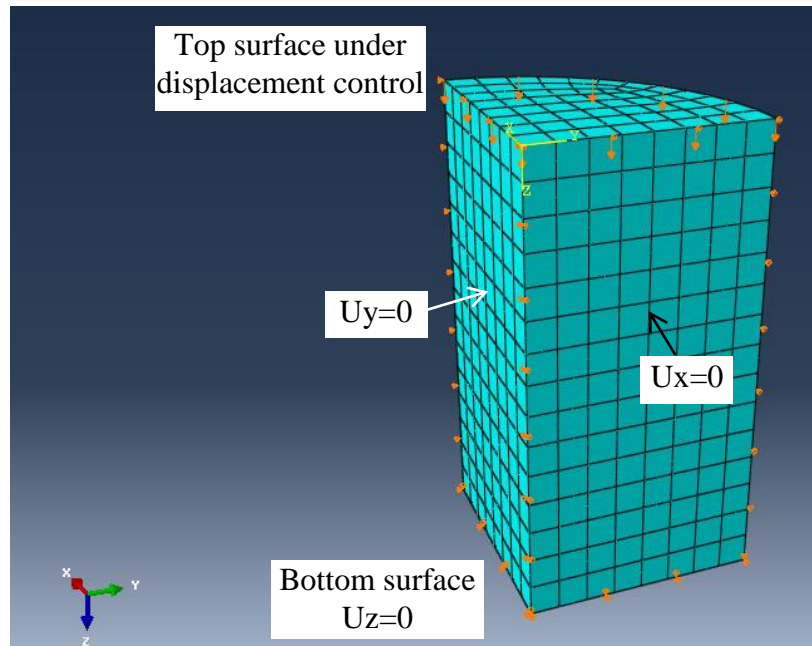


**Figure 6-7: FE modeling of FRP-confined concrete cylinders - boundary condition and loading**

### 6.5 Sensitivity Analysis

In this section, the sensitivity of the developed FE model to h- and p- refinement, by changing the element size and element type, respectively is analyzed. Since the computational cost of any FE model increases as the FE mesh is refined (the number of elements increases) and higher order of types of element are used (order of polynomial used as interpolation function increases), it is imperative to use a FE mesh with the lower order and minimum number of elements for which the FE results are satisfactory (close enough for the user to “actual”). The effect of varying concrete Poisson’s ratio on the FE results will be also examined.

### ***6.5.1 Effect of FE Mesh Size***

A sensitivity analysis of the FE mesh size was performed to examine the effect of mesh refinement on the accuracy of the FE results. Four FE analyses were performed on the FE model of 1/8 of the 150 x 300 mm cylinder of 35 MPa unconfined concrete strength, wrapped with 1.2 mm thickness of SFRP sheet ( $E_{\text{frp}} = 66.1$  GPa). The element types used were C3D8R and S4R for concrete and SFRP, respectively. The only parameter changed each time was the size of the element used; the number of the elements was changed between 32 and 7200. However, the aspect ratio of the element has been kept the same in all cases as shown in Figure 6-8. The effect of the element size as presented by the number of elements on the analysis results is summarized in Table 6-1 and shown in Figure 6-9. The computational cost in terms of total CPU time is also reported.

Figure 6-9 shows that the element size indeed affects the accuracy of FE results: the effect was pronounced on stress results but negligible on strain results. It also shows that the element size has a decreasing effect that becomes insignificant beyond certain limit (near the start of the horizontal part of the curve). The element size at this limit (1080 total number of elements) is used during the rest of the FE analysis performed in this study.

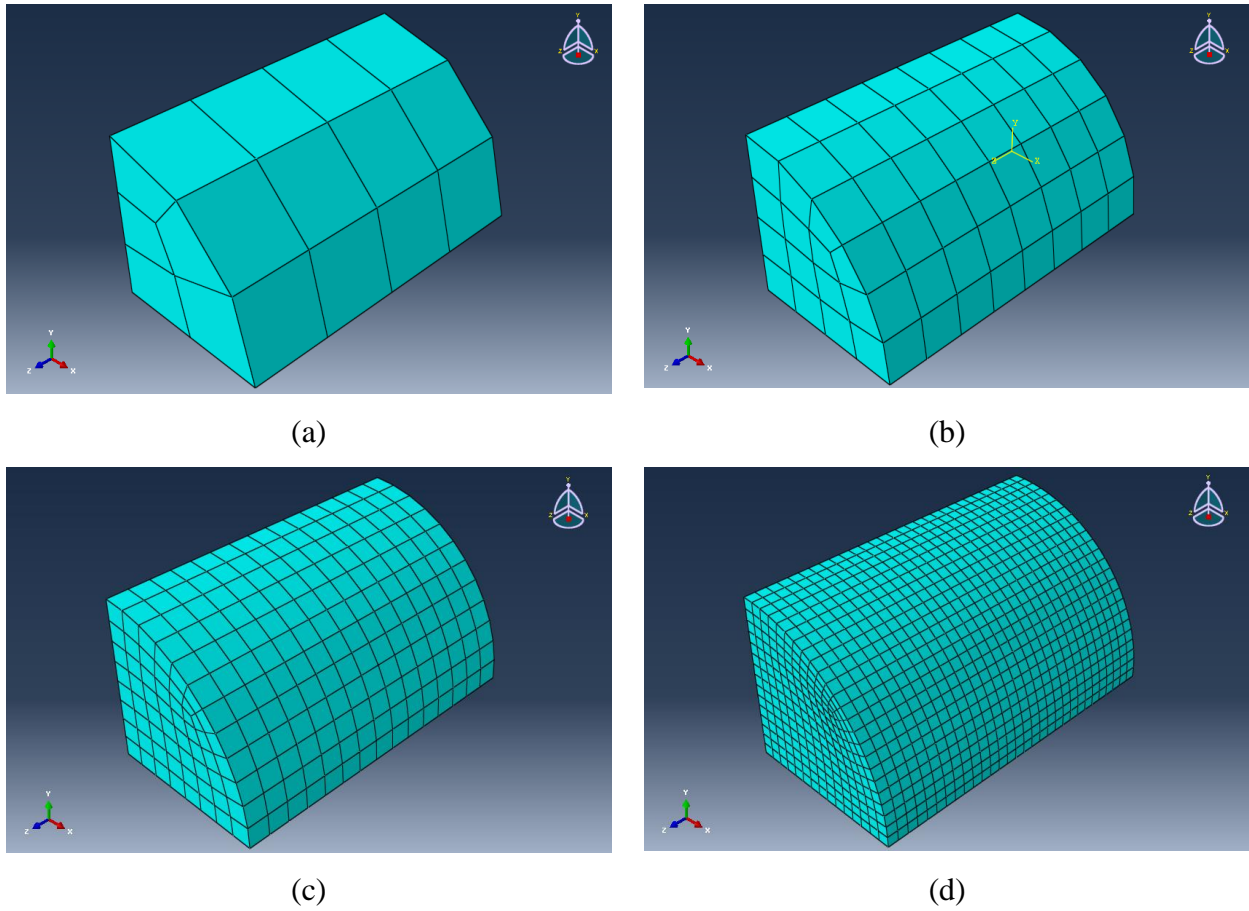


**Figure 6-8: Sensitivity analysis – mesh size**

**Table 6-1: Summary of mesh size sensitivity analysis**

FE Model ID	Mesh Size Sensitivity Analysis					
	Number of Element			FE Results		
	<i>Concrete</i>	<i>FRP</i>	<i>Total</i>	Axial Stress	<i>Axial Strain</i>	Total CPU Time
			(MPa)	(%)	(s)	
I	20	12	32	91.7	3.16	5.8
II	120	48	168	90.8	3.16	11.6
III	900	180	1080	90.6	3.16	65.4
IV	6480	720	7200	90.5	3.16	963

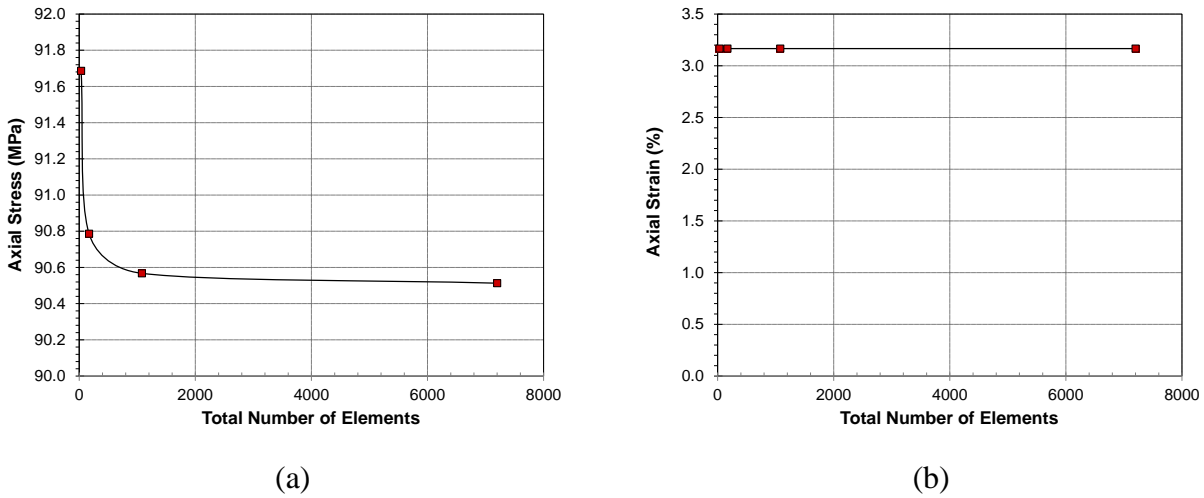


**Figure 6-9: Mesh size sensitivity analysis results**

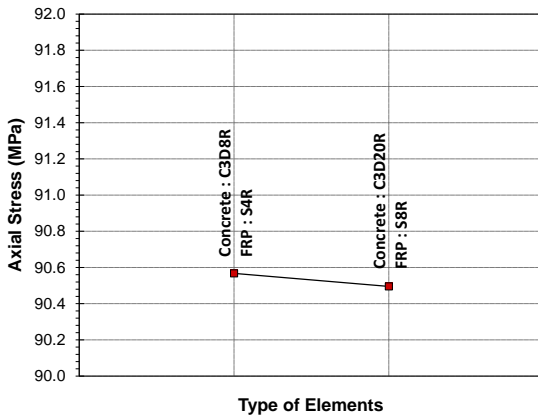
### 6.5.2 Effect of FE Element Type

A sensitivity analysis of the FE element type was performed to examine the effect of first order versus second order element type on the accuracy of the FE results. Two analyses were performed on the FE model of 1/8 of the 150 x 300 mm cylinder of 35 MPa unconfined concrete strength, wrapped with 1.2 mm thickness of SFRP sheet ( $E_{frp} = 66.1$  GPa). The number of elements in both models was 1080; 900 concrete elements and 180 FRP elements. The parameter changed was the type of elements used; first order elements C3D8R and S4R for concrete and FRP, respectively in the first model and second order elements C3D30R and S8R for concrete and FRP, respectively in the second model. The effect of the element type is summarized in Table 6-2 and shown in Figure 6-10. The computational cost in terms of total CPU time is also reported.

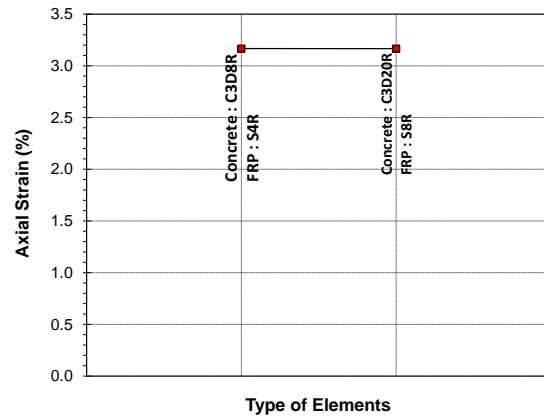
Figure 6-10 shows that the element type has negligible effect on the accuracy of FE results in terms of stress and strain ( $<0.1\%$ ). However, second order elements were significantly more expensive in terms of computational cost. Therefore, first order elements were used during the rest of the FE analyses performed in this study

**Table 6-2: Summary of element type sensitivity analysis**

FE Model ID	Element Type Sensitivity Analysis				
	Element Type		FE Results		Total CPU Time
	Concrete	FRP	Axial Stress	Axial Strain	
			(MPa)	(%)	(s)
I	C3D8R	S4R	90.6	3.16	56.4
II	C3D20R	S8R	90.5	3.16	670.4



(a)



(b)

**Figure 6-10: Element type sensitivity analysis results**

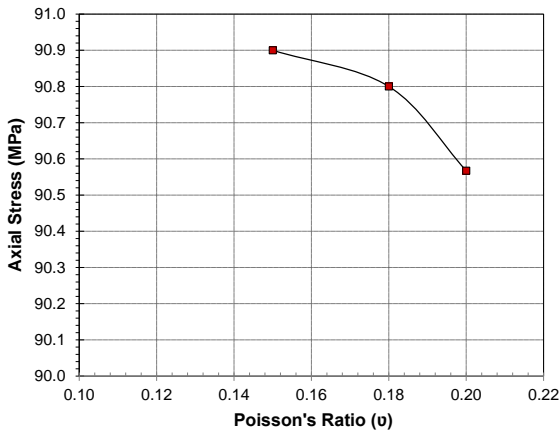
### 6.5.3 Effect of Concrete Poisson's Ratio

The effect of varying Poisson's ratio on the accuracy of the FE results was assessed by performing FE analyses on 1/8 of the 150 x 300 mm cylinder of 35 MPa unconfined concrete strength, wrapped with 1.2 mm thickness of SFRP sheet ( $E_{frp} = 66.1$  GPa). The number of elements in all models was 1080; 900 concrete elements and 180 FRP elements, and first order C3D8R and S4R are used for concrete and FRP, respectively. The only parameter changed was Poisson's ratio, the value changed between 0.15 and 0.2. The effect of Poisson's ratio on results is summarized in Table 6-3 and shown in Figure 6-11: Poisson's ratio sensitivity analysis results.

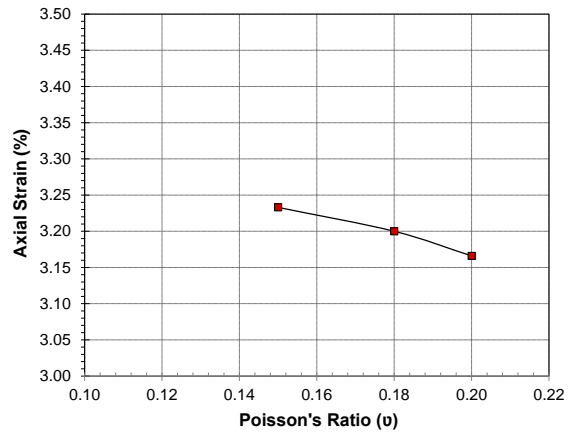
Figure 6 10 shows that Poisson’s ratio has a negligible effect on the FE results, less than 0.36% for stress results and 2.1% for strain results. Hence, a Poisson’s ratio of 0.2 was used during the rest of the FE analysis performed in this study

**Table 6-3: Summary of Poisson’s ratio sensitivity analysis**

FE Model ID	Poisson’s Ratio Sensitivity Analysis		
	Poisson’s Ratio ( $\nu$ )	FE Results	
		Axial Stress (MPa)	Axial Strain (%)
I	0.15	90.9	3.23
II	0.18	90.8	3.20
III	0.2	90.6	3.16



(a)



(b)

**Figure 6-11: Poisson’s ratio sensitivity analysis results**

## 6.6 FE Results and Discussion

### 6.6.1 Model Validation

The proposed FE model previously described is validated in this section against the herein experimental results in addition to three existing published experimental programs by other researchers, all of which are for standard circular normal strength concrete standard cylinders 150 x 300 mm with FRP sheet oriented in the lateral direction. The detail of the reference experimental programs used for the validation purposes are shown in Table 6-4.

**Table 6-4: Details of the reference experimental programs**

Reference Experiments	Cylinder Designation	Reference Experiments Details							
		Cylinders details			FRP Strengthening Scheme				
		$d$	$h$	$f'_{co}$	FRP Type	$E_{frp}$	$\epsilon_{frp}$	# of layers	$t_{frp}$
(mm)	(mm)	(MPa)		(GPa)	(%)		(mm)		
Xiao and Wu (2000)	XW-C33.68-CFRP1	152	305	33.68	CFRP	105	1.5	1	0.381
	XW-C33.68-CFRP2	152	305	33.68	CFRP	105	1.5	2	0.381
	XW-C33.68-CFRP3	152	305	33.68	CFRP	105	1.5	3	0.381
Lam and Teng (2004)	LT-C35.9-CFRP1	152	305	35.9	CFRP	230	1.5	1	0.165
	LT-C35.9-CFRP2	152	305	35.9	CFRP	230	1.5	2	0.330
	LT-C34.3-CFRP3	152	305	34.3	CFRP	230	1.5	3	0.495
Abdelrahman (2011)	AK-C42.0-SFRP1	150	300	42.0	SFRP	66.1	1.5	1	1.23

6.6.1.1 Ultimate Axial Strength and Ultimate Axial Strain

The comparison between the experimental and the FEA results is summarized in Table 6-5 and plotted in Figure 6-8 and Figure 6-13, respectively. The average errors are 6.7% and 16.5% for ultimate stress and ultimate strain, respectively.

**Table 6-5: Numerical and experimental results comparison**

Experiment Reference	Configuration Designation	Numerical and Experimental Results Comparison					
		Ultimate Stress ( $f'_{cu}$ )			Ultimate Strain ( $\epsilon_{cu}$ )		
		Exper.	FE	Error	Exper.	FE	Error
		(MPa)	(MPa)	(%)	(%)	(%)	(%)
Salameh and El-Hacha (2015)	C37.3-CFRP1	51.4	52.1	1.3	1.47	1.23	15.8
	C37.3-CFRP2	69.5	66.4	4.4	1.93	2.17	12.5
	C37.3-CFRP3	92.4	94.2	2.0	2.54	2.87	12.7
	C37.3-SFRP1	94.5	90.0	4.8	3.21	3.03	5.5
	C37.3-SFRP2	146.6	146.2	0.4	4.37	4.67	6.9
	C37.3-SFRP3	194.6	201.3	3.5	5.45	5.60	2.8
	C42.4-CFRP1	59.6	57.6	3.3	1.07	1.03	3.1
	C42.4-CFRP2	75.8	73.3	3.3	1.15	1.40	21.8
	C42.4-CFRP3	94.6	91.6	3.2	1.55	2.07	33.1
	C42.4-SFRP1	98.8	101.9	3.2	2.70	2.77	2.4
Xiao and Wu (2000)	XW-C33.68-CFRP1	48.1	49.5	-2.8	1.3	1.2	7.3
	XW-C33.68-CFRP2	69.7	70.7	-1.4	2.0	1.9	7.0
	XW-C33.68-CFRP3	86.0	85.6	0.5	2.7	2.2	19.2
Lam and Teng (2004)	LT-C35.90-CFRP1	50.3	51.6	2.7	1.2	1.2	-1.9
	LT-C35.90-CFRP2	70.1	72.1	2.9	1.8	1.9	3.7
	LT-C34.30-CFRP3	90.1	85.3	-5.3	2.4	2.1	-8.2
Abdelrahman (2011)	AK-C42.0-SFRP1	97.0	85.6	-11.7	1.65	1.83	11.1

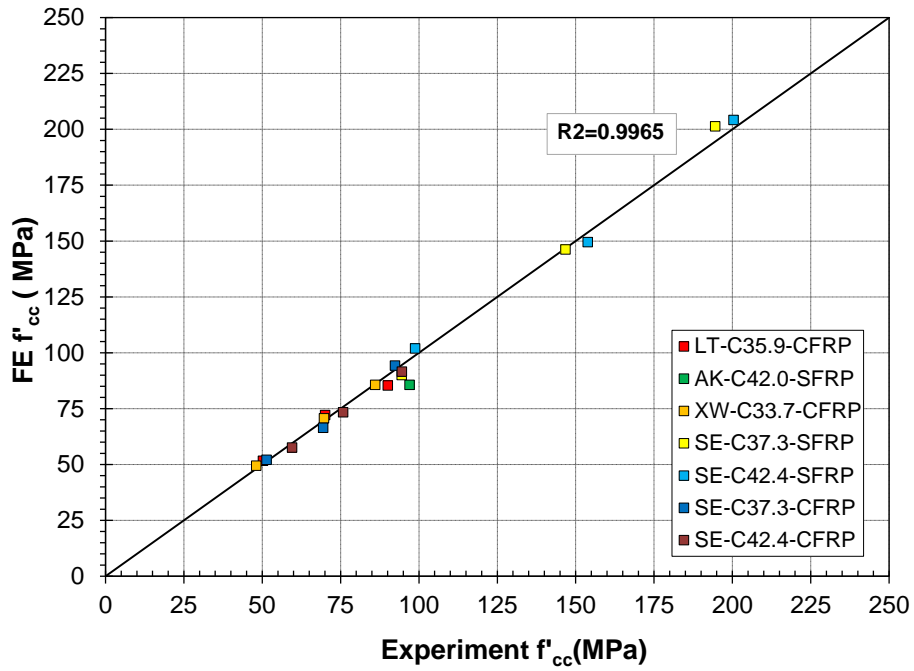


Figure 6-12: Numerical and experimental results comparison of ultimate strength

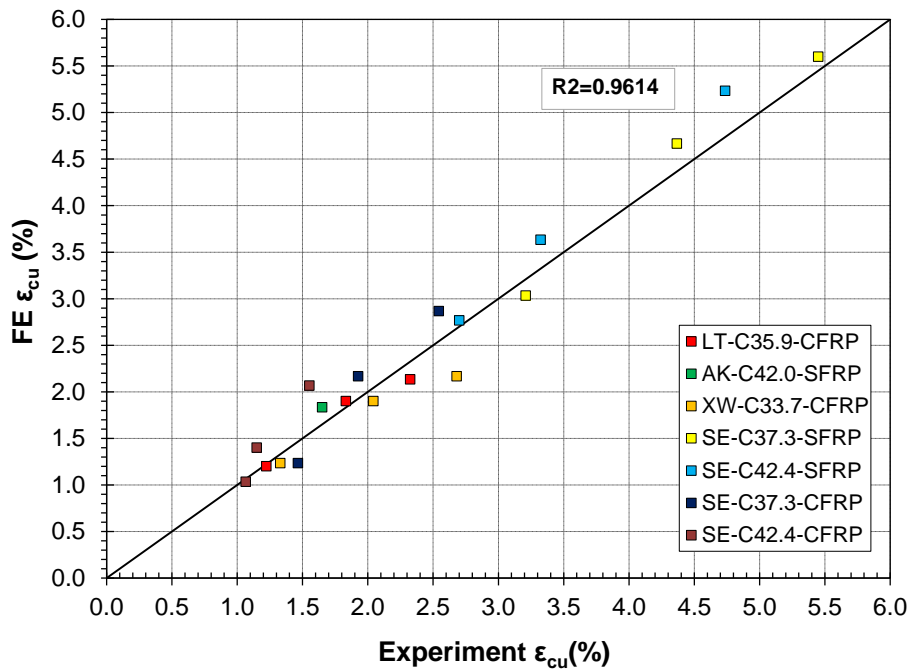
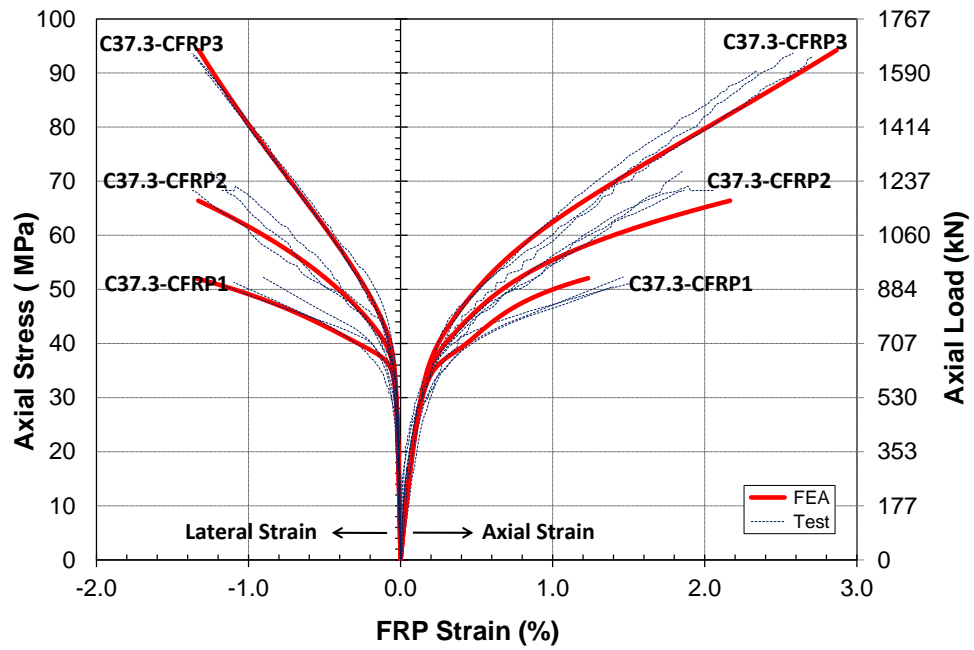
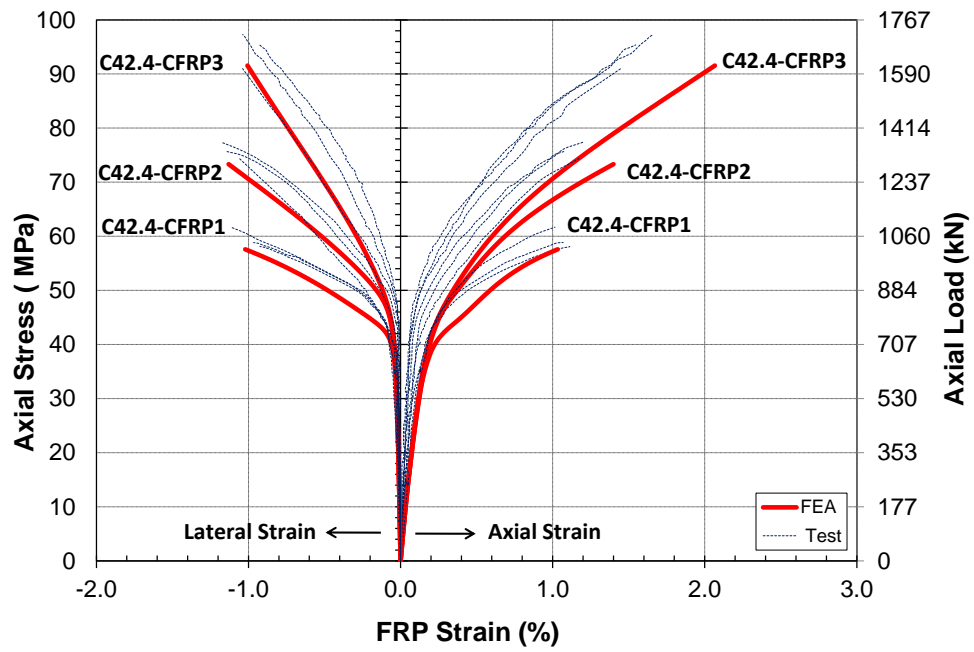


Figure 6-13: Numerical and experimental results comparison of ultimate strain

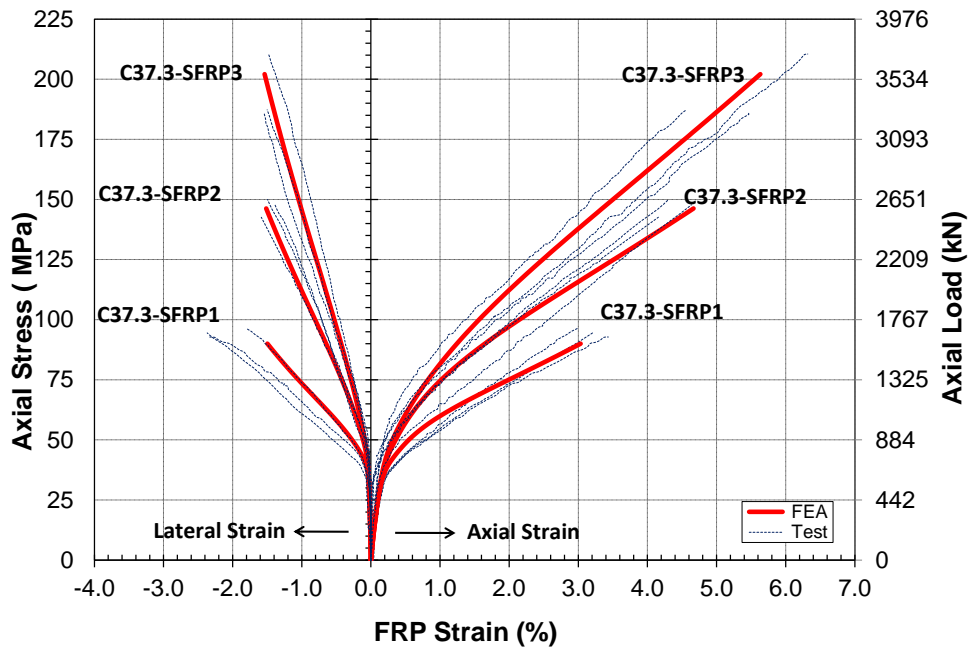
### 6.6.1.2 Stress – Strain Response



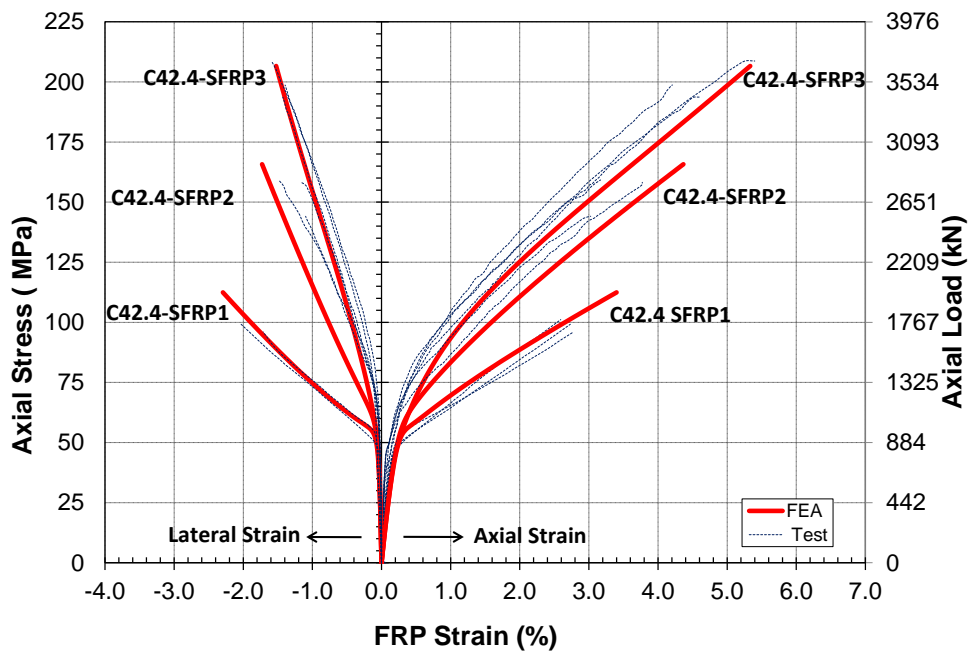
(a)



(b)



(c)



(d)

**Figure 6-14: Numerical and experimental results comparison for SFRP-confined cylinders: (a) C37.3-CFRP (b) C42.4-CFRP (c) C37.3-SFRP (d) C42.4-SFRP**

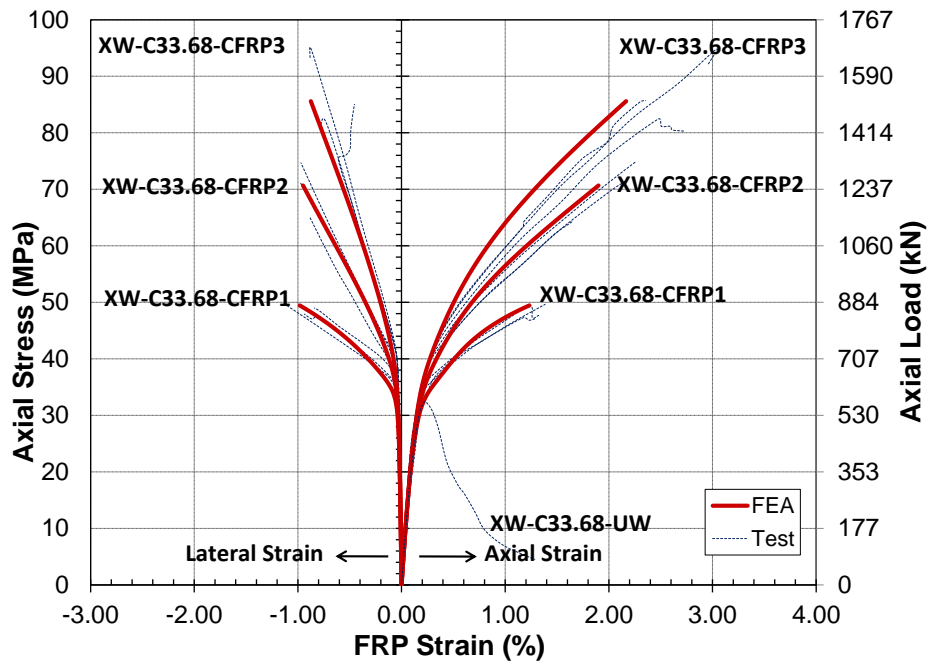


Figure 6-15: Numerical and experimental results comparison for Xiao and Wu (2000)

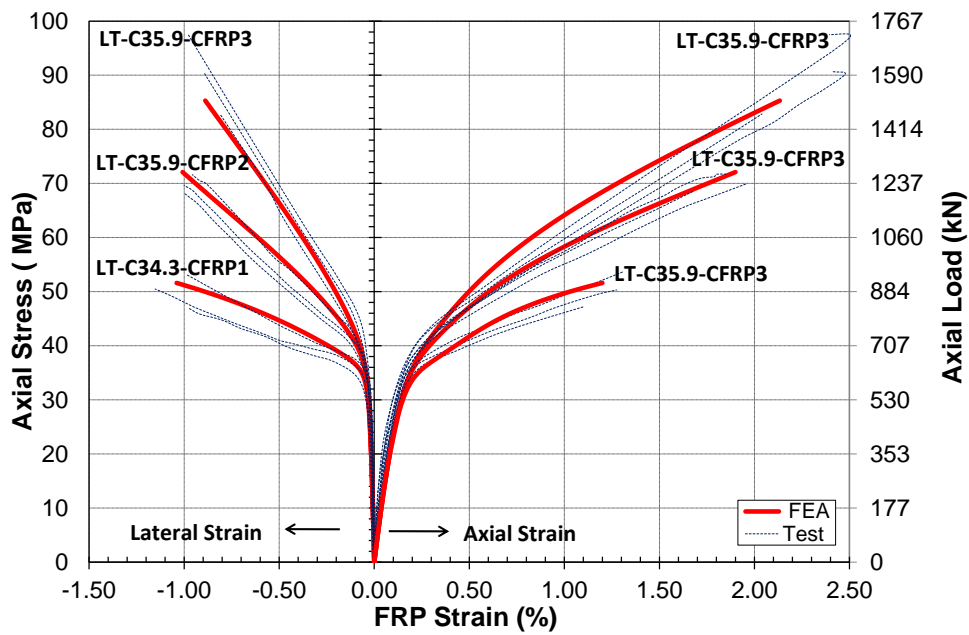
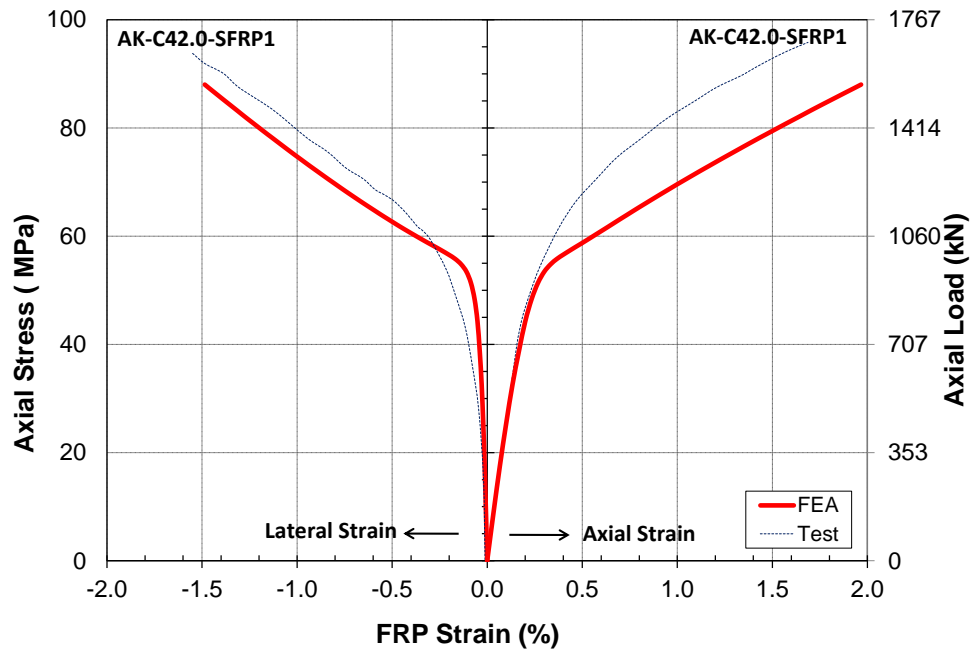


Figure 6-16: Numerical and experimental results comparison for Lam and Teng (2004)



**Figure 6-17: Numerical and experimental results comparison for Abdelrahman (2011)**

### 6.6.2 Parametric Study

The numerical predictions from the proposed FE model were generally in good agreement with the experimental results as demonstrated in the previous section, as such, the FE model is utilised in a parametric study to evaluate the effect of a wide range of the most critical parameters that influence the compressive behaviour of FRP-confined concrete.

All the models developed for the parametric study were comprised of the same number of elements, each model having 900 and 180 elements for the concrete and the FRP jacket respectively.

### 6.6.3 Effect of FRP Jacket Thickness

Finite Element Analysis of five models of the 150 x 300 mm cylinder having the same grade of concrete 35 MPa and wrapped with the same SFRP sheet material ( $E_{frp} = 66.1$  GPa) but varying jacket thickness in the range of 1.2 mm – 6.0 mm was conducted.

The FE analysis results of SFRP jacket thickness variation are summarized in Table 6-6.

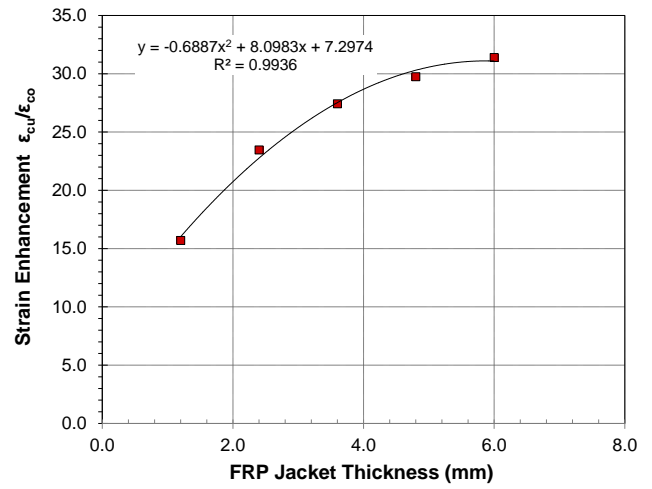
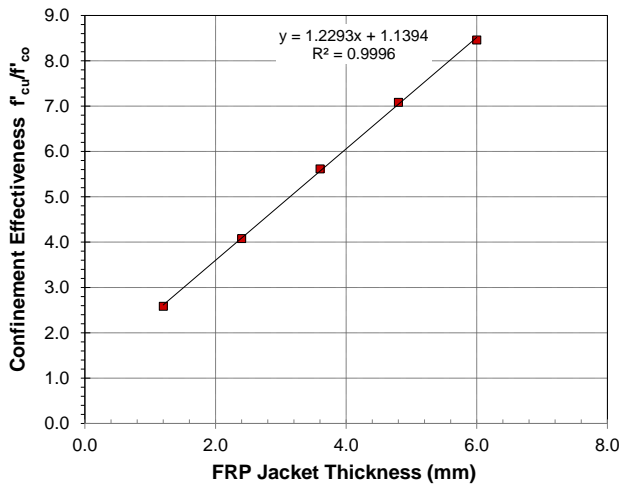
Furthermore, the results in terms of confinement effectiveness and strain enhancement are also plotted in Figure 6-18 (a) and Figure 6-18 (b), respectively.

It is evident that the axial strength in terms of confinement effectiveness is increased from for 159% for a single layer to 746% for 5 layers. In addition, the strain enhancement is also increased from 1469% for a single layer to 3039% for 5 layers. The maximum confinement effectiveness and strain enhancement was achieved for cylinders confined by 5 layers.

The stress-strain responses of the five models of various jacket thicknesses are shown in Figure 6-19. It can be observed that both ultimate strength and ultimate strain are maximum for the model of maximum number of layers, it is also clear that increasing the thickness of the SFRP jacket increases the slope of the second branch and the radius of curvature at response transition point.

**Table 6-6: Summary of FEA results for SFRP jacket thickness variation**

SFRP jacket Thk. $t_{frp}$ (mm)	FE results on SFRP jacket thickness variation $\rho$					
	Confinement effectiveness ( $f'_{cu}/f'_{co}$ )			Strain enhancement ( $\epsilon_{cu}/\epsilon_{co}$ )		
	$f'_{cu}$ (MPa)	$(f'_{cu}/f'_{co})$	% Increase (%)	$\epsilon_{co}$	$\epsilon_{cu}/\epsilon_{co}$	% Increase (%)
1.2	90.6	2.6	159	0.0317	15.7	1469
2.4	142.8	4.1	308	0.0473	23.5	2246
3.6	196.6	5.6	462	0.0553	27.4	2643
4.8	247.9	7.1	608	0.0600	29.7	2874
6.0	296.1	8.5	746	0.0633	31.4	3039



(a)

(b)

Figure 6-18: Effect of SFRP jacket thickness on: (a) Confinement effectiveness (b) Strain enhancement

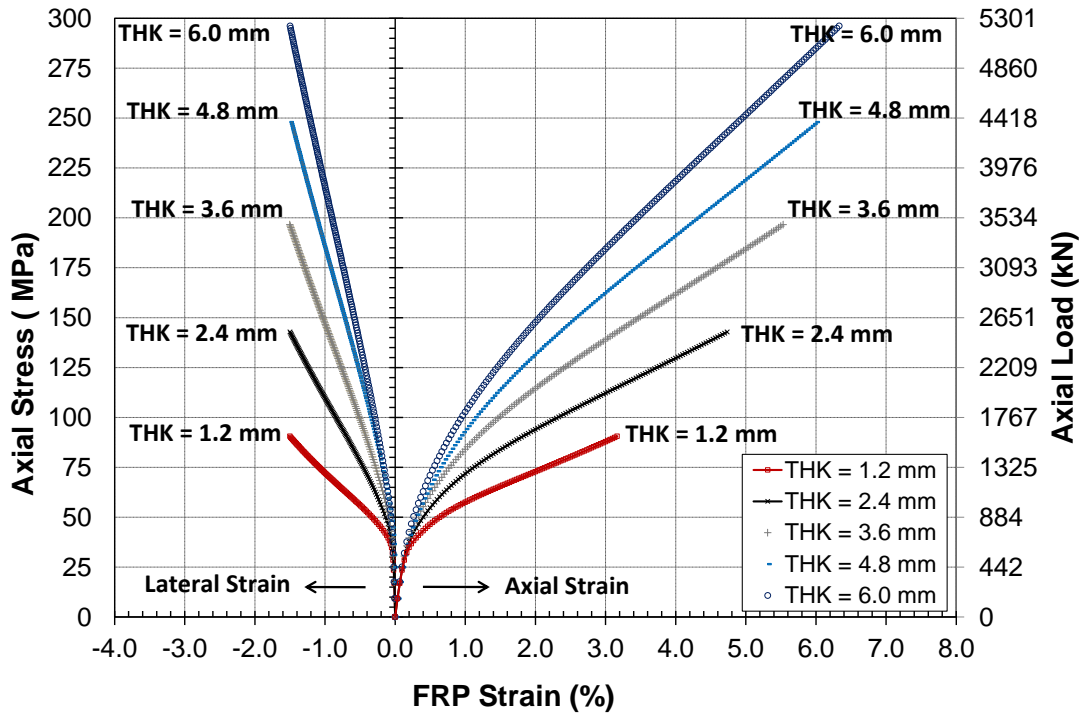


Figure 6-19: Effect of SFRP jacket thickness on stress – strain response

#### 6.6.4 Effect of FRP Mechanical Properties

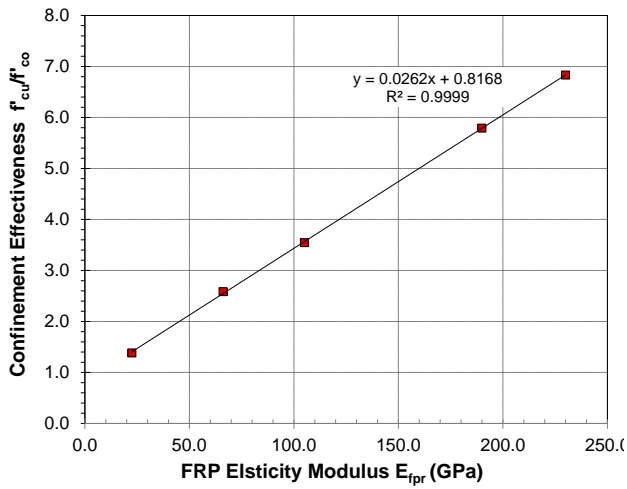
Finite Element Analysis of five models of the 150 ×x 300 mm cylinder of the same concrete grade, 35 MPa but wrapped with different types of FRP material was conducted. The FRP materials and their modulus of elasticity were CFRP (230 GPa), CFRP (190 GPa), CFRP (105 GPa), SFRP (66.1 GPa) and GFRP (22.46 GPa), however, the thickness of 1.2 mm was kept constant in all models.

The results of the FE analysis of FRP type variation are summarized in Table 6-7. The results in terms of confinement effectiveness, strain enhancement and stress-strain response are plotted Figure 6-20 (a), Figure 6-20 (b) and Figure 6-21, respectively.

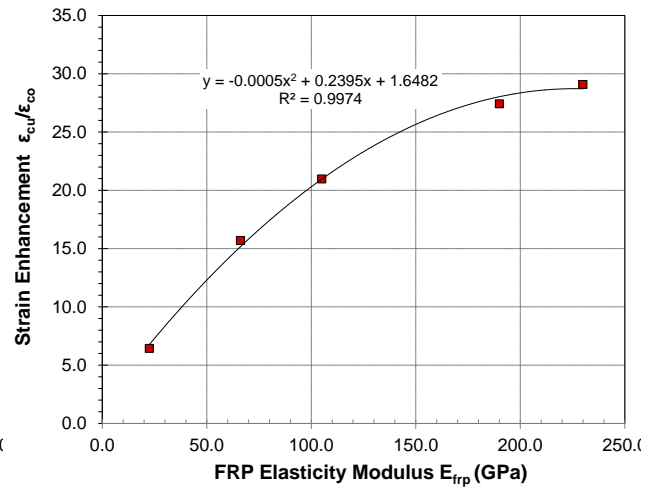
It can be concluded that that the compressive behaviour in terms of confinement effectiveness and strain enhancement was enhanced for higher FRP modulus of elasticity with the highest of 6.8 for the former and 29.1 for the latter achieved for 230 GPa modulus of elasticity.

**Table 6-7: Summary of FEA results for FRP type variation**

FRP Type	FRP modulus (GPa)	FE results on FRP type variation					
		Confinement effectiveness ( $f'_{cu}/f'_{co}$ )			Strain enhancement ( $\epsilon_{cu}/\epsilon_{co}$ )		
		$f'_{cu}$ (MPa)	$(f'_{cu}/f'_{co})$	% Increase (%)	$\epsilon_{co}$	$\epsilon_{cu}/\epsilon_{co}$	% Increase (%)
CFRP	230	239.1	6.8	583	0.0587	29.1	2808
CFRP	190	202.7	5.8	479	0.0553	27.4	2643
CFRP	105	124.1	3.5	255	0.0423	21.0	1998
SFRP	66.1	90.6	2.6	159	0.0317	15.7	1469
GFRP	22.46	48.4	1.4	38	0.0130	6.4	544



(a)



(b)

**Figure 6-20: Effect of FRP jacket type on: (a) Confinement effectiveness (b) Strain enhancement**

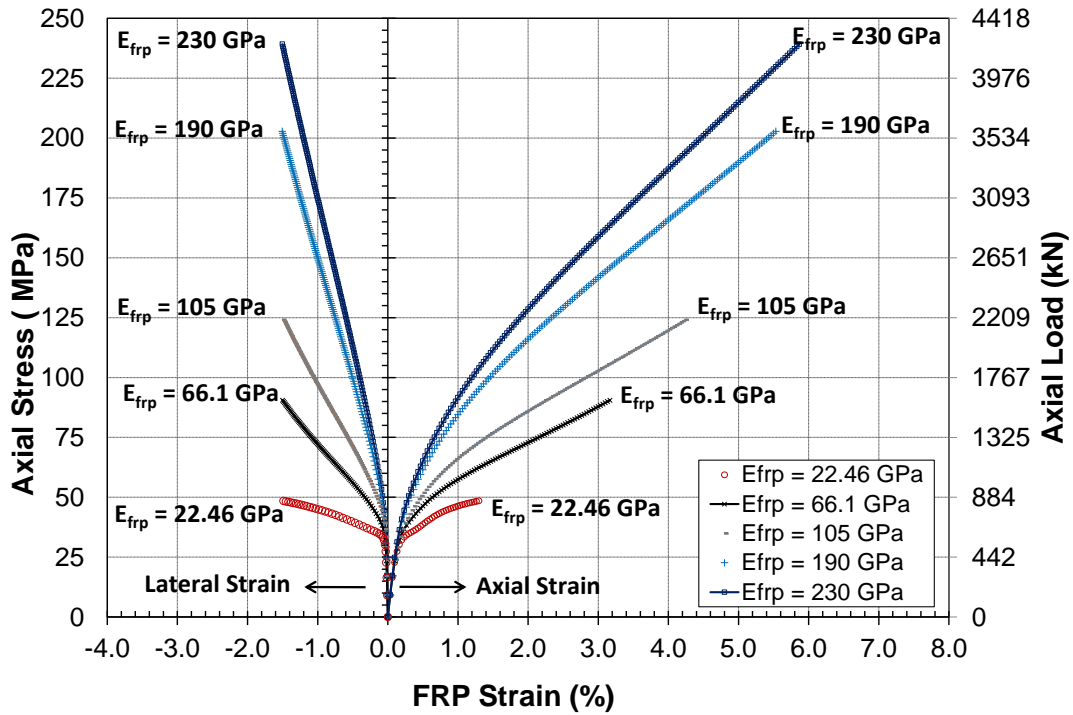


**Figure 6-21: Effect of FRP jacket type on the stress – strain response**

## **6.7 Summary**

This chapter presented a numerical analysis of FRP-confined concrete using the FE technique. Material parameters for concrete constitutive model in the framework of DP type plasticity model, namely, the friction angle, hardening/softening rule and the flow rule were derived from regression analysis of the current research experimental results and implemented in the FE model. The proposed FE model was validated against the herein experimental database as well as three published test results from different researchers. Finally, the validated FE model was used to perform a parametric study to investigate the influence of the FRP jacket thickness and the FRP type on the confinement effectiveness and strain enhancement as well as the stress-strain response of FRP-confined concrete cylinders.

The numerical predictions of the proposed FE model exhibited a good agreement with author's own experimental results as well as published experimental results by others. It has been found that the confinement effectiveness and strain enhancement increase as the FRP jacket thickness and modulus of elasticity increases.

The next chapter presents a summary of the major findings and conclusions drawn from the experimental, analytical and numerical investigation conducted in the current research as well as recommendations for future research so that a better understanding of the compressive behaviour of FRP-confined concrete can be reached.

## Chapter Seven: **Summary, Conclusions and Recommendations**

### **7.1 Introduction**

An experimental investigation on the compressive behaviour of small scale plain concrete cylinders confined with SFRP and CFRP wraps and subjected to uniaxial monotonic loading is reported in this thesis. A new analytical model to capture this experimentally-observed behaviour accurately is also presented. Furthermore, a constitutive law for concrete is suggested and implemented in a FE model to simulate the behaviour of FRP-confined concrete.

In the sections that follow, the methodology and main objectives of the current research are first summarized followed by the major findings. Finally, recommendations for future research are given so that better knowledge on the behaviour and modeling technique of FRP-confined concrete can be reached.

### **7.2 Research Summary**

The compressive behaviour of small scale (150 mm × 300 mm) plain concrete cylinders confined with CFRP and SFRP sheets under uniaxial monotonic loading has been investigated experimentally, analytically and numerically through FE modeling. Experimentally, the effect of parameters, mainly, the unconfined concrete compressive strength, type and thickness of FRP jackets on the ultimate axial strength, ultimate axial strain, the entire stress-strain response and the dilation behaviour of FRP-confined concrete were closely examined. Furthermore, the performance of CFRP-and SFRP-confined concrete were compared through a series of parameters, mainly confinement effectiveness coefficient, strain ductility index, energy ductility index and FRP efficiency factor. In addition, a DIC technique was utilised to quantify the axial and lateral strain variation over the surface of the CFRP-and SFRP-confined cylinders, the data collected was used to derive more reliable strain efficiency factors for CFRP and SFRP sheets

for design purposes use. Analytically, the accuracy of eleven confinement models; seven empirical, two analytical and two from Canadian design codes confinement models were carefully assessed and the theoretical predictions from these models were compared against the herein experimental results. An analytical model was proposed by modifying one of the existing confinement models so that the new predictive model fits better with the current experimental data and accurately captures all the characteristic behaviour of FRP-confined concrete. Finally, numerical FE model was implemented to simulate the behaviour of the FRP-confined concrete, and a constitutive model for concrete within the framework of DP plasticity and of which the model parameters were calibrated from the herein experimental database was developed. Finally, the FE model was compared against independent experimental data for verification purposes and then used in a parametric study to quantify the effect of FRP jacket thickness and the FRP elastic modulus in the overall compressive behaviour of FRP-confined concrete. The knowledge resulting from the current research adds and enhances the understanding of the compressive behaviour of FRP-confined concrete, and the proposed analytical and FE models serve as accurate analysis tools so that FRP wraps can be implemented more efficiently in column strengthening and retrofitting applications.

## **7.3 Conclusions**

### ***7.3.1 Compressive Behaviour of FRP-Confined Concrete***

1. Statistical analysis of experimental results using ANOVA analysis revealed that thickness and type of FRP jacket parameters are significant on the ultimate strength of FRP-confined concrete cylinders. On the other hand, the unconfined concrete compressive strength parameter is significant for weakly confined concrete while insignificant for moderately and highly FRP-confined concrete cylinders.

2. Concrete cylinders wrapped with CFRP sheets exhibited a conical failure mode due to concrete crushing in the middle third of the cylinder and fibre rupture typically initiated at the beginning of the overlap zone. Concrete cylinders wrapped with SFRP sheets exhibited a similar failure mode although some cylinders failed due to partial or full debonding of the SFRP sheet at the overlap region. In all cases and regardless of the type of the FRP jacket used, the failure of the FRP-confined cylinders was brittle and catastrophic.
3. The provision of one, two and three layers of CFRP and SFRP sheets significantly enhanced the axial load-carrying capacity. The increase in the axial strength, when all other parameters are the same, was higher for cylinders confined with SFRP sheets rather than CFRP sheets. The axial strength of confined cylinders increased as the unconfined concrete strength and the thickness of FRP jacket increased. Furthermore, a higher percentage increase in the axial strength was achieved for cylinders of lower unconfined concrete strength and thicker FRP jacket.
4. A substantial increase in the ultimate axial strain was achieved when concrete cylinders were wrapped with CFRP and SFRP sheets. When all other parameters are the same, a significant higher axial strain at ultimate was achieved for SFRP-confined concrete cylinders when compared to those confined with CFRP sheets. The ultimate axial strain increased as FRP jacket thickness increased and the unconfined concrete strength decreased.
5. Axial strain from foil strain gauge and the axial strain calculated from the axial shortening from LSC's device reading varied up to 22%. This is due to the different nature of measurement between foil strain gauges and LSC's devices; the former measure

the localised axial strain within the gauge length while the latter capture the global shortening of the tested cylinder.

6. The stress-strain response of CFRP- and SFRP-confined cylinder comprises three distinct regions; the first region is similar to that of unconfined concrete, which indicates that the lateral expansion of concrete core is insignificant and FRP wraps are not yet activated. As micro cracks in the concrete core grow rapidly, the response softens and a nonlinear transition zone is entered where the FRP wraps start to exert a confining pressure on concrete core to counteract its increasingly lateral expansion, eventually the concrete is fully cracked and the FRP is fully activated and the response is then linear up to failure, the slope of response in this stage is significantly, if not completely dependent on the lateral stiffness and strength of the FRP wraps. It was further observed that the stress at which the kink point in stress-strain response occurs is affected by the lateral stiffness of the FRP jacket.
7. The dilation behaviour of FRP-confined concrete cylinders is significantly dependent on the lateral stiffness ratio of the FRP jacket. Concrete cylinders confined with SFRP sheets exhibited superior performance than those exhibited by corresponding cylinders confined with CFRP sheets in curtailing the lateral expansion of concrete core, and maintaining volume reduction till failure.
8. The validation results of the DIC technique revealed that the strain measurements from conventional foil gauges and virtual gauges are in good agreement in terms of trend and magnitude, despite the fact that readings from virtual strain gauges at the initial loading stage were slightly scattered, and that the axial and lateral strain at failure were underestimated in limited cases due to the high frame rate used.

9. The trend on how the lateral strain profile developed as the cylinders were loaded to failure was similar for all tested cylinders, irrespective of the FRP jacket thickness or concrete unconfined strength; at load levels close to the unconfined concrete strength, lateral strain is negligible, after which it starts to increase rapidly as the concrete dilates. The lateral strain profile develops consistently at all subsequent load levels till the maximum lateral strain is reached at or close to the mid height of the cylinder.
10. Significant axial and lateral strain variations over the surface of the FRP-confined cylinders were detected. The average lateral strain variation for CFRP-confined cylinders was in the order of 5000,  $\mu\epsilon$  and the axial strain variation was in the order of 12500  $\mu\epsilon$ . On the other hand, the axial and lateral strain variations were more pronounced for SFRP-confined concrete cylinders and were in the order of 8200  $\mu\epsilon$  and 25500  $\mu\epsilon$  for lateral and axial strain variation, respectively.
11. FRP strain efficiency varied between concrete grades. For C37.3 and C42.4, respectively, CFRP strain efficiency calculated from discrete strain gauge readings was in the range of 0.92 - 0.78 based on manufacturer's rupture strain and in the range of 1.09 - 0.93 based on the flat coupon test. On the other hand, CFRP strain efficiency from virtual strain gauges was in the range of 0.85 - 0.79 based on the manufacturer's rupture strain and in the range of 1.04 - 0.97 based on the flat coupon test value. Similarly, it has been found that the SFRP strain efficiency, for C37.3 and C42.4, respectively, calculated from discrete strain gauge readings are in the range of 1.16 - 1.03 based on manufacturer's rupture strain and in the range of 1.25 - 1.11 based on the flat coupon test. On the other hand, the SFRP strain efficiency from virtual strain gauges are in the range of 1.07 - 1.04

based on the manufacturer's rupture strain and 1.16 - 1.12 based on the flat coupon test value.

12. Confinement effectiveness coefficient,  $k_t$ , and regardless of the unconfined concrete compressive strength ( $f'_{co}$ ), increases as thickness of FRP jacket increases for cylinders wrapped with CFRP sheets. However, the confinement effectiveness coefficient marginally reduces as FRP jacket thickness increases for cylinders wrapped with SFRP sheets due to the failure mode exhibited by some cylinders. Furthermore, the increase in  $f'_{co}$  resulted in an increase in the confinement effectiveness for cylinders wrapped with one, and two layers of CFRP wraps but a reduction in the confinement effectiveness for cylinders wrapped with three layers of CFRP wraps. On the other hand, confinement effectiveness coefficient shows no dependency on  $f'_{co}$  for SFRP-confined cylinders.
13. SFRP-confined cylinders, when concrete strength and number of wraps are the same, exhibited far superior performance than corresponding CFRP in terms of strain ductility and energy absorption capacity. Strain and energy ductility, when unconfined concrete compressive strength ( $f'_{co}$ ) is the same, enhanced significantly due to the increase in the FRP jacket thickness for CFRP-and SFRP-confined cylinders. Higher  $f'_{co}$  has an adverse effect on strain and energy ductility of CFRP-confined cylinders; however, higher  $f'_{co}$  resulted in a reduction in the strain ductility and an increase in energy ductility for SFRP-confined concrete cylinders.
14. SFRP-confined cylinders when compared to CFRP-confined cylinders of the same lateral stiffness ratio, exhibited comparable performance in terms of strength and superior performance in terms of the axial deformability.

### ***7.3.2 Analytical Modeling of FRP-Confined Concrete***

1. Performance analysis of various existing empirical and analytical confinement models revealed that none of these existing models is capable of predicting the ultimate conditions and the stress-strain response with a reasonable accuracy.
2. The accuracy of existing confinement models was generally higher in predicting the ultimate axial strength rather than the ultimate axial strain, with a minimum average absolute error of 3.4% for the former and 15.6% for the latter.
3. Out of the nine confinement models examined, models by Berthet et al. and Lam and Teng were the most accurate in predicting the ultimate axial strength. On the other hand, models by Spoelstra and Monti and Toutanji were the most accurate in predicting the ultimate axial strain. In general, models that performed well in predicting the ultimate axial strength did not perform equally well in predicting the ultimate axial strain.
4. An analytical confinement model is proposed based on the analytical model originally developed by Spoelstra and Monti. The proposed model exhibited superior behaviour over the investigated confinement models in predicting the ultimate axial strength, ultimate axial strain and the entire stress-strain behaviour of weakly, moderately and highly FRP confined concrete.

### ***7.3.3 FE Numerical Modeling of FRP-Confined concrete***

1. The DP type plasticity model's three main parameters, namely; the friction angle, hardening and softening rule and dilation angle have been derived based on a regression analysis of the author's own experimental program. Comparison between the herein and other published experimental results and the model numerical prediction shows very

good agreement with the model. The proposed model can be directly implemented in FE modeling of concrete confined by FRP sheets.

2. Implementing the developed concrete constitutive model in FE modeling to perform parametric study confirmed the experimental observations of the beneficial effect of increasing the FRP jacket and the FRP elastic modulus in enhancing the overall performance of FRP-confined concrete.

#### **7.4 Recommendations for Future Work**

1. Additional parameters that might affect the overall compressive behaviour of FRP-confined circular concrete sections should be further investigated such as concrete mix design, varying loading rate and FRP jacket orientation.
2. The compressive behaviour of other sections type such as square and rectangular sections should be investigated and proper analytical and numerical models to simulate their behaviour should be developed.
3. The compressive behaviour of confined concrete subjected to eccentric compressive loading should be investigated. The accuracy of the proposed analytical and numerical models in predicting the compressive behaviour characteristics of confined concrete when subjected to such type of loading condition should be examined and proper modifications, if necessary, should be suggested.
4. The compressive behaviour of concrete sections confined with other new developed FRP materials such as BFRP should be investigated and compared to that of GFRP, CFRP and SFRP.

5. Further validation of the proposed analytical model to confirm its accuracy in predicting the ultimate strength and axial strain is necessary before the proposed model can be used with a reasonable degree of confidence.
6. Further investigation of the validity of the proposed concrete material parameters' models outside the parameters range that the models have been derived based on such as high strength concrete, very low FRP lateral confinement level, FRP jacket orientation and the provision of internal steel reinforcement is required. Accordingly, modification to the proposed model may be necessary before a universal acceptance to the proposed model can be obtained.

## References

- ABAQUS 6.9, "ABAQUS Analysis User's Manual, version 6.9.", ABAQUS Inc., 2009.
- Abbasnia R, Ziaadiny H. "Behavior of Concrete Prisms Confined with FRP Composites under Axial Cyclic Compression." *Eng Struct.*, Vol. 32, No. 3, pp. 648–55, 2010.
- Abdelrahman, K., "Effectiveness of Steel Fibre Reinforced Polymer Sheets for Confining Circular Concrete Columns." MSc Thesis, Department of Civil Engineering, University of Calgary, Calgary, Alberta, Canada, 2011.
- Abdelrahman, K., and El-Hacha, R., "Finite Element Modeling of Concrete Columns Wrapped with SFRP and CFRP Sheets." *AMCM, 8th International Conference*. Wroclaw, Poland, 2014.
- Abdelrahman, K., and El-Hacha, R., "Ultimate Axial Strain Predictions of SFRP Confined Concrete Columns." *The 7th International Conference on FRP Composites in Civil Engineering*. Vancouver, Canada, 2014.
- Abdelrahman, K., El-Hacha, R., "Review of Confinement Models for FRP Wrapped Reinforced Concrete Columns." *Proceedings of the 3rd International Conference on Seismic Retrofitting (ICSR)*. Tabriz, Iran, October 20-22, 2010
- Ahamd, S. H., Khaloo, A. R., and Irshaid, A., "Behaviour of Concrete Spirally Confined by Fibreglass Filament." *Mag. Concrete Res.*, Vol. 43, No.156, pp. 143–148, 1991.
- Ahmad, S. H., and Shah, S. P., "Complete Triaxial Stress-Strain Curves for Concrete." *Journal Structures Div. ASCE*, Vol. 108, No. 4, pp. 728–742, 1982a.
- Ahmad, S. H., and Shah, S. P., "Stress–Strain Curves of Confined by Spiral Reinforcement." *ACI Journal*, Vol. 79, pp. 484–490, 1982b.

- Aire, C., Gettu, R., and Casas, J. R., "Study of the Compressive Behavior of Concrete Confined by Fiber Reinforced Composites." *Composites in Constructions, Proc. of the Int. Conf.*, A. A. Balkema, Lisse. The Netherlands, pp. 239–243, 2001.
- Au, C., "*Behaviour of FRP-Confined Concrete*", MSc Thesis, Massachusetts Institute of Technology, 2001.
- Bank, L.C., "*Composites For Construction: Structural Design with FRP Materials*", Hoboken, New Jersey: John Wiley and Sons, Inc., 2006.
- Benzaid, R., Chikh, N.E., and Mesbah, H, "Behaviour of Square Concrete Column Confined with GFRP Composite Wrap." *Journal of Civil Engineering and Management*, Vol. 14, No. 2, pp. 115–120, 2008
- Berthet, J.F., Ferrier, E., and Hamelin, P., "Compressive Behaviour of Concrete Externally Confined by Composite Jackets. Part A: Experimental Study". *Construction and Building Materials*, Vol. 19, No. 3, pp. 223-232, April 2005.
- Berthet, J.F., Ferrier, E., and Hamelin, P., "Compressive Behaviour of Concrete Externally Confined by Composite Jackets. Part B: Model". *Construction and Building Materials*, Vol. 20, No. 5, pp. 338-347, 2006.
- Binici B. "An Analytical Model for Stress–Strain Behavior of Confined Concrete." *Eng Struct.*, Vol. 27, No. 7, pp. 1040–51, 2005.
- Binici B. "Design of FRPs in Circular Bridge Column Retrofits for Ductility Enhancement." *Eng Struct.*, Vol. 30, No. 3, pp. 766–76, 2008.
- Bisby, L., and Stratford, T.; "The Ultimate Condition of FRP Confined Concrete Columns: New Experimental Observations and Insights.", *Proceedings of the 5th International*

- Conference on FRP Composites in Civil Engineering (CICE 2010)*. Beijing, China, pp. 599-602, September 27-29, 2010.
- Bisby, L., and Take, W., "Strain Localisations in FRP Confined Concrete: New Insights." *Structures and Buildings*, Vol. 165, No. 5, pp. 301-309, 2009.
- Bisby, L., Take, W., and Bolton, M., "Quantifying Strain Variation in FRP Confined Concrete using Digital Image Analysis.", *Proceedings of the 1st Asia-Pacific Conference on FRP in Structures (APFIS 2007)*, Hong Kong, China, pp. 599-604, December 12-14, 2007.
- Bisby, L.A., Dent, A.J.S., and Green, M.F., "Comparison of Confinement Models for Fibre-Reinforcement Polymer-Wrapped Concrete.", *ACI Structural Journal*, Vol. 102, No. 1, pp. 62-72, January 2005.
- Canadian Standards Association. "Canadian Highway Bridge Design Code." CAN/CSA S6-14, Ontario, Canada, 2014.
- Canadian Standards Association. "Concrete Materials and Methods of Concrete Construction" CAN/CSA A23.1-14, Ontario, Canada, 2014.
- Canadian Standards Association. "Test Methods and Standard Practices for Concrete" CAN/CSA A23.2-14, Ontario, Canada, 2014.
- Canadian Standards Association. "Design and Construction of Building Components with Fibre Reinforced Design Code." CAN/CSA S806-12, Ontario, Canada, 2012.
- Campione, G., and Miraglia, N., "Strength and Strain Capacities of Concrete Compression Members Reinforced with FRP." *Cem. Concr. Compos.*, Vol. 25, pp. 31-41, 2003.
- Campione, G., "Influence of FRP Wrapping Techniques on the Compressive Behavior of Concrete Prisms." *Cem. Concr. Compos.*, Vol. 28, pp. 497-505, 2006.

- Campione G, Minafo G. "Compressive Behavior of Short High-Strength Concrete Columns." *Eng Struct.*, Vol. 32, No. 9, pp. 2755–66, 2010.
- Carey SA, Harries KA. "Axial Behavior and Modeling of Confined Small, Medium, and Large Scale Circular Sections with Carbon Fiber-Reinforced Polymer Jackets." *ACI Struct J.*, Vol. 102, No. 4, pp. 596–604, 2005.
- Cervenka J, Papanikolaou VK. "Three Dimensional Combined Fracture-Plastic Material Model for Concrete." *Int. J Plasticity.*, Vol. 24, No. 12, pp. 2192–220, 2008.
- Chaallal, O., Hassan, M., and Shahawy, M., "Confinement Model for Axially Loaded Short Rectangular Columns Strengthened with Fiber-Reinforced Polymer Wrapping." *ACI Struct. J.*, Vol. 100, No. 2, pp. 215–221, 2003.
- Chastre C, Silva MAG. "Monotonic Axial Behavior and Modelling of RC Circular Columns Confined with CFRP." *Eng Struct.*, Vol. 32, No. 8, pp. 2268–77, 2010.
- Chen, Wai-Fah, "*Plasticity in Reinforced Concrete*", New York: McGraw-Hill Book Company, 1982.
- Chun, S. S., and Park, H. C., "Load Carrying Capacity and Ductility of RC Columns Confined by Carbon Fiber Reinforced Polymer." *Proc., 3rd Int. Conf. on Composites in Infrastructure (CD-Rom)*, Univ. of Arizona, San Francisco, 2002.
- Cui, C., "Behaviour of Normal and High Strength Concrete Confined with Fibre Reinforced Polymers (FRP)", *Ph.D thesis, Department of Civil Engineering, University of Toronto*, 2009.
- Cui, C., and Sheikh, S.A., "Experimental Study of Normal- and High-Strength Concrete Confined with Fibre-Reinforced Polymers", *Journal of Composites for Construction*, ASCE, Vol. 14, No. 5, pp. 553-561, October 2010.

- Daniel, Isaac M., and Ishai, O., "*Engineering Mechanics of Composite Materials*", New York: Oxford University Press, Inc., 1994.
- De Lorenzis L, Tepfers R. "Comparative Study of Models on Confinement of Concret Cylinders with Fiber Reinforced Polymer Composites." *ASCE J Compos Constr.*, Vol. 7, No. 3, pp. 219–37, 2003.
- Demers, M., "Determination of Parameters Influencing the Behavior of Concrete Columns Confined with Advanced Composite." *MSc Thesis, Univesite de Sherbrooke, France, 1994.*
- Demers, M., and Neale, K. W., "Strengthening of Concrete Columns with Unidirectional Composite Sheets." *Development in Short and Medium Span Bridge Engineering '94, Proc. of the 4th Int. Conf.on Short and Medium Span Bridges*, A. A. Mufti, B. Bakht, and L. G.Jaeger, eds., Canadian Society for Civil Engineering, Montreal, pp. 895–905, 1994.
- Demers, M., and Neale, K.W., "Confinement of Reinforced Concrete Columns with Fiber-Reinforced Composite Sheets – An Expeirmental Study", *Canadian Journal of Civil Engineering*, Vol. 26, No. 2, pp. 226-241, April, 1999
- Devore, L. Jay, "*Probability and Statistics For Engineering and the Sciences*", Duxbury-Thomson Learning, 2000.
- Drucker, D.C., and Prager, W., "Soil Mechanics and Plastic Analysis or Limit Design." *Quart Applied Mechanics*, Vol. 10, No. 2, pp. 157-165, 1952.
- Eid R, Dancygier AN. "Confinement Effectiveness in Circular Concrete Columns." *Eng Struct.*, Vol. 28, No. 13, pp. 1885–96, 2006.
- Eid R, Paultre P. "Plasticity-Based Model for Circular Concrete Columns Confined with Fibre-Composite Sheets." *Eng Struct.*, Vol. 29, pp. 3301–11, 2007.

- El-Hacha, R., and Mashrik, M.A., "Effect of SFRP Confinement on Circular and Square Concrete Columns." *Engineering Structures*, Vol. 36, pp. 379-393, 2012.
- El-Hacha, R., Green, M., and Wight, G., "Effect of Severe Environmental Exposures on CFRP Wrapped Concrete Columns." *Journal of Composites for Construction, ASCE*, Vol. 14, No. 1, pp. 83-93, February 2010.
- Esfahani, M.R. and Kianoush, M.R., "Axial Compressive Strength of Reinforced Concrete Columns Wrapped with Fibre Reinforced Polymers (FRP)." *International Journal of Engineering*, Iran, Vol. 18, No. 1, pp. 73-83, February 2000
- Fahmy, M.F.F., and Wu, Z., "Evaluating and Proposing Models of Circulars Concrete Columns Confined with Different FRP Composites." *Journal of Composites: Part B*, Vol. 41, No. 3, pp. 199-213, April 2010.
- Fam, A. Z., and Rizkalla, S. H., "Confinement Model for Axially Loaded Concrete Confined by Circular Fiber-Reinforced Polymer Tubes." *ACI Struct. J.*, Vol. 98, No. 4, pp. 451–461, 2001.
- Fam, A.Z., Flisak, B., and Rizkalla, S.H., "Experimental and Analytical Modeling of Concrete-Filled Fibre Reinforced Tubes Subjected to Combined Bending and Axial Loads." *Journal of Structural Engineering, ACI*, Vol. 100, No. 4, pp. 499-506, July 2003.
- Fang JH. "Finite Element Analysis of FRP-Retrofitted RC beams." *MSc. thesis. Department of Civil Engineering*, National Taiwan University, 1999.
- Fardis, M. N., and Khalili, H., "Concrete Encased in Fiberglass-Reinforced Plastic." *ACI J.*, Vol. 78, No. 6, pp. 440–446, 1981.
- Fardis, MN, and Khalili, H., "FRP-Encased Concrete as a structural material." *Mag Concrete Resources*, Vol. 34, No. 122, pp. 191-202, 1982.

- Feng, P., Lu, X.Z., and Ye, L.P., "Experimental Research and Finite Element Analysis of Square Concrete Columns Confined by FRP Sheets Under Uniaxial Compression." *In Proceedings of the 17th Australasian Conference on the Mechanics of Structures and Materials*, Gold Coast, Queensland, Australia, pp. 12-14, 2002
- GangaRao, H., Taly, N., and Vijay, P., "*Reinforced Concrete Design with FRP Composites*", Taylor and Francis Group, LLC, 2007.
- GBF, "GBF Basalt Fibre", July 13, 2015.  
<http://basaltfiber-gbf.com/basalt-multi-axial-fabric-supplier.html>
- Gunaslan, S.E., Karasin, A., and Oncu, M.E., "Properties of FRP Materials for Strengthening." *IJISSET - International Journal of Innovative Science, Engineering and Technology*, Vol. 1, No. 9, November 2014.
- HARDWIRE, "Hardwire Composite Armor System", March 01, 2014.  
<http://www.hardwirellc.com>.
- Harries, K. A., Kestner, J., Pessiki, S., Sause, R., and Ricles, J., "Axial Behavior of Reinforced Concrete Columns Retrofit with FRPC Jackets." *Proc., 2nd Int. Conf. on Composites in Infrastructures (ICCI)*, H. Saadatmanesh and M. R. Ehsani, eds., Tucson, Ariz., pp. 411–425, 1998.
- Harries, K. A., and Kharel, G., "Behavior and Modeling of Concrete Subject to Variable Confining Pressure." *ACI Mater. J.*, Vol. 99, No. 2, pp. 180–189, 2002.
- Hognestad, E., "A Study of Combined Bending and Axial Load in Reinforced Concrete Members." *Bulletin Series No. 399*, Engineering Experiment Station, Univ. of Illinois, Urbana, Ill, 1951.

- Hosotani, M., Kawashima, K., and Hoshikuma, J. I., “A Study of Confinement Effect of Concrete Cylinders by Carbon Fiber Sheets.” *Non-Metallic (FRP) Reinforcement for Concrete Structures, Proc., 3rd Int.Symposium*, Japan Concrete Institute, Sapporo, Japan, Vol. 1, pp. 209–216, 1997.
- Howie, I., and Karbhari, V. M., “Effect of Materials Architecture on Strengthening Efficiency of Composite Wraps for Deteriorating Columns in the North-East.” *Infrastructure: New Materials and Methods of Repair, Proc., 3rd Materials Engineering Conf.*, K. D. Basham, ed., Material Engineering Division, ASCE, pp. 199–206, 1994.
- Huang YL. “Analysis-Oriented and Constitutive Modeling of FRP-Confined Concrete.” *MSc thesis*, Tsing-Hua University, 2005.
- Huang, Z., and Zhou, Y., "*Strength of Fibrous Composites*", Zhejiang University Press, Hangzhou and Springer-Verlag Berlin Heidelberg, 2011.
- Ilki, A., and Kumbasar, N., “Behavior of Damaged and Undamaged Concrete Strengthened by Carbon Fiber Composite Sheets.” *Struct.Eng. Mech.*, Vol. 13, No. 1, pp. 75–90, 2002.
- Ilki A, Kumbasar N, Koc V. “Low Strength Concrete Members Externally Confined with FRP Sheets.” *Struct Eng Mech.*, Vol. 18, No. 2, pp. 167–94, 2004.
- Ilki, A., Peker, O., Karamuk, E., and Kumbasar, N., “External Confinement of Low Strength Brittle Reinforced Concrete Short Columns.” *Proc., ACI SP-238, Int. Symp. on Confined Concrete*, Y. Xiao, S. Kunnath, and W. Yi, eds., Farmington Hills, Mich., pp. 363–380, 2006.
- ISIS Education Module 2, "*An Introduction to FRP Composites for Construction*", The Canadian Network of Centre of Excellence on Intelligent Sensing for Innovative Structures, ISIS Canada, University of Manitoba, Winnipeg, Manitoba, Canada, March 2006.

- Jiang, J., and Wu, Y., "Identification of Material Parameters for Drucker-Prager Plasticity Model for FRP Confined Circular Concrete Columns." *International Journal of Solids and Structures*, Vol. 49, pp. 445-456, 2012.
- Jiang, T., and Teng, J.G., "Analysis-Oriented Stress-Strain Models For FRP-Confined Concrete." *Journal Engineering Structure, ASCE*, Vol. 29, No. 11, pp. 2968-2986, 2007.
- Jolly CK, Lilistone D. "The Stress–Strain Behavior of Concrete Confined by Advanced Fibre Composites." *In: Proc. 8th BCA conference higher education and the concrete industry. Southampton*, 1998.
- Karabinis, A.I., and Rousakis, T.C., "Concrete Confined by FRP material: A Plasticity approach." *Engineering Structures*, Vol. 24, pp. 923-932, 2002.
- Karabinis AI, Rousakis TC, Manolitsi GE. "3D Finite-Element Analysis of Substandard RC Columns Strengthened by Fiber-Reinforced Polymer Sheets." *J Compos Constr ASCE.*, Vol. 12, No. 5, pp. 531–40, 2008.
- Karabinis, A.I., and Kiouisis, P.D., "Effects of Confinement on Concrete Columns: Plasticity Approach." *Journal of Structural Engineering, ASCE*, Vol. 120, No. 9, pp. 2747-2766, 1994.
- Karabinis, A.I., and Kiouisis, P.D., "Strength and Ductility of Rectangular Concrete Columns: a Plasticity Approach." *Journal of Structural Engineering, ASCE*, Vol.122, No. 3, pp. 267-274, 1996
- Karbhari, V. M., and Gao, Y., "Composite Jacketed Concrete Under Uniaxial Compression—Verification of Simple Design Equations." *J.Mater. Civ. Eng.*, Vol. 9, No. 4, pp. 185–193, 1997.

- Kawashima K., Hosotani M., and Hoshikuma J., “ A Model for Confinement Effect for Concrete Cylinders Confined by Carbon Fiber Sheets.” *NCEER-INCEDE Workshop on Earthquake Engrg. Frontiers of Transp. Fac.*, NCEER, State University of New York, Buffalo, N.Y, 1997.
- Kono, S., Inazuni, M., and Kaku, T., “Evaluation of Confining Effects of CFRP Sheets on Reinforced Concrete Members.” *Proc., 2nd Int. Conf. on Composites in Infrastructures (ICCI '98)*, Tucson, Ariz., pp. 343–355, 1998.
- Kumutha, R., Vaidyanathan, R., and Palanichamy, M.S., “Behaviour of Reinforced Concrete Rectangular Columns Strengthened Using GFRP.” *Cement and Concrete Composites*, Vol. 29, pp. 609–615, 2007
- Lam, L., and Teng, J. G., “A New Stress–Strain Model for FRP-Confined Concrete.” *Proc., Int. Conf. on FRP Composites in Civil En-gineering*, Hong Kong, pp. 283–292, 2001.
- Lam, L., and Teng, J.G., "Strength Models for FRP-Confined Concrete." *Journal of Structural Engineering*, ASCE, Vol. 128, No. 5, pp. 612-623, 2002.
- Lam, L., and Teng, J. G., “Hoop Rupture Strains of FRP Jackets in FRP-Confined Concrete.” *Proc., 6th Int. Symp. on Fibre-Reinforced Polymer (FRP) Reinforcement for Concrete Structures*, K. H. Tan, ed., Vol. 1, World Scientific, Singapore, pp. 601–612, 2003a.
- Lam, L., and Teng, J.G., "Design-Oriented Stress-Strain Model for FRP-Confined Concrete." *Construction and Building Materials*, Vol.17, No. 6, pp. 471-489, 2003b.
- Lam, L., and Teng, J. G., “Stress–Strain Model for FRP-Confined Concrete for Design Applications.” *Proc., 6th Int. Symp. on Fibre-Reinforced Polymer (FRP) Reinforcement for Concrete Structures*, K.H. Tan, ed., Vol. 1, World Scientific, Singapore, pp. 99–110, 2003c.

- Lam, L., and Teng, J. G., "Design-Oriented Stress-Strain Model for FRP-Confined Concrete in Rectangular Columns." *J. Reinf. Plast. Compos.*, 22(13), 1149–1186, 2003d.
- Lam, L., and Teng, J.G., "Ultimate Condition of FRP-Confined Concrete." *Journal of Composites for Construction, ASCE*, Vol. 8, No. 6, pp. 539-548, December 2004.
- Lam, L., Teng, J. G., Cheung, C. H., and Xiao, Y., "Behavior of FRP-Confined Concrete Under Cyclic Axial Compression." *Proceedings(CD-ROM), International Symposium on Confined Concrete, Changsha, China*, pp. 12–14 June, 2004.
- Lam, L., Teng, J. G., Cheung, C. H., and Xiao, Y., "FRP-Confined Concrete Under Axial Cyclic Compression." *Cem. Concr. Compos.*, Vol. 28, pp. 949–958, June 2006.
- Lam L, Teng JG. "Stress–Strain Model for FRP-Confined Concrete under Cyclic Axial Compression". *Eng Struct.*, Vol. 31, No. 2, pp. 308–21, 2009.
- Lan, Y.M., "*Finite Element Study of Concrete Columns with Fibre Composite Jackets*", PhD Dissertation, School of Civil Engineering, Purdue University, 1998.
- Li, G. "Experimental Study of FRP Confined Concrete Cylinders." *Engineering Structures*, Vol. 28, pp 1001-1008, 2006.
- Lin, H. J., and Chen, C. T., "Strength of Concrete Cylinder Confined by Composite Materials." *J. Reinf. Plast. Compos.*, Vol. 20, No. 18, pp. 1577–1601, 2001.
- Lin, H., and Liao, C., "Compressive Strength of Reinforced Concrete Column Confined by Composite Material." *Compos. Struct.*, Vol. 65, No. 2, pp. 239–250, 2004.
- Luccioni BM, Rougier VC. "A Plastic Damage Approach for Confined Concrete." *Comput & Structures.*, Vol. 83, pp. 2238–56, 2005.
- Maalej, M., Tanwongsva, S., and Paramasivam, P., "Modelling of Rectangular RC Columns Strengthened with FRP." *Cem. Concr. Compos.*, Vol. 25, pp. 263–276, 2003.

- Mahfouz I, Rizk T, Sarkani S. “An Innovative FRP Confining System for Repairing Rectangular Columns”. *In: Construction and Materials Issues, Proceedings of the Second Congress, ASCE and Construction Institute.*, pp. 16–25, 2001.
- Malvar LJ, Morrill KB, Crawford JE. “Numerical Modeling of Concrete Confined by Fiber-Reinforced Composites.” *J Compos Constr, ASCE.*, Vol. 8, No. 4, pp. 315–22, 2004.
- Mandal S, Hoskin A, Fam A. “Influence of Concrete Strength on Confinement Effectiveness of Fiber-Reinforced Polymer Circular Jackets.” *ACI Struct J.*, Vol. 102(3): pp. 383–92, 2005.
- Mander, J.B., Priestley, M.J.N., and Park, R., "Theoretical Stress-Strain Model for Confined Concrete." *Journal Structural Engineering, ASCE*, Vol. 114, No. 8, ppl. 1804-1826, 1988.
- Mashrik, M.A., "Performance Evaluation of Circular and Square Concrete Columns Wrapped with CFRP and SFRP Sheets." MSc Thesis, Department of Civil Engineering, University of Calgary, Calgary, Alberta, Canada, 2011.
- Mashrik, M.A., El-Hacha, R., and Tran, K., "Performance Evaluation of SFRP-Confined Circular Concrete Columns." *The 5th International Conference on FRP Composites in Civil Engineering, CICE*, Beijing, China, 2010.
- Masia, M.J., Gale, T.N., and Shrive, N.G., “Size Effects in Axially Loaded Square-Section Concrete Prisms Strengthened Using Carbon Fiber Reinforced Polymer Wrapping”, *Canadian Journal of Civil Engineering.*, Vol. 31, No. 1, pp. 1-13, January 2004.
- Matthys, S., Taerwe, L., and Audenaert, K., “Test on Axially Loaded Concrete Columns Confined by Fiber Reinforced Polymer Sheet Wrapping.” *Proc., 4th Int. Symposium on Fiber Reinforced Polymer Reinforcement for Reinforced Concrete Structures*, C. W.

- Dolan, S. H., Rizkalla, and A. Nanni., eds., SP-188, American Concrete Institute, Farmington, Mich., pp. 217–229, 1999.
- Matthys S, Toutanji H, Taerwe L. “Stress–Strain Behavior of Large-Scale Circular Columns Confined with FRP Composites.” *ASCE J Struct. Eng.*, Vol. 132, No. 1, 123–33, 2006
- Mazumdar, Sanjay k. *Composite Manufacturing: Materials, Products, and Process Engineering*. CRC Press LLC, 2002.
- Minnaugh, P., "The Experimental Behaviour of Steel Fibre Reinforced Polymer Retrofit Measures." MSc Thesis, University of Pittsburgh, 2006.
- Mirmiran, A., and Shahawy, M., "A New Concrete-Filled Hollow FRP Composite Column." *Composites Part B: Engineering*, Vol. 27B, No. 3-4, pp. 263-268, 1996.
- Mirmiran, A., and Shahawy, M., "Behaviour of Concrete Columns Confined by Fibre Composites." *Journal Structural Engineering, ASCE*, Vol. 123, No. 5, pp. 583-590, 1997a.
- Mirmiran, A., and Shahawy, M., “Dilation Characteristics of Confined Concrete.” *Mech. Cohesive-Frict. Mater.*, Vol. 2, pp. 237–249, 1997b.
- Mirmiran, A., Shahawy, M., Samaan, M., and El-Echary, H., “Effect of Column Parameters on FRP-Confined Concrete.” *J. Compos. Constr.*, Vol. 2, No. 4, pp. 175–185, 1998.
- Mirmiran, A., Shahawy, M., and Samaan, M., "Strength and Ductility of Hybrid FRP-Concrete Beam-Columns." *Journal of Structural Engineering, ASCE*, Vol. 125, No. 10, pp. 1085-1093, 1999.
- Mirmiran, A., Zagers, K., and Yuan, W., "Nonlinear Finite Element Modeling of Concrete Confined by Fibre Composites." *Finite Elements In Analysis and Design*, Vol. 35, pp. 79-96, 2000.

- Miyauchi, K., Inoue, S., Kuroda, T., and Kobayashi, A., "Strengthening Effects of Concrete Columns with Carbon Fiber Sheet." *Trans. Japan Concrete Inst.*, Vol. 21, pp. 143–150, 1999.
- Miyauchi, K., Nishibayashi, S., and Inoue, S., "Estimation of Strengthening Effects with Carbon Fiber Sheet for Concrete Column." *Proc., 3rd Int. Symp. (FRPRCS-3) on Non-Metallic (FRP) Reinforcement for Concrete Structures*, Vol. 1, Sapporo, Japan, pp. 217–224, 1997.
- Moran DA, Pantelides CP. "Variable Strain Ductility Ratio for Fiber Reinforced Polymer-Confined Concrete." *ASCE J Compos Constr.*, Vol. 6, No. 4, pp. 224–32, 2002.
- Mohamed H, Masmoudi R. "Axial Load Capacity of Concrete-Filled FRP Tube Columns: Experimental Versus Predictions." *ASCE J Compos Constr.*, Vol. 14, No. 2, pp. 231–43, 2010.
- Nanni, A., and Bradford, N.M., "FRP Jacketed Concrete Under Uniaxial Compression." *Construction Building Material*, Vol. 9, No. 2, pp. 115-124, 1995.
- Napoli, A., and Realfonzo, R., "Behaviour of Concrete Confined by Steel Fibre Reinforced Polymer Wraps: Experimental Study", 2013.
- Newman, K., and Newman, J.B., "Failure Theories and Design Criteria for Plain Concrete" *Proceeding int. Civil Engineering Materials*, New York: Wiley Interscience, 1969.
- Oh, B., "A Plasticity Model for Confined Concrete Under Uniaxial Loading", PhD Thesis, Lehigh University, 2002.
- Ottosen NS. "Constitutive Model for Short-Time Loading of Concrete." *J Eng Mech Div, ASCE*, Vol. 105, No.1, pp. 127–41, 1979.

- Ozbakkaloglu, T., Lim, J.C., and Vincent, T., "FRP-Confined Concrete in Circular Sections: Review and Assessment of Stress-Strain Models." *Engineering Structures*, Vol. 49, pp. 1068-1088, 2013.
- Pan, J. L., Jin, X. N., Wang, F. L., Wang, Y. G., and Lai, W. H., "Behavior of Short Reinforced Concrete Columns Wrapped with FRP under Axial Compression." *J. Harbin University Civil Eng. Architecture.*, Vol. 35, No. 3, pp. 14–19, 2002.
- Papanikolaou VK, Kappos AJ. "Confinement-Sensitive Plasticity Constitutive Model for Concrete in Triaxial Compression." *Internat J Solids Structures.*, Vol. 44, No.21, pp. 7021–48, 2007.
- Park JH, Jo BW, Yoon SJ, Park SK. "Experimental Investigation on the Structural Behavior of Concrete Filled FRP Tubes with/without Steel Rebar." *KSCE J Civ Eng.*, Vol. 15, No. 2, pp. 337–45, 2011.
- Parnas, R., Shaw, M., and Liu, Q., "Basalt Fiber Reinforced Polymer Composites", *The New England Transportation Consortium*, NETCR63, August, 2007.
- Parvin A, Jamwal AS. "Performance of Externally FRP Reinforced Columns for Changes in Angle and Thickness of the Wrap and Concrete Strength." *Compos Struct.*, Vol. 73, pp. 451–7, 2006.
- Parvin, A., and Wang, W., "Behaviour of FRP Jacketed Concrete Columns under Eccentric Loading." *Journal of Composites for Construction, ASCE.*, Vol. 5, No.3, pp. 146-152, August, 2001.
- Pekau, O.A.,Zhang, Z.X., and Liu, G.T., "Constitutive Model for Concrete in Strain Space." *Journal of Engineering Mechanics*, Vol. 118, pp. 1907-1927, 1992.

- Pessiki, S., Harries, K., Kestner, J., Sause, R., Ricles, J., “Axial Behaviour of Reinforced Concrete Columns Confined with FRP Jackets.” *Journal of Composites for Construction*, ASCE, Vol. 5, No. 4, pp. 237-245, November 2001.
- Picher, F., Rochette, P., and Labossiere, P., “Confinement of Concrete Cylinders with CFRP.” *Proc., 1st Int. Conf. on Composites for Infra-Structures*, H. Saadatmanesh, and M. R. Ehsani, eds., Univ. of Arizona, Tucson, Ariz., pp. 829–841, 1996.
- Popovics, S., "A Numerical Approach to the Complete Stress-Strain Curves for Concrete." *Cement Concrete Resources*, Vol. 3, No. 5, pp. 583-599, 1973.
- Pramono, E. and Willam K., “Fracture-Energy Based Plasticity Formulation of Plain Concrete”, *Journal of Engineering Mechanics*, ASCE, Vol. 115, No. 6, pp. 1183-1204, 1989.
- Pulido, C., Saiidi, M. S., Sanders, D., and Itani, A., “Experimental Validation and Analysis of a CFRP-Retrofit of a Two-Column Bent.” *Proc., 3rd Int. Conf. on Composites in Infrastructure, (CD-Rom)*, 2002.
- Purba, B. K., and Mufti, A. A., “Investigation of the Behavior of Circular Concrete Columns Reinforced with Carbon Fiber Reinforced Polymer CFRP Jackets.” *Can. J. Civ. Eng.*, Vol. 26, pp. 590–596, 1999.
- Rajasekaran A., Raghunath, P.N., and Suguna, K., “Effect of Confinement on the Axial Performance of Fibre Reinforced Polymer Wrapped RC Column.” *American Journal of Engineering and Applied Sciences*, Vol. 1, No. 2, pp. 110-117, 2008.
- Realfonzo R, Napoli A. “Concrete Confined by FRP Systems: Confinement Efficiency and Design Strength Models.” *Compos Part B: Eng.*, Vol. 42, pp. 736–55, 2011.
- Restrepol, J. I. and De Vito, B., “Enhancement of the Axial Load Capacity of Reinforced Concrete Columns by Means of Fiberglass Epoxy Jackets.” *Proc., 2nd Int. Conf. on*

- Advanced Composite Materials in Bridges and Structures*, M. M. El-Badry, ed., Montreal, pp. 547–690, 1996.
- Richard, R. M., and Abbott, B. J., “Versatile Elastic-Plastic Stress-Strain Formula.” *J. Eng. Mech. Div.*, Vol. 101, No. 4, pp. 511–515, 1975.
- Richart, F. E., Brandtzaeg, A., and Brown, R. L., “A Study of the Failure of Concrete under Combined Compressive Stresses.” Engineering Experiment Station, Univ. of Illinois, Urbana, Ill., 1928.
- Rocca, S., Galati, N., and Nanni, A., “Large-Size Reinforced Concrete Columns Strengthened with Carbon FRP: Experimental Evaluation.” *Proc., Third Int. Conf. on FRP Composites in Civil Engineering*, Miami, Fla., pp. 491–494, 2006.
- Rochette, P., and Labossière, P., "A Plasticity Approach For Concrete Columns Confined with Composite Materials." *Proc., 2nd interantional conference on advanced compsoite materials in bridges and structures.*, Montreal, Canada, pp. 359-366, 1996.
- Rochette, P., and Labossiere, P., “Axial Testing of Rectangular Column Models Confined with Composites.” *J. Compos. Constr.*, Vol. 4, No. 3, pp. 129–136, 2000.
- Rodrigues, C. C., and Silva, M. G., “Experimental Investigation of CFRP Reinforced Concrete Columns under Uniaxial Cyclic Compression.” *Proc., 5th Int. Conf. on Fibre-Reinforced Plastics for Reinforced Concrete Structures*, C. J. Burgoyne, ed., Thomas Telford, London, pp. 783–792, 2001a.
- Rodrigues, C. C., and Silva, M. G., “The Behaviour of GFRP Reinforced Concrete Columns under Monotonic and Cyclic Axial Compression.” *Composites in Constructions, Proc., Int. Conf.*, Balkema, Lisse. The Netherlands, pp. 245–250, 2001b.

- Rousakis TC, Karabinis AI, Kiouisis PD. "FRP-Confined Concrete Members: Axial Compression Experiments and Plasticity Modeling." *Eng Struct.*, Vol. 29: pp. 1343–53, 2007.
- Rousakis, T. C., Karabinis, A.I., Kiouisis, P.D., and Tepfers, R., "Analytical Modeling of Plastic Behaviour of Uniformly FRP Confined Concrete Members." *Composites Part B-Engineering*, Vol. 39, pp. 1104-1113, 2008.
- Saadatmanesh, H., Ehsani, M. R., and Li, M. W., "Strength and Ductility of Concrete Columns Externally Reinforced with Fiber Composite Straps." *ACI Struct. J.*, Vol. 91, No. 4, pp. 434–447, 1994.
- Saafi, M., Toutanji, H. A., and Li, Z., "Behavior of Concrete Columns Confined with Fiber Reinforced Polymer Tubes." *ACI Mater. J.*, Vol. 96, No. 4, pp. 500–509, 1999.
- Saatcioglu, M., and Razvi, S.R., "Strength and Ductility of Confined Concrete", *Journal of Structural Engineering, ASCE*, Vol. 118, No. 6, pp. 1150-1607, June 1992.
- Saiidi MS, Sureshkumar K, Pulido C. "Simple Carbon-Fiber-Reinforced-Plastic- Confined Concrete Model for Moment-Curvature Analysis." *ASCE J Compos Constr.*, Vol. 9, No. 1, pp. 101–4, 2005.
- Samaan, M., Mirmiran, A., and Shahawy, M., "Model of Concrete Confined by Fiber Composites." *J. Struct. Eng.*, Vol. 124, No. 9, pp. 1025–1031, 1998.
- Sargin, M. "Stress-Strain Relationship for Concrete and the Analysis of Structural Concrete Section" *PhD thesis*, University of Waterloo, Ontario, Canada, 1971.
- Shahawy, M., Mirmiran, A., and Beitlman, T., "Tests and Modeling of Carbon-Wrapped Concrete Columns." *Composits: Part B-Engineering*, Vol. 31, No. 6 & 7, pp. 471-480, 2000.

- Shehata, I. A. E. M., Corneiro, L. A. V., and Shehata, L. C. D., "Strength of Short Concrete Columns Confined with CFRP Sheets." *Mater. Struct.*, Vol. 35, pp. 50–58, 2002.
- Shrive PL, Azarnejad A, Tadros G, McWhinnie C, Shrive NG. "Strengthening of Concrete Columns with Carbon Fibre Reinforced Polymer Wrap". *Can J Civil Eng.*, Vol. 30, No. 3, pp. 543–54, 2003.
- Sikadure<sup>®</sup> 330, "*Product Data Sheet: Impregnation Resin for Fabric Reinforcement*" (edition 06.2010/v1), March, 2014. <http://ca01.webdms.sika.com/fileshow.do?documentID=111>.
- Sikawrap Hex<sup>®</sup> 230C, "*Product Data Sheet: Carbon Fibre Fabric for Structural Stregthening System*", (edition 06.2010/v1), March 2014.  
<http://ca01.webms.sika.com/fileshow.do?documentID=582>
- Spoelstra, M.R., and Monti, G., "FRP-Confined Concrete Model." *Journal of Composites For Construction, ASCE* Vol. 3, No. 3, pp. 143-150, 1999.
- Soudki, K. A., and Green, M. F., "Performance of CFRP Retrofitted Concrete Columns at Low Temperature." *Advanced Composite Materials in Bridges and Structures, Proc., 2nd Int. Conf.*, M. M. El-Badry, ed., Canadian Society for Civil Engineering, Montreal, pp. 427–434, 1996.
- Tan, K. H., "Strength Enhancement of Rectangular Reinforced Concrete Columns using Fiber-Reinforced Polymer." *J. Compos. Constr.*, Vol. 6, No. 3, pp. 175–183, 2002.
- Tegola, L. A., and Manni, D., "Experimental Investigation on Concrete Confined by Fiber Reinforced Polymer and Comparison with Theoretical Model." *Proc., 4th Int. Symposium on Fiber Reinforced Polymer Reinforcement for Reinforced Concrete Structures*, C. W.Dolan, S. H. Rizkalla, and A. Nanni., eds., SP-188, American Concrete Institute, Farmington, Mich., pp. 243–254, 1999.

- Teng, J. G., and Lam, L., "Compressive Behavior of Carbon Fiber Reinforced Polymer-Confined Concrete in Elliptical Columns." *J. Struct.Eng.*, Vol. 128, No. 12, pp. 1535–1543, 2002.
- Teng, J. G., and Lam, L., "Behaviour and Modeling of Fibre Reinforced Polymer-Confined Concrete." *Journal of Structural Engineering, ASCE*, Vol. 130, No. 11, pp. 1713-1723, November 2004.
- Teng, J.G., Huang, Y.L., Lam, L., Ye, L.P., "Theoretical Model for Fiber-Reinforced Polymer-Confined Concrete." *Journal of Composites for Construction*, Vol. 11, pp. 201–210, 2007a.
- Teng, J.G., Yu, T., Wong, Y.L., Dong, S.L., "Hybrid FRP-Concrete-Steel Tubular Columns: Concept and Behavior." *Construction and Building Materials*, pp. 846–854, 2007b.
- Teng, J.G., Wong, Y.L., and Dong, S.L., "Finite Element Modeling of Confined Concrete-I: Drucker-Prager Type Plasticity Model." *Engineering Structures*, Vol. 32, pp. 665-679, 2010.
- Thériault M, Neale KW, Claude S. "Fiber Reinforced Polymer-Confined Circular Concrete Columns: Investigation of Size and Slenderness Effects." *J Compos Constr.*, Vol. 8, No. 4, pp. 323–31, 2004.
- Toutanji, H.A. "Stress-Strain Characteristics of Concrete Columns Externally Confined with Advanced Fibre Composite Sheets." *ACI Materials Journal*, Vol. 96, No. 3, pp. 397-404, 1999.
- Tsai, K.C., and Lin, M.L., " Seismic Jacketing of RC Columns for Enhanced Axial Load Carrying Performace." *Journal of the Chinese Institute of Engineers*, Vol. 25, No. 4, pp. 389-402, 2002.

- Tsionis G, Pinto A. "Numerical Analysis of RC Bridge Piers with Rectangular Hollow Cross-Section Retrofitted with FRP Jackets." *J Earth Eng.*, Vol. 11: pp. 607–30, 2007.
- Vermeer, P.A., de Borst, R., "Non-Associated Plasticity for Soils", *Concrete and Rock. Heron* 29, pp. 1–64, 1984.
- Wang, E.Z., and Shrive, N.G., "Brittle Fracture in Compression: Mechanisms, Models and Criteria", *Engineering Fracture Mechanics*, Vol. 52, No. 6, pp. 1107-1126, December 1995.
- Wang, L.M., and Wu, Y.F., "Effect of Corner Radius on the Performance of CFRP-Confined Square Concrete Columns: Test II." *Engineering Structures*, Vol. 30, pp. 493–505, 2008.
- Wang, Y. C., and Restrepo, J. I., "Investigation of Concentrically Loaded Reinforced Concrete Columns Confined with Glass Fiber Reinforced Polymer Jackets." *ACI Struct. J.*, Vol. 98, No. 3, pp. 377–385, 2001.
- Wang YF, Wu HL. "Size Effect of Concrete Short Columns Confined with Aramid FRP Jackets." *ASCE J Compos Constr.*, Vol. 15, No. 4, pp. 535–44, 2011.
- Watanable, K., Nakamura, H., Honda, T., Toyoshima, M., Iso, M., Fujimaki, T., Kaneto, M., and Shirai, N., "Confinement Effect of FRP Sheet on Strength and Ductility of Concrete Cylinders Under Uniaxial Compression." *Non-Metallic (FRP) Reinforcement for Concrete Structures, Proc., 3rd Int. Symposium*, Japan Concrete Institute, Sapporo, Japan, Vol. 1, pp. 233–240, 1997.
- White, D., and A. Take, A., "Particle Image Velocimetry (PIV) Software for Use in Geotechnical Testing." *CUED/D-SOILS/TR322*, pp. 1-14, 2002.
- White, D., Take, W., and Bolton, M., "Soil Deformation Measurement using Particle Image Velocity (PIV) and Photogrammetry." *Geotechnique*, Vol. 53, No. 7, pp. 619-663, 2003.

- William, K. J., and Warnke, E. P., “ Constitutive Model for the Triaxial Behaviour of Concrete.”  
*Proc., Int. Assoc. Bridge Structural Eng.*, Vol. 19, pp.1–30, 1975.
- World-Trades.com*. March, 2014. <http://www.world-trades.com>.
- Wu G, Lu ZT, Wu ZS. “Strength and Ductility of Concrete Cylinders Confined with FRP Composites.” *Constr Build Mater.*, Vol. 20, No. 3, pp. 134–48, 2006.
- Wu, G., Gu, D.S.Wu, Z.S., Jiang, J.B. and Hu, X.Q., “Comparative Study on Seismic Performance of Circular Concrete Columns Strengthened with BFRP and CFRP Composites.” In: *Proceedings of the Asia-Pacific Conference on FRP in Structures (APFIS 2007)*, Vol. 1, Hong Kong, China, pp. 199-204, 2007.
- Wu H, Wang Y, Yu L, Li X. “Experimental and Computational Studies on High Strength Concrete Circular Columns Confined by Aramid Fiber-Reinforced Polymer Sheets.” *ASCE J Compos Constr.*, Vol. 13, No. 2, pp. 125–34, 2009.
- Wu H, Wang Y. “Experimental Study on High Strength Concrete Short Columns Confined with AFRP Sheets.” *Steel Compos Struct.*, Vol. 10, No. 6, pp. 501–16, 2010.
- Wu YF, Wei YY. “Effect of Cross-Sectional Aspect Ratio on the Strength of CFRP- Confined Rectangular Concrete Columns.” *Eng Struct.*, Vol. 32, No. 1, pp. 32–45, 2010.
- Xiao, Y., and Wu, H., "Compressive Behaviour of Concret Confiend by Carbon Fibre Composite Jackets." *Journal of Materials in Civil Engineering, ASCE*, Vol. 12, No. 2, pp. 139-149, May 2000.
- Xiao, Y., and Wu, H., "Compressive Behaviour of Concrete Confined by Various Types of FRP Composites Jackets." *Journal of Reinforced Plastics and Composites*, Vol. 22, No. 13, 2003.

- Xiao Q, Teng JG, Yu T. "Behavior and Modeling of Confined High Strength Concrete." *ASCE J Compos Constr.*, Vol. 14, No. 3, pp. 249–59, 2010.
- Youssef, M.N., Feng, M.Q., and Mosallam, A.S., "Stress-Strain Model For Concrete Confined by FRP Composites" *Composites: Part B*, Vol. 38, pp. 614-628, 2007.
- Yu, T., Teng, J.G., Wong, Y.L., and Dong, S.L., "Finite Element Modeling of Confined Concrete-I: Drucker-Prager type Plasticity model." *Engineering Structures*, Vol. 32, pp. 665-679, 2010.
- Yu, T., "Structural Behaviour of Hybrid FRP-Concrete-Steel Double-Skin Tubular Columns", PhD Thesis, *The Hong Kong Polytechnic University*, August, 2006.
- Yan Z, Pantelides CP. "Fiber-Reinforced Polymer Jacketed and Shape-Modified Compression Members-II: Model." *ACI Struct J.*, Vol. 103, No.6, pp. 894–903, 2006.
- Zhang, S., Ye, L., and Mai, Y. W., "A Study on Polymer Composites Strengthening Systems for Concrete Columns." *Appl. Compos. Mater.*, Vol. 7, pp. 125–138, 2000.
- Zhang DJ, Wang YF, Ma YS. "Compressive Behaviour of FRP-Confined Square Concrete Columns after Creep." *Eng Struct.*, Vol. 32, No. 8, pp. 1957–63, 2010.

## APPENDIX A: FAILURE MODES

### A.1. Group I

#### A.1.1. C37.3-CFRP1



C37.3-CFRP1-SP#1



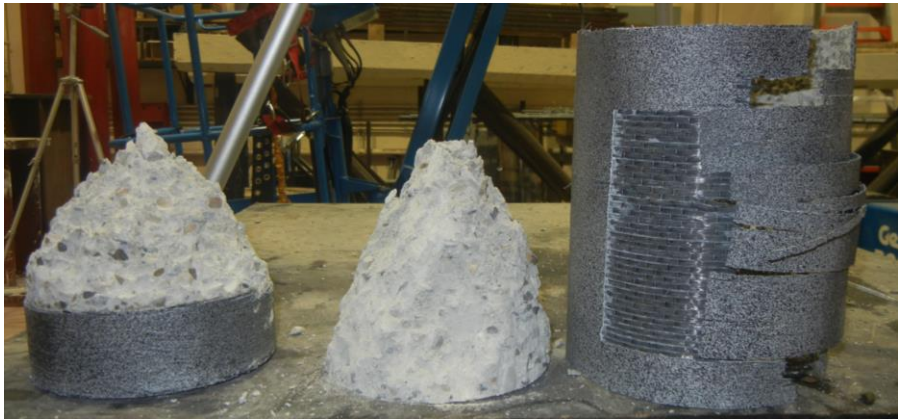
C37.3-CFRP1-SP#2



C37.3-CFRP1-SP#3

**Figure A-1: Failure modes of group I – C37.3-CFRP1**

A.1.2. C37.3-CFRP2



C37.3-CFRP2-SP#1



C37.3-CFRP2-SP#2



C37.3-CFRP2-SP#3

Figure A-2: Failure modes of group I – C37.3-CFRP2

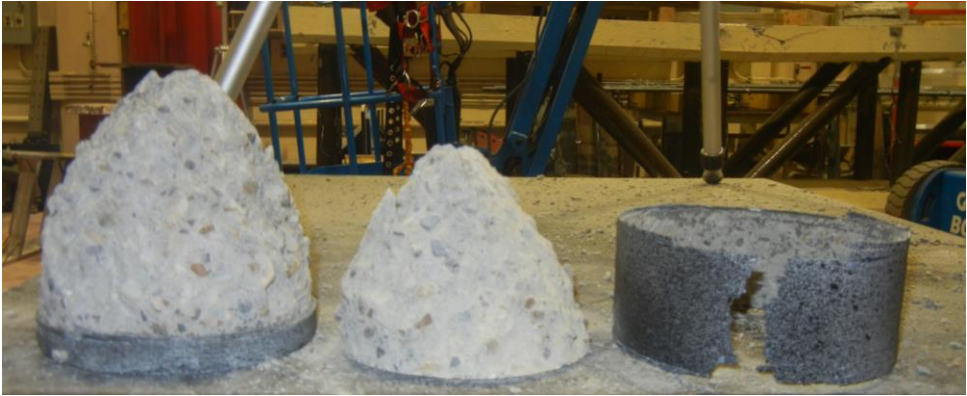
**A.1.3. C37.3-CFRP3**



**C37.3-CFRP3-SP#1**



**C37.3-CFRP3-SP#2**



**C37.3-CFRP3-SP#3**

**Figure A-3: Failure modes of group I – C37.3-CFRP3**

**A.1.4. C37.3-SFRP1**



**C37.3-SFRP1-SP#1**



**C37.3-SFRP1-SP#2**



**C37.3-SFRP1-SP#3**

**Figure A-4: Failure modes of group I – C37.3-SFRP1**

**A.1.5. C37.3-SFRP2**



**C37.3-SFRP2-SP#1**



**C37.3-SFRP2-SP#2**



**C37.3-SFRP2-SP#3**

**Figure A-5: Failure modes of group I – C37.3-SFRP2**

**A.1.6. C37.3-SFRP3**



**C37.3-SFRP3-SP#1**



**C37.3-SFRP3-SP#2**



**C37.3-SFRP3-SP#3**

**Figure A-6: Failure modes of group I – C37.3-SFRP3**

**A.2. Group II**

**A.2.1. C42.4-CFRP1**



C42.4-CFRP1-SP#1



C42.4-CFRP1-SP#2



C42.4-CFRP1-SP#3

**Figure A-7: Failure modes of group II – C42.4-CFRP1**

**A.2.2. C42.4-CFRP2**



**C42.4-CFRP2-SP#1**



**C42.4-CFRP2-SP#2**



**C42.4-CFRP2-SP#3**

**Figure A-8: Failure modes of group II – C42.4-CFRP2**

**A.2.3. C42.4-CFRP3**



**C42.4-CFRP3-SP#1**



**C42.4-CFRP3-SP#2**



**C42.4-CFRP3-SP#3**

**Figure A-9: Failure modes of group II – C42.4-CFRP3**

**A.2.4. C42.4-SFRP1**



**C42.4-SFRP1-SP#1**



**C42.4-SFRP1-SP#2**



**C42.4-SFRP1-SP#3**

**Figure A-10: Failure modes of group II – C42.4-SFRP1**

**A.2.5. C42.4-SFRP2**



**C42.4-SFRP2-SP#1**



**C42.4-SFRP2-SP#2**



**C42.4-SFRP2-SP#3**

**Figure A-11: Failure modes of group II – C42.4-SFRP2**

**A.2.6. C42.4-SFRP3**



**C42.4-SFRP3-SP#1**



**C42.4-SFRP3-SP#2**



**C42.4-SFRP3-SP#3**

**Figure A-12: Failure modes of group II – C42.4-SFRP3**

## APPENDIX B: STRESS-STRAIN CURVES

### B.1. Group I

#### B.1.1. C37.3-CFRP1

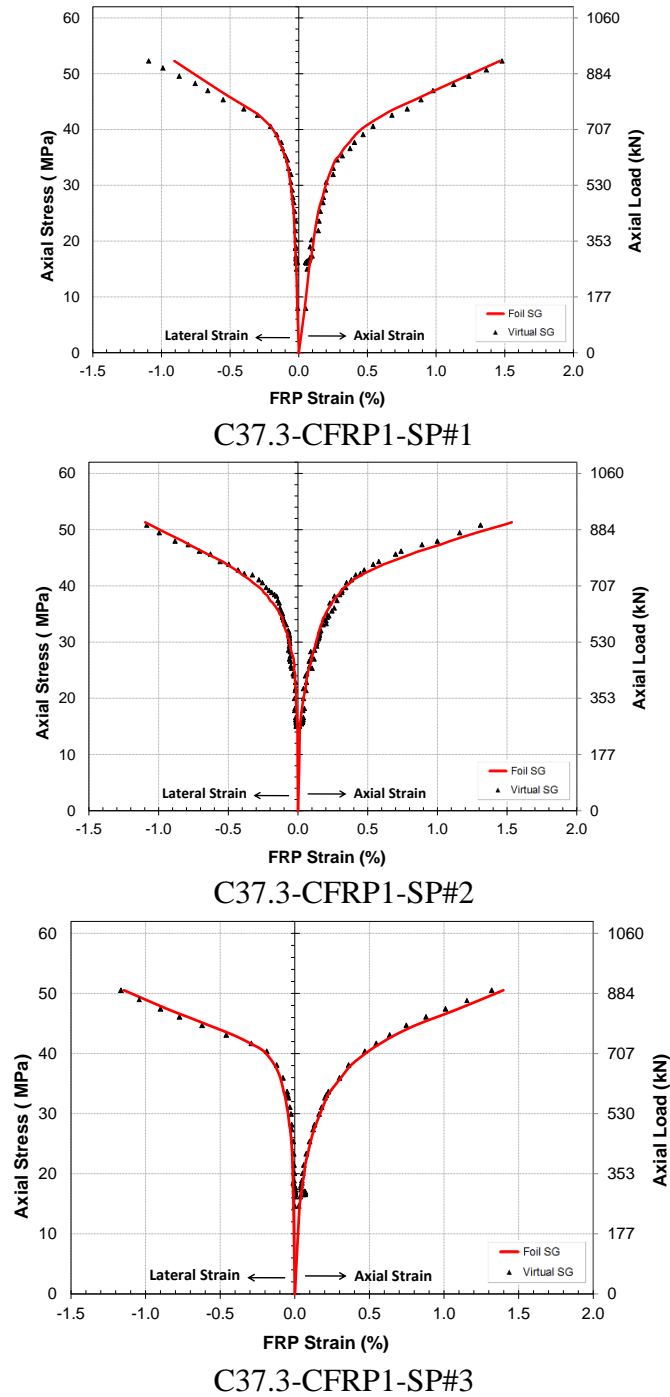
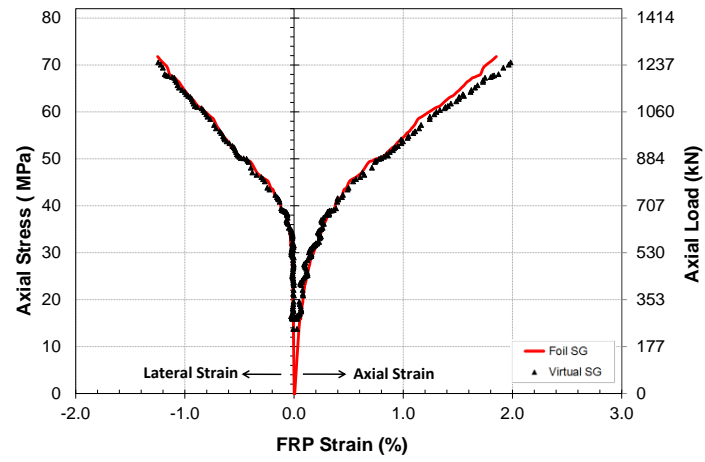
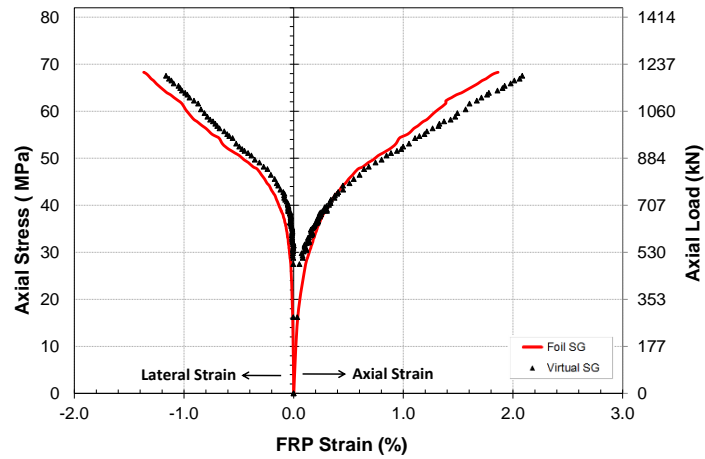


Figure B-1: Stress-strain curves for group I – C37.3-CFRP1

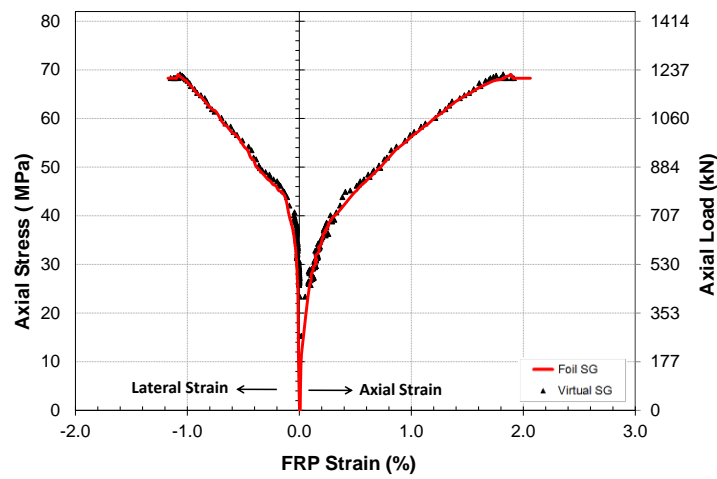
**B.1.2. C37.3-CFRP2**



**C37.3-CFRP2-SP#1**



**C37.3-CFRP2-SP#2**



**C37.3-CFRP2-SP#3**

**Figure B-2: Stress-strain curves for group I – C37.3-CFRP2**

### B.1.3. C37.3-CFRP3

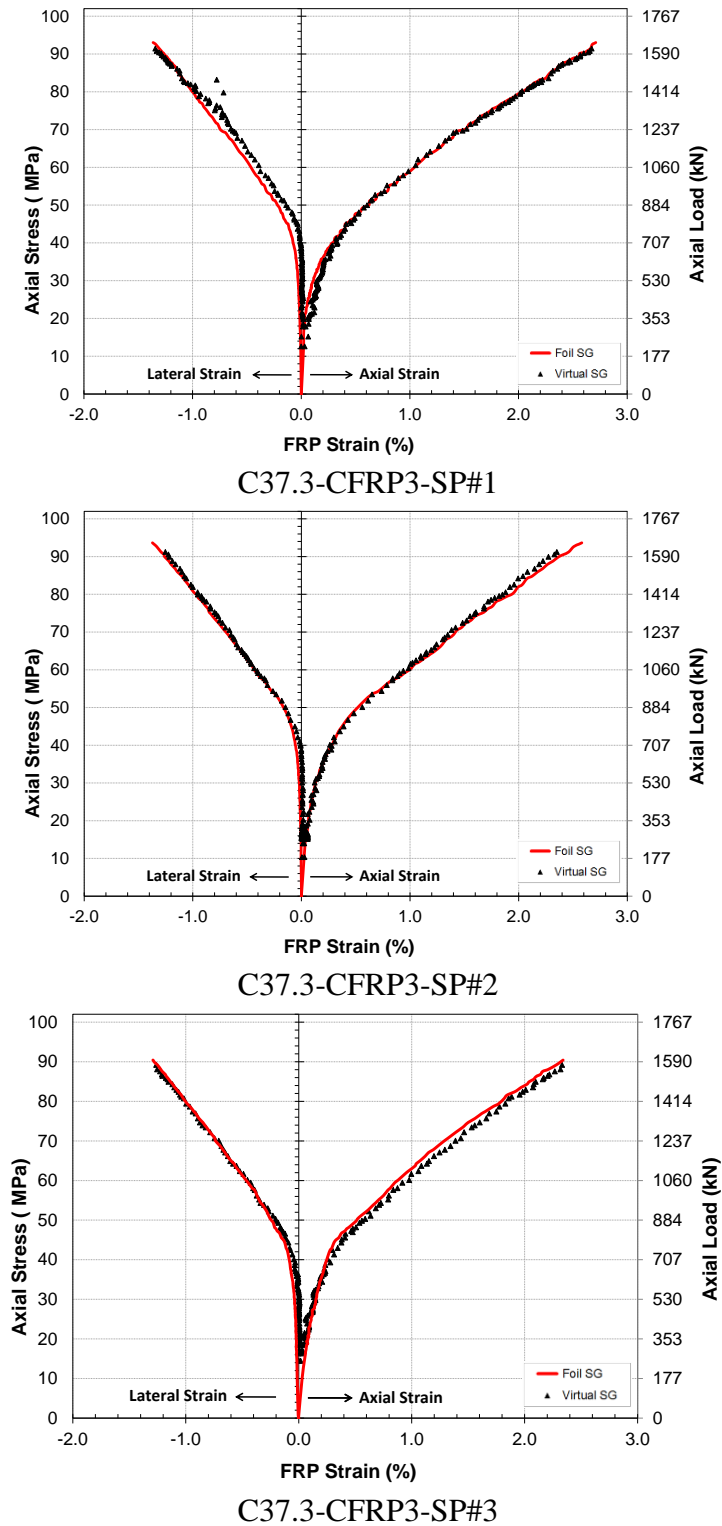
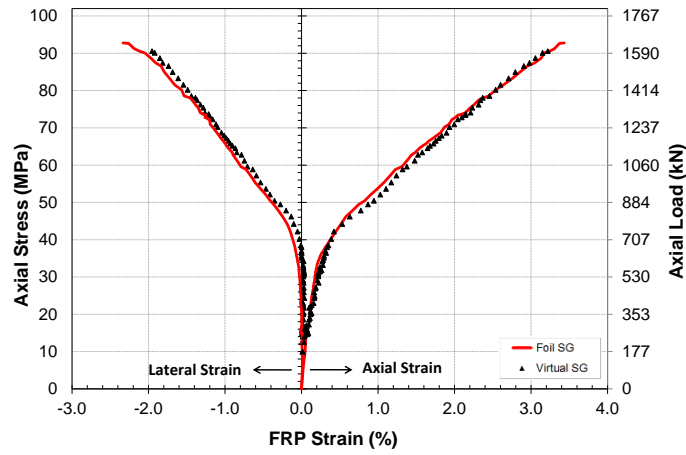
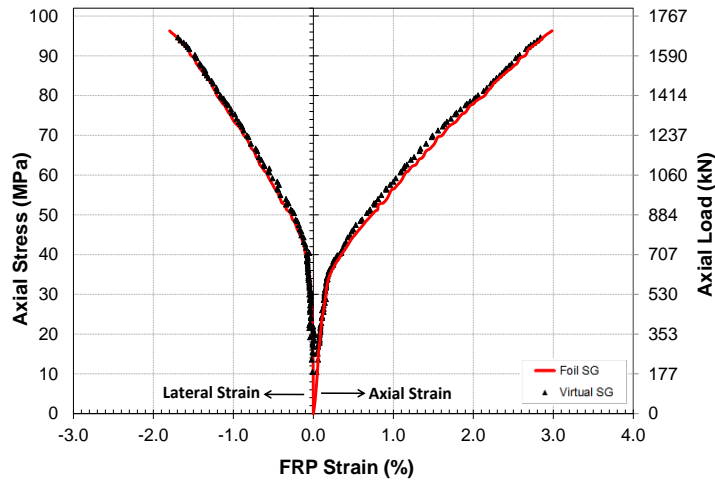


Figure B-3: Stress-strain curves for group I – C37.3-CFRP3

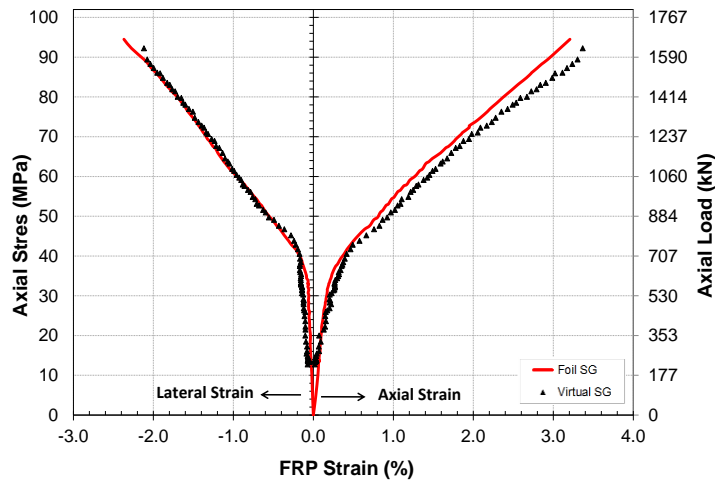
**B.1.4. C37.3-SFRP1**



**C37.3-SFRP1-SP#1**



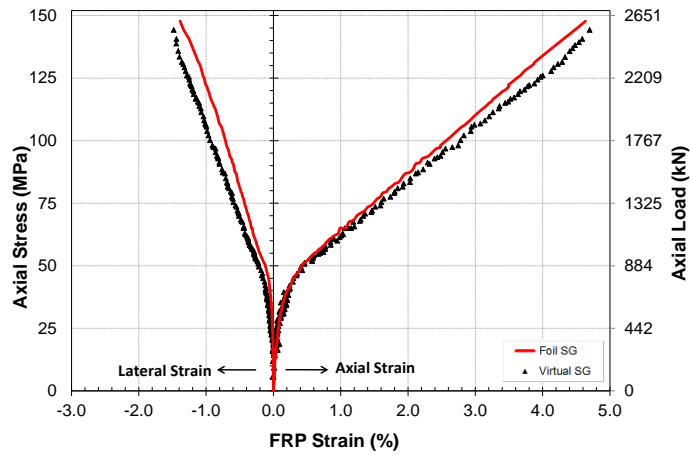
**C37.3-SFRP1-SP#2**



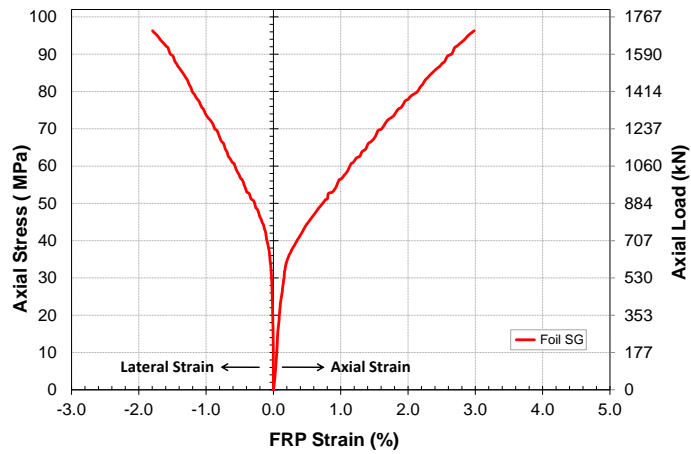
**C37.3-SFRP1-SP#3**

**Figure B-4: Stress-strain curves for group I – C37.3-SFRP1**

**B.1.5. C37.3-SFRP2**

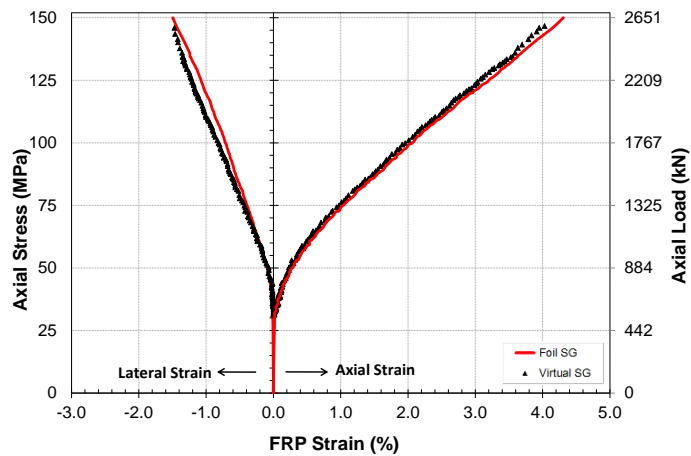


**C37.3-SFRP2-SP#1**



**C37.3-SFRP2-SP#2\***

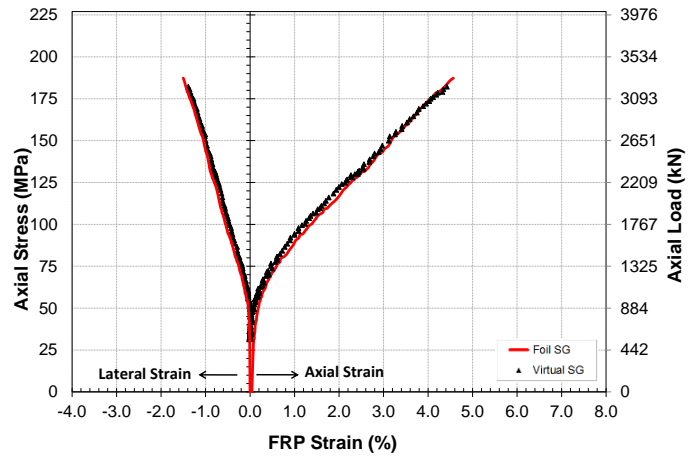
\* DIC results were lost due to a technical error



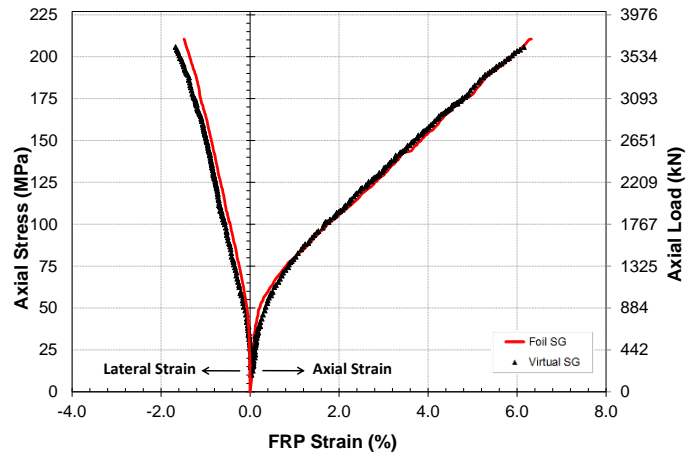
**C37.3-SFRP2-SP#3**

**Figure B-5: Stress-strain curves for group I – C37.3-SFRP2**

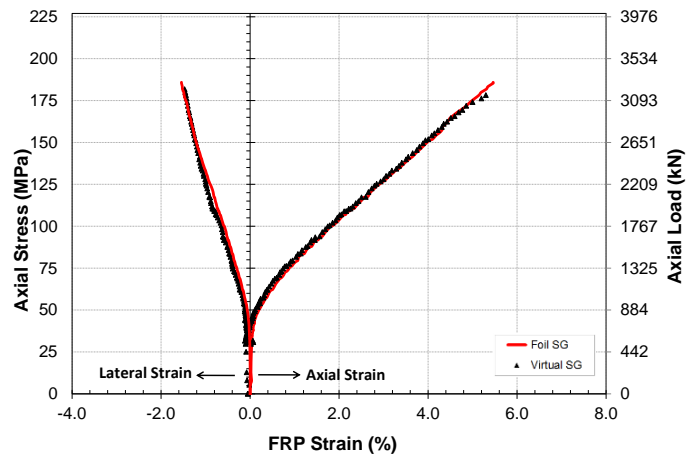
**B.1.6. C37.3-SFRP3**



**C37.3-SFRP3-SP#1**



**C37.3-SFRP3-SP#2**



**C37.3-SFRP3-SP#3**

**Figure B-6: Stress-strain curves for group I – C37.3-SFRP3**

## B.2. Group II

### B.2.1. C42.4-CFRP1

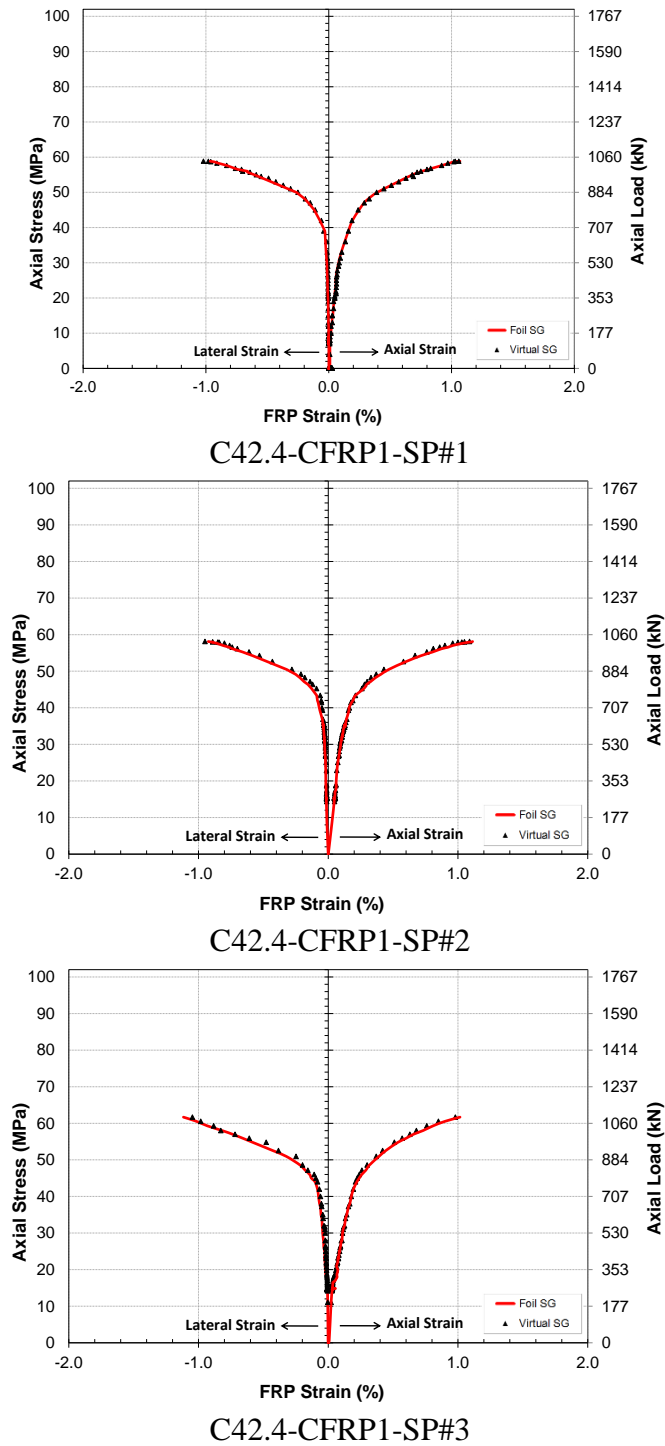
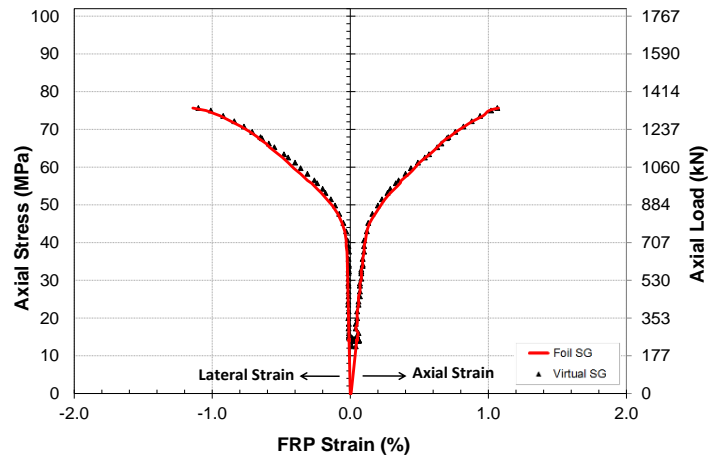
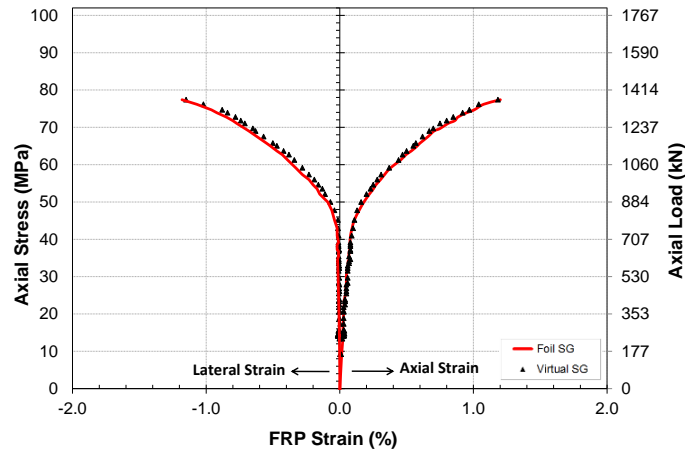


Figure B-7: Stress-strain curves for group II – C42.4-CFRP1

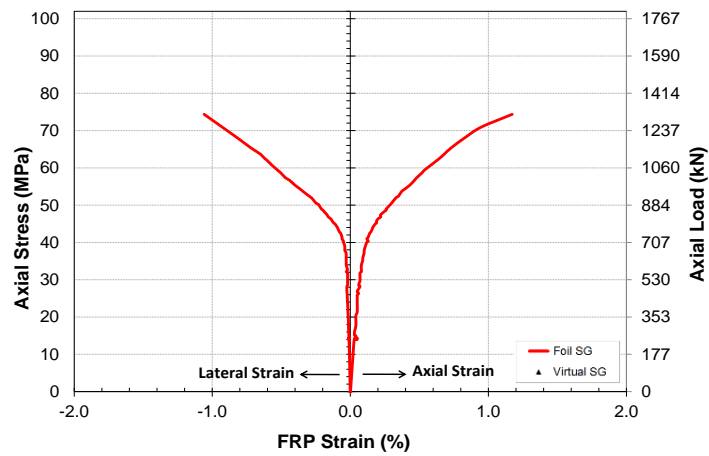
B.2.2. C42.4-CFRP2



C42.4-CFRP2-SP#1



C42.4-CFRP2-SP#2

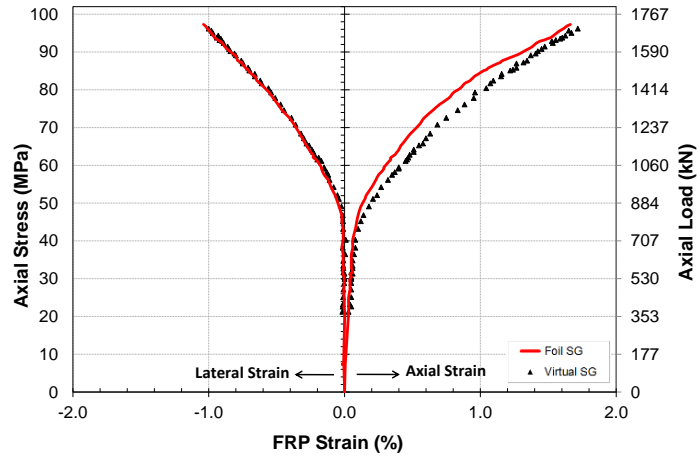


C42.4-CFRP2-SP#3\*

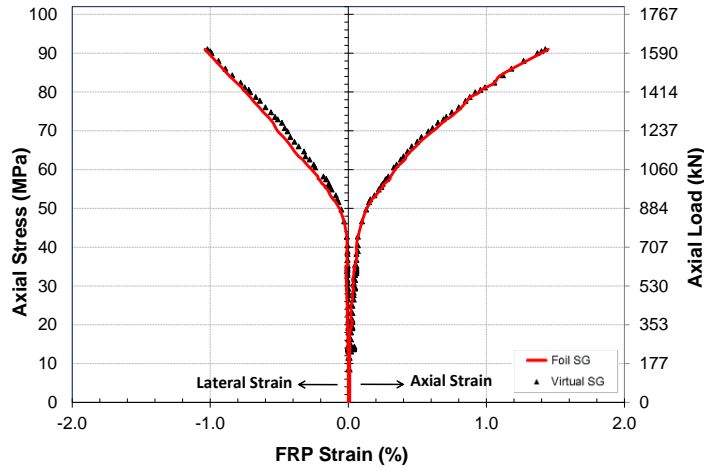
\* DIC results were lost due to a technical error

Figure B-8: Stress-strain curves for group II – C42.4-CFRP2

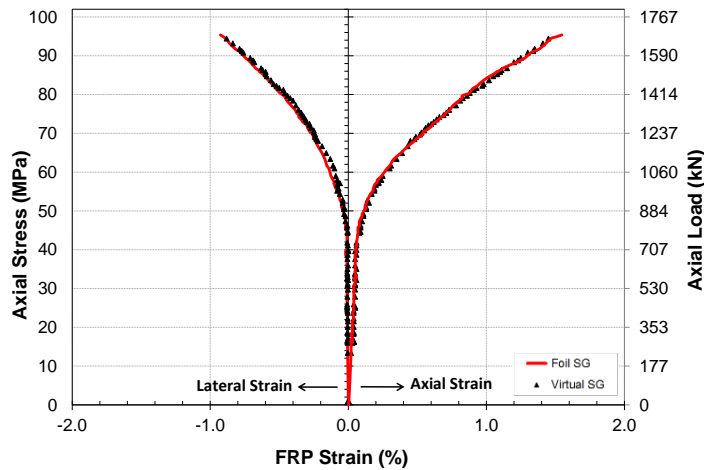
B.2.3. C42.4-CFRP3



C42.4-CFRP3-SP#1



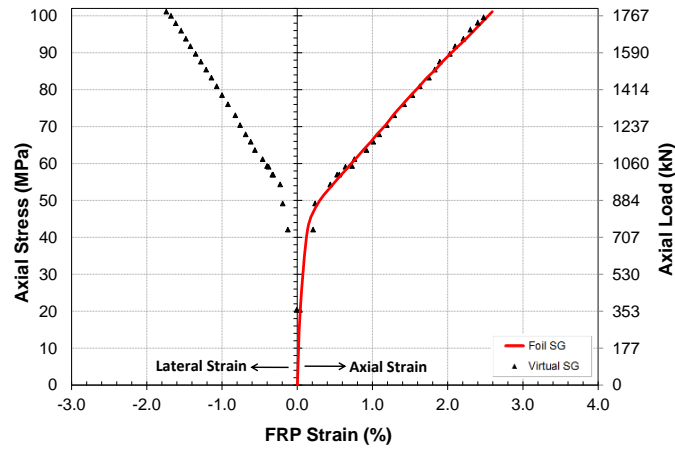
C42.4-CFRP3-SP#2



C42.4-CFRP3-SP#3

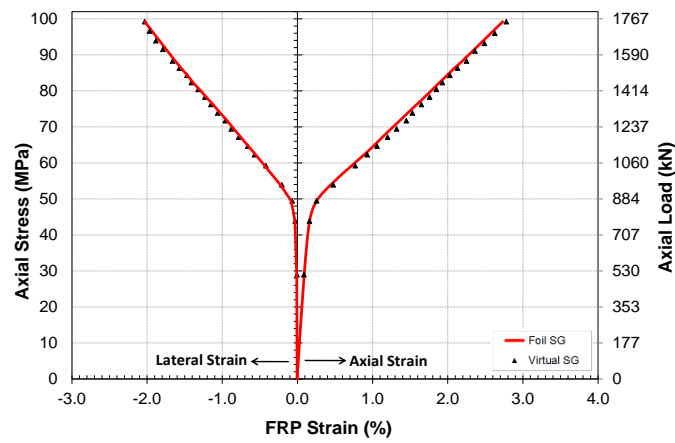
Figure B-9: Stress-strain curves for group II – C42.4-CFRP3

**B.2.4. C42.4-SFRP1**

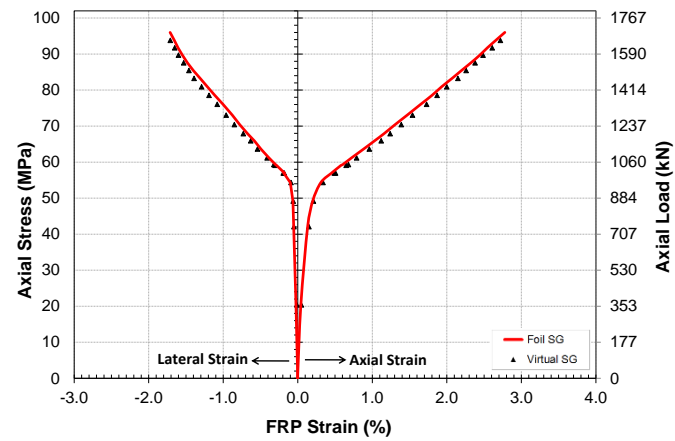


**C42.4-SFRP1-SP#1\***

\* Lateral strain gauge was detached during testing



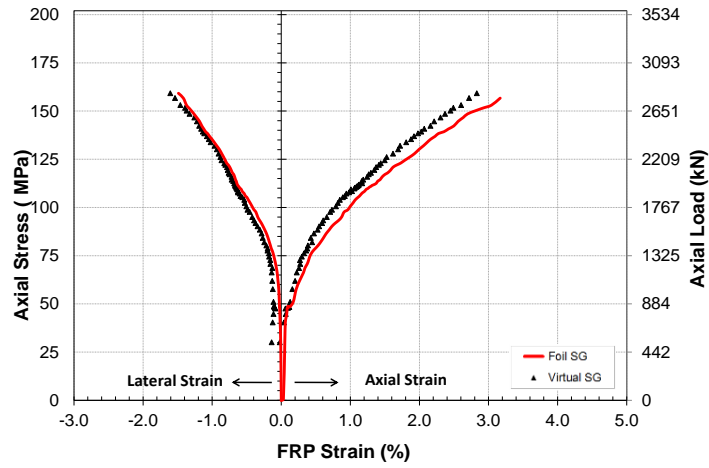
**C42.4-SFRP1-SP#2**



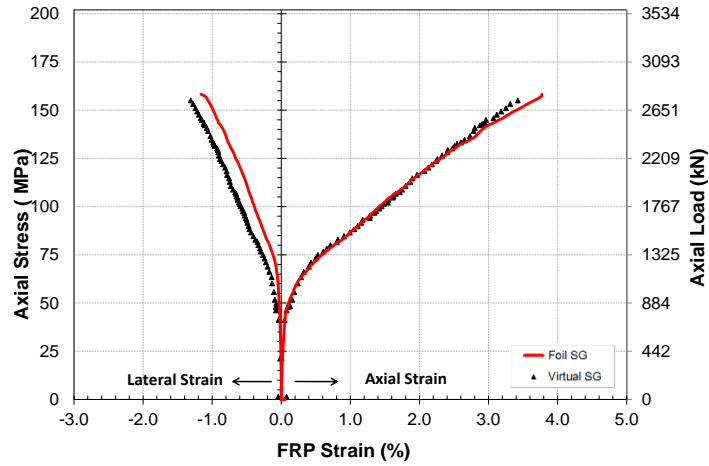
**C42.4-SFRP1-SP#3**

**Figure B-10: Stress-strain curves for group II – C42.4-SFRP1**

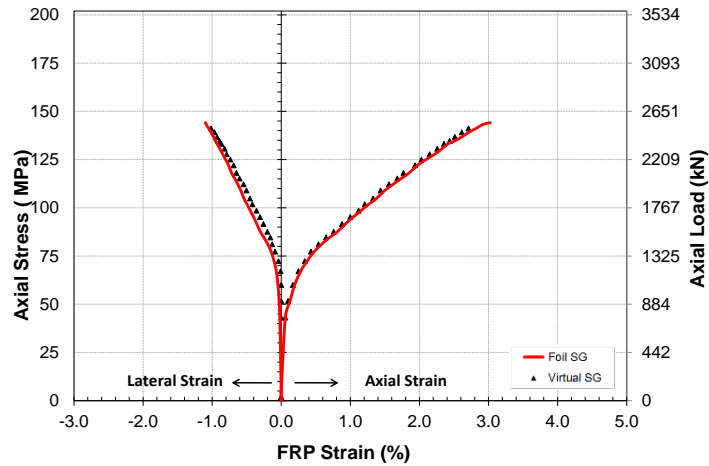
**B.2.5. C42.4-SFRP2**



**C42.4-SFRP2-SP#1**



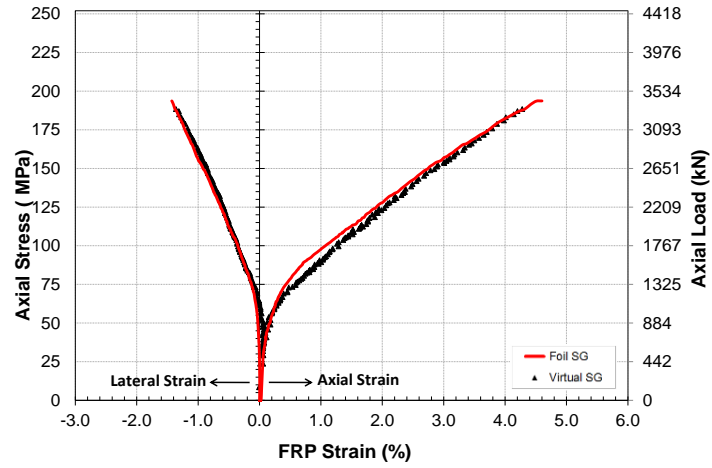
**C42.4-SFRP2-SP#2**



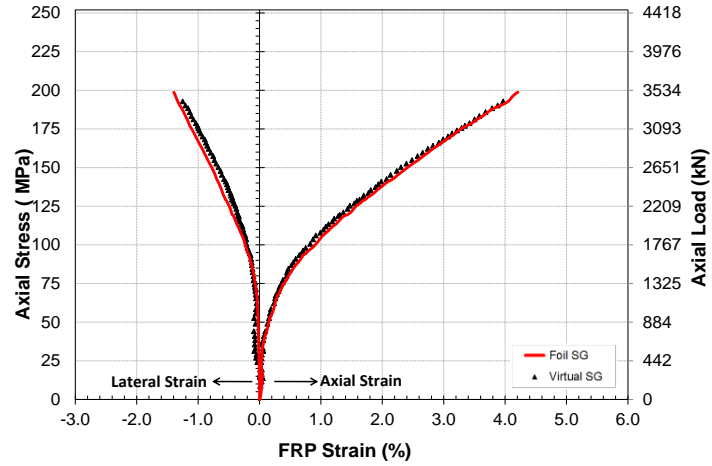
**C42.4-SFRP2-SP#3**

**Figure B-11: Stress-strain curves for group II – C42.4-SFRP2**

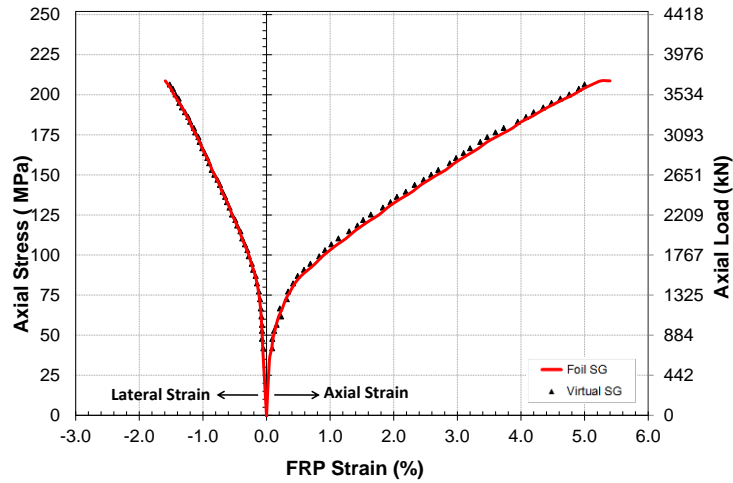
**B.2.6. C42.4-SFRP3**



**C42.4-SFRP3-SP#1**



**C42.4-SFRP3-SP#2**



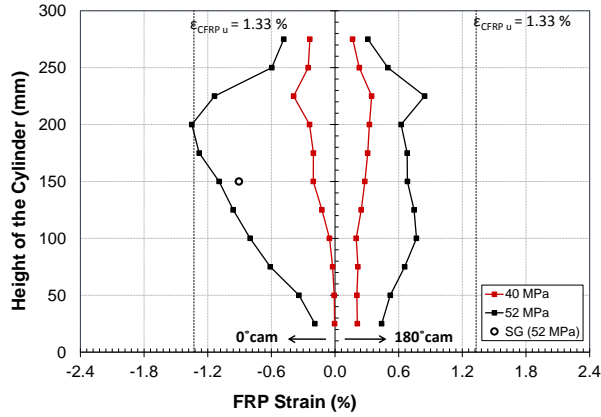
**C42.4-SFRP3-SP#3**

**Figure B-12: Stress-strain curves for group II – C42.4-SFRP3**

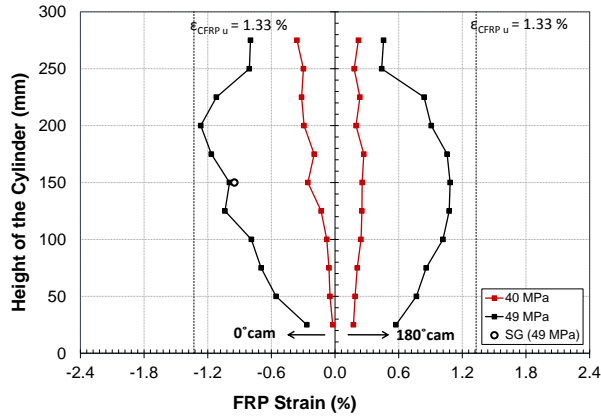
## APPENDIX C: LATERAL STRAIN PROFILE EVOLUTION

### C.1. Group I

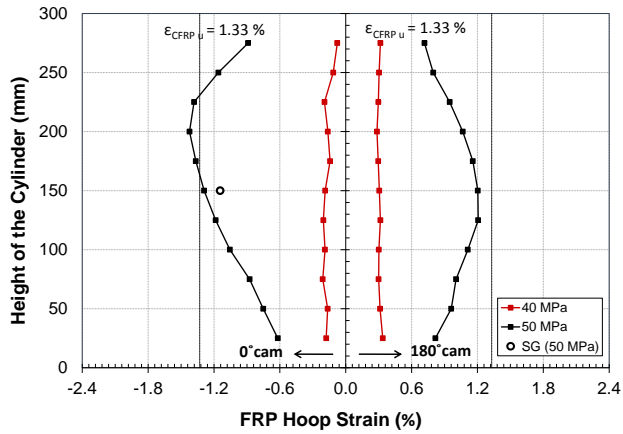
#### C.1.1. C37.3-CFRP1



**C37.3-CFRP1-SP#1**



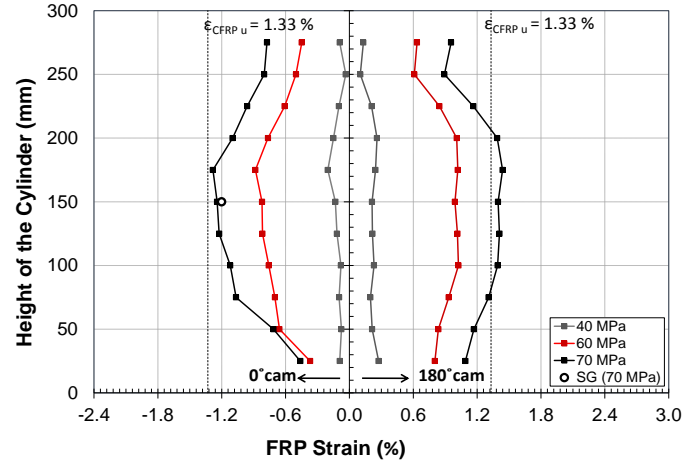
**C37.3-CFRP1-SP#2**



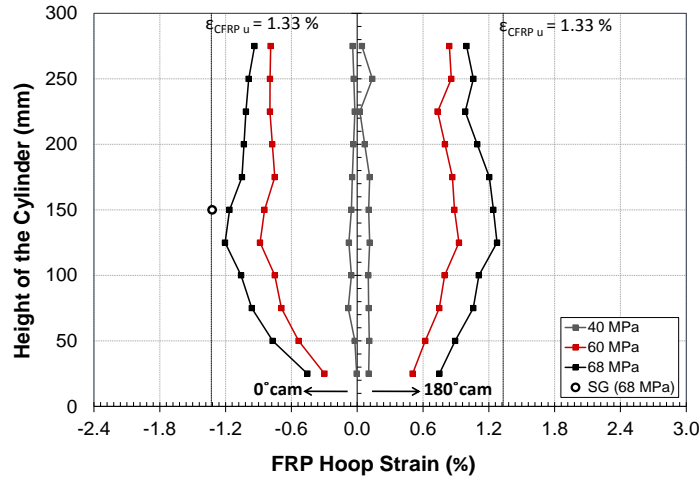
**C37.3-CFRP1-SP#3**

**Figure C-1: Lateral strain profiles for group I – C37.3-CFRP1**

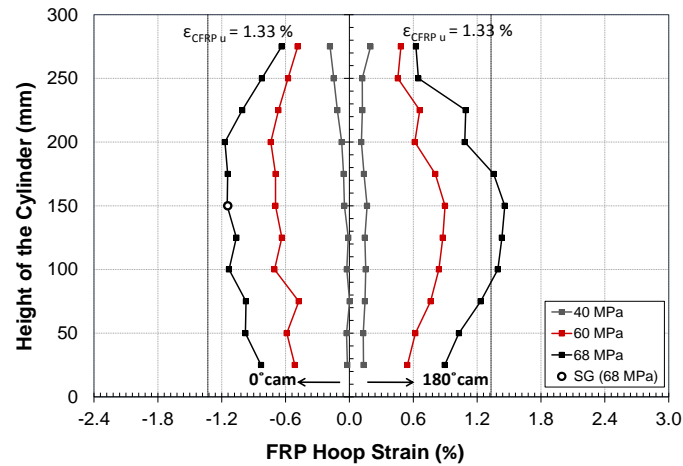
C.1.2. C37.3-CFRP2



C37.3-CFRP2-SP#1



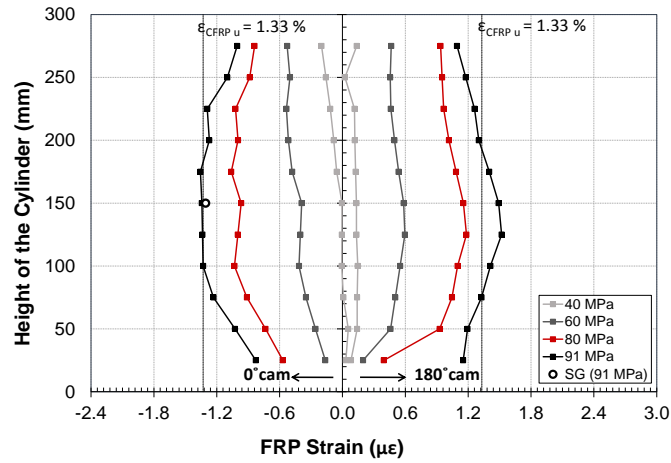
C37.3-CFRP2-SP#2



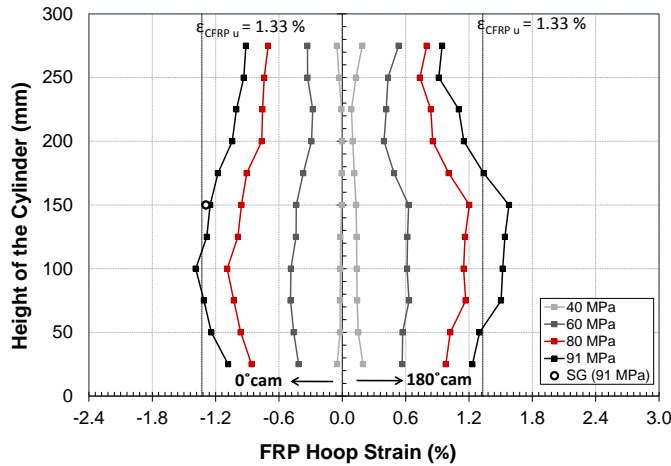
C37.3-CFRP2-SP#3

Figure C-2: Lateral strain profiles for group I – C37.3-CFRP2

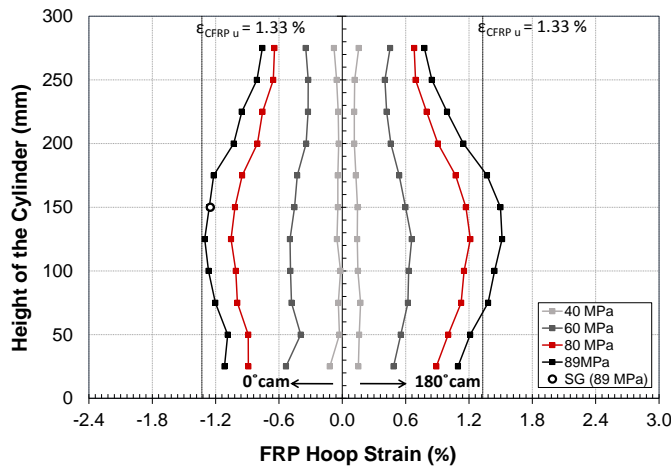
C.1.3. C37.3-CFRP3



C37.3-CFRP3-SP#1



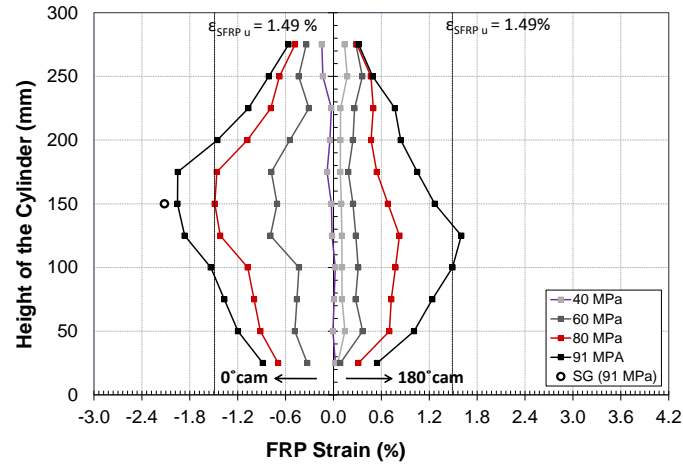
C37.3-CFRP3-SP#2



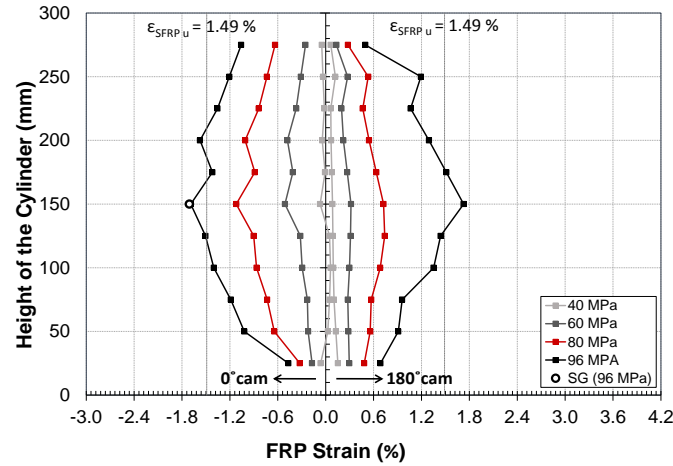
C37.3-CFRP3-SP#3

Figure C-3: Lateral strain profiles for group I – C37.3-CFRP3

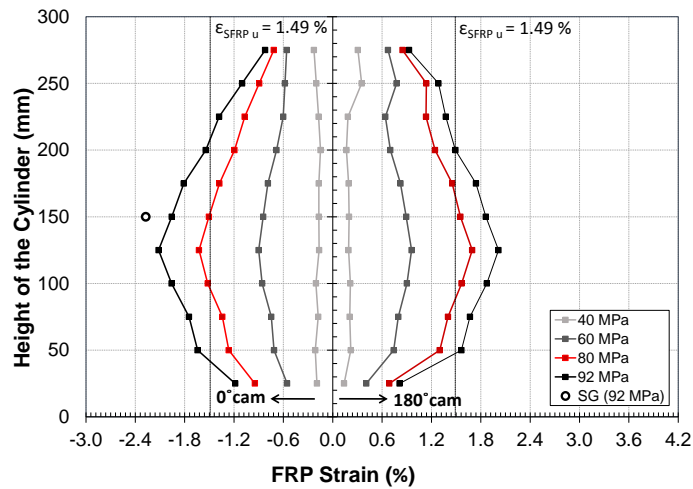
C.1.4. C37.3-SFRP1



C37.3-SFRP1-SP#1



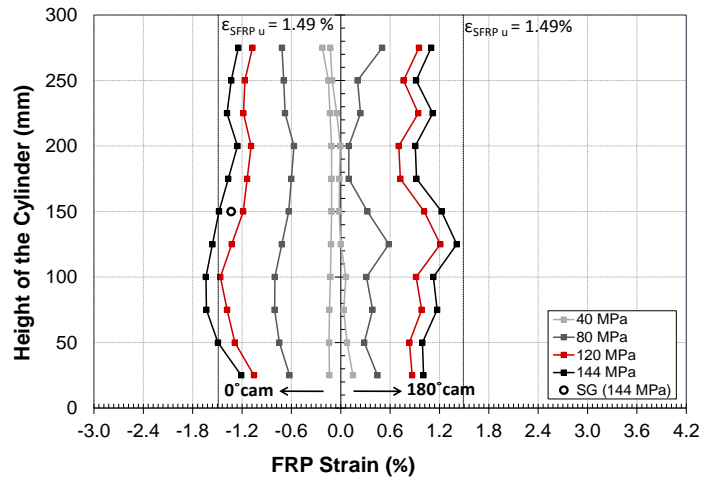
C37.3-SFRP1-SP#2



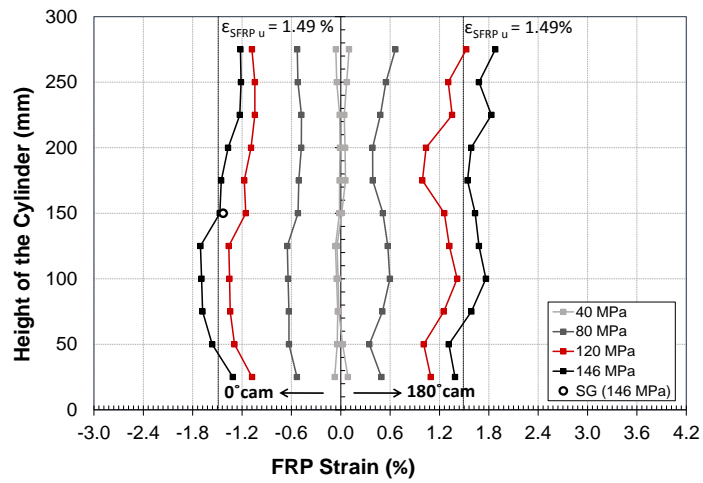
C37.3-SFRP1-SP#3

Figure C-4: Lateral strain profiles for group I – C37.3-SFRP1

**C.1.5. C37.3-SFRP2**



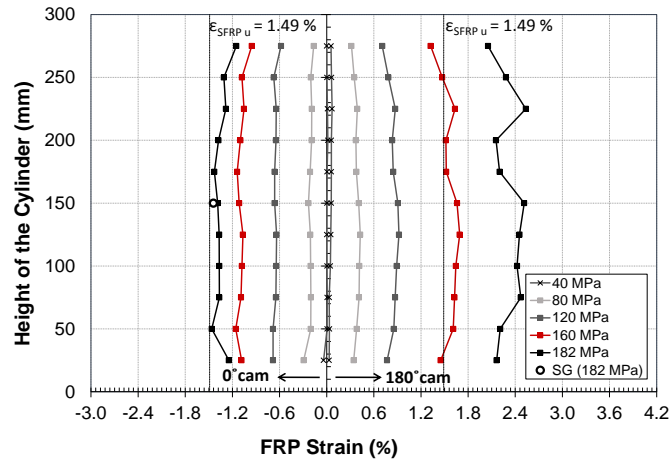
**C37.3-SFRP2-SP#1**



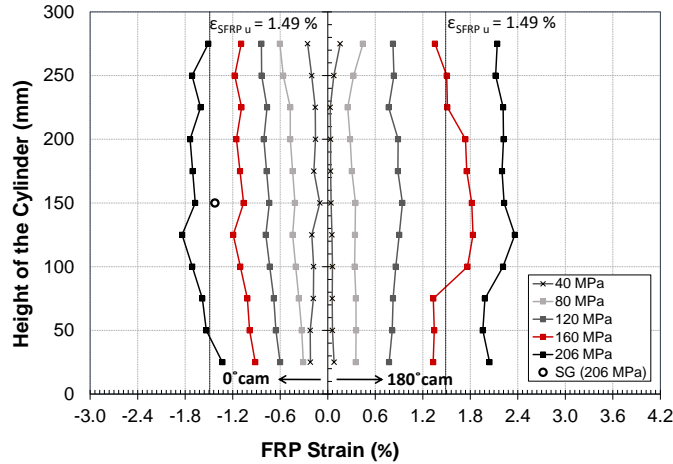
**C37.3-SFRP2-SP#3**

**Figure C-5: Lateral strain profiles for group I – C37.3-SFRP2**

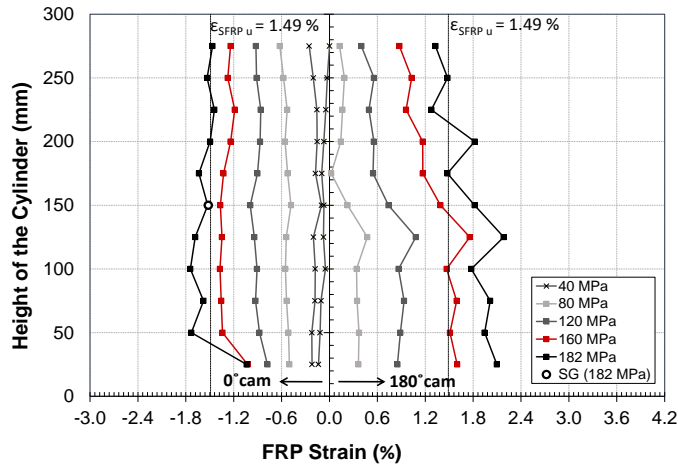
C.1.6. C37.3-SFRP3



C37.3-SFRP3-SP#1



C37.3-SFRP3-SP#2

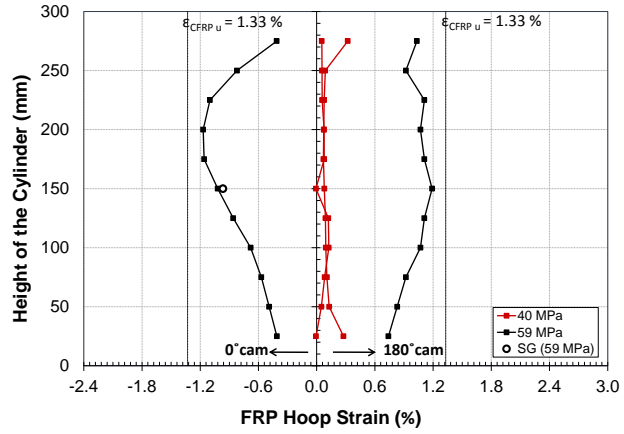


C37.3-SFRP3-SP#3

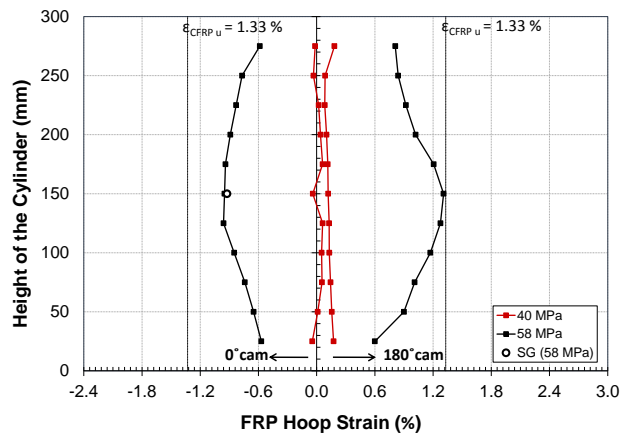
Figure C-6: Lateral strain profiles for group I – C37.3-SFRP3

## C.2. Group II

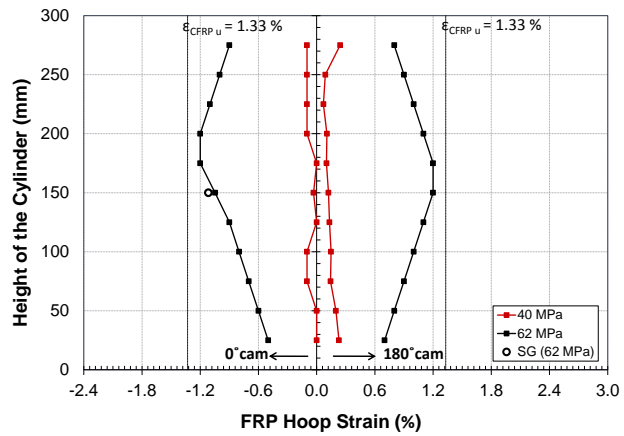
### C.2.1. C42.4-CFRP1



C42.4-CFRP1-SP#1



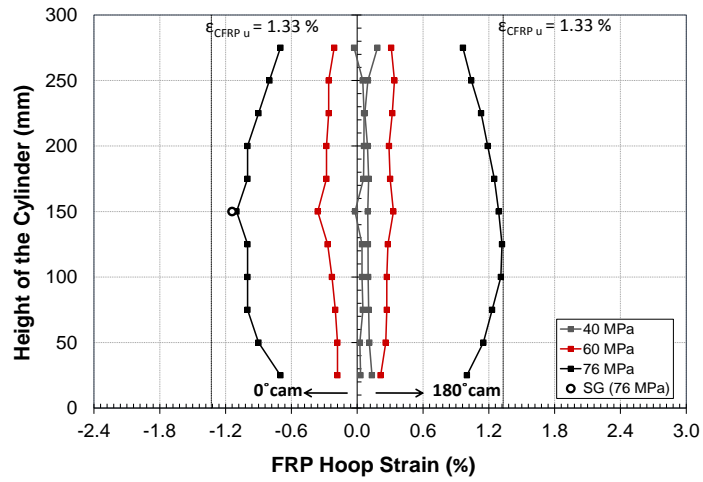
C42.4-CFRP1-SP#2



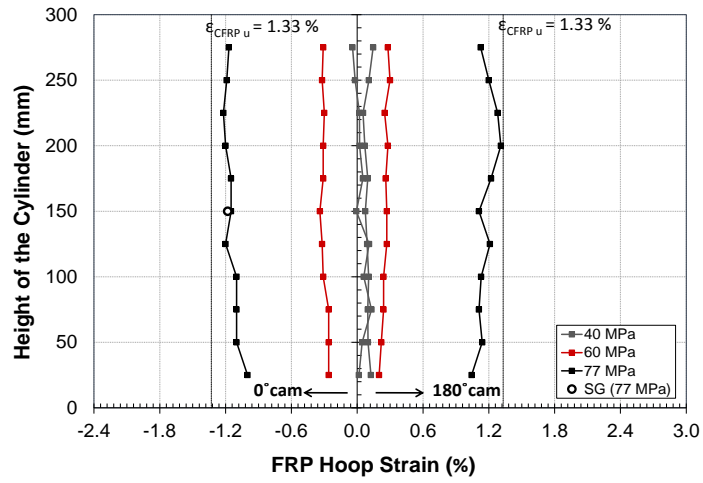
C42.4-CFRP1-SP#3

Figure C-7: Lateral strain profiles for group II – C42.4-CFRP1

C.2.2. C42.4-CFRP2



C42.4-CFRP2-SP#1



C42.4-CFRP2-SP#2

Figure C-8: Lateral strain profiles for group II – C42.4-CFRP2

C.2.3. C42.4-CFRP3

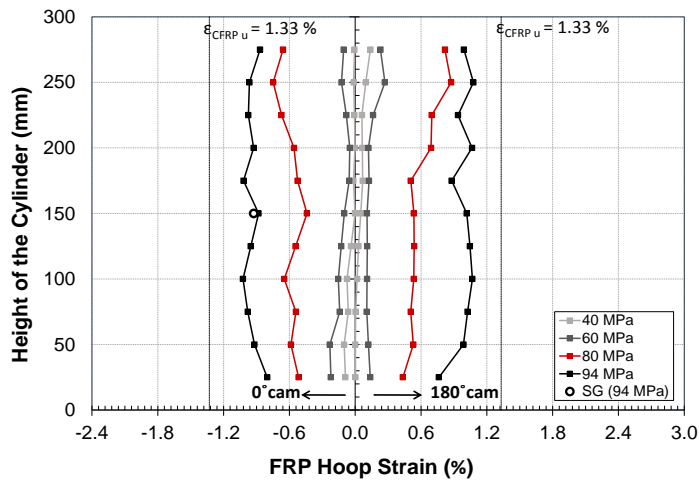
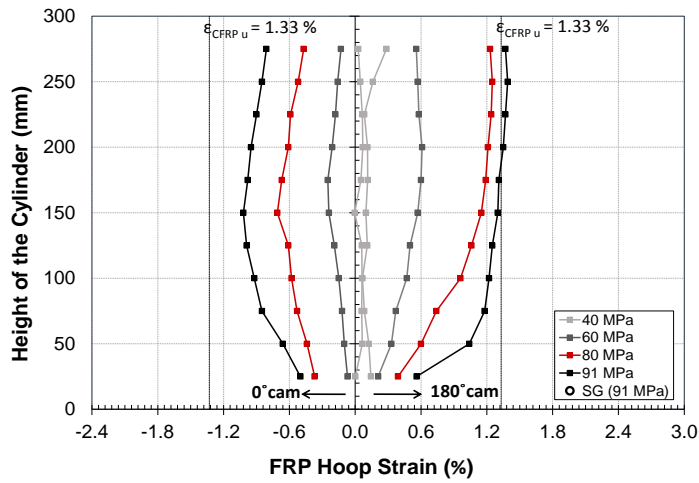
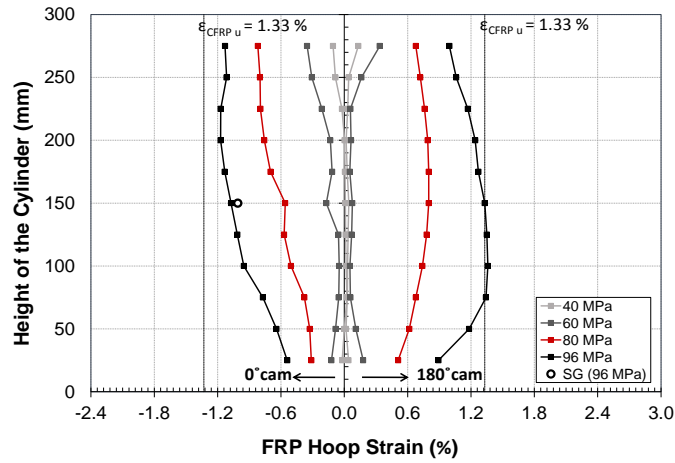
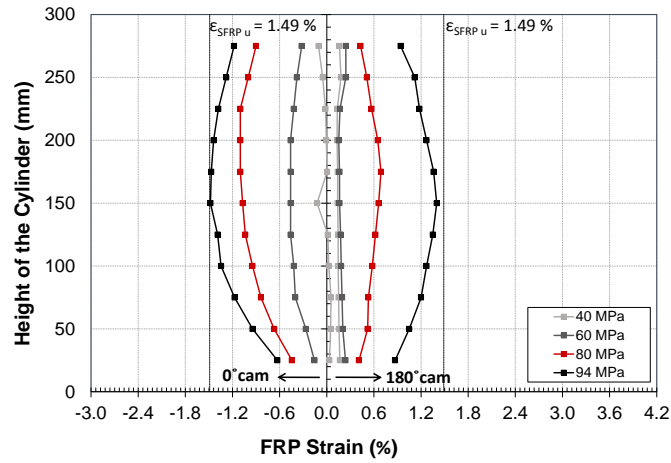
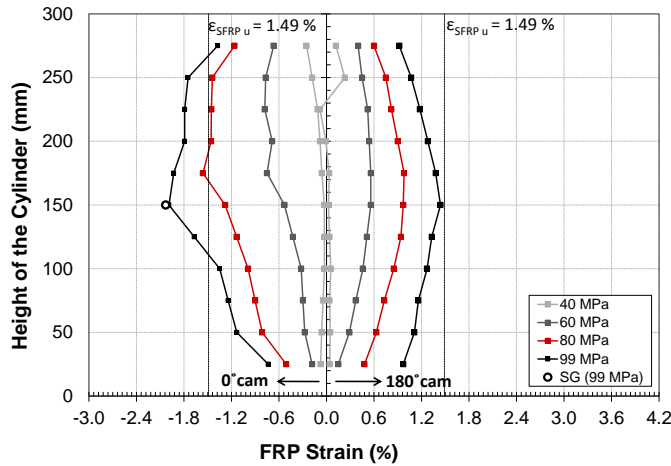


**Figure C-9: Lateral strain profiles for group II – C42.4-CFRP3**

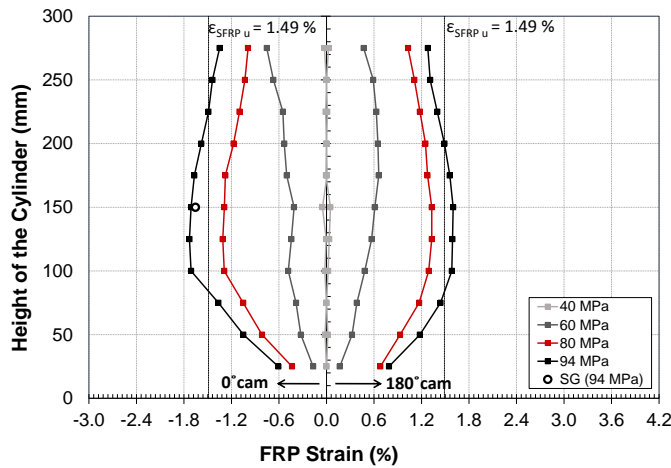
C.2.4. C42.4-SFRP1



C42.4-SFRP1-SP#1



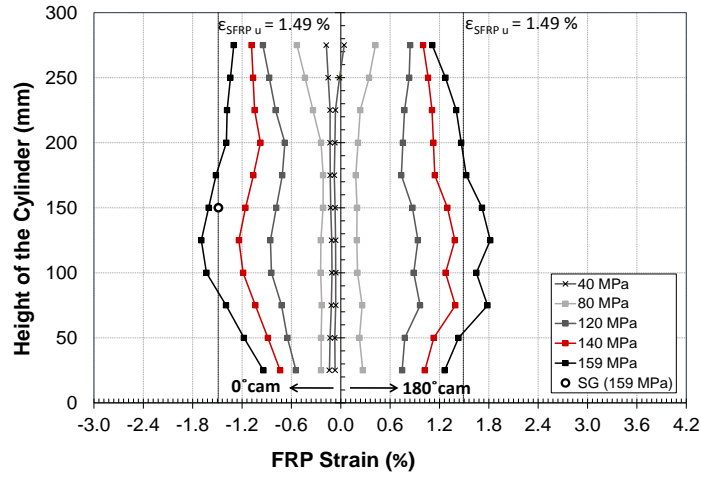
C42.4-SFRP1-SP#2



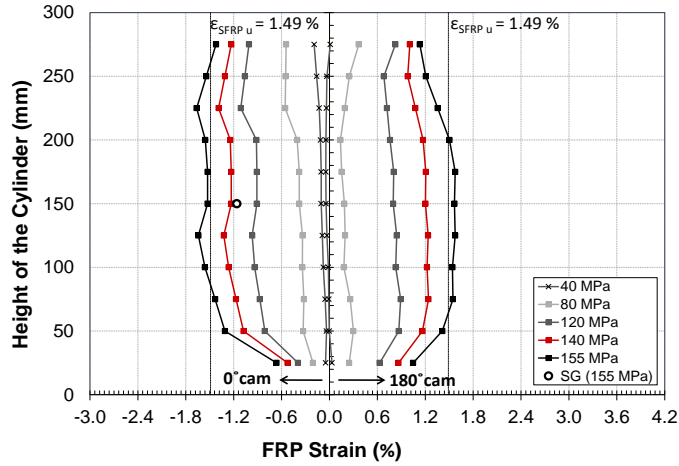
C42.4-SFRP1-SP#3

Figure C-10: Lateral strain profiles for group II – C42.4-SFRP1

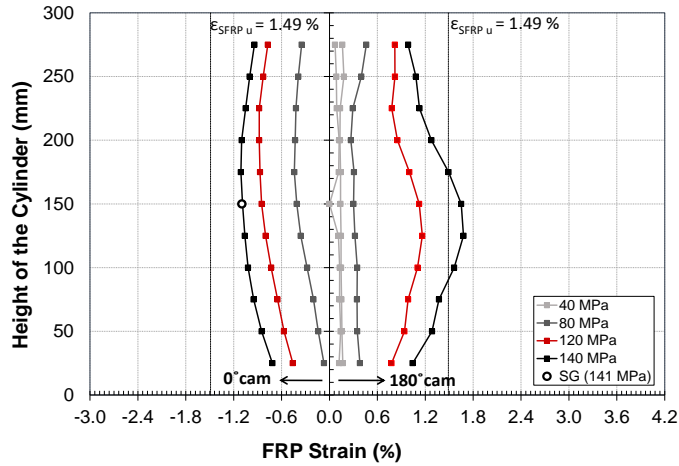
C.2.5. C42.4-SFRP2



C42.4-SFRP2-SP#1



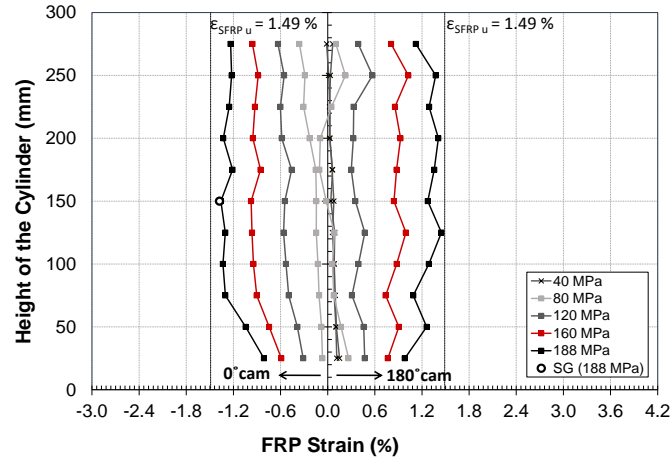
C42.4-SFRP2-SP#2



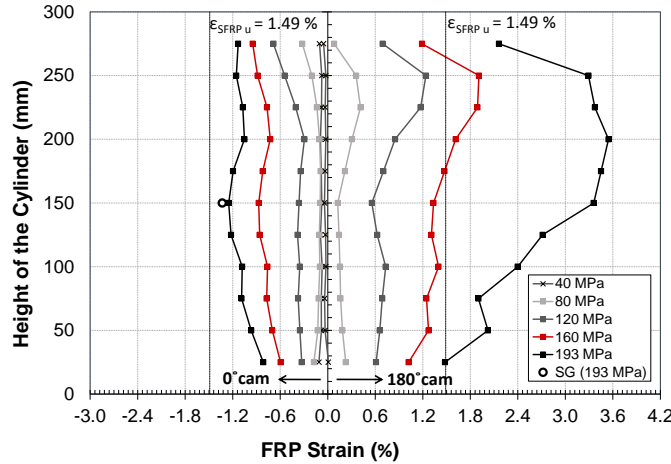
C42.4-SFRP2-SP#3

Figure C-11: Lateral strain profiles for group II – C42.4-SFRP2

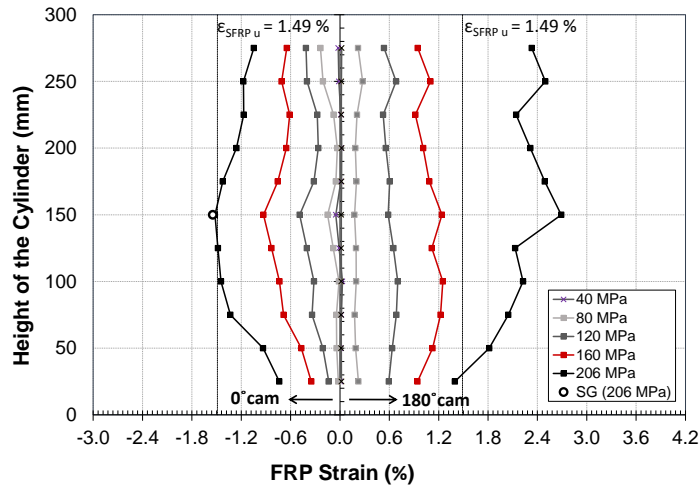
C.2.6. C42.4-SFRP3



C42.4-SFRP3-SP#1



C42.4-SFRP3-SP#2



C42.4-SFRP3-SP#3

Figure C-12: Lateral strain profiles for group II – C42.4-SFRP3

## APPENDIX D: AXIAL AND LATERAL STRAIN DISTRIBUTION AT FAILURE

### D.1. Group I

#### D.1.1. C37.3-CFRP1

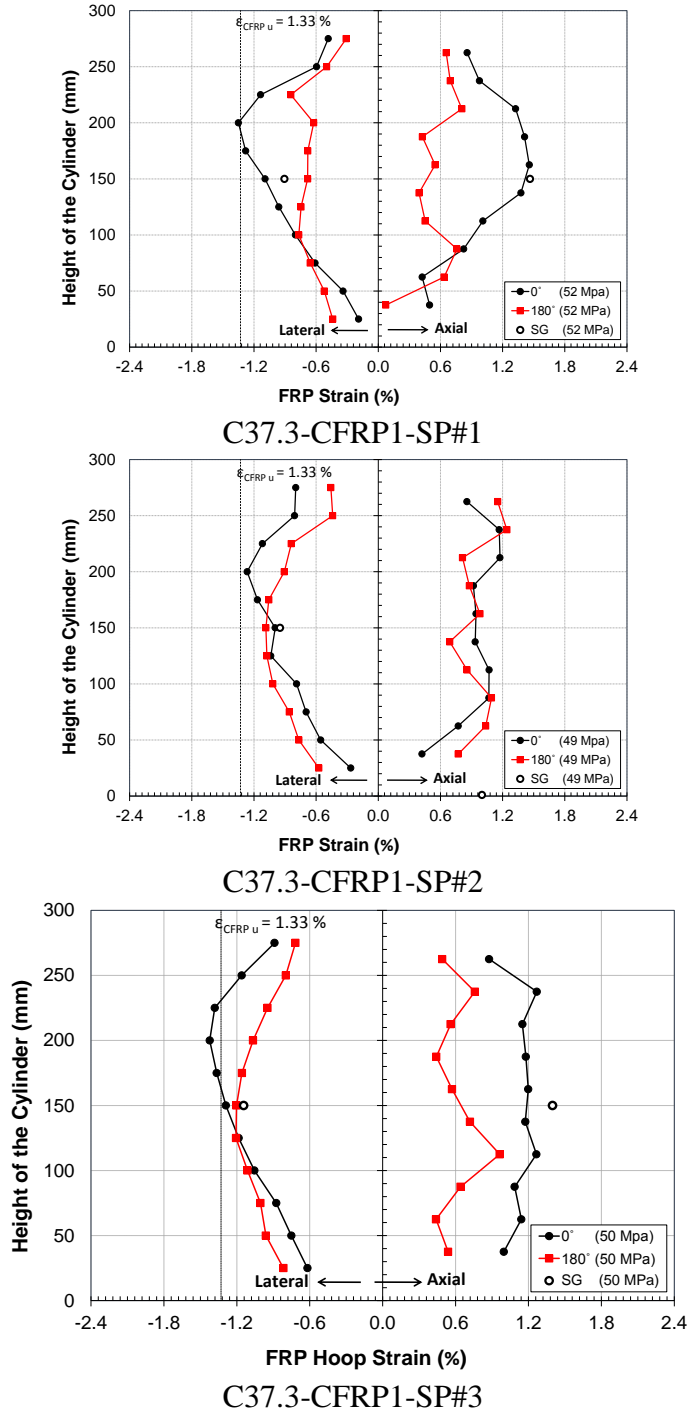
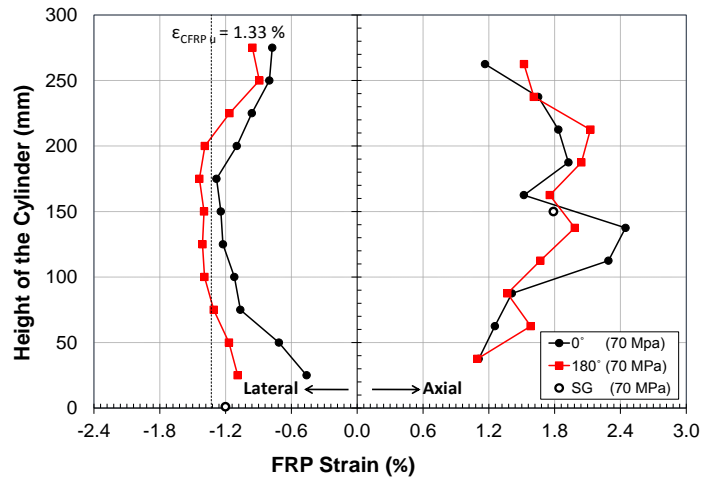
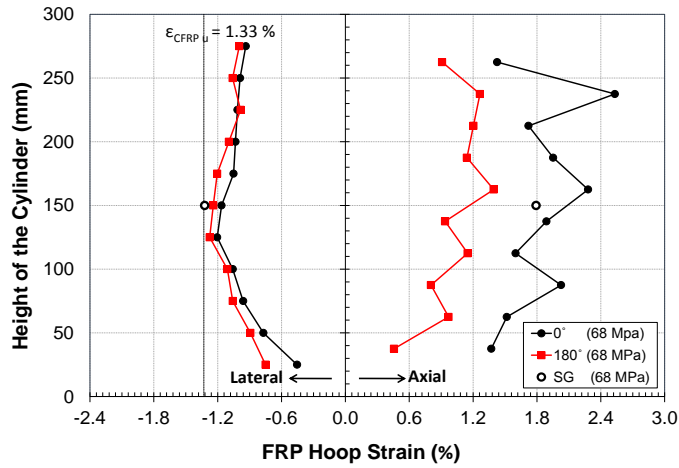


Figure D-1: Axial and lateral strain at failure distribution for Group I – C37.3-CFRP1

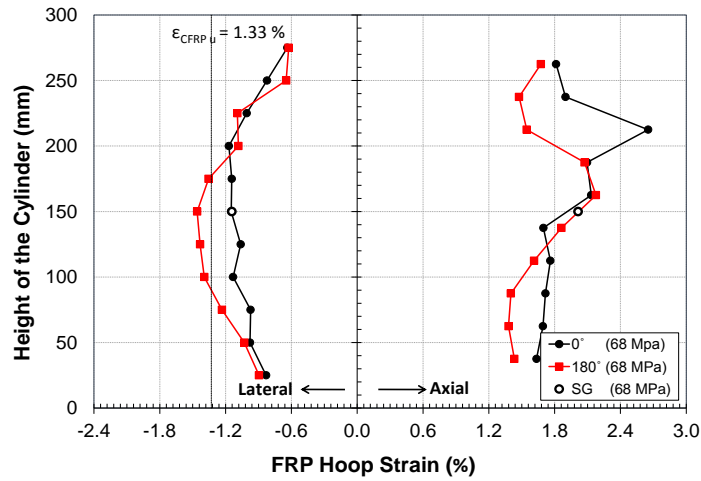
D.1.2. C37.3-CFRP2



C37.3-CFRP2-SP#1



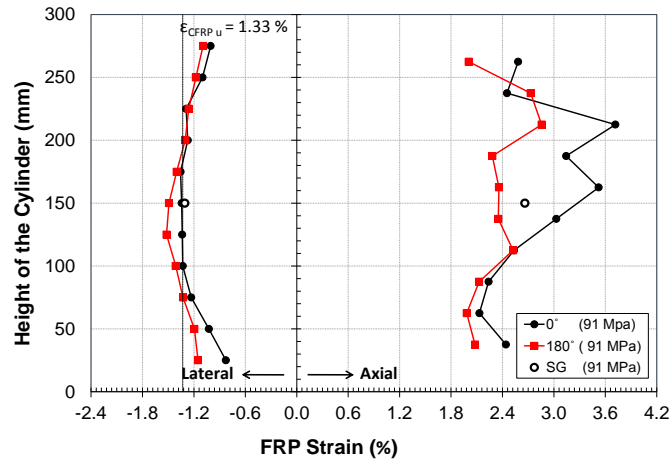
C37.3-CFRP2-SP#2



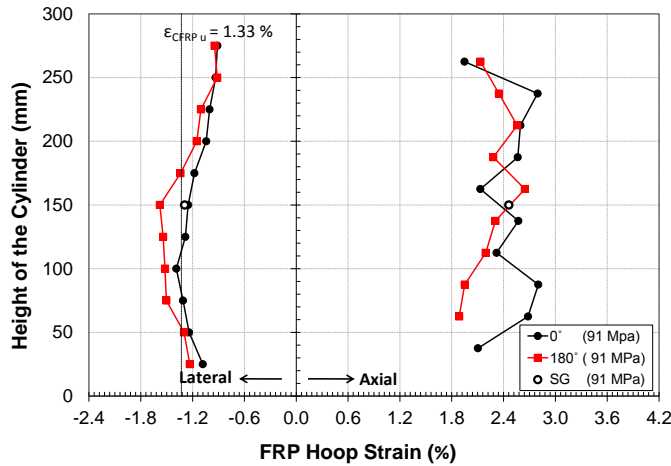
C37.3-CFRP2-SP#3

Figure D-2: Axial and lateral strain at failure distribution for Group I – C37.3-CFRP2

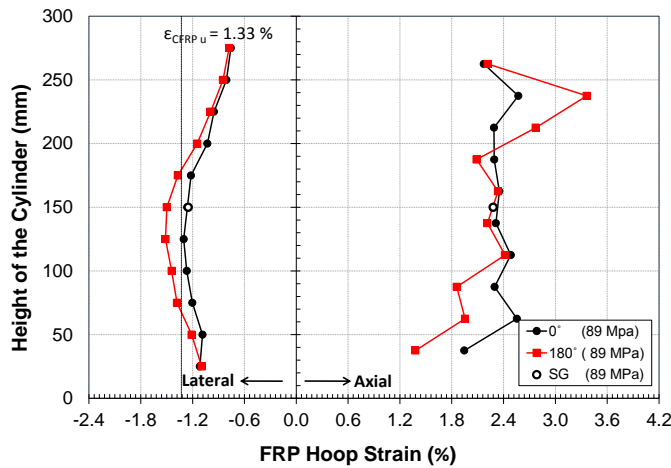
D.1.3. C37.3-CFRP3



C37.3-CFRP3-SP#1



C37.3-CFRP3-SP#2



C37.3-CFRP3-SP#3

Figure D-3: Axial and lateral strain at failure distribution for Group I – C37.3-CFRP3

**D.1.4. C37.3-SFRP1**

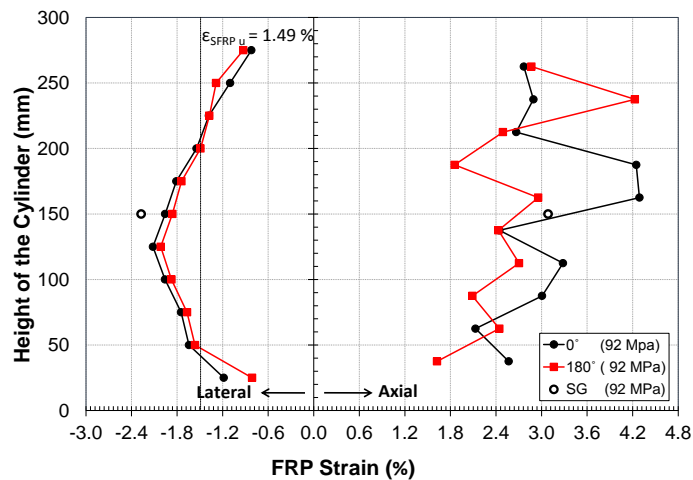
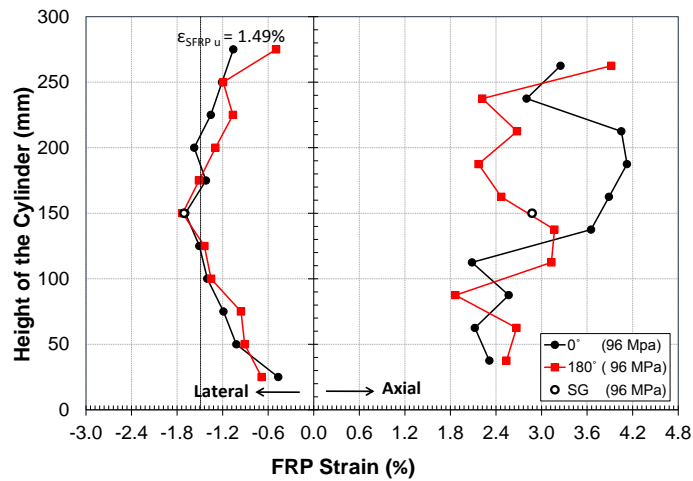
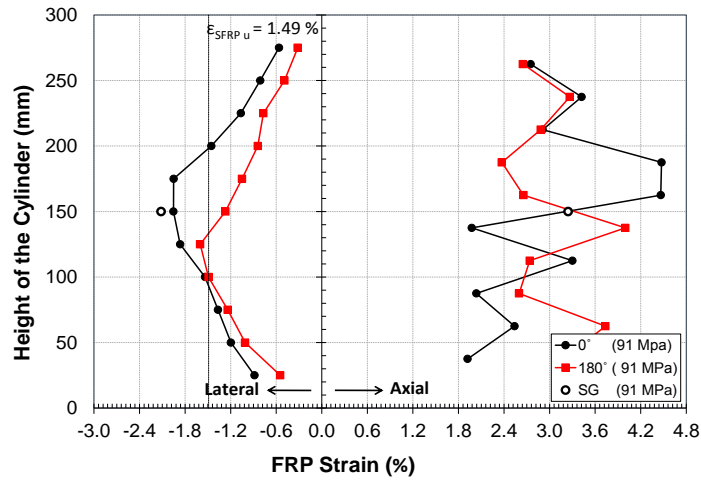
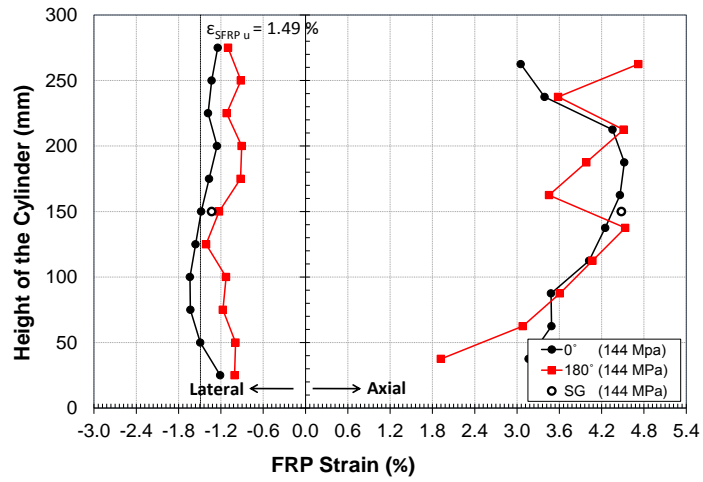
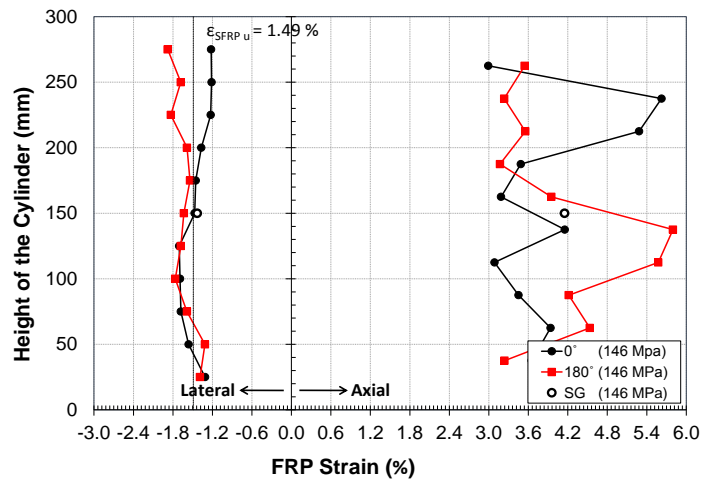


**Figure D-4: Axial and lateral strain at failure distribution for Group I – C37.3-SFRP1**

D.1.5. C37.3-SFRP2



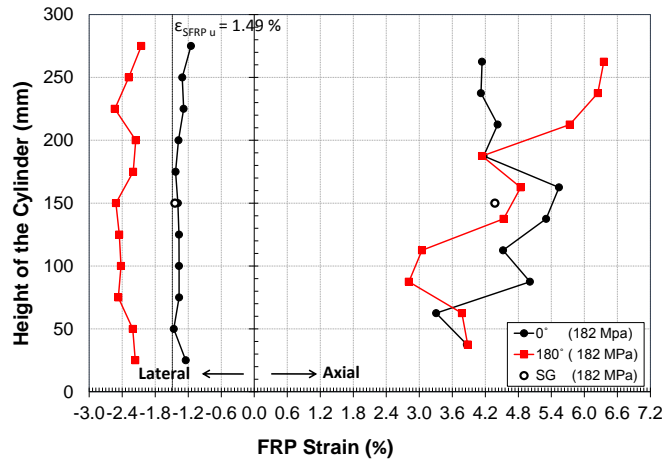
C37.3-SFRP2-SP#1



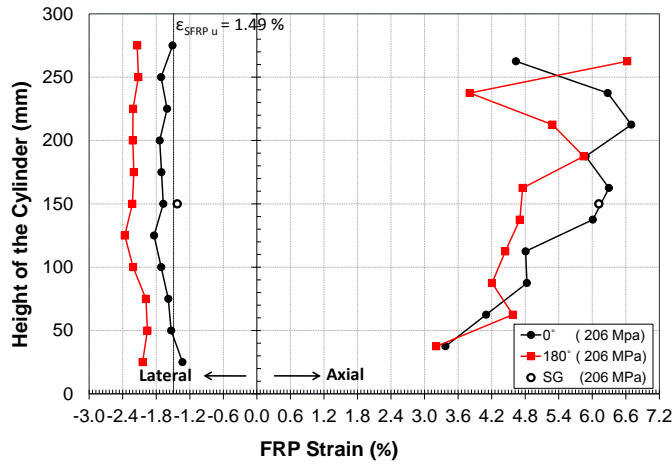
C37.3-SFRP2-SP#3

Figure D-5: Axial and lateral strain at failure distribution for Group I – C37.3-SFRP2

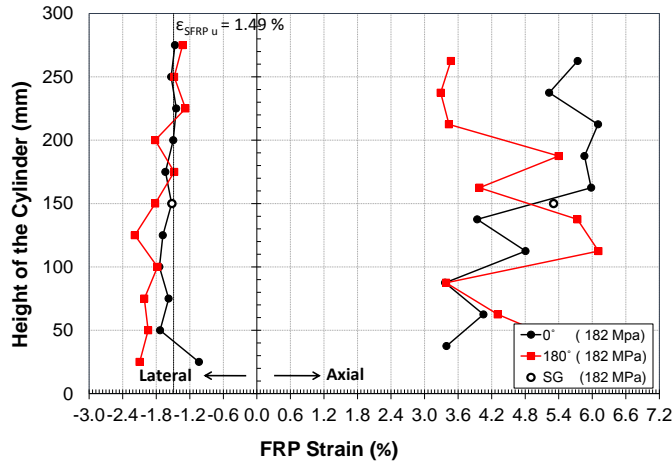
D.1.6. C37.3-SFRP3



C37.3-SFRP3-SP#1



C37.3-SFRP3-SP#2

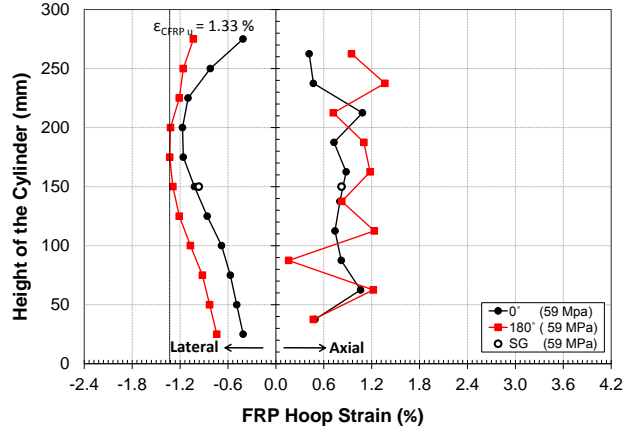


C37.3-SFRP3-SP#3

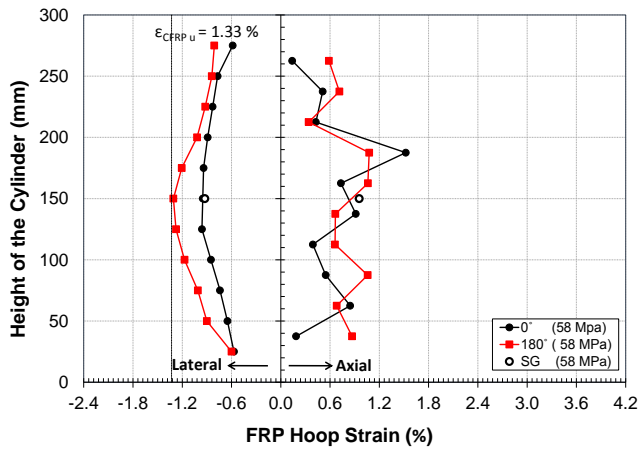
Figure D-6: Axial and lateral strain at failure distribution for Group I – C37.3-SFRP3

## D.2. Group II

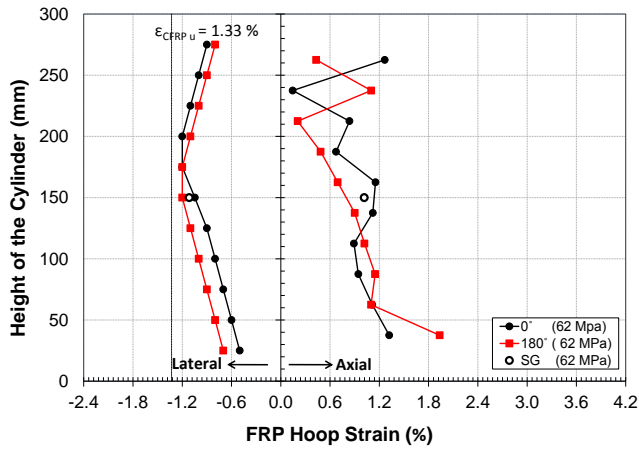
### D.2.1. C42.4-CFRP1



C42.4-CFRP1-SP#1



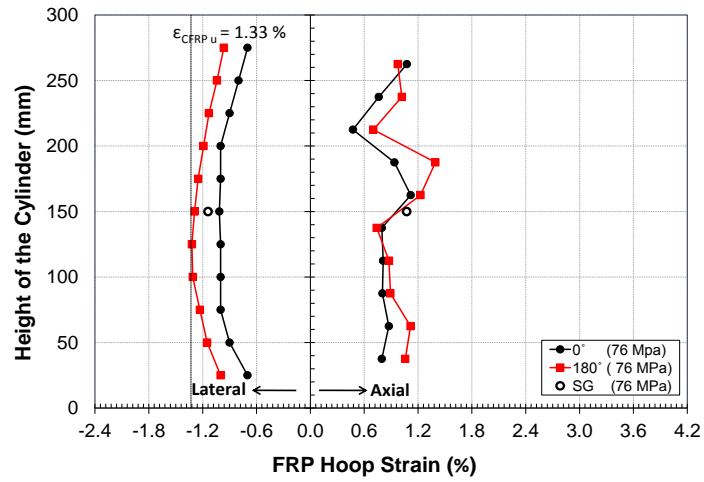
C42.4-CFRP1-SP#2



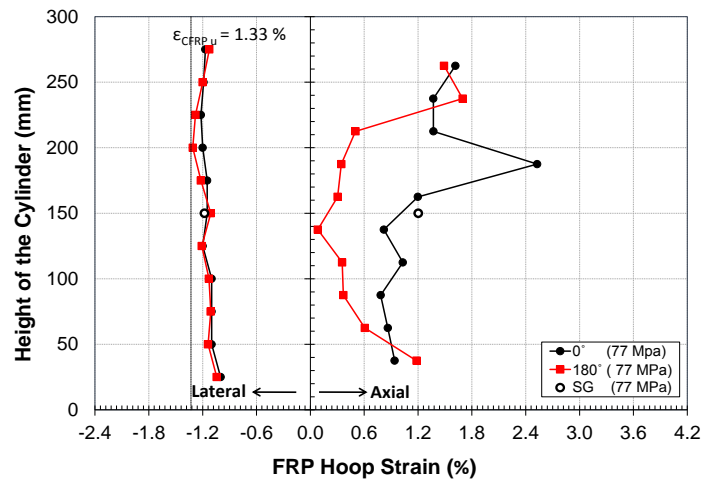
C42.4-CFRP1-SP#3

Figure D-7: Axial and lateral strain at failure distribution for Group II – C42.4-CFRP1

D.2.2. C42.4-CFRP2



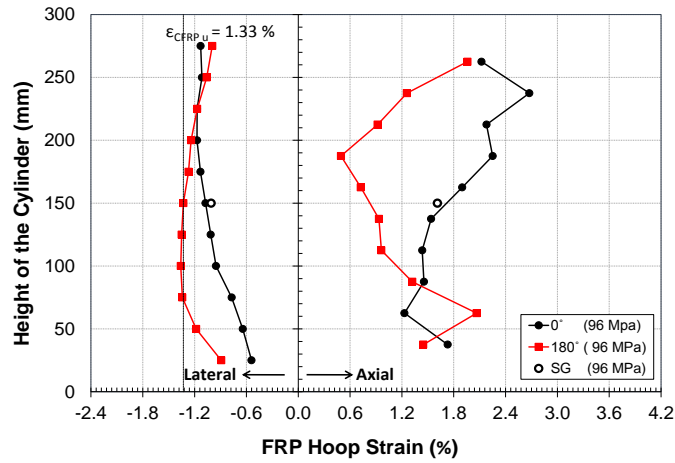
C42.4-CFRP2-SP#1



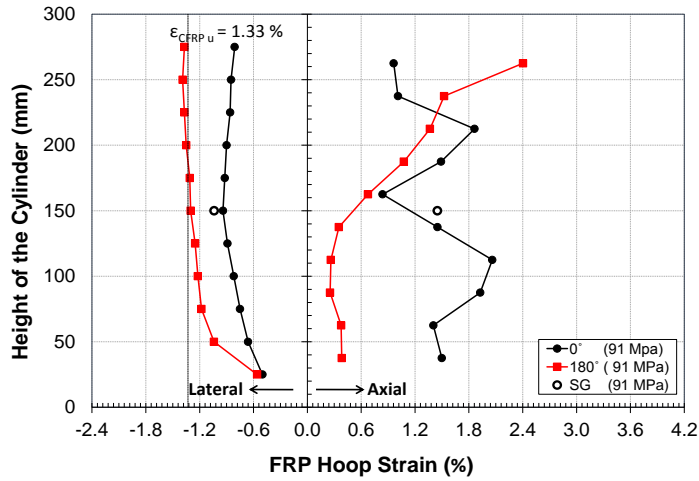
C42.4-CFRP2-SP#2

Figure D-8: Axial and lateral strain at failure distribution for Group II – C42.4-CFRP2

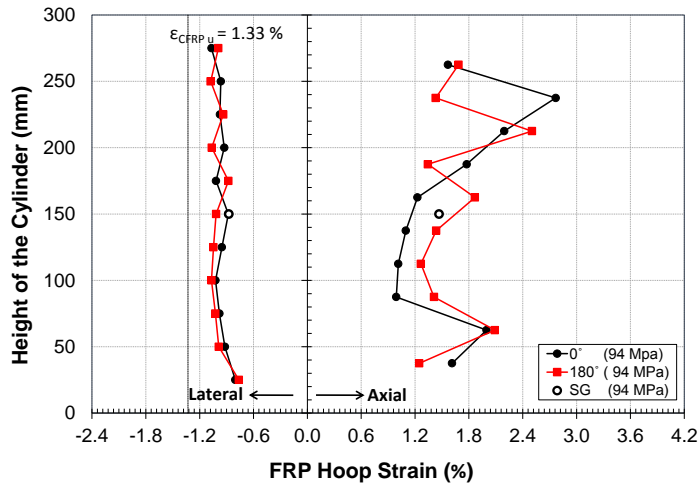
D.2.3. C42.4-CFRP3



C42.4-CFRP3-SP#1



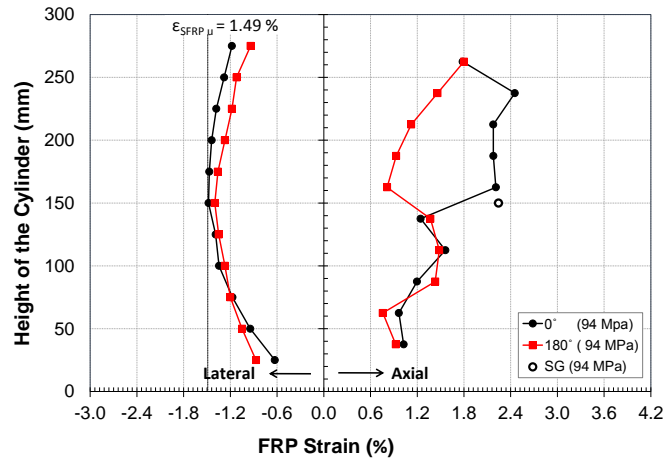
C42.4-CFRP3-SP#2



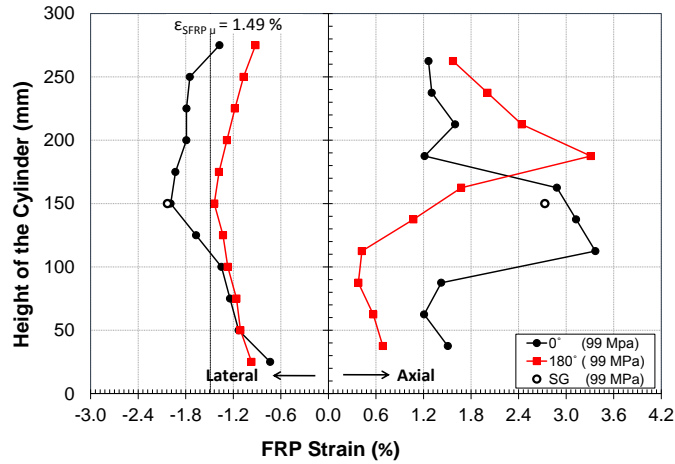
C42.4-CFRP3-SP#3

Figure D-9: Axial and lateral strain at failure distribution for Group II – C42.4-CFRP3

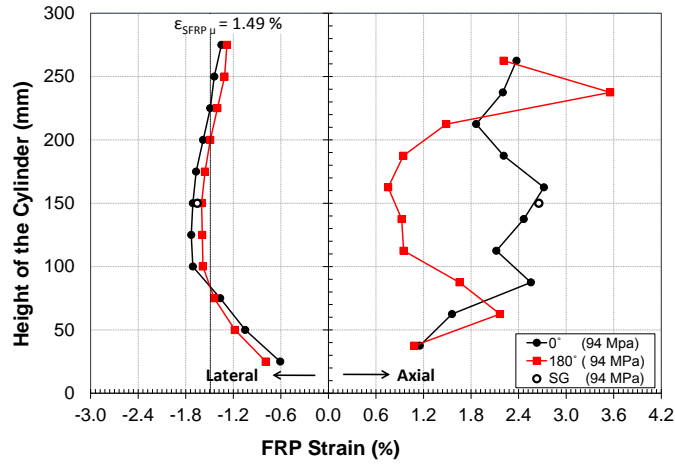
D.2.4. C42.4-SFRP1



C42.4-SFRP1-SP#1



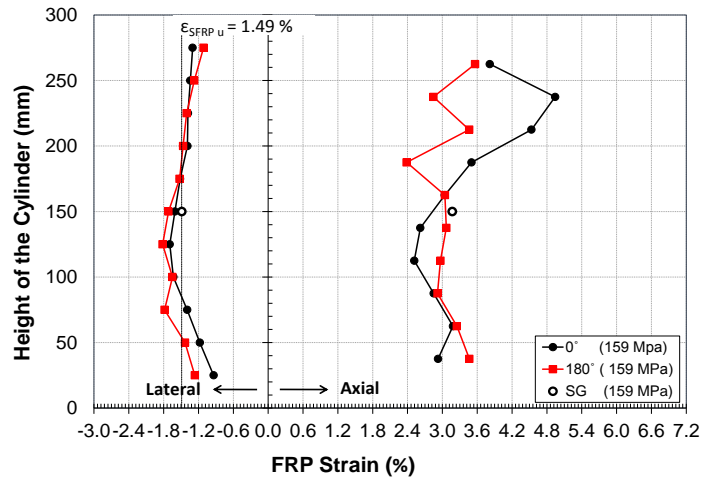
C42.4-SFRP1-SP#2



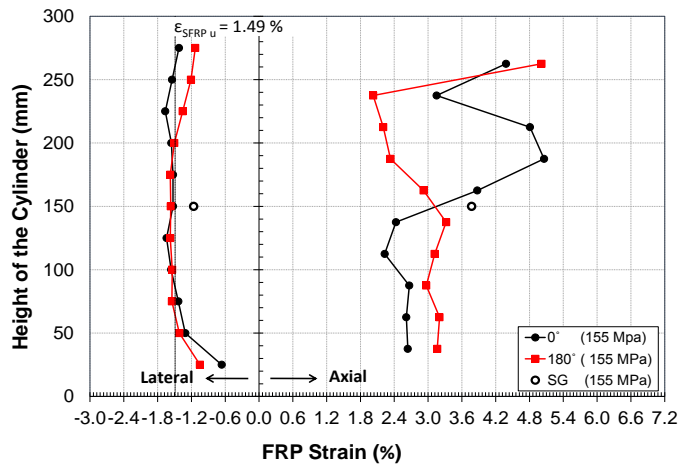
C42.4-SFRP1-SP#3

Figure D-10: Axial and lateral strain at failure distribution for Group II – C42.4-SFRP1

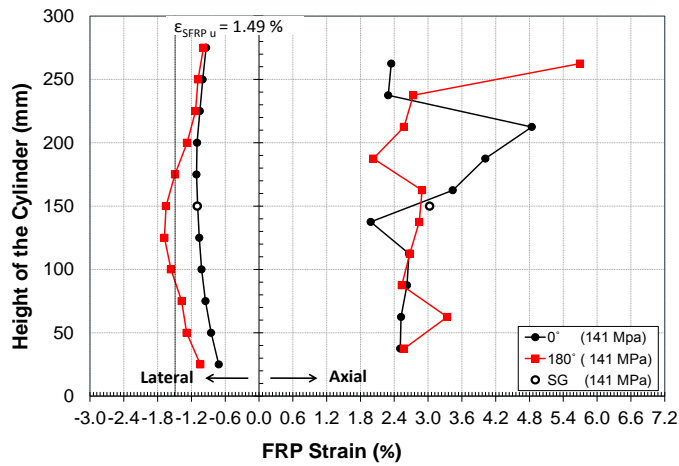
D.2.5. C42.4-SFRP2



C42.4-SFRP2-SP#1



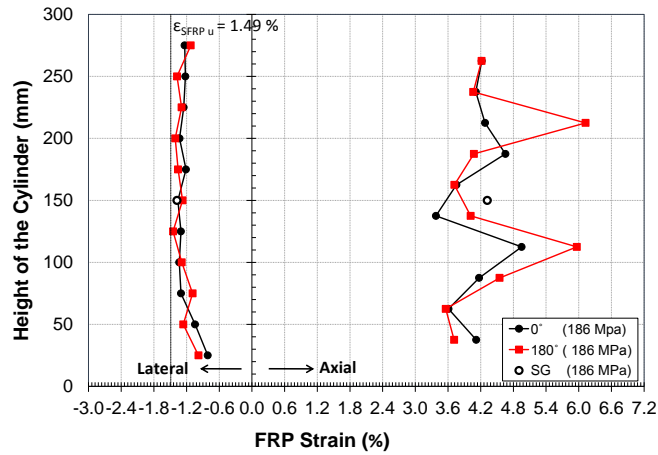
C42.4-SFRP2-SP#2



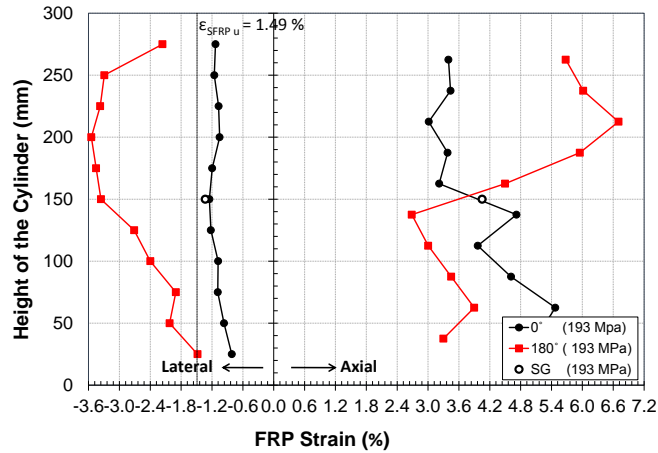
C42.4-SFRP2-SP#3

Figure D-11: Axial and lateral strain at failure distribution for Group II – C42.4-SFRP2

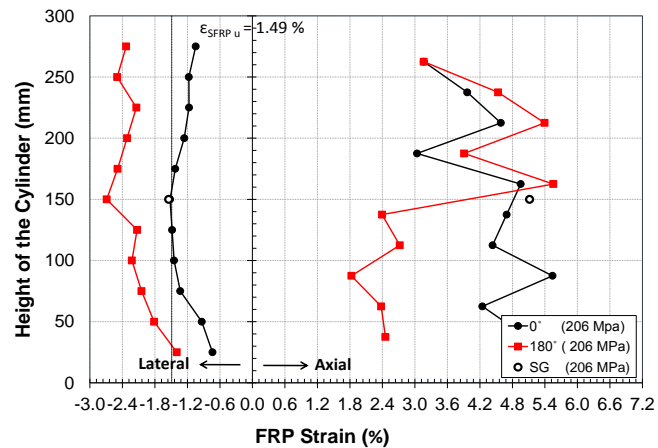
D.2.6. C42.4-SFRP3



C42.4-SFRP3-SP#1



C42.4-SFRP3-SP#2



C42.4-SFRP3-SP#3

Figure D-12: Axial and lateral strain at failure distribution for Group II – C42.4-SFRP3